

UNIVERSITÉ DE NANTES
Ecole polytechnique de l'Université de Nantes
ÉCOLE DOCTORALE

**SCIENCES POUR L'INGENIEUR, GEOSCIENCES, ARCHITECTURE
DE NANTES**

N° attribué par la bibliothèque

Année 2014

--	--	--	--	--	--	--	--	--	--

Transferts thermiques et mélange dans les écoulements pulsés en présence de force centrifuge

THÈSE DE DOCTORAT
Discipline : Sciences pour l'Ingénieur
Spécialité : Thermique et Énergétique

*Présentée
et soutenue publiquement par*

Fareed Hussain MANGI

Le 14 avril 2014, devant le jury ci-dessous

Président		
Rapporteurs	M. Fethi ALOUI	Professeur, Université de Valenciennes
	M. Yves BERTIN	Professeur, ENSMA, Poitiers
Examineurs	M. Abdelhak AMBARI	Professeur, ENSAM, Angers
	M. Ahmed OULD EL MOCTAR	Maître de Conférences HDR, Polytech' Nantes
	M ^{me} Dominique DELLA VALLE	Maître de Conférences HDR, ONIRIS Nantes
	M. Mojtaba JARRAHI	Maître de Conférences, Université Paris Sud
	M. Thierry LEMENAND	Maître de Conférences HDR, Université d'Angers
	M. Hassan PEERHOSSAINI	Professeur, Université Paris VII

Directeur de thèse : Professeur Hassan PEERHOSSAINI

ED :
(Uniquement pour STIM et SPIGA)

Symbols	Unit	Definition
\bar{c}	$\mu\text{g/L}$	• Mean concentration measured by PLIF
C_o	$\mu\text{g/L}$	• Concentration injected
d	m	• Diameter of pipe/tube section
D_1, D_2	m	• Diameters of the pullies
D_n	--	• Dean number
\bar{g}	m/s^2	• Gravity
L	m	• Length
I_{mix}	--	• Mixing degree
I_{seg}		• Segregation index
N_o	rpm	• Rotational speed of motor
N_{crank}	rpm	• Crank velocity
P	Pa	• Pressure
r	m	• Radius
r_c	m	• Radius of curvature
r_o	m	• Radius of the pipe section/tube
Re_{st}	----	• Reynolds number
t	s	• Time
t_d	s	• Time delay
T	s	• Time period
T_{inlet}	$^{\circ}\text{C}$	• Inlet temperature
T_{outlet}	$^{\circ}\text{C}$	• Outlet temperature
T_s	$^{\circ}\text{C}$	• Shell side temperature
ΔT	$^{\circ}\text{C}$	• Temperature difference
U	m/s	• Velocity
u, v, w	m/s	• Cartesian velocity components
u_{θ}	m/s	• Tangential velocity component
X_{piston}	m	• Piston displacement
\dot{X}_{piston}	m/s	• Piston velocity

Greek letteres

Symbols	Unit	Definition
α	--	• Womersley frequency parameter
β	--	• Velocity amplitude ratio
ε	s^{-1}	• Deformation rate
ζ	s^{-1}	• Vorticity
η	%	• Heat exchanger efficiency
θ	--	• Radius of curvature
ν	m	• Kinematic viscosity
ψ	%	• Mixing intensification
χ	%	• Heat exchanger efficiency intensification
ω	rad. s^{-1}	• Angular velocity

Table of contents	1
General introduction	5
Chapter 1 Time dependent alternated Dean flow	11
Objective	13
I.1. Chaos terminology	13
I.1.1. Dynamical systems	14
I.1.1.1. Deterministic system	14
I.1.1.2. Non deterministic system	14
I.1.2. Chaotic system	14
I.1.2.1. Temporal chaos	15
I.1.2.2. Spatial chaos	15
I.1.2.3. Spatiotemporal chaos	15
I.1.3. Different approaches to study the chaos	15
I.1.4. Different methods to emphasize chaos	15
I.1.4.1. Sensitivity to initial conditions - Lyapunov exponents	16
I-1.4.2. Poincaré section	16
I.1.4.3. Horseshoe transformation	18
I.1.5. Chaotic advection	19
I.2. Chaotic advection in alternated Dean flow	21
I.2.1. Dean flow	21
I.2.2. Spatial chaos in alternating Dean flow	23
I.3. Dean alternating pulsatile flow	24
I.3.1. Pulsatile flow and characteristic parameters	25
I.3.2. Complexity of secondary flow – Lyne structure	27
I.3.3. Equations for alternating pulsatile Dean flow	32
I.3.4. Quantitative description of mixing	34
I.4. Previous studies on mixing enhancement by alternating pulsatile Dean flow	36
I.5. Main results of Timité (2005)	36
I.5.1. At the exit of the first 90° curved pipe	36
I.5.2. At the exit of the second to sixth 90° curved pipes	38
I.5. 3. Rate of elongation	38
I.6. Main results of Jarrahi (2010)	41
I.6. 1. At the exit of a 90° curved pipe	42

I.6. 1.1. Phase angle $\omega t = 0^\circ$	43
I.6. 1.2. Phase angle $\omega t = 90^\circ$	45
I.6. 1.3. Phase angle $\omega t = 180^\circ$	46
I.6. 1.4. Phase angle $\omega t = 270^\circ$	47
I.6.2. Mixing analysis in a curved pipe	49
I.7. Pulsatile chaotic advection in micro fluidic mixers	50
I.8. Previous studies on heat transfer enhancement by pulsatile flows	52
I.8.1. Heat transfer enhancement techniques	52
I.8.1.1. Active heat transfer enhancement techniques	52
I.8.2. Passive heat transfer enhancement techniques	53
I.8.2. Using different kind of geometries to enhance heat transfer	53
I.9. Pulsation impositions on the flow to enhance heat transfer	54
1.9.1. Pulsation impositions on the flow to enhance heat transfer (older studies)	54
1.9. 2. Pulsation impositions on the flow to enhance heat transfer (recent studies)	57
Chapter 2 Materials and methods	63
Objective	65
II.1. Experimental setup for mixing study in pulsatile flows through a bend	65
II.1.1. Pulsatile flow generation	65
II.1.2. Pulsation generator	68
II.1.2.1. Scotch yoke mechanism	68
II.1.2.2. Crank length and piston diameter	69
II.1.2.3. Adjustments to obtain different conditions of pulsation	71
II.2. PLIF technique	77
II.2.1 Fluorescence and tracer dye	78
II.2.1.1. General considerations on fluorescent dyes	79
II.2.1.2. Laser / Dye combination – notion of spectral conflict	80
II.2.1.3. Notion of photo bleaching	81
II.2.1.4. Tracer dye Rhodamine 6G	81
II.2.2. PLIF system	83
II.2.2.1. Description of the PLIF system used	83
II.2.2.2. Synchronization	84
II.2.2.3. PLIF measurements and data treatment	86

II.3.The intermittent heat exchanger	88
II.3.1. Schematic arrangement	88
II.3.2. Pulsation pumping system	89
II.3.3. Chaotic heat exchanger	91
II.3.4.Pulsation parameters and conditions	92
Chapter 3 Mixing intensification by pulsatile flow	95
Objectives	97
III.1. PLIF measurements	98
III.1.1. Operating conditions	98
III.1.2. PLIF calibration	100
III.1.3. Mass balance of tracer dye for steady cases	102
III.2. Qualitative study of mixing in pulsatile flow	103
III.2.1. Flow visualization in steady cases	103
III.2.2. Flow visualization in pulsated cases	104
III.2.2.1. Influence of Reynolds number	104
III.2.2.2. Influence of velocity amplitude	108
III.2.2.3. Influence of the frequency	108
III.3. Mixing intensification analysis in pulsatile flow	112
III.3.1. Determination of the degree of mixing	112
III.3.2. Influence of Reynolds number	114
III.3.3. Influence of the frequency	119
III.3.4. Influence of velocity amplitude	128
III.3.5. Influence of phase angle ωt	132
III.4. Conclusions	139
Chapter 4 Heat transfer intensification by pulsatile flow	141
Objective	143
IV.2.Introduction	143
IV.3.Pulsatile flow and Dean configuration	143
IV.4.Pulsation conditions and measurements	145

IV.3.1.Verification of the pulsation flow	146
IV.3.2.Quality of measurement	150
IV.3.2.1 Temperature measurement accuracy	150
IV.3.2.2.Standard deviation of measurement	153
IV.3.2.3. Reproducibility of measurement	154
IV.5.Study of heat transfer	156
IV.4.1. Influence of frequency	156
IV.4.2. Influence of velocity amplitude	158
IV.4.3. Influence of Reynolds number	158
IV.4.4. Influence of pulsation signal	159
IV.6.Intensification of heat transfer	160
IV.5.1. Influence of frequency	161
IV.5.2. Influence of velocity amplitude	164
IV.5.3.Influence of Reynolds number	168
IV.5.4.Influence of pulsation signal	171
IV.7. Conclusions	179
Chapter 5 Conclusion and prospects	181
Résumé français	187
References	195

Chapter 0

General introduction

General introduction

Mixing and heat transfer intensification in laminar flow regime are of great importance for some industry sectors (food, pharmaceuticals, plastics, process and polymers) where the quality of products should not be altered because of high shear stresses. These products are often high viscosity structured fluids, with cells or long molecular chains likely to be broken in a turbulent regime. Improving the performance of mixers which operate in laminar regime is still the core subject of many engineering studies.

Helical tube mixers are already used in industry since the mixing occurs more efficiently in curved channels than in the straight ones. This is due to the secondary flow generated by the centrifugal force. With this secondary flow, the transverse displacements of the fluid particles increases and the axial dispersion decreases: Dean roll-cells formed [Dean (1927) and Dean (1928)] in the secondary flow act as internal agitators which homogenize the flow. To improve the mixing and the heat transfer in the laminar regime, a more complex geometric configuration compared to helical has been proposed and studied in the “Laboratoire de Thermocinétique de Nantes” (LTN) [Le Guer (1993), Castelain (1995) Mokrani (1997), Chagny-Regardin (2000)]. This geometry is composed of series of bends $\pm 90^\circ$ of alternated chiralities between the planes of curvature. This geometry induces a spatial chaos in the fluid trajectories (the state variables being the particle location). At each change of the plane of curvature, the Dean roll-cells are destroyed and reformed under the new orientation of the centrifugal force, which intensifies the mixing by chaotic advection. This has been assessed in numerous previous studies like (Aref, 1984), (Jones et al., 1989), (Acharya et al., 1992, Peerhossaini et al., 1993), (Castelain, 1995), (Mokrani, 1997), (Chagny et al. 2000), (Castelain et al., 2001), (Lemenand and Peerhossaini, 2002), (Timité, 2005), (Habchi et al., 2009), (Jarrahi, 2010) and (Funakoshi and Jang, 2012). The flow in this type of mixer is called "Dean alternating flow".

In the present work, this chaotically twisted geometry is used as a mixer and heat exchanger.

In 2005, Timité studied the effects of the superimposition of time dependence on a steady Dean alternating flow.

The idea was to impose pulsations on a steady flow to obtain a more complex flow.

Actually, the apparition of an extra pair of counter rotating cells that co-exist with the Dean cells in a sinusoidal flow in a bend has been demonstrated for the first time by Lyne (1970). This complex structure of secondary flow obtained in the presence of the pulsation might therefore result in a better mixing in a chaotic regime compared to the steady cases. By qualitative visualizations conducted through LIF (laser induced fluorescence), in a chaotic configuration, consisting a series of six alternating bends, Timité (2005) analyzed the evolution of vortices of the secondary flow that develops during the pulsation in the bends. He has experimentally demonstrated the appearance of this chaotic flow by monitoring the deformation of the tracer lines. An increasing of the chaos that provides a better mixing by the pulsations was confirmed by the analysis of the stretching of these tracer lines.

Jarrahi (2010) analyzed more deeply the role of complex secondary flow structures formed through pulsation on mixing enhancement. For this purpose, the velocity fields of the secondary flow at the exit of each bend of a chaotic configuration (same geometry of Timité (2005)) were obtained by using the particle image velocimetry (PIV) technique. Jarrahi (2010) used these velocity fields to describe the topology of the various structures that develop within a pulsated developing laminar flow in a single bend, and in the chaotic geometry (Dean alternating). Moreover, he defined favorable pulsation conditions for the mixing enhancement by criteria for the quantification of the mixing based on calculations of vorticity fields and strain rates.

Encouraged by the thermal results of Mokrani (1997) and (Chagny et al. 2000), and the results of Timité (2005) and Jarrahi (2010), the objective of the present thesis is to analyze the effect of pulsation on mixing and heat transfer intensification, compared to the steady flow. Two different experimental set-up are used in this purpose, a transparent duct for the optical mixing study, and a metal duct for the thermal study. The influence of the different operating parameters -of the Reynolds numbers, frequencies and amplitudes of sinusoidal pulsation-, on heat and mass transfer intensification is presented and analyzed in each case.

To study the mixing criteria in a curved pipe (same set up used by Timité (2005) and Jarrahi (2010)), the PLIF (planar laser induced fluorescence) technique is implemented for the first time in LTN laboratory.

Concerning the heat transfer study a shell and chaotically twisted tube heat exchanger is designed and constructed in LTN laboratory. The effect of the pulsation shape (sinusoidal,

triangular and square) is also investigated in the thermal study, in laminar as well as in turbulent regime.

In the first chapter of this thesis, some definitions of chaos are recalled and the chaotic advection in a flow of alternating Dean is explained. Previous studies on the role of the time dependence of the modification of the flow lines structure in the bends are shown.

The second chapter is devoted to a detailed presentation of the two different experimental setups, the first one for mixing study and the second one for the heat exchanger. The first experimental device is mainly that of Jarrahi study (2010), with adaptations to PLIF measurements. The second experimental device is a completely new setup especially built for this work. The measurement techniques, especially the PLIF technique are explained.

The objective of the third chapter is to present the results obtained by the PLIF technique for the mixing intensity through pulsations imposition on steady laminar flow. Effects of different pulsation parameters (steady Reynolds number, frequency parameter and velocity amplitude ratio) on the mixing degree in a single 90° curved pipe are discussed.

The fourth chapter is devoted to study the heat transfer intensification by pulsatile flow in a shell and tube heat exchanger. Tubes are chaotically twisted. Effects of pulsation, studied *via* four parameters i.e. steady Reynolds number, frequency parameter, velocity amplitude ratio and different pulsation wave forms, are observed, measured and analyzed. Optimum values (favorable for more efficient heat exchanger) for pulsation parameters are observed,.

Finally, in the fifth chapter, the general conclusions of this research are presented as well as the prospects for future work to be done in the continuity of this study.

Chapter 1

Time dependent alternated Dean flow

Objective

The objective of this chapter is to present the need and motivation of the usage of the pulsation flow in chaotic configurations, for the purpose of mixing and heat transfer enhancement.

The chapter consists of five sections: first, a reminder of the terminology of chaos, and the different approaches to define, describe and study chaotic systems is proposed. The notion of chaotic advection is also introduced in this section. In the second section, the Dean flow properties in a unique pipe bend are presented, and subsequently the development of chaotic advection in the case of spatially alternating chiralities. In the following (third) section, the idea of superimposing a time dependence to the basic alternating Dean flow is introduced, including a description of the mechanisms that impact the mixing and heat transfer process. The complex secondary flow observed in a pulsed or sinusoidal flow in a curved duct is also detailed.

In the last two sections, the governing equations and dimensionless parameters are presented, with the most important results from the bibliography devoted to highlight the advantage of using alternating flows Dean time dependent to increase mixing and heat transfers.

Chaos terminology

Chaos is a structured random behavior of a non-linear, complex, dynamical system. The behavior over long-time scales is unpredictable, seemingly random but not arbitrarily so, sensitive to initial conditions, and characterized by a strange attractor that is often a fractal. Chaotic behavior is different from random behavior in that it is not completely random and

the strange attractor governs its structure. The different terms of chaos terminology are defined hereafter.

I.1.1. Dynamical systems

A dynamical system is a physical system that evolves with time or with respect to another variable following the phase space considered through deterministic equations. A dynamic system can be random or deterministic.

I.1.1.1. Deterministic system

A deterministic system is governed by a known mathematical law, therefore an exact prediction of its evolution over time is possible, as far as a unique trajectory of the state variables is associated to each initial condition.

I.1.1.2. Non deterministic system

A non deterministic system is not governed by any equation. This type of system evolves randomly and no accurate prediction is possible in time. In these systems, output responses are not linearly related to input changes.

I.1.2. Chaotic system

A chaotic system can be considered as a deterministic system when it is perfectly described by mathematical equations, but what differs this kind of system is that it remains unpredictable for some parameters values. Determinism and unpredictability of a chaotic system seem paradoxical. This paradox can be explained by the main property of a chaotic system: the sensitivity to initial conditions. This sensitivity is so strong that two very close initial conditions can result in completely different final states of the system. Since this sensitivity is not detectable by the actual tools, therefore a chaotic system remains unpredictable in the long term despite its determinism. The term "chaos" in the flow fluid is used for two different cases: the temporal chaos and spatial chaos.

I.1.2.1. Temporal chaos

The temporal consideration of the chaos is entirely linked to the velocity field. Therefore an initially stable flow, which has random variations velocity in time is often studied under the term temporal chaos.

I.1.2.2. Spatial chaos

Spatial chaos is meant to chaotic spatial trajectories of the particles. The evolution of these spatial trajectories is sensitive to the initial conditions. Trajectories are disordered but are still reproducible because the system is deterministic. The term "spatial chaos" is directly related to our study and "Lagrangian chaos" is also used for this type of chaos.

I.1.2.3. Spatiotemporal chaos

The systems which show disorder in both space and time are said to exhibit spatiotemporal chaos. These chaos occur for instance in turbulent regime.

I.1.3. Different approaches to study the chaos

There are two different approaches in the fluid mechanics to study all kinds of flows including chaotic flows : the Eulerian coordinates and the Lagrangian coordinates. In the Eulerian description, a fixed point of the flow medium is observed and observers study the changes in the properties of the flow at that point. In the Lagrangian one, the flow properties are described by following each particle in its movement, meaning throughout its dynamic history while moving through space and time.

I.1.4. Different methods to emphasize chaos

Emphasizing chaos is directly related to the approach (Lagrangian or Eulerian) to study the flow.

I.1.4.1. Sensitivity to initial conditions - Lyapunov exponents

When a Lagrangian approach is chosen for the description of the flow, the measurement of Lyapunov exponents appears the most appropriate method to characterize the chaos. This method is related to the key property of a chaotic system, let be the sensitivity to initial conditions. In a chaotic system, two initially very close particles follow divergent paths that exponentially move away (Figure I-1). Lyapunov exponents characterize the divergence rate of trajectories and thus determine the chaos degree in the flow, it is defined by:

$$\lambda = \lim_{\substack{t \rightarrow \infty \\ \varepsilon(0) \rightarrow 0}} \frac{1}{t} \ln \left(\frac{\varepsilon(t)}{\varepsilon(0)} \right) \quad (\text{I- 1})$$

where $\varepsilon(0)$ is the initial distance between two particles and $\varepsilon(t)$ is the distance between these two particles over time. While $\varepsilon(0) \rightarrow 0$, Lyapunov exponent λ is an indicator of the divergence rate of the trajectories over time.

If $\lambda \leq 0$, the behavior of the system is regular. On the contrary, a Lyapunov exponent $\lambda > 0$ is the necessary and sufficient condition to exhibit the existence of chaos. The advantage of this method is that it provides a safe and direct quantification of chaos, but the disadvantage is related to difficulties in experimental measurements in complex geometries where the Lagrangian approach becomes very complicated to carry out.

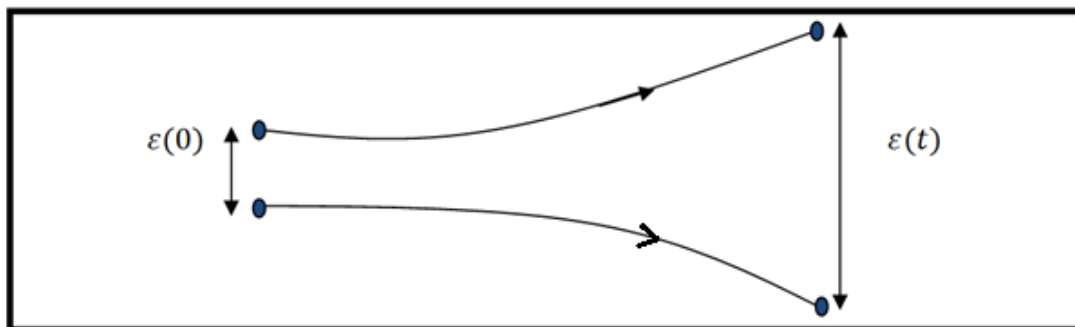


Figure I- 1. Particles initially very close then exponentially move away in a chaotic system.

I-1.4.2. Poincaré section

In numerous flow configurations, regular zones and chaotic zones can coexist, and the Poincaré section determination is a relatively simple method to characterize qualitatively the

chaotic zones associated to different trajectories of the flow. This method is relevant with the Eulerian approach, in the sense that defined locations in the flow are observed.

For example, the technique of Poincaré sections in a three-dimensional flow consists to observe the intersection points of the considered trajectories with plans to periodic abscissa or periodic time. Elliptical points and hyperbolic points are among the specific issues that may exist in the structure of the flow. Figure I-2 shows schematically these two specific points.

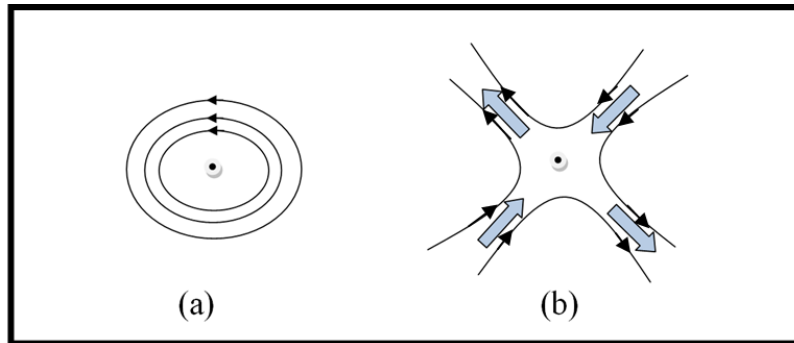


Figure I- 2. (a) Elliptical point; (b) Hyperbolic point.

The fluid surrounding an elliptical point has a few convective mass transfer with the core flow. The area around an elliptical point is hence not favorable for mixing because the particles that are trapped in this area cannot cross the current lines and therefore do not mix with the other part of the flow.

Conversely, in an hyperbolic point of the flow structure, the fluid is brought and ejected in another direction, because a part of the area around a hyperbolic point is stretched in a given direction (non-colored arrows in Figure I-2b) and contracted in the orthogonal direction (the colored arrows Figure I-2b). The hyperbolic points are known as points of interest because they favor the mixing process by the stretching / folding mechanism. We observe that each particular point in the flow may deviate the trajectories of a differently way depending on the nature of the point. This is why the study of positioning, forming and disappearance of these points is a method developed to highlight chaos. Although this method is indirect, it remains interesting for experimental measurements because it is based on the Eulerian approach.

I.1.4.3. Horseshoe transformation

A flow through a chaotic geometry might be stretched and folded in certain regions. This process of stretching and folding is called a horseshoe transformation. The process of stretching and folding was first described by (Ottino, 1989). He investigated the temporal evolution of a tracer in a cavity flow, and found that flow has a regular structure when the cavity walls move simultaneously in opposite direction, but on the other hand when they move in opposite direction alternatively and periodically, the flow becomes chaotic and tracer is distributed in more area than in the regular case.



Figure I- 3. Horseshoe transformation (Ottino, 1989).

In this transformation, an element is stretched which incites the contraction in its perpendicular direction and then it folds on its original position (LeGuer, 1993, Le-Guer-Y, 1993). Figure I-4 illustrates the different steps of this transformation. The present study is based on this type of transformation.

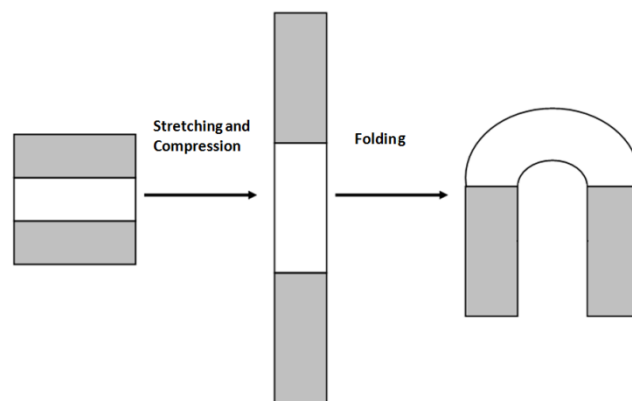


Figure I- 4. Horseshoe transformation principle.

The existence of a horseshoe transformation implies the existence of homoclinic points. Identification of only one of them ensures the existence of this transformation.

For example, we can refer to the Figure I-5 (LeGuer, 1993) which is obtained in an open three dimensional system composed of series of alternative bends in a steady regime. The Figure I-5 shows different operations of stretching and folding in a line of 5000 points initially positioned at 45° . Geometric alternance of the flow causes the stretching and folding process in it, therefore we may see at the exit of 100th bend that particles have travelling almost the whole of the section.

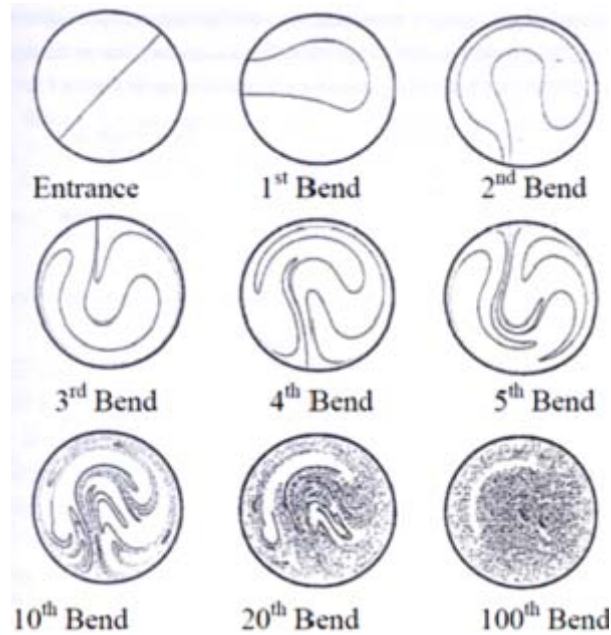


Figure I- 5. Deformation of a line of 5000 points initially positioned at 45° (Le Guer, 1993).

I.1.5. Chaotic advection

Chaotic advection, first introduced by (Aref, 1984), can be understood as the macroscopic phenomena of transportation in which the trajectories of the flow tracers are spatially chaotic, even obtained from initially simple velocity fields. A particularity of the chaotic advection is that it can appear even in laminar regime. The chaotic advection can be demonstrated in two dimensional time-dependent systems (Aref, 1984) or three-dimensional steady systems (Timité, 2005) who was the first to study the chaotic advection in a three-dimensional time-dependent system.

The motion equations for a two dimensional time dependant incompressible flow can be written as:

$$\frac{dx}{dt} = u(x, y, t) \quad (\text{I- 2})$$

$$\frac{dy}{dt} = v(x, y, t) \quad (\text{I- 3})$$

This is a Hamiltonian function and velocity is derived from stream function ψ ;

$$u = \frac{\partial \psi}{\partial y} \quad \text{and} \quad v = -\frac{\partial \psi}{\partial x} \quad (\text{I- 4})$$

Therefore, from equation (I-2), (I-3) and (I-4) we may have:

$$\frac{\partial x}{\partial t} = \frac{\partial \psi(x, y, t)}{\partial y} \quad \text{and} \quad \frac{\partial y}{\partial t} = -\frac{\partial \psi(x, y, t)}{\partial x} \quad (\text{I- 5})$$

In a steady flow, the stream function is independent of time and the system (I-5) is integrable. Trajectories are regular for this steady system (regular advection). However, the system (I-5) is non-integrable if the function y depends on time, in other words, if the flow is two dimensional incompressible time dependant. This situation can lead to chaotic trajectories (chaotic advection).

The motion equations for a three dimensional incompressible steady flow can be written:

$$\begin{aligned} \frac{dx}{dt} &= u(x, y, z) \\ \frac{dy}{dt} &= v(x, y, z) \\ \frac{dz}{dt} &= w(x, y, z) \end{aligned} \quad (\text{I- 6})$$

By dividing first and second equation of (I-6) by third one, we get:

$$\frac{dx}{dz} = \frac{u(x, y, z)}{w(x, y, z)} \quad \text{and} \quad \frac{dy}{dz} = \frac{v(x, y, z)}{w(x, y, z)} \quad (\text{I- 7})$$

The analogy between equations (1-2, I-3) and (1-7), for which the space variable z can be identified as time t , shows that the three-dimensional steady flows are equivalent to two dimensional time-dependent flow. Thus, we can conclude that the chaotic trajectories

generation (and therefore chaotic advection) is possible in a steady three dimensional flow. For example, a simple geometric disturbance may generate chaotic trajectories in an open three-dimensional steady flow while remaining in a laminar regime. The studies of (Khakhar et al., 1987) and (LeGuer, 1993) are based on this idea.

Chaotic advection in alternated Dean flow

I.2.1. Dean flow

When a steady flow is through a curved pipe, two opposite forces act on the fluid particles perpendicularly to the direction of the main flow: the centrifugal force due to the curvature of the pipe and the force generated by the pressure gradient. If we call the wall closest to the center of curvature "internal wall" and the wall far from the center of curvature as "outer wall" (Figure I-6), the centrifugal force acts in the direction from the inner wall to the outer wall although the pressure force acts in the opposite direction. In the median plane, shown by a symmetry line on the Figure (I-6) the centrifugal force over rides the pressure force and therefore the fluid particles move to the outer wall. The particle motion is slowed near the outer wall due to viscous forces. Then to ensure the momentum conservation, the fluid particles back towards the inner wall, passing in the vicinity of the upper and lowerfaces where the velocities are lower and the forces balance is in favor of the pressure-driven centrifugal force. The competition between the centrifugal force and the pressure force, forms two counter rotating cells in the plane perpendicular to the main flow (Figure I-6). These cells are named Dean roll cells (Dean, 1927, Dean, 1928). (White, 1929) experimentally confirmed the existence of Dean roll cells but the experimental work of (Eustice, 1911) must be mentioned as the first study that has shown these counter rotating cells in a bend pipe.

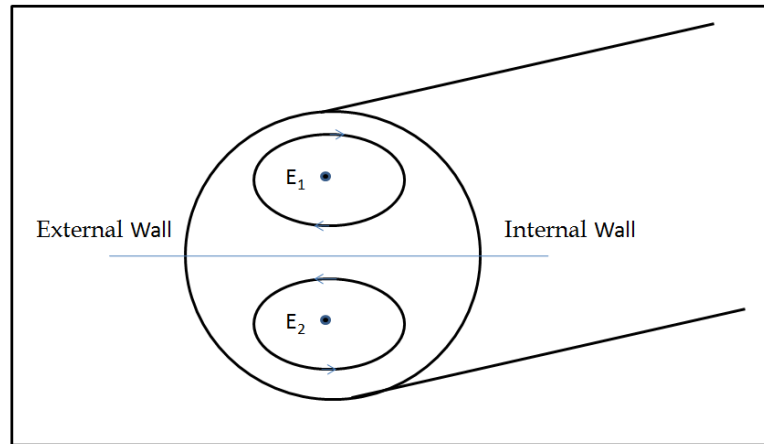


Figure I- 6. Dean cells.

The Dean flow is governed by the following three parameters:

- (i) Φ : the opening angle of the pipe.
- (ii) θ : the curvature ratio of the pipe, defined as:

$$\theta = \frac{r_o}{r_c} \quad (\text{I- 8})$$

where r_o is the radius of the circular section of the pipe and r_c is the radius of curvature of the pipe.

(iii) D_n : the Dean number is a non-dimensional number that characterizes the flow in curved channels. It represents the ratio of centrifugal force and inertial forces to viscous forces and is defined as:

$$D_n = Re(\theta)^{\frac{1}{2}} \quad (\text{I- 9})$$

The analytical study of (Dean, 1927 and Dean, 1928) was carried out for a case for which the flow is developed (a relatively large opening angle) and the curvature ratio is very small. In that special case, the flow is only governed by the Dean number. But for a general case, one must consider all three parameters (Φ , θ , D_n).

I.2.2. Spatial chaos in alternating Dean flow

The center of each Dean cell is an elliptical point development and this particular type of point is not favorable to the mixing, E_1 and E_2 on Figure (I-6) illustrate these points. On the other hand, Dean vortices (cells) play the role of internal agitators for mixing the particles in

the flow. By analogy with the time-dependent two dimensional system of (Aref, 1984) which is a chaotic system, the agitator materials may be replaced by the inherent stirring by the Dean vortex/cells. In addition, the time period of the vortices of the system proposed by (Aref, 1984) may be substituted by a spatial period of a geometric parameter (see equations I-2 and I-6). Thus the system obtained by these replacements is a three-dimensional chaotic system. If the orientation of the curvature plane of the pipe is chosen as the geometric parameter which periodically varies, the system is called Dean alternating flow because with each change of the plan direction, positioning of the Dean vortex/cells centers and also their chirality (Figure I-7). The trajectories of the particles in this flow are chaotic. The formation and subsequent disappearance of Dean cells in this system also solve the problem of elliptic points which are obstacles to the better mixing. Thus the Dean alternating flow system seems a highly suitable system for mixing process in laminar flows.

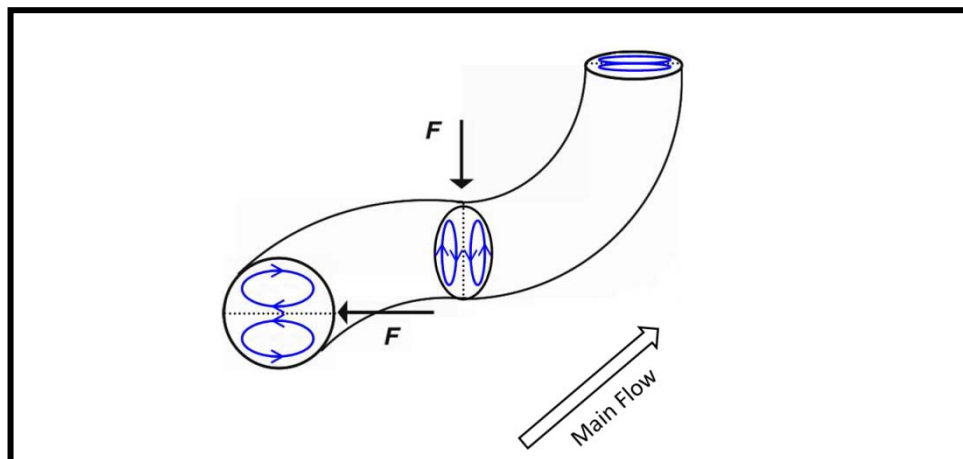


Figure I- 7. Dean alternating flow (F : centrifugal force).

If the angle of orientation between the curvature planes is 0° , i.e. a helical or toroidal geometry, the system is completely integrable and the particle trajectories are regular. In this case, once the trapping zones around elliptical points (Dean cells centers) form, they do not disappear and thus the mixing is restricted. If the angle is non zero, the regular trajectories begins to decrease. For an angle equal to 90° , the fraction volumes of islands is minimum in the flow and the regime is at maximum chaos (S.W.Jones 1989), (Le-Guer-Y, 1993). This geometry is that studied during the present work.

Chaotic advection in the alternating Dean flow can appear in a laminar regime at low Reynolds numbers, this can be very interesting for some industrial applications. For example, the mixing of highly viscous fluids or products of fragile structures which can be damaged under the action of too high shear stresses is not feasible in a turbulent regime. This kind of mixing processes are widely carried out in the food, pharmaceutical, plastics, chemical and polymer industries. In addition, Dean alternating flow is interesting for a more uniform and efficient heat transfer. In a heat exchanger designed on this principle, heat is advected from the walls to the fluid through the Dean cells (heat transfer efficiency increased) and the direction of this advection changes periodically by the alternating geometry of the heat exchanger (homogeneous heat transfer). Due to these advantages, the Dean alternating flow has been the subject of several studies, especially experimental ones in the “Laboratoire de Thermocinétique de Nantes” [(Le-Guer-Y, 1993, Castelain, 1995, Mokrani, 1997, Chagny-Regardin-C, 2000) (Habchi et al., 2009)]. These studies resulted in the design of prototypes chaotic mixers/exchangers applicable in the industry.

Dean alternating pulsatile flow

In a laminar flow regime, the superimposition of a time-dependence on an stationary flow in a curved duct (Dean flow), modifies the structure of the main flow and the secondary flow. If the time dependence is imposed in the form of a sinusoidal axial velocity, the flow structure can become more complex, for certain conditions, due to this modification (Lyne, 1970). As the secondary flow is more complex, fluid particles better travel across the duct section, so that the residence time of the particles is more uniform (sharper RTD), that is a good criteria for the macro-mixing. In addition, velocity gradients are stronger in a complex structure compared to the gradients in a steady flow. Strong velocity gradients intensify the rate of stretching and folding, which are the main mechanisms of the mixing. Another advantage of this time dependence is that the flow and thus the quality of the mixing can be controlled by varying the parameters of this dependence. All these arguments reinforce the idea that the mixing will be increased by adding a temporal dependence to the Dean flow. In the literature, the pulsatile flow in curved channels is much studied for broad applications in the area of physiology and cardiovascular flows. These works include the following studies: (Pedley, 1980), (Chang, 1985), (Zabielski L., 1998, Deplano V., 1999), (Siouffi M., 1998) and (Siggers J.H., 2008). The pulsating flow in a curved duct was also the subject of study in

order to increase the heat transfer (Simon., 1977), but the effect of pulsation on the quality mixture (Timité., 2009) is not much studied.

I.3.1. Pulsatile flow and characteristic parameters

The pulsatile flow used in this study is on the one hand, a result of a pure sinusoidal flow imposed on a steady flow in the experimental mixing study, and on the other hand it is composed of the surimposition of either sinusoidal, triangular or square signals on a steady flow in the experimental heat transfer study. In the following, and in order to clarify the manuscript, the oscillation that creates the pulsatile flow is described as a sinusoidal signal and details about triangular and square signals are given in section II.3 relatively to the experimental heat transfer study in which they are exclusively use. Therefore analyzing pulsatile flow, it is obvious to consider the pulsatile velocity U_p can be written as:

$$U_p(t) = U_{st} + U_{sin}(t) \quad (\text{I- 10})$$

where U_{st} is the mean steady velocity and $U_{sin}(t)$ is the pure sinusoidal flow, which is the time-dependent component of the pulsatile velocity. If the amplitude of the sinusoidal flow is U_{sinmax} , and the angular frequency of the oscillation is ω , then Equation I.10 can be written as:

$$U_p(t) = U_{st} + U_{sinmax} \sin(\omega t) \quad (\text{I- 11})$$

Different characteristic parameters are useful and are recapitulated below.

- the angular frequency, ω , can also be described by a dimensionless parameter, α , called the Womersley parameter, defined as:

$$\alpha = r_o \left(\frac{\omega}{\vartheta} \right)^{\frac{1}{2}} \quad (\text{I- 12})$$

where r_o is the radius of the pipe and ϑ is the kinematic viscosity of the fluid. The Womersley number is a dimensionless expression of the inertial effects due to pulsatile flow frequency in relation to viscous effects and is used in what follows to express the angular frequency of the oscillation.

The Womersley parameter indicates the ratio of inertial forces associated with the local acceleration and viscous forces that determine the movement for a time scale equal to the oscillation period. It also provides information on the relative magnitude of the boundary layer disturbed by the pulsation from the magnitude of the boundary layer flow stationary:

$$\delta = \left(\frac{2\nu}{\omega} \right)^{\frac{1}{2}} = r_o \cdot 2^{\frac{1}{2}} \cdot \frac{1}{\alpha} \quad (\text{I- 13})$$

The ratio α can also be interpreted as the square root of viscous time diffusion, $\frac{r_o^2}{\nu}$, and the oscillation period, $\frac{1}{\omega}$, (Timité, 2005). In a pulsating flow, if the Womersley parameter is small ($\alpha \leq 1$), the pulsation frequency is sufficiently low that the flow remains almost in phase with the pressure gradient which generates the flow. As a consequence, for large Womersley parameter values ($\alpha \gg 1$) i.e. for high frequencies pulsation, the flow is no longer in phase with the pressure gradient, with a shift of about 90° between the flow and the pressure gradient.

- a velocity component ratio β is defined as the ratio between the maximum sinusoidal amplitude of the sinusoidal velocity term and the average value of the steady velocity term:

$$\beta = \frac{U_{sinmax}}{U_{st}} \quad (\text{I- 14})$$

If the value of β is very small ($\beta \ll 1$), the steady component predominates over the sinusoidal component of flow quasi steady (Takami., 1984). But on the contrary, for large values of β ($\beta > 1$), the axial velocity distribution and structures of the secondary flow are complex and do not resemble to those of steady flow.

- the steady Reynolds number Re_{st} which is based on the average value of steady components of velocity is expressed as:

$$Re_{st} = \frac{U_{st} \cdot d}{\nu} \quad (\text{I- 15})$$

- the sinusoidal Reynolds number Re_{sin} is based on the maximum amplitude of sinusoidal component of the velocity:

$$Re_{sin} = \frac{U_{max, sin} \cdot d}{\nu} \quad (\text{I- 16})$$

- the Reynolds number Re_p that represents the maximum peak value of Reynolds number in a pulsatile flow is the sum of the steady and sinusoidal Reynolds numbers.

$$Re_p = Re_{st} + Re_{sin} \quad (I- 17)$$

If the radius of the curvature of the pipe is equal to r_c , then three more dimensionless parameters can be defined:

- the steady Dean number Dn_{st} which takes into account the effect of steady Reynolds number and curvature of the pipe at the same time:

$$Dn_{st} = Re_{st} \cdot (\theta)^{\frac{1}{2}} \quad (I- 18)$$

- the sinusoidal Dean number Dn_{sin} whose definition is based on the sinusoidal velocity component and also on the curvature of the pipe:

$$Dn_{st} = Re_{sin} \cdot (\theta)^{\frac{1}{2}} \quad (I- 19)$$

- the Dean number Dn_p which shows the maximum peak value of the Dean number in pulsatile flow in a curved pipe:

$$Dn_p = Dn_{st} + Dn_{sin} = (Re_{st} + Re_{sin}) \cdot (\theta)^{\frac{1}{2}} = Re_p \cdot (\theta)^{\frac{1}{2}} \quad (I- 20)$$

In the following study, the pulsatile flow is described via three characteristic parameters that are Re_{st} , α and β .

I.3.2. Complexity of secondary flow – Lyne structure

For the first time (Lyne, 1970) considered a purely sinusoidal flow ($Re_{st}=0$) flowing through a curve. In his analytical study, the flow is generated by a pressure gradient which varies sinusoidally in time. The results showed that for some pulsation conditions ($\alpha \geq 12.9$), a new pair of cells appears and adds two Dean cells observed in a steady flow. Figure I-8 shows this structure, known as the Lyne structure, which is more complex compared to that of Dean

cells (Figure I-6). A little later, (Zalosh., 1973) showed the same structure using a different analytical approach.

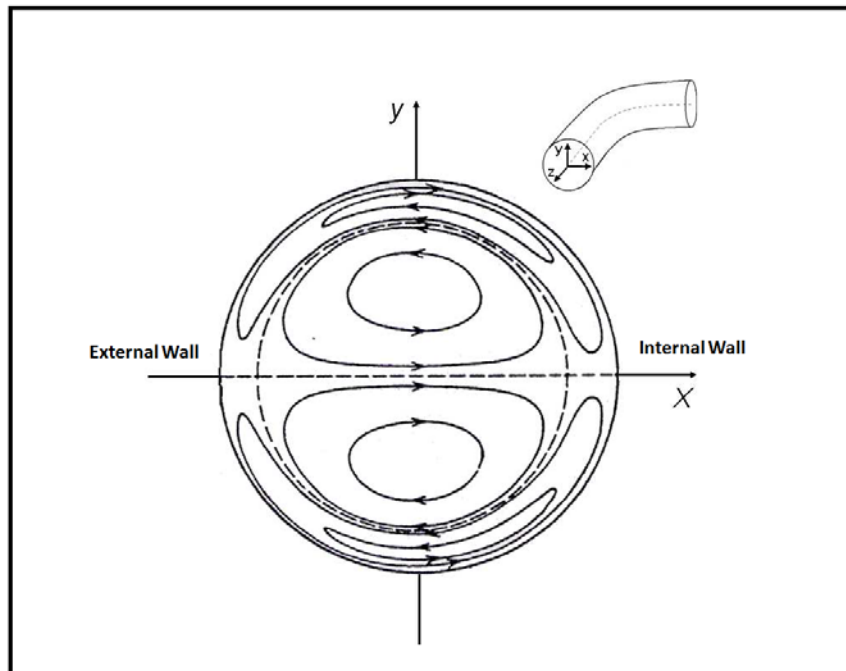


Figure I- 8. Lyne's secondary flow structure.

Based on the (Lyne, 1970) analysis, for Womersley parameter (α) less than 12.9 the secondary flow is always composed of two Dean cells, although this structure is slightly deformed for values close to 12.9. For $\alpha \geq 12.9$, the fluid near the outer wall slows the secondary flow. It follows a stagnation zone near the outer wall of the curved pipe. The pressure gradient becomes greater than the centrifugal force in the center of the pipe and at certain time periods, the fluid in the stagnation region and close to the outer wall, starts a rotational movement. Then there is the addition of a vortices pair in the nearby region of the outer wall, which amplifies and pushes the previous two vortex centers the section. The secondary flow is thus composed of four counter rotating vortices (Figure I-8). Most of the analytical studies (Lyne, 1970), (Zalosh., 1973), (Simon., 1977 and Siggers., 2008) were devoted to analyze a sinusoidal or pulsatile flow in a curve duct, using some assumptions such as: the flow is fully established, the curvature ratio is very small ($\theta \rightarrow 0$), and / or the symmetry conditions hypothesis with respect to median plane of the curve. These assumptions help to better understand the phenomena but simplified expressions obtained for the velocity field (after applying assumptions) are sometimes far from what happens in reality. For example in our study, 90° curve is considered the basic element that builds the mixer structure and according to (Swanson., 1993) and (Timité., 2005), a 90° angle is not sufficient so that

the flow is established at the outlet of the bend. Therefore we cannot rely only on existing analytical studies. This remark is also valid in relation to numerical studies. Even if the imposed conditions in the numerical calculations [(Lin., 1980), (Takami., 1984), (Chang, 1985, Hamakiotes., 1990, Tada., 1996), (Timité., 2005), (Siggers., 2008)] are less simplified compared to analytical studies, these numerical studies often involve flow completely established at the outlet of the curve.

To validate analytical and numerical studies on the behavior of a pulsating flow in a curved pipe, and also to have a more reliable base to discuss results, several experimental works were carried out. Most measurements are limited to weak axial flow velocity in the center plane of curvature and the secondary flow measurements are often made to observe and classify the change in the structure of the secondary flow [(Mullin., 1980), (Talbot., 1983), (Swanson., 1993), (Timité., 2005), (Sumida, 2007), (Timité., 2009)]. In all these experimental studies, there are no reliable measurements of velocity vectors of the secondary flow. One reason for this lack may be due to problem of light refraction that occurs through curve walls.

(Lyne, 1970) who initiated the analytical study on this subject, has also conducted an experiment to validate his analytical work. However, because of the small thickness of Stokes layer, he was able to detect the movements of fluid in the secondary flow only within the central region of the pipe. The experimental study of (Munson, 1975) on a flow generated by an oscillating pressure gradient in a curved pipe was performed by recording the time which had a floating tracer initially located at the center of the tube to travel a known distance. (Munson, 1975) had decreased (without totally eliminated) the optical distortion caused by the curvature of the walls by putting the curved pipe in a Plexiglas box filled with a fluid. The results of his work for $7 \leq \alpha \leq 32$ have validated the analysis of (Lyne, 1970). (Bertelsen, 1975) used the same technique to reduce the optical distortion and the measured displacement of the aluminum particles to calculate the radial velocity along the diameter of the section of the curved pipe. The result is another confirmation of the analytical study of (Lyne, 1970). (Sumida., 1989) observed the different structures of the secondary flow using the method of solid-tracer: the nylon spherical particles are illuminated by a light plane emitted by a stroboscope, synchronized with the piston movement which produces the oscillation in the flow. Figure I-9 shows schematically the experimental setup of (Sumida., 1989).

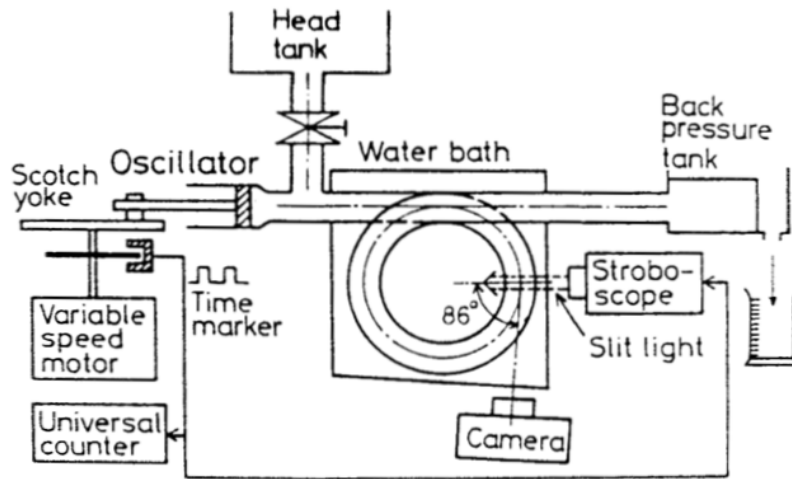


Figure I- 9. Experimental setup of Sumida et al.(1989).

At each emission of the light plane, a picture was taken of the particles which were illuminated during a time long enough and thus the trajectories and velocities of the particles were determined from each photograph at a given time of the oscillation period. A digitizer and a computer were used for calculations of velocity and image saving was done for four main phases of the oscillation cycle. The experimental work of (Sumida M., 1989) is among the most precise measurements found in literature but there were still some inaccuracies. First, the camera was not perfectly perpendicular to the section of the curved pipe. The angle between the camera and the pipe section is equal to 86° in this work. Second, the optical distortion caused by the walls curvature of the pipe was reduced by placing the pipe bend in a box filled with water, but the deformation was not completely removed.

Measurements carried out by (Sumida., 1989) were made for different conditions of pulsatile flow (steady + sinusoidal) completely developed at the outlet of the curve whose opening angle is $\Phi = 450^\circ$. Two steady Dean numbers $Dn_{st} = 90$ and $Dn_{st} = 200$, with two velocity amplitude ratios, $\beta = 0.5$ and $\beta = 1$, and a Womersley parameter varied in the range $\alpha = 5.5$ to $\alpha = 18$ were selected as the pulsation conditions. Finally, three properties have been observed for the secondary flow structure (Figure I-10).

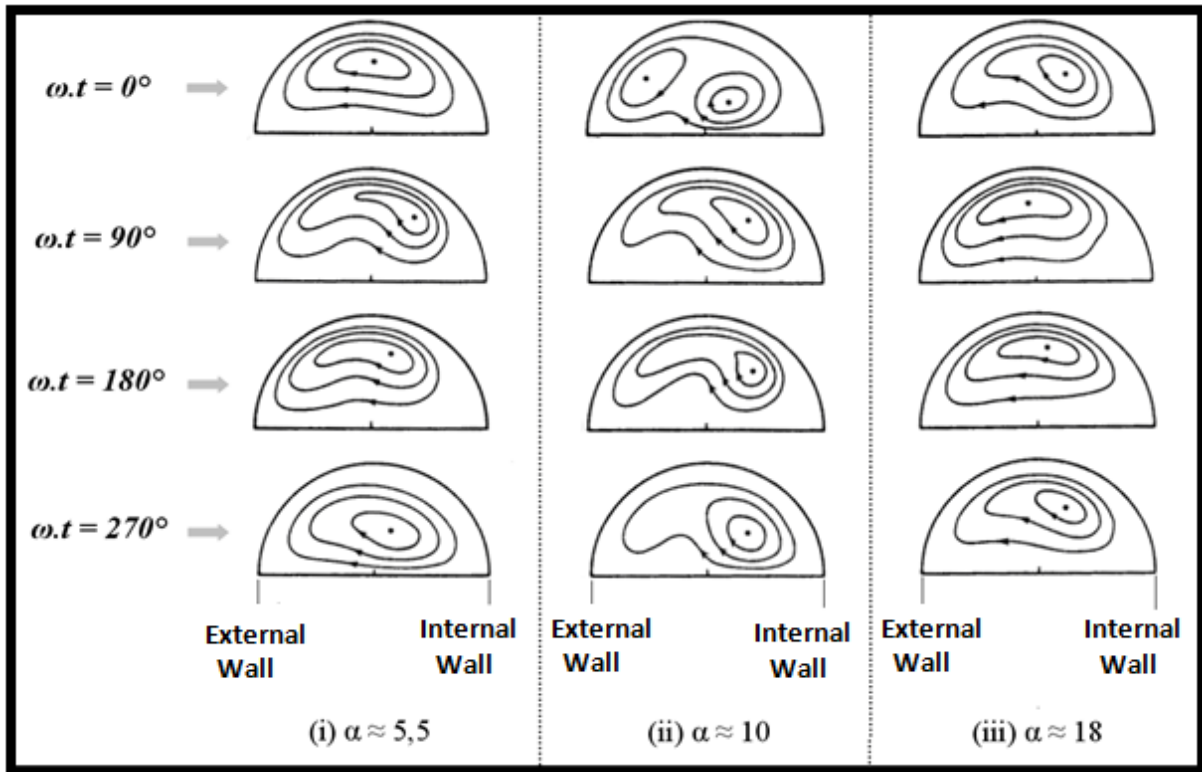


Figure I- 10. Classification of flow by Sumida et al.(1989).

- For a small Womersley parameter value ($\alpha \approx 5.5$), except for a part of the oscillation cycle, the secondary flow structure is similar to that of observed in a steady flow.
- For a medium Womersley parameter values ($\alpha \approx 10$), the secondary flow has a complex structure.
- For large values of the Womersley parameter ($\alpha \approx 18$), the secondary flow structure varies a little during the different phases of the cycle.

The same experimental setup (Figure I-8) and the same measurement technique were used by Sudo et al. (1992) but for a completely developed purely sinusoidal flow. The different structures of the secondary flow observed in this study shown in Figure I-11 were classified into five categories:

- Type I: Dean circulation
- Type II: Dean deformed circulation
- Type III: Intermediate circulation between the Dean structure and the Lyne structure
- Type IV: Lyne deformed circulation
- Type V: Lyne circulation

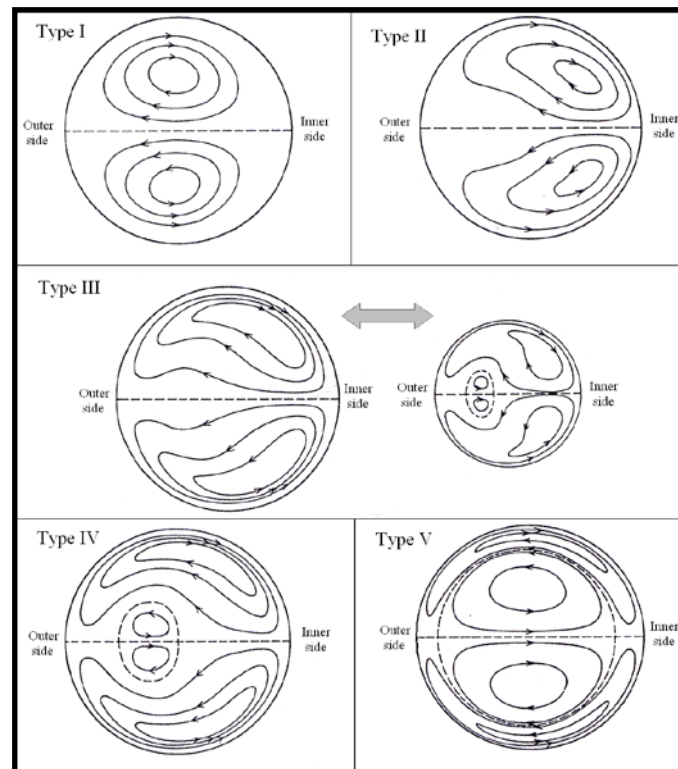


Figure I- 11. Classification of secondary flow patterns by Sudo et al. (1992).

Comparing the different structures in Figures I-10 and I-11 with that of Figure I-6, the secondary flow structures in a time-dependent flow, pulsatile or sinusoidal, compared to those of a steady flow appears clearly.

This complexity is one of the motivation that supports the idea of this work, focused on a developed pulsatile flow in a curve whose opening angle is $\Phi=90^\circ$.

I.3.3. Equations for alternating pulsatile Dean flow

The term "alternating pulsatile Dean flow" from now is used in the present study for an incompressible pulsatile laminar flow flowing through curved pipes installed in a series of alternated curvature planes, in order to create a spatially chaotic geometry. As the basic geometry for a Dean alternating pulsatile flow in the study is a 90° curved pipe, the flow equations of a unsteady flow through a curved pipe are presented here.

Consider an incompressible flow through a curved pipe and assume that the velocity vector at each position of the flow is $\vec{U}(t)$. If t, \vec{g}, ρ, P, ν respectively represent the time, gravity, density, pressure and the kinematic viscosity, the Navier-Stokes equations for the general case are presented as:

- Continuity equation:

$$\frac{\partial \rho}{\partial t} + \text{div}(\vec{U}) = 0 \quad (\text{I- 21})$$

- Momentum equation:

$$\frac{\partial \vec{U}}{\partial t} + (\vec{U} \cdot \vec{\nabla}) \vec{U} = \vec{g} - \frac{1}{\rho} \vec{\nabla}(P) + \nu \nabla^2(\vec{U}) \quad (\text{I- 22})$$

Writing these equations in dimensionless form requires the following non dimensional variables:

$$\underline{t} = a \cdot t, \quad \underline{\vec{\nabla}} = r_o \cdot \vec{\nabla}, \quad \underline{\vec{U}} = \frac{\vec{U}}{U_{av}}, \quad \underline{P} = \frac{P}{\rho \cdot U_{av}^2} \quad (\text{I- 23})$$

where a is a parameter of dimension s^{-1} and U_{av} is the average velocity in the duct. By putting the equations (I-23) in equation (I-22), multiplying by $\frac{r_o^2}{\nu U_{av}}$, and if the gravity is negligible:

$$\frac{r_o^2}{\nu U_{av}} \frac{\partial \underline{\vec{U}}}{\partial \underline{t}} + \frac{U_{av} \cdot r_o}{\nu} (\underline{\vec{U}} \cdot \underline{\vec{\nabla}}) \underline{\vec{U}} = - \frac{U_{av} \cdot r_o}{\nu} \underline{\vec{\nabla}}(\underline{P}) + \underline{\nabla}^2(\underline{\vec{U}}) \quad (\text{I- 24})$$

or

$$\frac{r_o^2}{\nu U_{av}} \frac{\partial \underline{\vec{U}}}{\partial \underline{t}} + \frac{R_e}{2} (\underline{\vec{U}} \cdot \underline{\vec{\nabla}}) \underline{\vec{U}} = - \frac{R_e}{2} \underline{\vec{\nabla}}(\underline{P}) + \underline{\nabla}^2(\underline{\vec{U}}) \quad (\text{I- 25})$$

For a pulsating flow, the parameter a may take the value of the angular velocity of the velocity sinusoidal component, ω , therefore the momentum equation (I-25) becomes:

$$\alpha^2 \frac{\partial \underline{\vec{U}}}{\partial \underline{t}} + \frac{R_{e, \text{st}}}{2} (\underline{\vec{U}} \cdot \underline{\vec{\nabla}}) \underline{\vec{U}} = - \frac{R_{e, \text{st}}}{2} \underline{\vec{\nabla}}(\underline{P}) + \underline{\nabla}^2(\underline{\vec{U}}) \quad (\text{I- 26})$$

where α is the Womersley parameter, defined in previous section.

I.3.4. Quantitative description of mixing

Quality of mixing of a given mixture can be developed by the comparison of the state of the mixture to the most complete mixing state achievable. The complete mixing corresponds to the statistical randomness of the ultimate properties of the ingredients being mixed which would follow the binomial distribution. Different parameters of mixing quantification are discussed.

1) Mean concentration

If one makes N measurements of concentration, C_i of the components i , the mean concentration \bar{C} is calculated according to

$$\bar{C} = \frac{1}{N} \sum_{i=1}^N C_i \quad (\text{I- 27})$$

where \bar{C} should not differ significantly from the overall concentration of the component, the difference between \bar{C} and overall concentration of the component decreases as the number of characterized samples N is increased.

2) Variance

A basic measurement of homogeneity of a mixture is the extent to which the concentration values at various regions of the volume of the mixture differs from the mean concentration. The variance σ^2 arising from the individual concentration C_i measurements provides such an index to quantitatively assess the degree of mixing. The variance σ^2 is expressed as

$$\sigma^2 = \frac{1}{N} \sum_{i=1}^N (C_i - \bar{C})^2 \quad (\text{I- 28})$$

A small variance implies that most of the samples yield concentration C_i values are close to the mean \bar{C} of all samples, thus suggesting a homogeneous system.

3) Standard deviation

The deviation of the sample measurements from the mean \bar{C} is given by the standard deviation:

$$\sigma = \sqrt{\sigma^2} \quad (\text{I- 29})$$

This is the square root of the variance, and is in the same unit as the concentration data.

4) Coefficient of variance

When the means of two concentration data sets differ greatly, a measure of relative variability is defined by coefficient of variance C_oV .

$$C_oV = \frac{\sigma}{\bar{C}} \quad (\text{I-30})$$

5) Maximum variance

$$\sigma_{max}^2 = \bar{C}(1 - \bar{C}) \quad (\text{I-31})$$

The maximum variance occurs if the components are completely segregated.

6) Intensity of segregation

If the variance is normalized to its maximum value, the resulting parameter is called the intensity of segregation. I_{seg} , given by

$$I_{seg} = \frac{\sigma^2}{\sigma_{max}^2} \quad (\text{I- 32})$$

The higher the I_{seg} value, the less homogeneity in the mixing, then the lowest I_{seg} value corresponds to better mixing.

7) Intensity of mixing

One can define intensity of mixing I_{mix} as:

$$I_{mix} = 1 - \frac{\sigma^2}{\sigma_{max}^2} \quad (\text{I-33})$$

Intensity of mixing values range from zero, for completely segregated to one for ideally homogeneous system.

Previous studies on mixing enhancement by alternating pulsatile Dean flow

To our knowledge, the PhD of (Timité, 2005) and (Jarrahi, 2010) are so far the only experimental studies on the alternating pulsatile Dean flow as an approach to mixing enhancement. (Timité, 2005) developed an experimental setup composed of a straight pipe and series of six consecutive 90° twisted pipes. Those pipes were attached in such a way that the orientation of one bend is changed to another. The pulsations were generated by a Scotch yoke mechanism. Measurements of axial velocity vectors along two axes x and y (see axes in Figure I-8) were carried out by laser Doppler velocimetry (LDV) and qualitative visualization of the structures of the secondary flow were carried out by the laser induced fluorescence (LIF) method. Along with these measurements (Timité, 2005) also did visualizations experiments and numerical calculations using commercial software Fluent for the same flow. His study was assigned to study the mixing at the outlet of each curved pipe for different pulsation conditions. (Timité, 2005) conducted the experiments for $300 \leq Re_{st} \leq 1300$, a frequency parameter/Womersley parameter α ($1 \leq \alpha \leq 20$) and two velocity amplitude ratio β ($\beta = 1$ and 2).

Main results of Timité (2005)

I.5.1. At the exit of the first 90° curved pipe

For $Re_{st} \leq 600$, $\alpha < 17$ and $\beta = 1$, the secondary flow at the exit of first bend is composed of two counter rotating cells during a pulsation cycle. Return movement is observed in regions close to the inner wall during the deceleration phases ($90^\circ < \omega.t < 270^\circ$), which intensify with increasing α . When $\alpha > 17$ (for $Re_{st} \leq 600$, and $\beta = 1$) instability of low intensity appears in the secondary flow and near outer wall at the end of the deceleration phase ($\omega.t = 270^\circ$). Figure (I-12) shows the different structures of the secondary flow observed by Timité (2005) at the exit of first bend for $\beta = 1$.

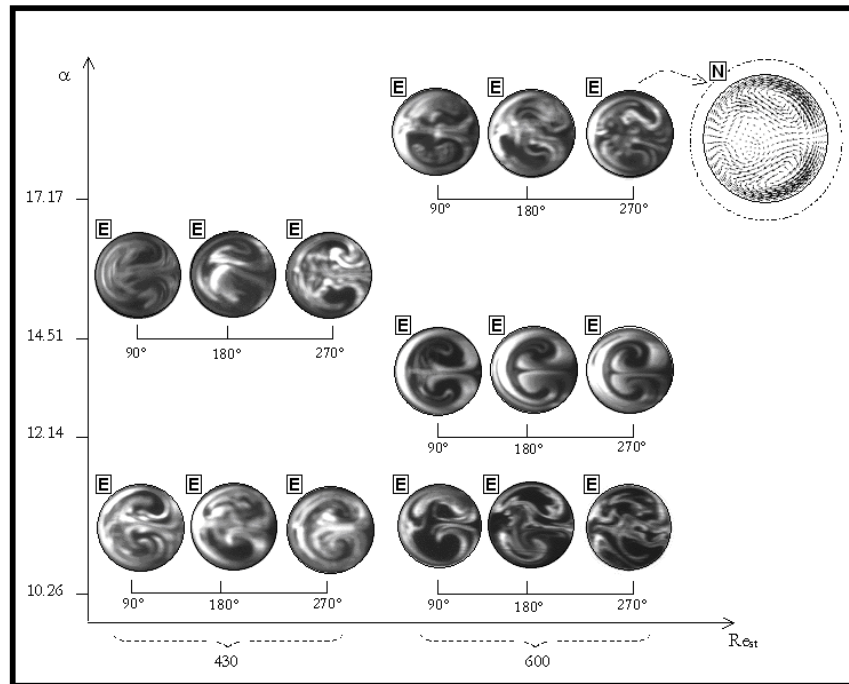


Figure I- 12. Different secondary flow structures observed at the exit of first curved pipe at different phase angles ($\omega.t$) for $\beta=1$ (Timité et al. 2009) (N : numerical and E : experimental).

For $Re_{st}=430$, $\beta= 2$ and $\alpha=10.26$ a phenomenon due to siphon effect is observed at center of the section during deceleration phases ($90^\circ < \omega.t < 270^\circ$) and especially at $\omega.t= 270^\circ$. By increasing the steady Reynolds number to 600 (for $\beta=2$ and $\alpha=10.26$), Lyne instability appears at the mid-deceleration ($\omega.t = 180^\circ$). The different structures observed in the secondary flow at the exit of first bend at $\beta=2$ are shown in Figure I-13.

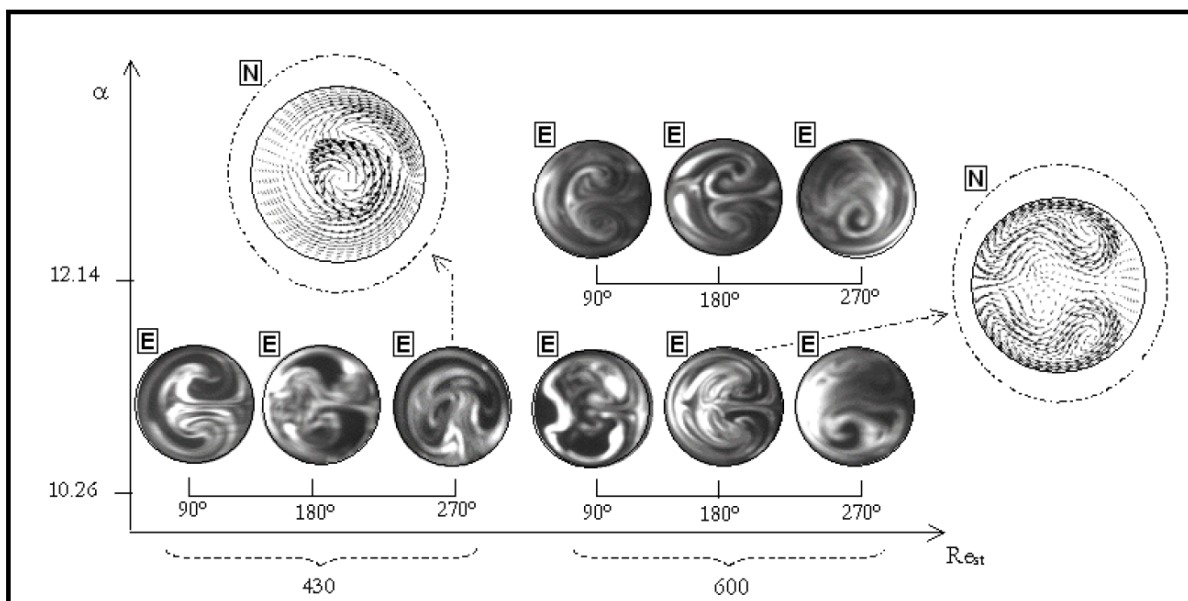


Figure I- 13. Different secondary flow structures observed at the exit of first curved pipe at different phase angles ($\omega.t$) for $\beta=2$ (Timité et al. 2009) (N : numerical and E : experimental).

I.5.2. At the exit of the second to sixth 90° curved pipes

At the exit of second to sixth 90° curved pipes, the secondary flow cells are reorganized in the direction of the centrifugal force of the bend in most of the cases, the structure of the secondary flow consists of two counter rotating cells. Specially when $\beta=2$, configurations of the secondary flow observed at the exit of second to sixth 90° curved pipes differ from that of the first bend. For example, four cells (Lyne instability) were observed at the exit of second, third and sixth 90° curved pipes while in the first bend the two cells remain as two. The siphon phenomenon observed in the first curve was also appeared in other curves. Figure I-14 shows the experimental observations and numerical calculations for the third, fourth and sixth curve when $Re_{st}=600$, $\beta=2$, $\alpha=10.26$ (Timité, 2005).

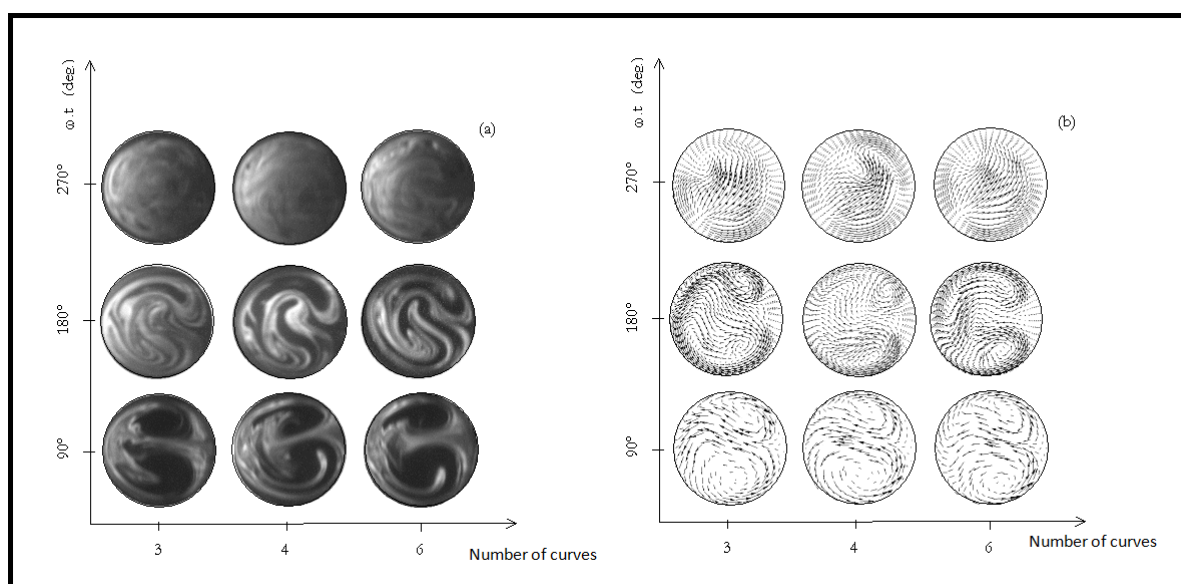


Figure I-14. Different secondary flow structures observed at the exit of 3rd, 4th and 6th curved pipe at different phase angles ($\omega.t$) for $Re_{st}=600$, $\beta=2$, $\alpha=10.26$ (N : numerical and E : experimental), a) LIF visualization and b) Numerical results by FLUENT (Timité et al. 2009).

I.5.3. Rate of elongation

Stretching or elongation is one of the most influential mechanisms for the mixing phenomenon. (Timité, 2005) studied the elongation rate of colored dye by following its spatial evolution. By image analysis for two injection tests, he determined the apparent area corresponding to colored spot at the exit of each curve. Figure I-15 provides, for the injection point ($x/r_o=0$, $y/r_o=0.7$), the evolution of the normalized area obtained as the function of the

longitudinal normalized abscissa. The area is normalized by dividing the apparent surface area of the colored spot by the total area of the image. The longitudinal abscissa is the normalized ratio between the position of the display section and the total length of the pipe. From Figure I-15 it can be concluded that there is no significant spread of dye in the steady flow ($Re_{st} = 430$), while the evolution of the dye spread of the colored spot in pulsatile flow is observed to be exponential for $Re_{st}=\{430, \beta=1 \text{ and } 2, \alpha=10.26\}$. (Timité, 2005) proposed to use the exponents of exponential curves obtained by this method as an equivalent of Lyapunov exponents (see section I.1.4.1). This allows us to compare different chaos levels reacted by different pulsation conditions and the effect of different positions of dye injections.

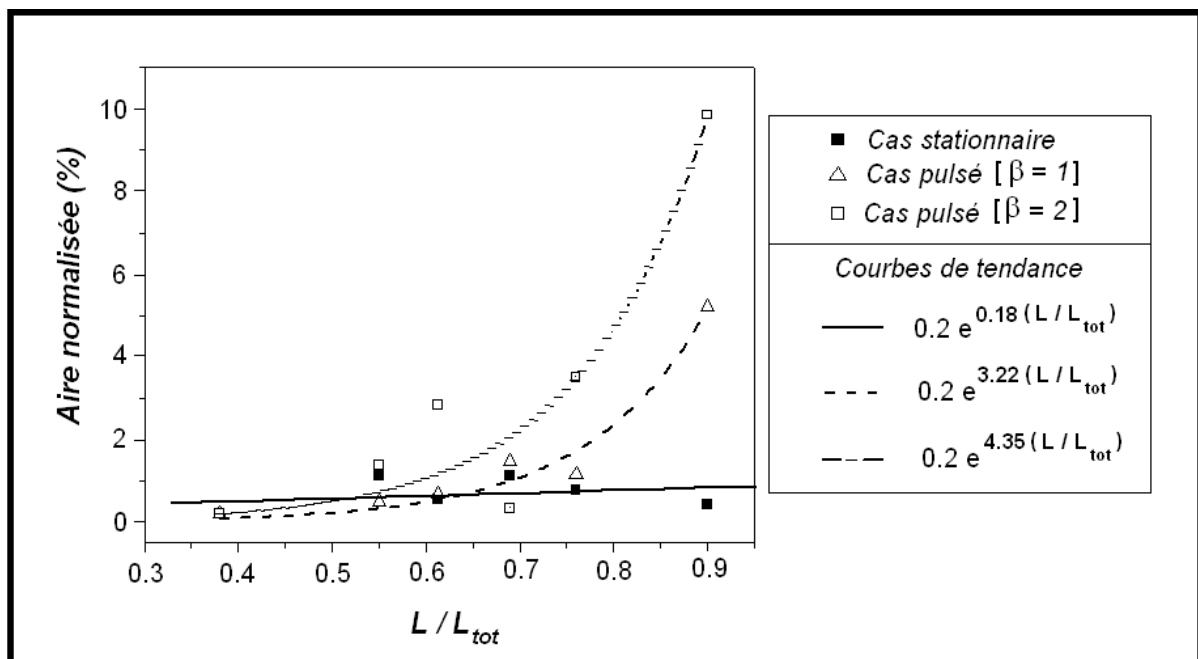


Figure I- 15. Normalized air evolution as the function of longitudinal normalized abscise for the point of injection ($x/r_0=0, y/r_0 =0.7$) with $Re_{st}=430, \beta=0,1 \text{ and } 2, \alpha = 10,26$ [Timité (2005)].

(Timité et al., 2011) carried out an experimental and numerical study of pulsatile alternating Dean Flow showing an important modification of the secondary flow structure due to the pulsation. They obtained velocity profiles and flow visualization images both numerically and experimentally for each bend and for a large range of characteristic parameters. They observed that for certain control parameters, the secondary flow becomes more complex, in some cases accompanied by Lyne instability or swirling structures due to the periodic movement. Therefore they concluded that the modification of the secondary flow cells, coupled with the destruction and rebuilding of the cells at each bend, generates a more

chaotic flow. The regular zones that disappear with increasing bend number are reduced with increasing pulsation parameters.

The mixing efficiency increases linearly with the Reynolds number. In the pulsated configuration, the mixing degree is represented in figure I-16 at $\omega.t = 360^\circ$, i.e. at the end of period T. The mixing degree in the configuration where the velocity-amplitude ratio β is equal to 2 reaches rather quickly (at the exit of the third bend) the limiting value characterizing perfect mixing. However, when the velocity amplitude ratio β is equal to 1, the mixing degree reaches the value 1 after the fifth bend. Comparison of the results obtained in the steady and pulsated cases show the influence of pulsation. Indeed, when the velocity-amplitudes ratio is unity ($\beta = 1$), mixing is better in the boundary layer near the wall. On the other hand, when the velocity-amplitude ratio is doubled ($\beta = 2$), the effective mixing zones increase by occupying a larger surface. The intensification of the reverse flow in the tube center induced by the increase of the velocity-amplitude ratio produces a reverse movement in the trajectories upstream of the first bend. Indeed, the fluid particles located in the first bend close to the inlet can be sucked up in the straight tube during the deceleration phase. In summary, the experimental and numerical results yielded certain information on tracer transport. The first type of information relates to the stretching and folding mechanisms responsible for chaotic mixing. Two initially close trajectories diverge exponentially due to bend reorientation and the effect of pulsation. Flow visualizations shows that the stretched and folded structures observed depend on initial tracer position and that the pulsation amplifies the stretching rate, thus making the appearance of small islands less likely. The regular zones (small islands) that tend to disappear as the number of bends increases are reduced with pulsation amplitude. Analysis of the dye stretching on the one hand showed that the pulsating character of the flow leads to the production of an overall chaotic flow and on the other hand suggested that the flow with less bends is more chaotic and can thus generate a better mixing.

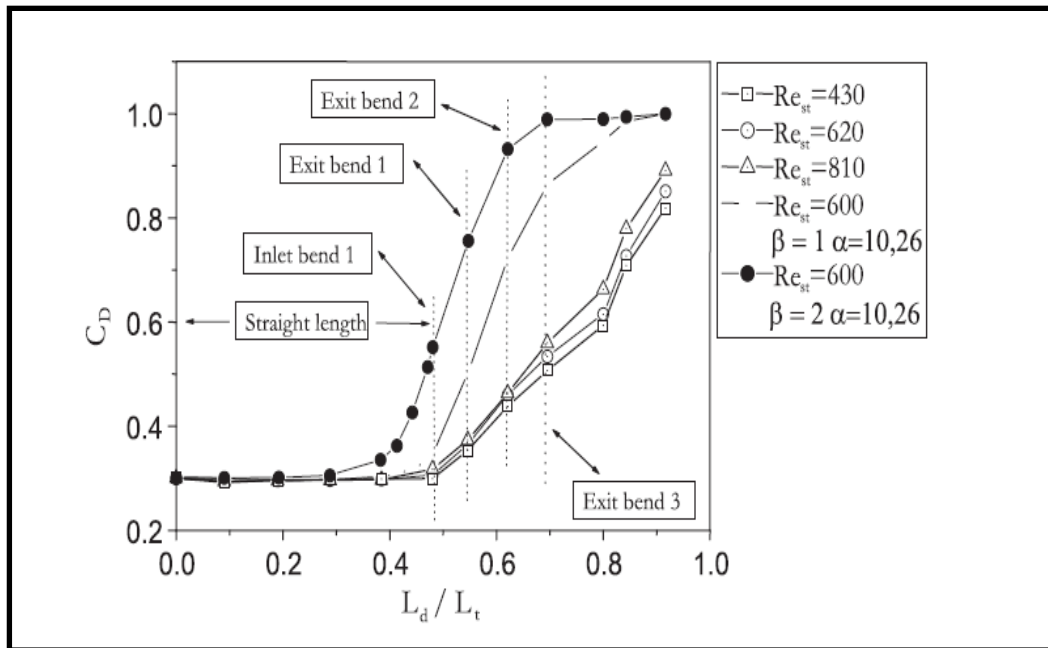


Figure I- 16. Evolution of mixing degree versus normalized longitudinal distance for the different cases (Timité et al., 2011).

Main results of Jarrahi (2010)

(Jarrahi, 2010) used the experimental setup developed by (Timité, 2005). He did measurements of axial velocity vectors along two axes x and y by particle image velocimetry (PIV) technique in a developed laminar pulsating flow through a circular series of curved pipes. He studied the different secondary flow patterns formed during an oscillation period due to competition among the centrifugal, inertial and viscous forces. These different secondary-flow structures lead to different transverse-mixing schemes in the flow. The transverse mixing enhancement was investigated by imposing different pulsating conditions (Dean number, velocity ratio and frequency parameter). Further more (Jarrahi, 2010) proposed favorable pulsating conditions for mixing.

To obviate light-diffraction effects during PIV measurements, (Jarrahi, 2010) designed and fabricated a T-shaped structure which was installed downstream of the curved pipe. He performed the experiments for the Reynolds numbers ranging between $420 \leq Re_{st} \leq 1000$ (Dean numbers $126.6 \leq Dn \leq 301.5$), velocity component ratios $1 \leq (\beta = U_{max,osc} / U_{m,st}) \leq 4$ and Womersley frequency parameters $8.37 < (\alpha = r_0(\omega/\nu)^{0.5}) < 24.5$. In order to quantify the mixing (Jarrahi, 2010) analyzed the variations in axial vorticity ξ and transverse strain rate ϵ .

He discussed the effects of each parameter (Re_{st} , β and α) on transverse mixing by comparing the dimensionless vorticities ($|\zeta_P|/|\zeta_S|$) and dimensionless transverse strain rates ($|\varepsilon_P|/|\varepsilon_S|$) during a complete oscillation period.

I.6. 1. At the exit of a 90° curved pipe

The PIV measurements concern the velocity fields of the secondary flow in *developing* pulsatile flows through a curved pipe. PIV measurements of the secondary flow for $Re = 600$, $\beta = 2$ and $\alpha = 10.26$ are shown in Figure I-17 as a representative example. Different pulsating conditions yield different secondary flow patterns. To describe the variations in observed secondary flow structures, the different pulsating conditions that yield similar patterns (in the same phase position) are grouped together. To this end, four main phase positions in a period of pulsation are selected: $\omega.t = 0^\circ$, 90° , 180° and 270° . The secondary flow structures observed in these four positions are shown in Figures I-18, I-19, I-20 and I-21.

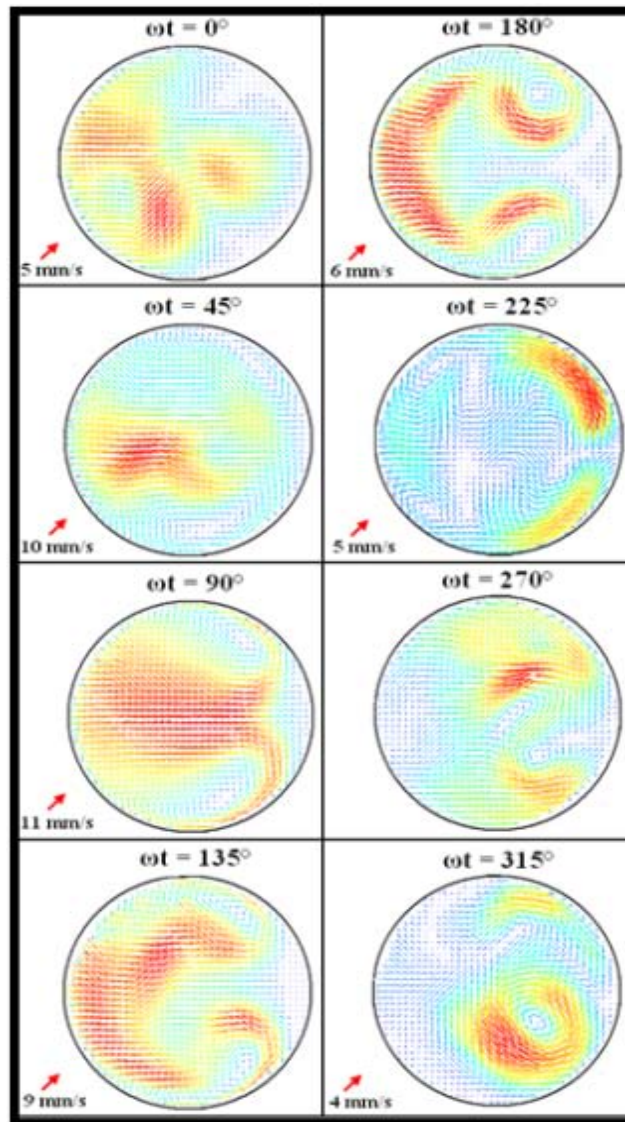


Figure I- 17. Secondary flow variation in an oscillation period, $Re=600$, $\beta=2$, $\alpha=10.26$. Velocity values at lower left indicate the highest velocities, shown as red vectors in the velocity field, for each case. The smallest velocities are the blue vectors, between 0 mm/s and 1 mm/s , (Jarrahi et al., 2010).

I.6. 1.1. Phase angle $\omega t = 0^\circ$

Figure I-18 shows secondary flow structures for different pulsating conditions, at the lowest phase position, $\omega.t = 0^\circ$, where the pulsatile velocity $U_p(t)$ at the entrance of the curved pipe is equal to the mean steady flow velocity, U_{mS} . Jarrahi et al., (2009) categorized the secondary flow structures in following way:

- For $\alpha \leq 12.14$, $420 \leq Re_{st} \leq 1000$ and $1 \leq \beta \leq 3$, the fluid particles move only from the inner side of the tube cross section to the outer side under the effect of centrifugal force; therefore no cells appear in the secondary flow structure.
- For $12.14 < \alpha < 17.77$, they observed three flow patterns. When $\beta = 2$, the role of the mean Reynolds number in the secondary flow structure becomes dominant and the observed structures differ for $Re_{st}=420$ and $Re_{st}=600$ at the same Womersley number ($\alpha = 14.51$). For $Re_{st} = 420$, the pattern consists of two counter-rotating cells at the inner side of the section: the cell closer to the upper wall rotates clockwise and that near to the lower wall rotates counter-clockwise. For $Re_{st} = 600$, a more complex structure consisting of four cells appears. Two asymmetrical counter-rotating cells move from the inner side of the curved tube wall to the outer side and two new counter-rotating cells at the inner side begin to form.
- For $\alpha \geq 17.77$, the secondary flow structures have the same general form for all values of the mean Reynolds number and velocity component ratio, i.e. for $Re_{st} \leq 1000$ and $1 \leq \beta \leq 4$. This means that in flows with high Womersley frequency numbers at $\omega.t = 0^\circ$, the secondary flow structure does not depend on the values of Re_{st} and β , and therefore the inertial force due to the oscillation is the dominant factor.

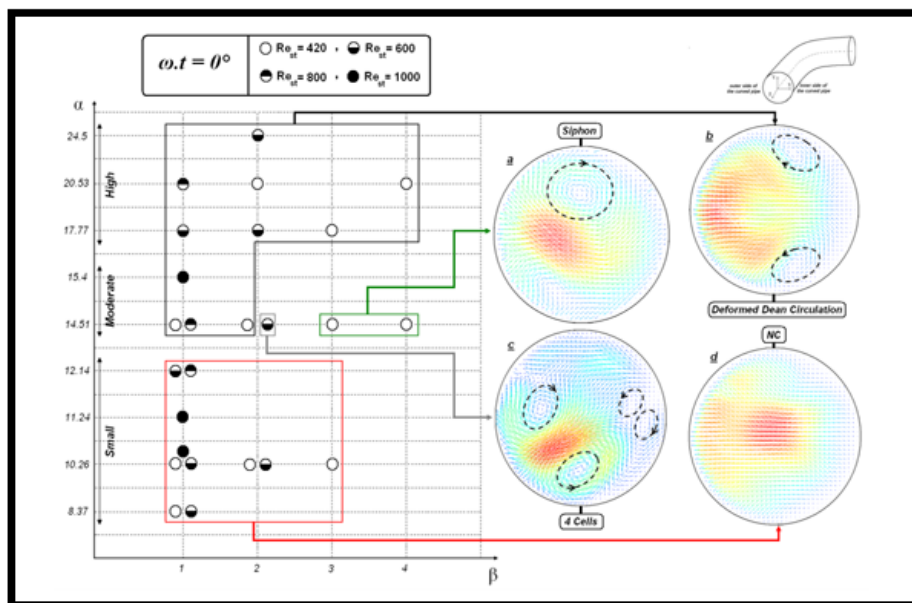


Figure I- 18. Secondary flow structures at $\omega.t=0^\circ$ for different pulsating conditions $\{420 \leq Re_{st} \leq 1000, 1 \leq \beta \leq 4 \text{ and } 8.37 \leq \alpha \leq 24.5\}$.

I.6. 1.2. Phase angle $\omega t = 90^\circ$

Figure I-19 shows secondary flow structures at $\omega.t = 90^\circ$ for different pulsating conditions. When the phase position is $\omega.t = 90^\circ$, the pulsatile velocity at the entrance of the curved pipe reaches its highest value, i.e. $(1 + \beta)U_{ms}$ and the flow rate through the curved pipe is maximum. At this phase position, where the deceleration zone of the oscillating velocity curve starts.

- For $\alpha < 17.77$, the secondary flow pattern does not depend on the mean Reynolds number and velocity component ratio. In this interval of Womersley numbers, for the range $420 \leq Re_{st} \leq 1000$ and $1 \leq \beta \leq 4$, the secondary flow structure is similar to a deformed Dean circulation. The laser-induced fluorescence (LIF) flow visualizations of Timité et al. (2009) show the same structure at this phase position ($\omega.t = 90^\circ$) for four pulsating conditions: $\{Re_{st} = 600, \beta = 1, \alpha = 10.26\}$, $\{Re_{st} = 600, \beta = 1, \alpha = 12.14\}$, $\{Re_{st} = 430, \beta = 2, \alpha = 10.26\}$ and $\{Re_{st} = 600, \beta = 2, \alpha = 12.14\}$. This deformed Dean roll pattern is similar to that observed at phase position $\omega.t = 0^\circ$ for high Womersley numbers ($\alpha \geq 17.77$) and, in some conditions, for moderate values ($12.14 < \alpha < 17.77$).
- When $\alpha = 17.77$ the secondary flow structure depends also on mean Reynolds number and velocity component ratio. When $\beta = 1$ or 2 (for $Re_{st} = 600$), the observed pattern is still a deformed Dean roll, but when the velocity component ratio is increased to $\beta = 3$ (for $Re_{st} = 420$) the cells disappear and a no-cell (NC) structure appears. As the Womersley number increases further ($\alpha > 17.77$), the secondary flow structure again becomes independent of the values of Re_{st} and β , so that the no-cell structure is the only structure found for all conditions in this range of α .

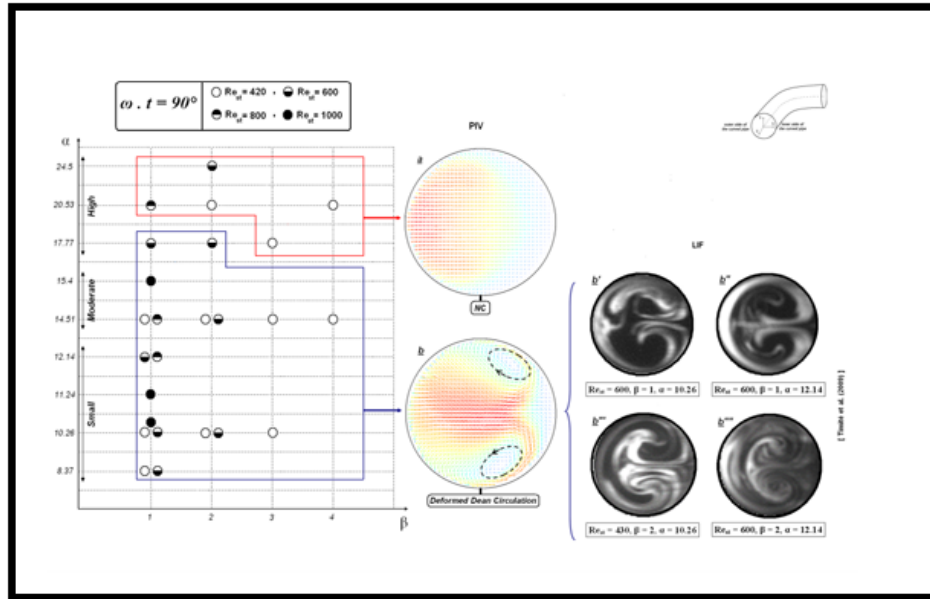


Figure I- 19. Secondary flow structures at $\omega.t=90^\circ$ for different pulsating conditions $\{420 \leq Re_{st} \leq 1000, 1 \leq \beta \leq 4, 8.37 \leq \alpha \leq 24.5\}$.

I.6. 1.3. Phase angle $\omega t = 180^\circ$

Figure I-20 shows secondary flow structures at $\omega.t = 180^\circ$ for different pulsating conditions. Similar to the phase position $\omega.t = 0^\circ$, the pulsatile velocity becomes equal to the mean steady flow velocity, U_{mS} , at $\omega.t = 180^\circ$; but, the observed secondary flow structures are not completely similar to that for $\omega.t = 0^\circ$. The fundamental difference between these two phase positions is that the flow is accelerating in $\omega.t = 0^\circ$, while it is decelerating in $\omega.t = 180^\circ$. At this phase position ($\omega.t = 180^\circ$), two patterns have been observed in the middle of deceleration zone in oscillating velocity curve. Both are composed of two counter-rotating cells but their structures are different.

- For $\alpha \leq 12.14$, the secondary flow structure is a recirculation flow intermediate between Dean and Lyne structures for all values of $420 \leq Re_{st} \leq 1000$ and $1 \leq \beta \leq 4$. The LIF visualization and also numerical simulations of Timité et al. (2009) confirm the formation of this pattern, called flow circulation intermediate between Dean and Lyne, when the pulsating condition is $\{Re_{st} = 600, \beta = 2, \alpha = 10.26 \text{ and } \omega.t = 180^\circ\}$.
- For $12.14 < \alpha < 17.77$ or $\alpha = 17.77$, the values of Re_{st} and β affect the secondary flow structure as well. At the $\beta=1$, for $Re_{st} \leq 600$, a deformed Dean circulation and for $Re_{st} > 600$ a recirculating flow intermediate between Dean and Lyne structures was

reported. When $\beta = 2$, the observed structure for $Re_{st} \leq 600$ transforms from a deformed Dean recirculation to a recirculation intermediate between Dean and Lyne structures.

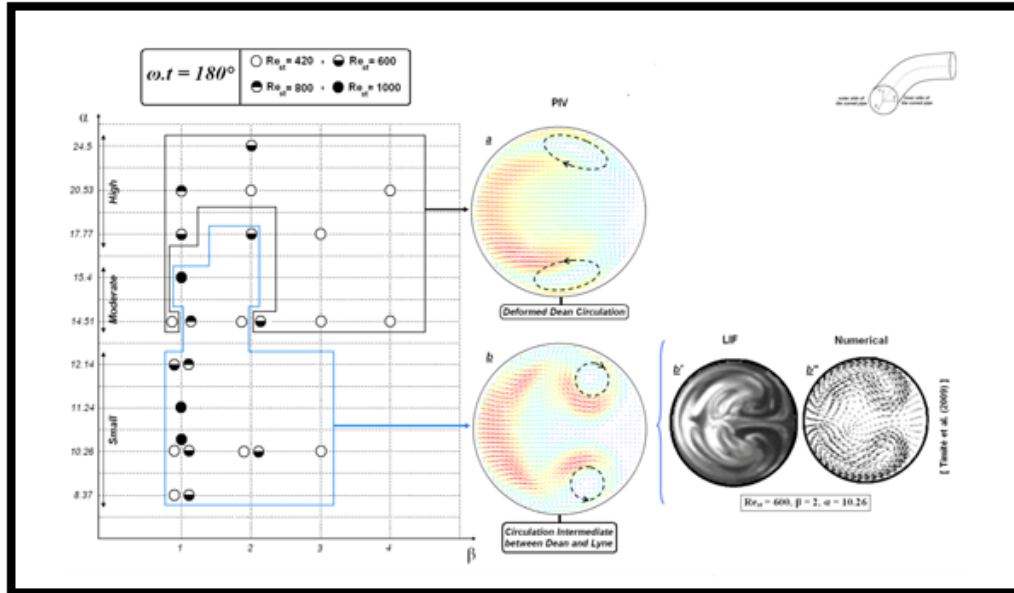


Figure I-20. Secondary flow structures at $\omega.t=180^\circ$ for different pulsating conditions $\{420 \leq Re_{st} \leq 1000, 1 \leq \beta \leq 4 \text{ and } 8.37 \leq \alpha \leq 24.5\}$.

I.6. 1.4. Phase angle $\omega t=270^\circ$

Figure I-21 shows secondary flow structures at $\omega.t=270^\circ$ for different pulsating conditions. This phase position is the beginning of acceleration zone and the end of the deceleration zone in the oscillating velocity curve. Here the flow rate through the pipe is minimum. The variety of the observed structures at $\omega.t = 270^\circ$ is much greater than what has been distinguished for previous phase positions. The sharp variations in secondary flow structure with strong dependence on Re_{st} , β and α at this phase position.

For $\beta=1$, where the axial flow is at least partially positive (forward), most pulsating conditions, $\alpha = 8.37$ and $\alpha \geq 17.77$, result in a deformed Dean recirculation flow, with smaller velocity vectors toward the outer wall in the central region compared to the same structure at previous phase positions studied. Timité et al. (2009) have also shown experimentally by LIF visualization and numerically the formation of a deformed Dean recirculation flow when $\{Re_{st} = 600, \beta = 1, \alpha = 17.77 \text{ and } \omega.t = 270^\circ\}$. A more complex structure with four cells has also been observed at small Womersley numbers for $Re_{st} \geq 600$. In this type of structure, the

two counter-rotating cells of deformed Dean recirculation type move closer to each other around the horizontal symmetry line of the section and two other cells begin to appear near the outer wall. The rotation direction of the cells in the upper half of the section is counter-clockwise, opposite to that of the cells in the lower half. For $\alpha = 14.51$ an asymmetric pattern with three cells forms when $Re_{st} = 800$.

For $\beta = 2$, the wide variety and the strong sensitivity of the secondary flow patterns to pulsating conditions prevent a simple grouping of the flow patterns. When $\beta = 2$ at $\alpha > 17.77$ and when $\beta \geq 2$ at $\alpha = 14.51$, the secondary flow structure is mainly composed of two counter-rotating cells close to the outer wall. For $\{Re_{st} = 420, \beta = 2, \alpha = 14.51\}$, however, the more complex observed structure consists of four cells. When $\alpha < 17.77$ for $\beta = 2$, the cells disappear and the fluid particles move from the outer wall toward the inner wall, i.e., opposite to the direction of the centrifugal force. At this phase position ($\omega.t = 270^\circ$), the siphon pattern forms at $\beta = 2$ and $\alpha = 10.26$ than that observed at $\omega.t = 0^\circ$. The LIF visualizations and also numerical simulations of Timité et al. (2009) confirm the formation of this siphon structure for $\{Re_{st} = 430, \beta = 2, \alpha = 10.26$ and $\omega.t = 270^\circ\}$. It should be mentioned that the location and rotation direction of the cell in the siphon pattern are not the same at $\omega.t = 0^\circ$, where the main flow is positive (forward), and $\omega.t = 270^\circ$, where the main flow becomes negative (backward).

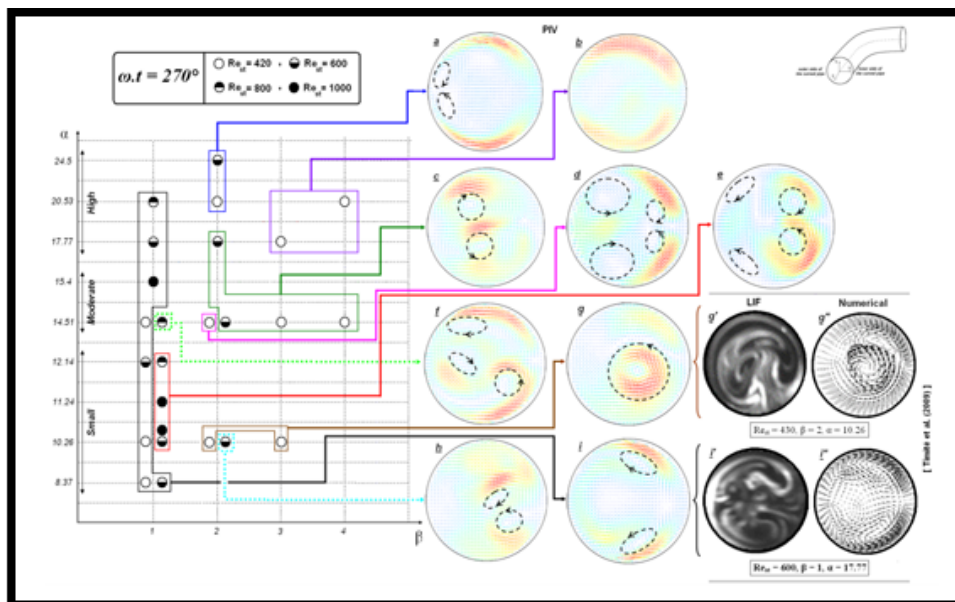


Figure I-21. Secondary flow structures at $\omega.t=270^\circ$ for different pulsating conditions $\{420 \leq Re_{st} \leq 1000, 1 \leq \beta \leq 4$ and $8.37 \leq \alpha \leq 24.5\}$.

I.6.2. Mixing analysis in a curved pipe

(Jarrahi 2009) established the theoretical grounds for the effects of vorticity and strain rate on mixing. In particular, for the case of transient diffusion, it was reported that the strain rate directly affects the scaling laws for the diffusion of species. In this case not only the diffusion coefficient and time but also the strain rate affect the diffusion flux. Another difference from pure transient diffusion is that when time tends to infinity the flux rate does not tend to zero (as in pure diffusion), but approaches a constant value $\rho \sqrt{\frac{2D\varepsilon}{\pi}}$ where ε is the strain rate and D is Dean number. It was also shown that the presence of vorticity enhances diffusion by creating stretching in fluid filaments, at the rate of $\left(\frac{\Gamma}{D}\right)^{\frac{2}{3}}$, where Γ is the vorticity.

The axial vorticity and transverse strain rate were calculated using the velocity fields measured by PIV in the tube exit cross section, and were compared to those in a steady curved-pipe flow. Conditions that provide a vorticity field and strain field stronger than those in a steady flow were called *favorable pulsating conditions* for mixing. The results show that these conditions are realized when $\beta > 2$ and $\alpha \leq 15$.

This study showed that pulsation can increase transverse mixing (as measured by strain rate or vorticity enhancement) in a curved pipe flow by 68% for $\beta = 1$ (for the strain rate at $Re = 420$, $\beta = 1$, $\alpha = 8.37$) and up to 400% for $\beta \leq 4$. It was also observed that small and moderate values of α (10 to 15) provide better mixing than higher α . Some phenomenological explanations were provided.

The different aspects of different flow conditions, i.e. steady state, pure sinusoidal, and pulsatile flow, on transverse mixing variation in a curved pipe were studied by (Jarrahi et al., 2011). They analyzed the variation in the axial vorticity and transverse strain for different conditions that contribute to the mixing evaluation under different flow conditions. Furthermore, the displacement of the centers of cells in the secondary flow (elliptic points) was studied and their complex movement was introduced as another index for mixing enhancement by pulsatile flow (Jarrahi et al., 2011).

Pulsatile chaotic advection in micro fluidic mixers

In recent years, micro fluidic systems are among the important topics of fluid mechanics. The cooling of electronic chips was the main reason to study micro fluidic systems whose applications are now in the fields of transport, materials, and mixing in chemistry and biology [(Cunningham, 2001), (Kakuta et al., 2001), (Beebe et al., 2002, Chován and Guttman, 2002), (Meldrum and Holl, 2002), (Schulte et al., 2002), (Sato et al., 2003) and (Weigl et al., 2003)]. One of the problems encountered is the small size of micro fluidic devices which creates difficulties in the mixing process: since the magnitudes of characteristic dimensions of these devices are generally between $10\ \mu\text{m}$ and $100\ \mu\text{m}$, the molecular diffusion is the only mechanism that generates the mixing, a mechanism which is too slow for most of the applications. In addition, the Reynolds number of the flow in these devices varies from the unit value to some hundreds such that the flow remains in laminar regime. This is the reason that using the turbulence to enhance mixing in micro fluidic systems is not a practical idea. The small size in micro fluidic systems also prevents applying some traditional techniques used in mixing process at the macroscopic scale. The use of mechanical stirrers is among these techniques which are not easily applicable to these micro fluidic systems. The proven benefits of chaotic advection in laminar regime to intensify the mixing in the usual scale devices have motivated researchers to propose and study the same technique for the improvement of the mixing in the microfluidic systems.

It is known that chaotic advection can play an important role in the effectiveness of microfluidic mixers (Stremler et al., 2004). For example, the use and manufacturing of complex geometries such as (Beebe et al., 2002), (Vijayendran et al., 2002), (Lasbet et al., 2006), (Lasbet, 2008), (Ansari and kim, 2009)] is an effective idea that is inspired by the study of (Jones et al., 1989) on chaotic advection in the ordinary scale.

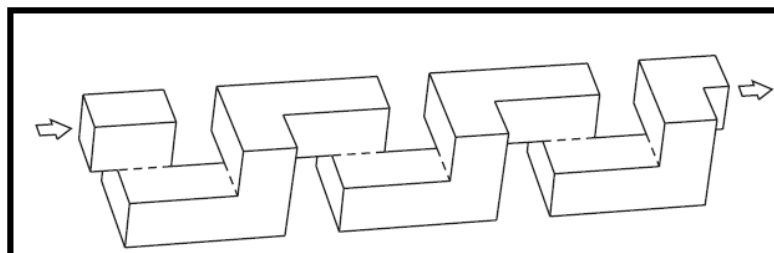


Figure I- 22. Zigzag micro channels with the cross sections of $300\ \mu\text{m} \times 300\ \mu\text{m}$ (Beebe et al., 2001).

Instead of fabricating complex geometries or applying external fields such as magnetic fields to improve the mixing, (Glasgow and Aubry, 2003) proposed to add a temporal dependence to microfluidic flow. Usage of pulsatile flow at the entrance of microchannels is a simple and easy idea to implement. The pulsations stretch and successively fold interfaces in the mixing process and thus it contributes to the intensification of the mixing. In addition, when the flow is pulsatile, the particles go through the mixing regions for several times and therefore, the mixing occurs on a shorter length.

The numerical analysis (CFD) from (Glasgow and Aubry, 2003) shows the positive effect of the flow pulsation on the mixing in a simple T-form geometry. The application of pulsatile flow in microchannel coils is also discussed in (Glasgow and Aubry, 2003) but to our knowledge there are not so much studies on this subject in the literature. We believe that the results presented in this work may also increase motivation to use the Dean alternated time dependent (pulsatile) flow in microfluidic system.

Previous studies on heat transfer enhancement by pulsatile flows

I.8.1. Heat transfer enhancement techniques

The uniform heating of delicate and viscous fluids is not an easy process. Increasing heat transfer and mixing enhancement are usual techniques to achieve homogeneous mixing and heating. Better fluids mixing and heat transfer can be achieved in the turbulent regime, but there is a disadvantage of higher shear stress and it is also difficult to obtain a turbulent regime in high viscous fluids, this leads to difficulties in heat transfer enhancement. Fluids like human blood, food liquids and pharmaceutical ones, can easily be damaged by higher shear stresses. Therefore a solution is that these fluids may be heated by mixing them efficiently in a laminar flow regime.

Generally, the heat transfer enhancement techniques can be classified in two types either as active techniques or passive techniques.

I.8.1.1. Active heat transfer enhancement techniques

Active heat transfer enhancement techniques requires an external source input to modify the flow and enhance the heat transfer in the heat exchangers or other energy systems. These type of techniques are difficult to use and complex to design. Moreover, while comparing to the passive techniques, the active techniques have less potential as it is not easy to provide an external source input in several applications.

Heat transfer enhancement by these type of techniques can be attained from:

- **Mechanical means:** To stir the fluid by mechanical resources or by rotating the surface. Rotating tube heat exchangers and scrapped surface heat and mass exchangers are examples of it.
- **Surface vibration:** This is applied in single phase flows to get higher heat transfer coefficients.
- **Fluid vibration:** Primarily used in single phase flows and are regarded as the most realistic type of vibration intensification approach.

- **Electrostatic fields:** In the form of electric or magnetic fields or a grouping of the both from dc or ac sources, this may be applied in heat transfer systems involving dielectric fluids.
- **Injection:** This technique is used in single phase flow and pertains to the method of injecting the same or a different fluid into the main fluid either through a porous heat transfer interface or upstream of the heat transfer section.
- **Suction:** It involves either vapor removal through a porous heated surface in nucleate or film boiling, or fluid withdrawal through a porous heated surface in single-phase flow.
- **Jet impingement:** It involves the direction of heating or cooling fluid perpendicularly or obliquely to the heat transfer surface.

1.8.2. Passive heat transfer enhancement techniques

The mechanism for heat transfer enhancement through passive techniques consists to reduce the thermal boundary layer thickness which constitutes an obstacle to heat transfer. It is obtained by several enhancing modified tubes configurations such as a finned tube, tube with rib, tube with spirally roughened wall, corrugated tube, fluted tube, helical tube, elliptical axis tube and micro-fin tube, etc.

Among the passive techniques, tremendous approaches for heat transfer augmentation have been introduced and tried to improve the overall thermal efficiency of heat exchangers. These approaches were devoted to get a better overall thermal performance of the heat exchangers by reducing the size of the heat exchanger and the cost of operation.

1.8.2. Using different kind of geometries to enhance heat transfer

Using different kind of geometries of heat exchangers like helical pipes and chaotically twisted pipes is the main passive technique in heat transfer enhancement. These geometries are designed to better mix the fluid by creating perturbation in the fluid streamlines thus enhancing the heat transfer.

A chaotically twisted pipe flow used as a mixer and/or heat exchanger have remained advantageous when compared to a helically coiled pipe or a straight pipe. This is concluded in prior studies (Aref, 1984), (Jones et al., 1989), (Acharya et al., 1992, Peerhossaini et al.,

1993), (Chagny et al. 2000), (Castelain et al., 2001), (Lemenand and Peerhossaini, 2002), (Timité, 2005), (Habchi et al., 2009), (Jarrahi, 2010) and (Funakoshi and Jang, 2012).

Pulsation impositions on the flow to enhance heat transfer

Recently, there has been growing interest in the effects of pulsating flow on convective heat transfer. Superimposition of pulsation on a steady flow affects the hydrodynamic and thermal boundary layers, which in turn affect the overall convective heat transfer rate. Pulsation generators can be used to increase heat transfer rates, because the pulsated flow enhances the heat transfer mainly due to increasing of turbulence levels in the boundary layer.

The effect of pulsations on heat transfer has been studied in previous studies with conflicting conclusions about heat transfer augmentation.

Some previous experimental studies (started for some of them in the sixties) show a **positive effect** of the pulsation on the thermal transfer.

1.9.1. Pulsation impositions on the flow to enhance heat transfer (older studies)

(Baird et al., 1966) examined the influence of pulsation on heat transfer in turbulent regime flow. They used a steam-water heat exchanger. The cold water was flown upward through a steam covered copper tube. Sinusoidal pulsations were created through an air pulsation generator installed upstream of the test section. They conducted experiments for Reynolds number ranging from 4300 to 16200 with the pulsation conditions of Womersley frequency parameter α varying from 6.7 to 10, and different velocity amplitudes. They concluded that sinusoidal pulsations can enhance heat transfer, particularly if the flow could be made to reverse in direction. Therefore they observed a maximum heat transfer augmentation about 41% for the Reynolds number 8000, based on the overall heat transfer coefficient.

(Karamercan and Gainer, 1979) conducted experiments to test the effect of pulsations on the heat transfer enhancement in a water stream double pipe heat exchanger. The pulsations were generated through a reciprocating pump installed first upstream and then downstream of the test section. They conducted experiments for Reynolds numbers ranging from 1000 to

50000 with the pulsation conditions of frequency ranged up to 5 Hz and five different amplitudes. Their results showed that heat transfer coefficient increases with pulsation imposition. The maximum heat transfer enhancement was observed in the transitional flow regime.

(Lemlich, 1961 and Lemlich, 1965) studied the influence of pulsation imposition on heat transfer coefficient of water in a double pipe, steam-water heat exchanger. Pulsations were generated through an electrical-hydraulic pulsation generator comprising of a solenoid valve activated by a regulating pressure switch. The solenoid valve was mounted at a short distance upstream the water line. Frequency of 1.5 Hz was managed and Reynolds number varied from 500 to 5000. They observed that pulsation increased the overall heat transfer coefficient by 80%, depending on the upstream position of the solenoid valve at Reynolds number equal to 2000. The better enhancement in the overall heat transfer coefficient was realized with the closer valve position to the test section inlet.

(Lemlich and Hwu, 1961) investigated the influence of acoustic vibration on forced convective heat transfer of air following in the core of a horizontal, double pipe stream-air heat exchanger. Pulsations were superimposed on the air flowing at Reynolds number between 560 and 5900 with frequencies of 198, 256 and 322 Hz. An electromagnetic driver, activated through an audio amplifier by changeable sinusoidal audio signal generator was used to generate sound vibration frequency. This driver was installed at the upstream of the test section. An increase of 51% in Nusselt number in the laminar regime and up to 27% in the turbulent regime was observed.

(Shuai, 1994) performed an experimental investigation on the effect of perturbations created through pulsation on convective heat transfer for laminar flow for Reynolds number ranging from 150 to 1000 in a co-axial cylindrical tube heat exchanger for a viscous fluid. A reciprocating pump installed at the upstream of the heat exchanger was used as a pulsation generator. Pulsation parameters frequency ranged from 0 to 2 Hz and different velocity amplitude was imposed. A significant increase in the heat transfer coefficient was observed, even more than 300%, obtained with strong-pulsed perturbations.

(West, 1952) pursued an experimental investigation to estimate the influence of the pulsations on heat transfer coefficient enhancement of water in a long horizontal tube of a steam-water heat exchanger. The pulsating stream of water was obtained by a reciprocating pump, located at upstream, with a variable air chamber, through a 50 mm inner diameter and 6130-mm length galvanized iron pipe of the test section. They performed experiments for Reynolds number between 30000 to 85000 with a fixed pulsation frequency of 1.6 Hz and a

varying amplitude ratio from 1 to 1.56. They evidenced an augmentation of 60 to 70% in the heat transfer coefficient with an amplitude ratio of 1.42.

(Havemann and Rao, 1954), employing pulsations at frequency between 5 to 33 Hz over a steady flow of turbulent regime, achieved an enhancement of about 42% in the heat flux.

(Keil and Baird, 1971) examined as much as a 100% increase in the overall heat transfer coefficient employing pulsating frequencies ranging from 0.4 to 1.1 Hz in a commercial shell and tube heat exchanger having steam in the shell.

(Ludlow, 1975) used a double pipe heat exchanger with hot water in the ring, and acquired a 500% boost in the tube side heat transfer coefficient in the transition flow regime with pulsation frequencies between 0.16 to 2.83 Hz.

(Martinelli, 1943) imposed semi-sinusoidal velocity perturbations on the tube side fluid in a concentric tube heat exchanger. They performed experimental investigations in laminar flow regime. They showed a 10% augmentation in the overall heat transfer coefficient over the steady flow coefficient.

However positive effects of the pulsation on the thermal transfer are not always observed and some authors measured moderated and even **negative effects** in experiments.

(Darling, 1959) reported something interesting about pulsation influence. He obtained an increase of 90% in the heat transfer coefficient by employing pulsation at the upstream of the heaters and observed no any enhancement when applying the pulsation at the downstream of the heaters. He carried out the experiments for Reynolds number 6000 and a pulsation frequency of 2.66 Hz.

(Muller, 1957) described the negative impact of pulsations in turbulent regime flow. He showed that the average Nusselt number was found to be less than the corresponding steady flow Nusselt number for pulsating flows with frequency between 0.03 to 0.248 Hz and Reynolds number range between 53000 to 76000.

(McMichael, 1975) have concluded through a theoretical development, that for laminar flow, pulsations cause a decrease in the rate of heat transfer at flow amplitudes which do not allow flow reversal to take place.

Experiments carried out by (Lemlich, 1961) studied the effect of acoustic vibration on forced convective heat transfer of air following in the core of a horizontal, double pipe stream-air heat exchanger. Frequencies of 198, 256, and 322 Hz were imposed on air flowing at Reynolds number of 560 to 5900. They observed an increase in overall heat transfer coefficient up to 80% when the pulsation generator was installed at upstream. On the contrary when the pulsation generator was installed at downstream, a decrease in the overall heat transfer coefficient was realized.

1.9. 2. Pulsation impositions on the flow to enhance heat transfer (recent studies)

Some analytical studies of laminar pulsating flow show a **frequency-dependent influence** on the heat transfer compared to steady flow, yet, overall the effect on the average heat transfer rate is found to be negligible (Moschandreou and Zamir, 1997, Hemida et al., 2002). However some numerical and experimental studies found enhancement factors of up to 11% for laminar flow (Craciunescu OI, 2001) and 9% for turbulent pulsating flow (Elshafei et al., 2008) in smooth channels. Some of the current experimental investigations on heat and mass transfer enhancement through pulsating flow in ducts with cross-stream ribbed walls report enhancement factors of 100% up to 250% compared to steady flow (Nishimura et al., 2000). The heat transfer enhancement is achieved more in laminar regime as compared to turbulent regime and it increases with Prandlt number (B. O. Olayiwola, 2009). The influence of flow pulsation on the heat transfer augmentation has been also investigated on impinging jets. Using synthetic (zero net mass flux) jets, heat transfer rates comparable to those of steady impinging jets have been obtained (Pavlova, 2006, Valiorgue et al., 2009, Persoons, 2009 and Persoons et al., 2011). A pulsed impinging jet can achieve a heat transfer enhancement of about 100% compared to a steady jet at the same Reynolds number (Zumbrunnen, 1993).

(Karagoz, 2001) considered laminar oscillatory flow over a heated plate flush mounted in the middle of the bottom wall in a 2-D channel. He analyzed the flow and temperature characteristics numerically for a range of Womersley number from about 3 to 25. He concluded that the thickness of the Stokes boundary layer decreases and the core region of the flow exhibits more uniform velocity profiles as the Womersley number increases. The velocity gradients at the wall are generally greater than the ones for steady laminar flows. When the flow velocity is low during flow reversal, increases of heat diffusion due to relatively longer residence time results in high flow temperature and low temperature gradient

at the wall. The depth of heat penetration into the fluid increases at those times. On the contrary, high flow velocities lead to low flow temperatures and steeper temperature gradients at the wall. The higher Womersley and Reynolds numbers, the smaller the thickness of the thermal boundary layer. High Reynolds numbers result in great velocity gradient at the wall; low flow temperature and high penetration depth of heat. Extensions of this numerical study would include the effects of tidal displacement, conjugate heat transfer, the role of turbulent at high frequency oscillating or pulsatile flow and pressure losses.

(Chen and Zhao, 2006) concluded from their numerical study on heat transfer enhancement due to pulsation in a shell and tube heat exchanger that the pulsation frequency has an influence on heat transfer coefficient and there is always an optimal frequency. (Elshafei et al., 2006) carried out their experimental study of heat transfer in a pulsating turbulent flow in a pipe for $1000 \leq Re \leq 40000$ and $6.6 \text{ Hz} \leq f \leq 68 \text{ Hz}$. The pipe was subjected to a uniform heat flux and the pulsation generator was placed downstream of the pipe. They observed that heat transfer coefficient increases or decreases with the different values of frequency and Reynolds number.

(Akdag, 2010) conducted a numerical investigation by using Fluent® CFD commercial software to understand the influence of pulsation on a laminar unsteady convective heat transfer around a discrete heater in a channel. In his study, the main parameters, Womersley frequency parameter α and dimensionless amplitude were considered as pulsation variables for a fixed Reynolds number, ($Re_{st}=125$). Six different values for frequencies and three different values for amplitudes were tested.

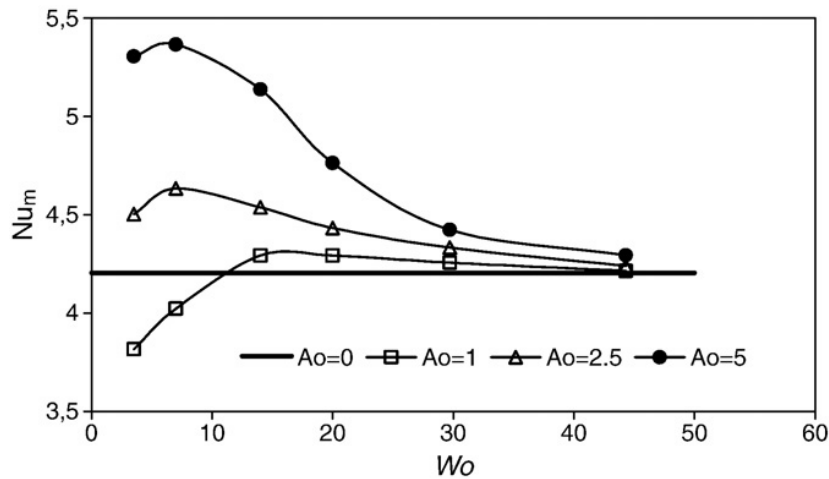


Figure I- 23 Average Nusselt numbers versus dimensionless pulsation parameters (Akdag, 2010)

Figure I-23 shows the results obtained by (Akdag, 2010). He observed that pulsations enhance the heat transfer at low frequency and high amplitude. Though heat transfer was also enhanced at lower amplitudes but that enhancement was not notable as compared to steady flow cases. The heat transfer characteristics meet the steady flow conditions with a gradual increase in the frequency values for any amplitude. With both at low amplitude and low frequency as seen in Figure I-23 there is a decrease in heat transfer characteristics.

Zohir (2011) investigated experimentally heat transfer characteristics of the turbulent pulsating water flow through the concentric tube heat exchanger equipped with a ball valve mounted at outlet of the outer pipe. The ball valve was used as a pulsation flow generator in the parallel and counter flows and results showed that the Nusselt number in the concentric double-pipe heat exchanger was increased from 20% to 90% for pulsated flow. For parallel flow these improvements were about 70% lower than that for the counter flow.

Persoons *et al.* (2012) studied experimentally the potential of overall heat transfer rate enhancement using pulsating flow in a single phase liquid flow heat sink, for use in electronics cooling. Heat sink was a single rectangular channel of 1.9 mm hydraulic diameter. They performed experiments for Reynolds number range [100–650] with the pulsation parameters β in the range [0.002–3] and frequency parameter α in the range [6–17]. Their results showed an increase in heat transfer enhancement factor up to 40% when compared to the heat transfer rate for steady flow at the same steady Reynolds number. They observed a consistent trend for heat transfer enhancement as a function of the ratio of the dimensionless pulsating amplitude β . For small pulsation amplitude ($\beta < 0.05$), a negligible yet slightly

negative enhancement is observed. For larger pulsation amplitudes ($\beta > 0.2$), the heat transfer enhancement is positive and increases with increase in β . In terms of practical relevance for electronics cooling, this study indicates that inline flow pulsation can be advantageous in terms of heat transfer performance. Circulation pumps with an inherent pulsatile nature such as membrane pumps could be considered instead of centrifugal or gear pumps. They confirmed the order of magnitude of the heat transfer enhancement which can be reasonably achieved.

(Jafari et al., 2013) studied, the effects of the pulsations on the forced convection in a corrugated channel by Lattice Boltzmann Method (LBM) based on Boundary Fitting Method (BFM). They observed the influences of dimensionless frequency at a form of Strouhal number $0.05 \leq St \leq 1$ and oscillation amplitude for a range $0 \leq \beta \leq 0.25$ on Reynolds number range $50 \leq Re_{st} \leq 150$. Their results showed that the role of flow pulsation on the heat transfer intensification on the targeted area is highly dependent on pulsation parameters.

Figure I-24 shows local and period averaged values of Nusselt number for pulsating flow with different St and Amplitudes. (a) $Re_{st} = 50$, (b) $Re_{st} = 100$, (c) $Re_{st} = 150$ of (Jafari et al., 2013) results. Their results show that the role of pulsation amplitude on heat transfer intensification is significant. For a $Re_{st} = 150$, by an increase of the pulsation amplitude from 0.05 to 0.25, the value of Nusselt number Nu increases about 2, 14, 18, 11, 3 and 0.5% respectively for $St = 0.05, 0.15, 0.25, 0.50, 0.75$ and 1. It may be noted that at $St = 0.25$ which is the peak value of the Strouhal number at $Re_{st} = 150$, the pulsation amplitude enhances more heat transfer.

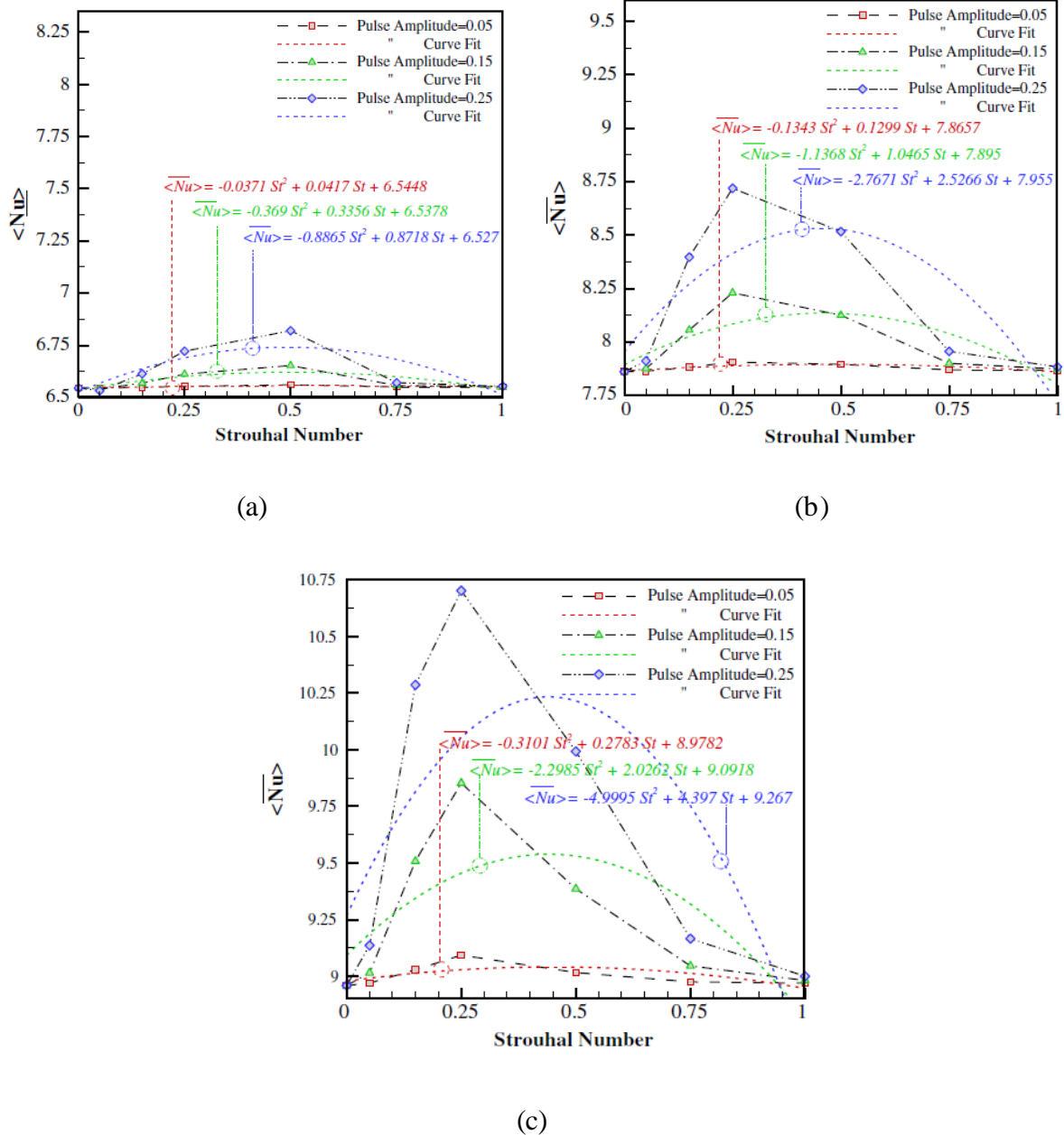


Figure I- 24 Local and period averaged values of Nusselt number for pulsating flow with different St and Amplitudes. (a) $Re_{st} = 50$, (b) $Re_{st} = 100$, (c) $Re_{st} = 150$ (Jafari et al., 2013).

(Yin and Ma, 2014) obtained analytical solution of velocity distribution, temperature distribution and Nusselt number of a laminar oscillating flow in capillary tube driven by a triangular pulsation signal. Their results showed that the peak Nusselt number for a triangular pulsation signal is very different from a sinusoidal pulsation signal. For an oscillating flow driven by a triangular pulsation signal, when the Womersley frequency parameter decreases or when the amplitude increases, the oscillating motion can enhance heat transfer. However,

when the Womersley frequency parameter is high enough, the pressure waveform effect on heat transfer enhancement disappears.

From the previous works, it can be observed that, due to variety of heat transfer control parameters, some conflicting results appear about effect of pulsation on heat transfer. Most investigators reported increase in heat transfer due to pulsated flow and few of them reported no increase or even decrease in heat transfer.

This study is devoted to examine the effect of pulsation on mixing in a developing flow in a 90° curved pipe of 4cm diameter through PLIF technique and heat transfer in a shell and tube heat exchanger. Circular cross-sectional tube of 8 mm consists of 12 successive 90° twisted bends. Experiments are conducted for Reynolds number ranging from 600 to 5000. Three different wave forms *i.e.* sinusoidal, triangular and square signals are generated to obtain different pulsation conditions composed of Womersley number α varying between 0 to 20, *i.e.* frequency ranges between 0 and 4 Hz, and velocity amplitude ratio β from 1 to 16.

Chapter 2

Materials and methods

Objective

This chapter is devoted to describe the two experimental setups used for mixing and heat transfer studies, the experimental techniques PLIF used for mixing analysis and the thermal measurements for heat transfer study. Concerning the mixing analysis, pulsations are imposed on the steady flow in a 90° curved pipe, a T-shaped arrangement is used to avoid optical refraction induced by the curvature of the pipe, and the various measurement steps of the PLIF technique are explained. For the thermal measurements pulsations in the form of three different wave signals are imposed on the steady flow in a chaotic twisted pipe to measure the heat transfer enhancement in a shell and tube heat exchanger.

II.1. Experimental setup for mixing study in pulsatile flows through a bend

II.1.1. Pulsatile flow generation

Figure II-1 shows a general circuit of the experimental setup used in this study. A reservoir of 300 liters is filled with the tap water. This reservoir is connected to a centrifugal pump to supply the permanent flow in the setup, which is the steady part of the pulsatile flow. The flow rate is measured by a monobloc flowmeter.

Sinusoidal component of the pulsatile flow is produced by a pulsation generator and the steady flow produced by the centrifugal pump. Pulsatile flow obtained by this superposition is circulated in the tube. Mathematically,

$$U_p(t) = U_{st} + U_{sin}(t) \quad (\text{II- 1})$$

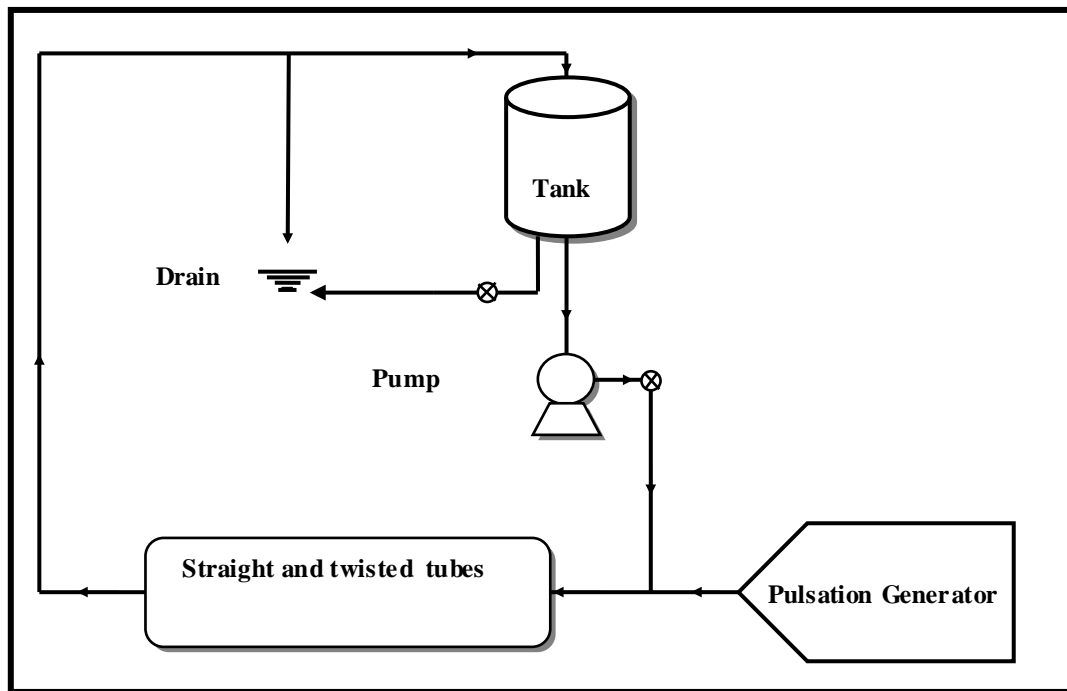


Figure II-1. Experimental setup circuit.

The testing section is composed of a 90° curved pipe in which the pulsatile flow is flown in order to observe the effects of pulsations on the mixing. This curved pipe section is followed by a straight pipe section of 2.5 m of length, to ensure a hydrodynamically developed flow entering the curved sections. The straight pipe and curved pipe section are of the same diameter $2r_o=0.04\text{m}$, and are fabricated from the plexiglas, a transparent and thermal insulated with the wall thickness of 5mm.

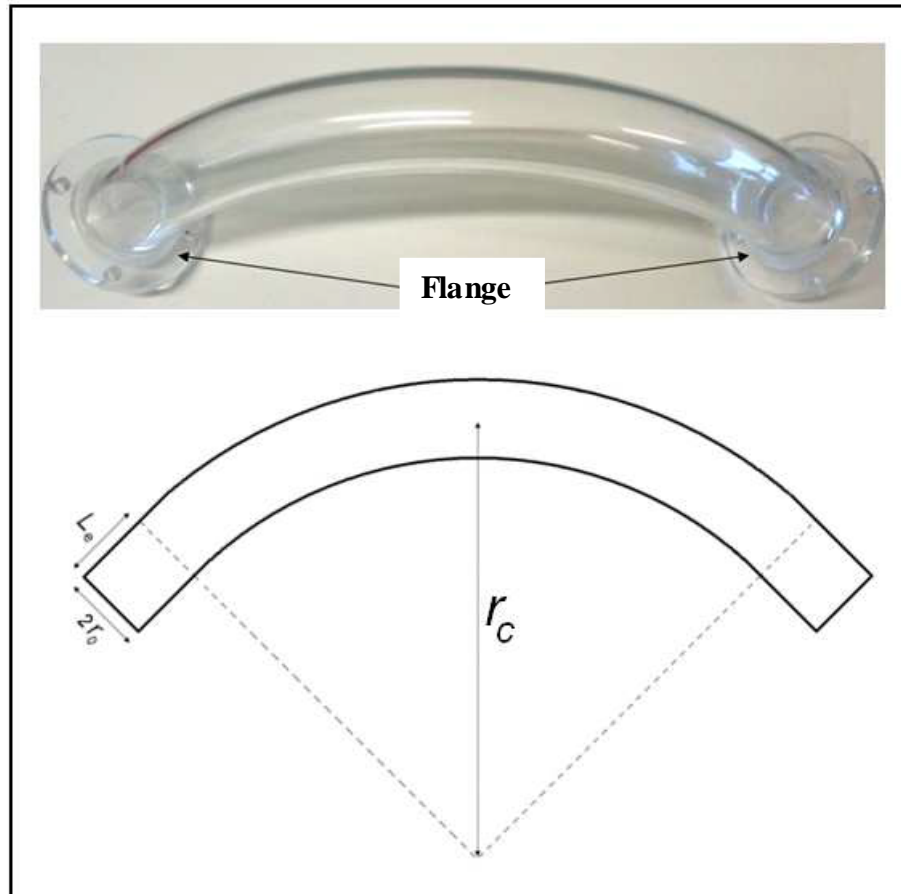


Figure II- 2. A 90° curved pipe section.

Figure II-2 represents a 90° curved pipe section. This element is constructed of three parts: an opening angle of 90° and two straight lengths at the ends. The mean curvature radius is equal to 0.22 m. Therefore, the curvature ratio is equal to $\theta = \frac{r_o}{r_c} = \frac{0.02}{0.22} = 0.091$. The straight lengths are added to perform PLIF measurements at the outlet of each curved pipe and to attach the flanges. The flanges are attached at the ends of the curved pipe sections in such a way that the outlet section of the curved pipe section to be added come in a perfectly dug in shape but in the inlet section of the next curved pipe section. The flange of the inlet section of the curved pipe has a groove cut and O ring is installed on it to avoid fluid leakage.

II.1.2. Pulsation generator

II.1.2.1. Scotch yoke mechanism

The Scotch yoke mechanism is used as a pulse generator which generates a sinusoidal component of the flow. The choice of this mechanism among other options possible (such as rod-crank system used by Ohmi and Iguchi (1984) or the used in the study of Sarpkaya (1966)) is based on the reliability of the Scotch yoke mechanism and has been validated by Timité (2005). This mechanism is composed of:

- A flywheel
- A piston and its cylinder
- Two pulleys
- An asynchronous electric motor

A complete scheme of this Scotch yoke mechanism is shown in Figure II- 4.

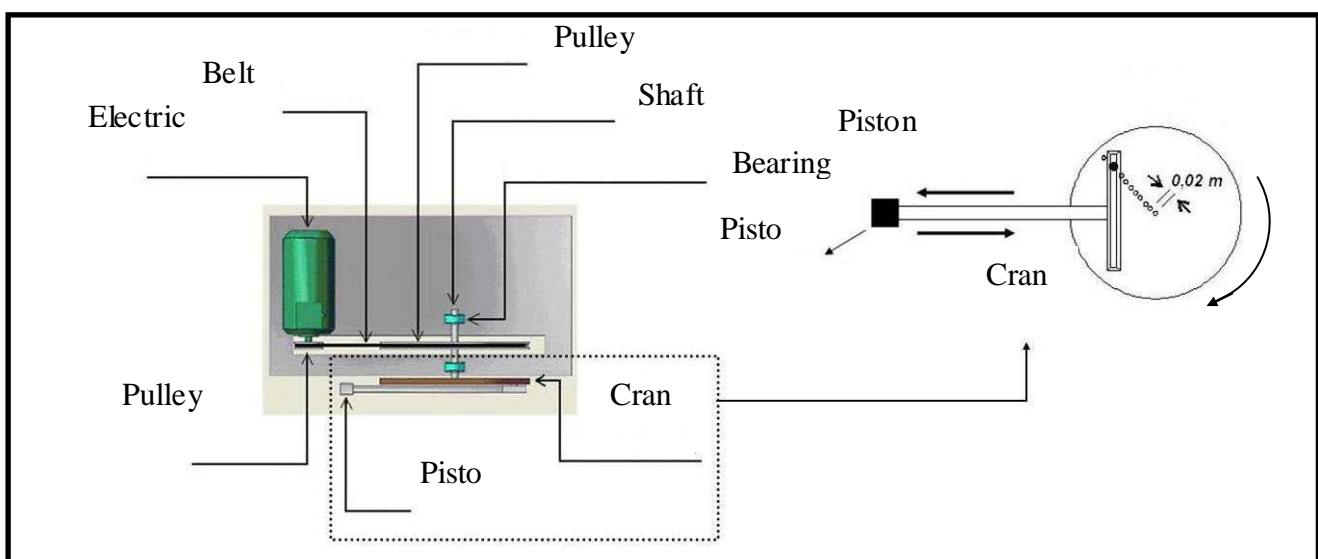


Figure II- 3. Scotch yoke mechanism (Top view).

To minimize the mass of the assembly, aluminum is used as a material constituting the moving parts of the system Scotch yoke. But the non moving parts like the volume of the junction between the main supply system (steady input flow) and the cylinder (piston chamber) are constructed of stainless steel Figure II- 5.

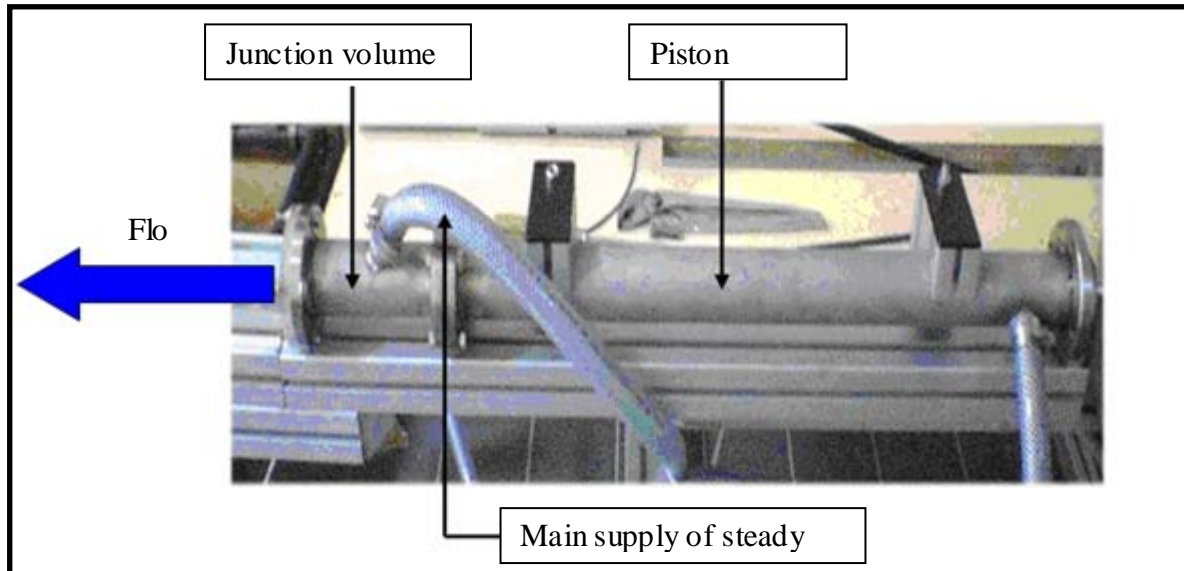


Figure II- 4. Piston assembly.

Scotch yoke system permits to adjust the Womersley parameter (α) and the velocity amplitude ratio (β) by varying the rotational speed of the crank and changing the piston stroke (by means of the holes made on the crank).

In the Scotch yoke system used in this study the piston displacement X_{Piston} , may be

$$X_{Piston} = L_{Crank} [(1 - \cos(\omega t))] \quad (\text{II- 2})$$

Then, the sinusoidal velocity of the piston becomes:

$$\dot{X}_{Piston} = \frac{d}{dt} X_{Piston} = \omega L_{Crank} \sin(\omega t) \quad (\text{II- 3})$$

where L_{Crank} and ω are the length of the crank and the angular frequency, respectively.

II.1.2.2. Crank length and piston diameter

Applying flow conservation principle, the sinusoidal Reynolds number Re_{sin} , is based on the maximum amplitude of the sinusoidal component of velocity $Re_{sin} = \frac{U_{sinmax}}{\nu} d$, and can be determined as a function of the crank length L_{Crank} , diameter of the piston d and Womersley parameter α .

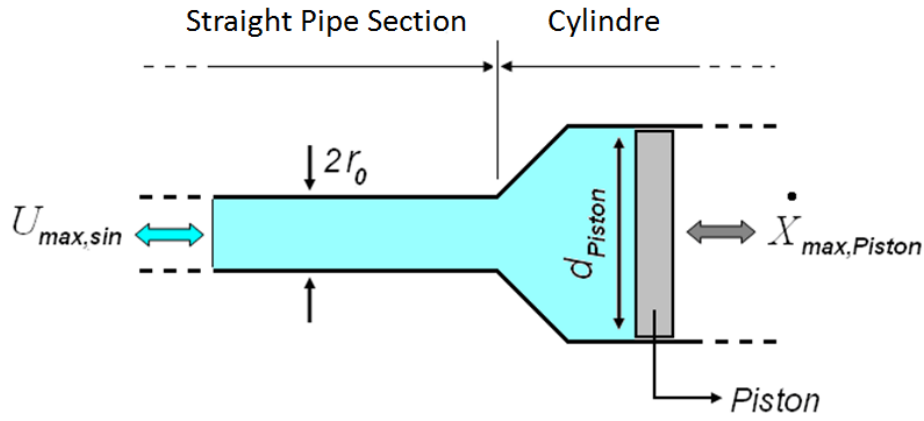


Figure II- 5. Junction zone between flow development straight length and the cylinder of pulsation generator.

Figure II-6 describes the schematic arrangement of the junction zone between flow development straight length and the cylinder of the pulsation generator. The conservation of the flow between cylinder and the straight pipe section is:

$$\dot{X}_{Pistonmax} \left(\frac{\pi d_{Piston}^2}{4} \right) = U_{sinmax} \left(\frac{\pi (2r_0)^2}{4} \right) \quad (\text{II- 4})$$

thus:

$$U_{sinmax} = \dot{X}_{Pistonmax} \left(\frac{\pi d_{Piston}^2}{(2r_0)^2} \right) = \omega L_{Crank} \left(\frac{\pi d_{Piston}^2}{(2r_0)^2} \right) \quad (\text{II- 5})$$

Then

$$Re_{sin} = \frac{U_{sinmax} (2r_0)}{\vartheta} = \frac{\omega L_{crank} d_{Piston}^2}{2r_0 \vartheta} = \frac{\omega L_{crank} d_{Piston}^2}{2 r_0 \vartheta} \quad (\text{II- 6})$$

Applying the definition of Womersley parameter α :

$$Re_{sin} = \left[r_0 \left(\frac{\omega}{\vartheta} \right)^{\frac{1}{2}} \right]^2 \frac{L_{crank} d_{Piston}^2}{2r_0^3} = \alpha^2 \frac{L_{crank} d_{Piston}^2}{2r_0^3} \quad (\text{II- 7})$$

As $d_{Piston}=2r_0=40$ mm then putting this value in the equation II-7, we get

$$Re_{sin} = \alpha^2 \frac{2L_{crank}}{r_0} \quad (\text{II- 8})$$

Dividing by Re_{st} the both sides of II-8 and using the definition of β , we get

$$\frac{\beta Re_{st}}{\alpha^2} = \frac{2L_{crank}}{r_0} = \frac{2L_{crank}}{0.02} = 100L_{crank} \quad (\text{II- 9})$$

The equation II-9 allows to obtain different pulsation parameters. In order to set L_{crank} , ten holes (20 mm to 200 mm from the crank center) with a constant distance of 20 mm are made on the crank .

II.1.2.3. Adjustments to obtain different conditions of pulsation

Pulsation generator designed by Timité (2005) is used in this study. This pulsation generator permits to generate the pulsatile flow with different pulsation conditions by adjusting Womersley parameter α and velocity amplitude ratio β separately. According to the definition of Womersley parameter α and by setting the kinematic viscosity of water $\nu = 10^{-6} m^2/s$ and the radius of the pipe section, $r_0 = 20 mm$; it can be seen that the Womersley parameter depends only on the angular velocity of the crank:

$$\alpha = 400 \omega \quad (\text{II- 10})$$

An alternating current asynchronous electric motor of 1.5 kW coupled with a speed regulator with a maximum value of $N_{0,max} = 1500 rpm$ is used for rotating the crank with desired velocity through a pulley. The rotation speed can be reduced with the gear ratio R (equal to 35.5) and a set of pulleys with a ratio of $D_2/D_1=2.8$; where $D_2 = 280 mm$ and $D_1=100 mm$ are the diameters of pulleys. Therefore the relation between the output angular velocity of this system which is in fact the velocity of the crank N_{crank} and that of the motor N_0 is expressed as:

$$N_{crank} = \frac{N_0}{R \left(\frac{D_2}{D_1} \right)} = \frac{N_0}{99.4} \quad (\text{II- 11})$$

Therefore, the crank angular velocity can be adjusted between 0 and 15.1 rpm. Then from equations (II-10) and (II-11) we obtain:

$$\alpha = 400 \omega = 400 \frac{2\pi N_{crank}}{60} = 0.42 N_o \quad (\text{II- 12})$$

This whole schematic arrangement is shown in the Figure II-7.

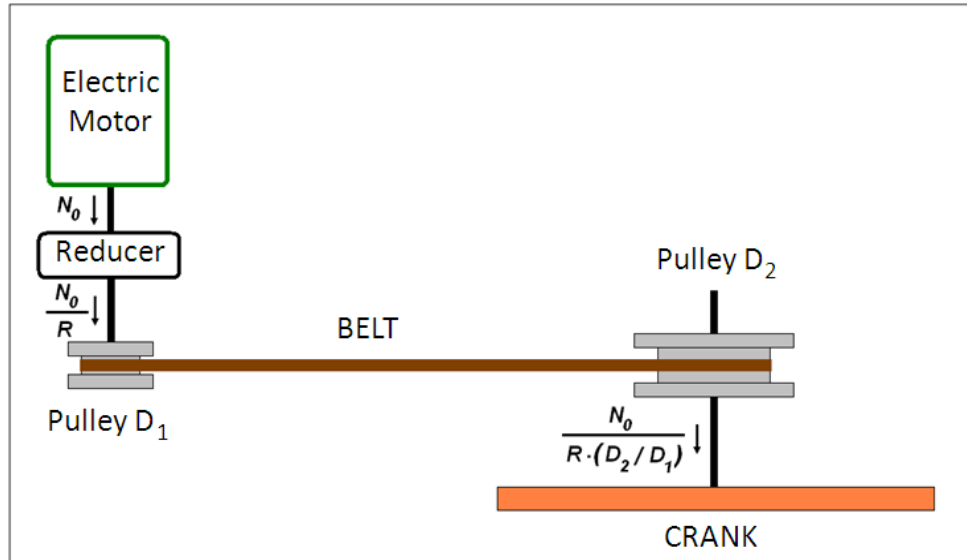


Figure II- 6. Pulley-Belt assembly.

Equations (II-9) and (II-12) are used to construct the table of measurements Table II-1 that summarizes all the settings needed to produce the different conditions of pulsation. First, the motor speed (N_o), associated with a desired Womersley parameter (α), is determined using the relationship (II-12). Then, for a specified steady Reynolds number Re_{st} , equation (II-9) is applied to find a crank length (L_{Crank}) that can give appropriate value of β (velocity amplitude ratio) close to the values 1, 2, 3 or 4.

Timité et al. (2005, 2009) showed that the pulse generator presented here produces a pure sinusoidal movement. They made measurements of the axial velocity by laser Doppler velocimetry (LDV) in the straight tube located upstream of the bend; where the flow is assumed hydrodynamically established.. The measurements are carried out at three different radial positions $\frac{r}{r_o} = 0, 0.4, 0.8$ in the cross section. These measurements were performed for two different conditions of pulsation: $\{Re_{st} = 600, \beta = 1, \alpha = 8\}$ and $\{Re_{st} = 280, \beta = 1, \alpha = 11.2\}$. Figure II-8 shows the results concerning the condition $\{Re_{st} = 280, \beta = 1, \alpha = 11.2\}$. A difference of less than 3% is observed between measurements of Timité et al. (2005, 2009) and analytical solutions of a purely sinusoidal flow.

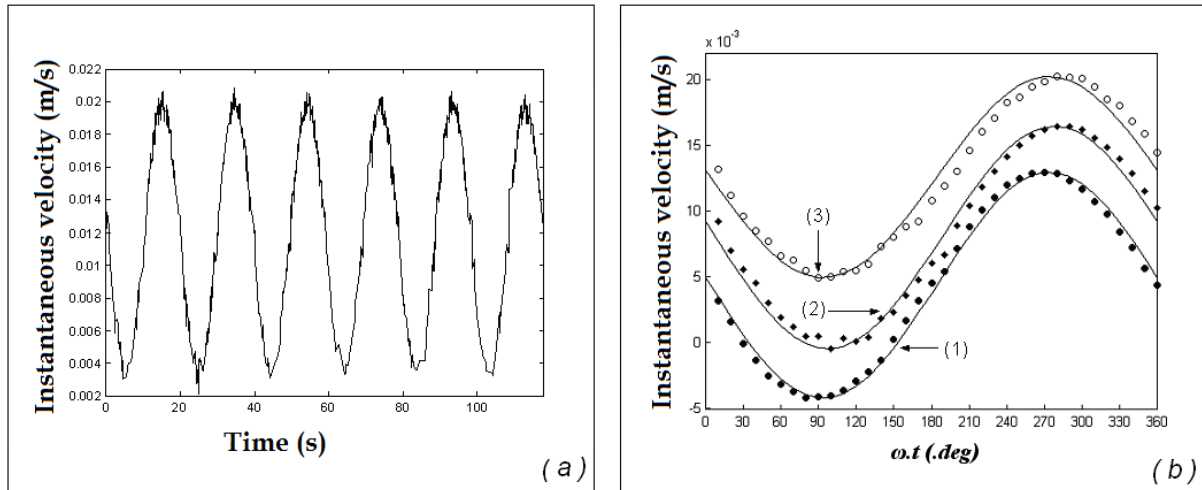


Figure II- 7. For $\{Re_{st} = 280, \beta = 1, \alpha = 11.2\}$: a) Instantaneous velocity at radial position ($r/r_0 = 0.4$) b) Instantaneous average axial velocity during a cycle for different radial positions; Experimental measurements ($\bullet, \blacklozenge, o$); analytical solutions ($---$); (1) $r/r_0 = 0.8$ (2) $r/r_0 = 0.4$, (3) $r/r_0 = 0$ [Timité et al. (2005 and 2009)].

The different pulsating conditions obtained by adjusting the different parameters, are recapitulated in Table II- 1.

Steady Reynolds number Re_{st}	Flow rate (L/min)	Womersley parameter α	Amplitude ratio β	Motor speed (rpm)	Crank position (m)		
420	0.80	8	1	167	0.06		
			2	167	0.12		
		10	1	251	0.04		
			2	251	0.08		
		15	1	501	0.02		
			2	501	0.04		
		21	2	1004	0.02		
600	1.10	8	1	167	0.08		
			2	167	0.18		
		10	1	251	0.06		
			2	251	0.12		
				12	1	351	0.04
		800	1.50	8	1	167	0.12
1	251				0.08		
12	1			351	0.06		
	1			501	0.04		
1000	1.90	8	1	167	0.14		
			1	251	0.1		
		11	1	301	0.08		
			1	565	0.04		

Table II- 2 The different pulsating conditions obtained by adjusting the different parameters

Figure II-9 illustrates the scheme of the experimental setup used in this work. A circular water duct made up of Plexiglas is used to provide controlled flow through the test section. Steady flow is pumped in the setup through a volumetric pump from a tank of 300 L capacity. The steady flow rate is measured by a monobloc flow meter. To be sure about clean and stable inlet conditions and to develop a Poiseuille flow in the setup a straight 2.50 m pipe is used. The Scotch yoke pulsation generator allows adjusting different pulsation conditions by regulating the dimensionless frequency parameter α and amplitude ratio β . This Scotch yoke mechanism consists of a crank of 40 mm diameter connected by a metallic stem. The piston stroke is controlled on the crank in steps of 20 mm to a maximum of 200 mm. A motor speed reducer is used to control the pulsation frequency ω .

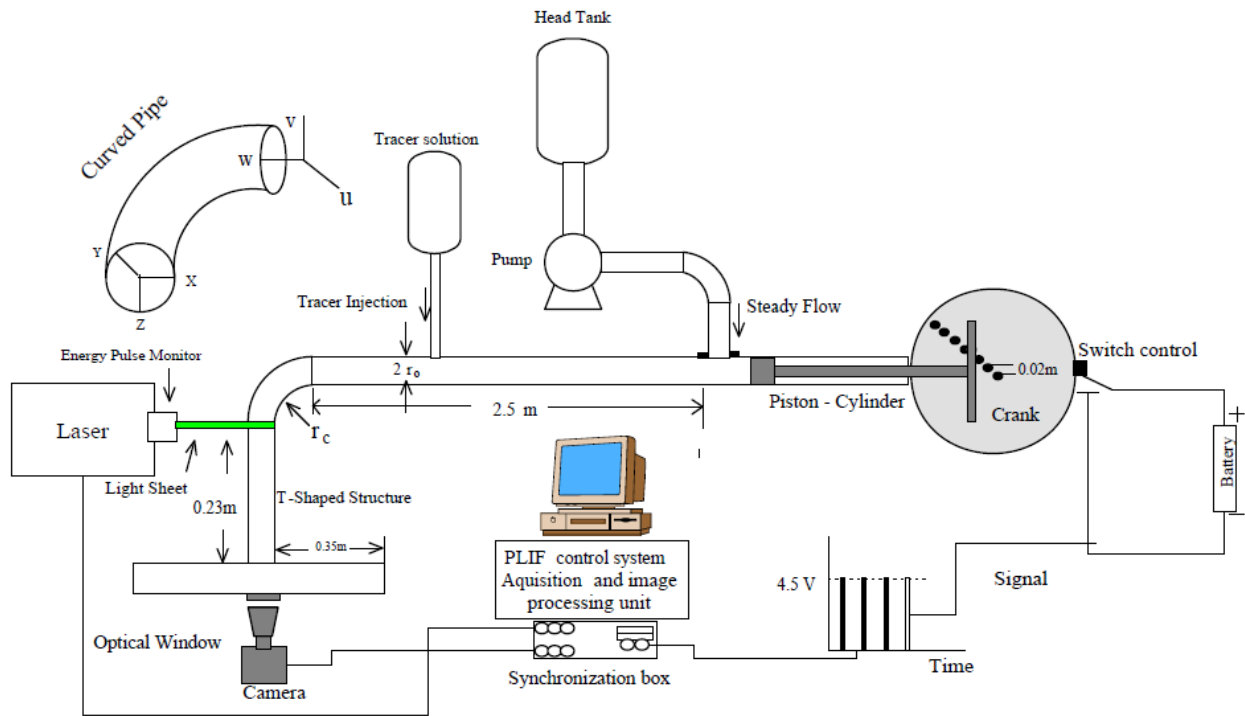


Figure II- 8. Experimental setup.

Therefore both parts of the flow *i.e.* steady and sinusoidal join upstream of the curved pipe in such a way that a fully developed flow enters in the 90° curved pipe of 40 mm diameter, radius of curvature 220 mm. A tracer injection setup was designed and fabricated to inject the tracer dye through an injecting needle of 1 mm diameter. Injecting needle is positioned at the center of the cross-sectional area of the duct. The distance between the injecting needle and the curved pipe inlet is 50 cm.

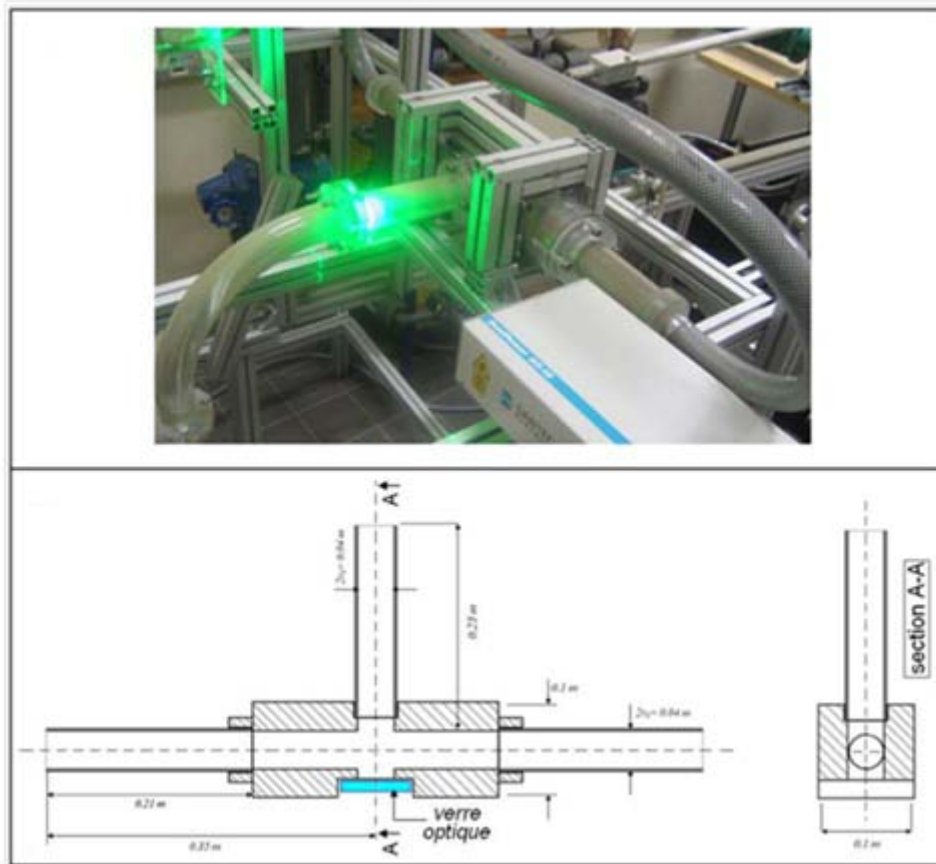


Figure II- 9. T-shaped flow divider.

Figure II-10 describes a T-shaped Plexiglas flow divider comprising a central tube with two symmetric tubes of the same diameter as the curved pipe (40 mm) is installed at the exit of the curved pipe to avoid the light refraction effects during PLIF measurements. The central branch connected to the curved pipe outlet is passed through a water box to get better flattened image quality. The length of the central tube is 230 mm, and each lateral branch is 350 mm long.

The camera with a filter captures the illuminated outlet section of the curved pipe through an optical window, a 3-mm-thick float glass with a multilayer anti-reflection coating on both sides. The T-shaped Plexiglas flow divider permits the camera to view the illuminated flow cross section perpendicularly, thus reducing measurement inaccuracies. Moreover, the light beam encounters no curved surfaces in its path between the illuminated section and the camera. Under these conditions, although the light passes through three different media (the fluid in the duct, the optical window and air) with three different refractive indices before entering the camera, there is no light refraction because the angle of incidence is zero on all interfaces.

II.2. PLIF technique

Planar laser-induced fluorescence (abbreviated PLIF in the following) is a fluorescence-based technique used to perform non-intrusive whole field concentration or temperature measurements in liquids. The measure is made possible thanks to a well-defined relationship between the intensity of fluorescence and the concentration and/or temperature when other experimental parameters are set. In the next sections, focus is first made on the principles of LIF technique and the practical aspects are then dealt with.

Applications can be found in process engineering (e.g. mixing in stirring vessels, heating and cooling systems), biomedical engineering (e.g. transport of drugs in biological flows such as in model veins) and fluid dynamics research (e.g. turbulent mixing and heat transfer modeling, indoor climate etc.)

The advantages and features are:

- Non intrusive technology, so it does not disturb flow
- Quantitative, precise and accurate measurements of concentration or temperature fields
- In combination with velocity measurements, transport properties (e.g. Reynolds flux, turbulent diffusion coefficients and other parameters) are made experimentally available.

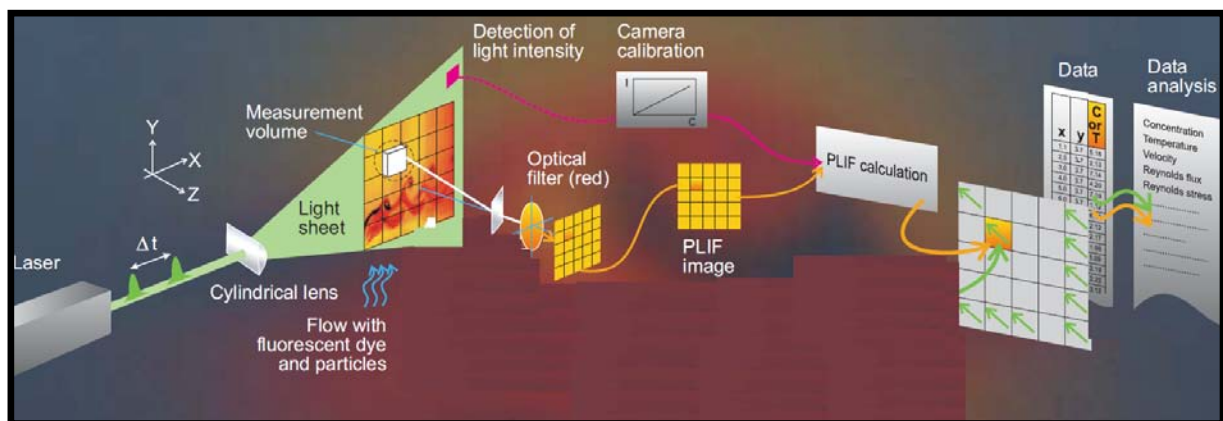


Figure II- 10. PLIF Principle (courtesy of Dantec Dynamics).

The basic principle of PLIF is shown in Figure II-10. The basic equipment needed to carry out PLIF measurement is:

- A laser source ,

- A fluorescent dye that marks the fluid and that is traced during the measurements. This chemical compound absorbs the laser light energy and re-emits light at a longer wavelength that can be detected by a photo detector.
- A CCD camera equipped with a sharp cut-off or narrow band filter, so that fluorescent light is recorded. This camera acts as an array of light detectors (pixels).

II.2.1 Fluorescence and tracer dye

Fluorescence is a natural property of matter. It physically corresponds to an atomic excitation process with emission of a photon of lower energy than that of the excitation light. In other words, when light is sent to excite a given medium, that medium re-emits light at a longer wavelength (λ_{Em}) than the excitation wavelength (λ_{Ex}). The technical challenge thus consists in capturing the fluorescence and filtering out the excitation (laser) light, which is considered as ‘noise source’. This is made possible thanks to the shift between excitation and emission spectra and the use of optical filters that only let the re-emitted light to enter the detector. The fluorescence intensity (noted F) varies with the local excitation energy inside the sampling volume considered (E and V_c respectively), the concentration (C) and the temperature (T) inside V_c and the physical properties of the medium used. Other optical parameters that vary from experiments to experiments also influence the fluorescence level. These parameters are regrouped under the variable f_{optic} and are determined by calibration. The second technical challenge consists in relating the intensity of fluorescence (minus that absorbed on the light pathway) to the local concentration or temperature, using the integral correlation:

$$F = f_{optic} \cdot A_C \cdot V_c \cdot (EC) \cdot Q_\lambda(T) \text{ with } A_C = e^{-\varepsilon L \cdot C} \quad (\text{II- 13})$$

where f_{optic} is a factor corresponding to the optic set-up, $Q_\lambda(T)$ is the quantum efficiency of the dye at the temperature T , when excited at the frequency λ , A_C corresponds to absorption phenomena, which are integrated on the light pathway L . The parameter ε represents the absorption factor of the fluid.

For a medium with a quantum efficiency that is not temperature dependent, one can derive the concentration directly from the fluorescence using the formula:

$$F = \alpha_c \cdot A_c \cdot (EC) \text{ with } \alpha_c = f_{optic} \cdot V_c \cdot Q_\lambda \quad (\text{II- 14})$$

For a medium with a quantum efficiency that varies with the temperature and a known (constant) concentration, the temperature can be determined from the fluorescence using the formula:

$$\Delta F \approx \alpha_T \cdot A_T \cdot (EC_0) \cdot \Delta(T) \cdot \Delta Q_\lambda \text{ with } \alpha_T = f_{optic} \cdot V_c \text{ and } \Delta\Phi = (\Phi - \Phi_{REF}),$$

$$\Phi = F, \text{ Tor } Q_\lambda \quad (\text{II- 15})$$

At low concentration levels, absorption phenomena are very weak (i.e. $A \approx \text{unity}$) and (when the laser excitation power is known: $E=E_0$) the local concentration or temperature are determined from the re-emitted fluorescence using the formulae:

For the concentration:

$$C \approx \frac{F}{\alpha_c \cdot E_0} \quad (\text{II- 16})$$

II.2.1.1. General considerations on fluorescent dyes

When implementing planar-LIF measurements in liquids e.g. for mixing analysis, one marks one fluid (say fluid F1) and mixes it into a fresh fluid F2 or vice-versa. Selecting the appropriate marker (fluorescence dye) to tag the fluid F1 can be a difficult task. To do so, one must match the properties of the dye selected with the equipment (the light source) used and the chemical property of the dye (e.g. diffusivity, fluorescence response, etc.), according to the physical data one wishes to collect.

All substances do not behave identically with respect to fluorescence. To choose the appropriate marker, several spectral factors are to be considered. These are the absorption wavelength range, the emission wavelength range and the quantum efficiency of the marker. Absorption and emission spectra provide information on the type of laser that can be used to excite the dye and the type of light re-emitted (consequently the filter to be used), respectively. The quantum efficiency on the other hand tells about the intensity of re-emitted light and is therefore related to the precision of the data, as is further discussed in the next chapters. In general, markers with high quantum efficiency are recommended to get planar-LIF measurements of good quality.

II.2.1.2. Laser / Dye combination –notion of spectral conflict

Among the variety of markers available, Rhodamine 6B is selected for our experiments. The absorption and emission spectra of this dye are drawn in Figure II-12. The energy absorption spectrum is found to be at wavelengths between 460 and 590 nm, with a peak around 520 nm. This characteristic makes the marker very well suited for experiments for which a frequency (single- or double-cavity) Nd:YAG laser is used ($\lambda_{\text{Nd:YAG}} = 532 \text{ nm}$). Furthermore, the fluorescence spectrum (between 550 and 650-670 nm) does not conflict too much with absorption spectrum. Filtering the signal with the appropriate filter with a cut-off at about 550/570 nm, the laser light can be blocked and only the fluorescence light reaches the sensor.

Spectral conflicts are the source of many problems because they cannot be detected during calibration. The only way to identify spectral conflicts is to refer to the literature or to carry out spectral analyses. Strong overlapping-spectra lead to the next physical events: the local fluorescence that is re-emitted by the excited marker (due to the laser light) sort of “re-excites itself and the surrounding molecules of marker” (self-quenching). In such configurations the local fluorescence is no more only related to the experimental set-up but varies with the local spatio-temporal signal; i.e. the physics of fluid motion. In turbulent flows, the use of such a type of marker renders quantitative analysis impossible. With Rhodamine, the overlapping is considered to have a relatively small impact on the final results. However, this has never been quantified in the literature.

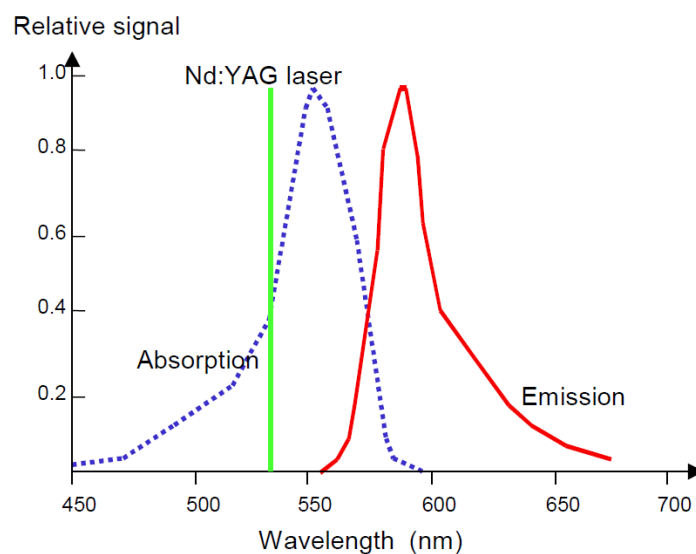


Figure II- 11. Laser signal response.(courtesy Dantec Dynamics)

II.2.1.3. Notion of photo bleaching

During LIF-experiments, if the laser energy is too high or if the photochemical stability of the dye used is too weak, the marker can be destroyed from laser pulse. This laser induced photo decomposition of the dye is known as *photobleaching* and leads to very large inaccuracy. Effectively, if a certain (unknown) amount of the marker does not respond to excitation, the fluorescence light re-emitted is considerably reduced in comparison with the initial system. Since it is impossible (or technically very difficult) to determine the quantity of dye that is locally destroyed, the results become obsolete.

II.2.1.4. Tracer dye Rhodamine 6G

Rhodamine 6G is a chemical compound and a dye. It is often used as a tracer dye within water to determine the rate and direction of flow and transport. Rhodamine B is the most frequently used dye for planar-LIF measurements in water for the following reasons:

(i) The dye is highly soluble in water (and in alcohol) and its chemical stability is high for very large range of concentration levels, which enables long storage periods.

(ii) The quantum efficiency of Rhodamine is very high, which leads to very high fluorescence signals.

(iii) Photo bleaching effects are known to be very weak (unless extremely high excitation energy levels are used, which is not necessary since the quantum efficiency of this marker is high).

(iv) The spectral characteristics of the dye are optimal, when used in combination with Argon ion (green) or preferably Nd:YAG lasers. Effectively, the laser wave length (514 and 532 nm respectively) matches perfectly the range of excitation of the dye and is close to the optimal excitation wave length (526 and 580 nm respectively) of the Rhodamine B.

(v) The quantum efficiency is very high and is used for concentration measurement. The main spectral and chemical characteristics of the molecule are reported in Table II-2.

Rhodamine 6G	Lower	Upper	Optimal
Absorption wavelengths (nm)	460	560	530
Emission wavelengths (nm)	540	640	560
pH sensitivity	No		
Temperature sensitivity	Very low - to none		

Table II- 3. Temperature dependency of the fluorescence signal of Rhodamine 6G (at the peak excitation wavelength).

The chemical structure of Rhodamine 6G ($C_{28}H_{31}N_2O_3Cl$, molar mass 479 g/mol, molecular Schmidt-number 800 in water) is shown in Figure II-12.

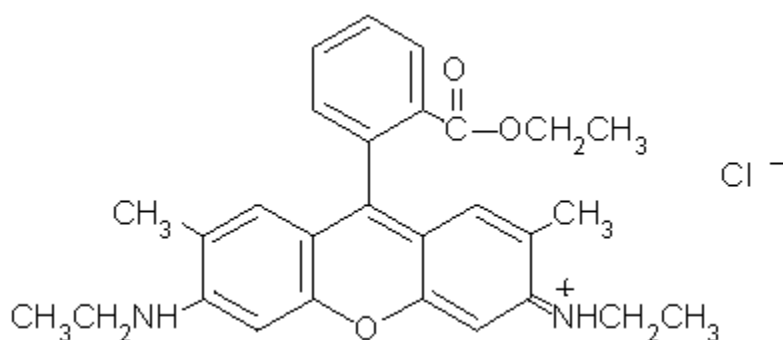


Figure II- 12. Chemical structure of Rhodamine 6G.

Due to its molecular configuration (presence of aromatics), the operator should be aware of potential toxicological hazards. Rhodamine 6G is about 400 times less toxic than nicotine, with an LD_{50} at 88.7 mg/kg in mice for oral injection, LD stands for "Lethal Dose". LD_{50} is the amount of a material, given all at once, which causes the death of 50% of a group of test animals. The LD_{50} is one way to measure the short-term poisoning potential (acute toxicity) of a material.

II.2.2. PLIF system

II.2.2.1. Description of the PLIF system used

PLIF system of "Dantec Dynamics" is used in this study. This system is composed of the following accessories:

(i) a laser source of the Nd: YAG double cavity (50 mJ) which emits laser beams whose wavelength is equal to 532 nm. In the midst of action and because of malfunction, the laser source has been replaced with another source, which is more powerful (65 mJ) (Fig. II-13).

(ii) HiSense Neo camera for high quality imaging, specifications are in the Figure II-16.

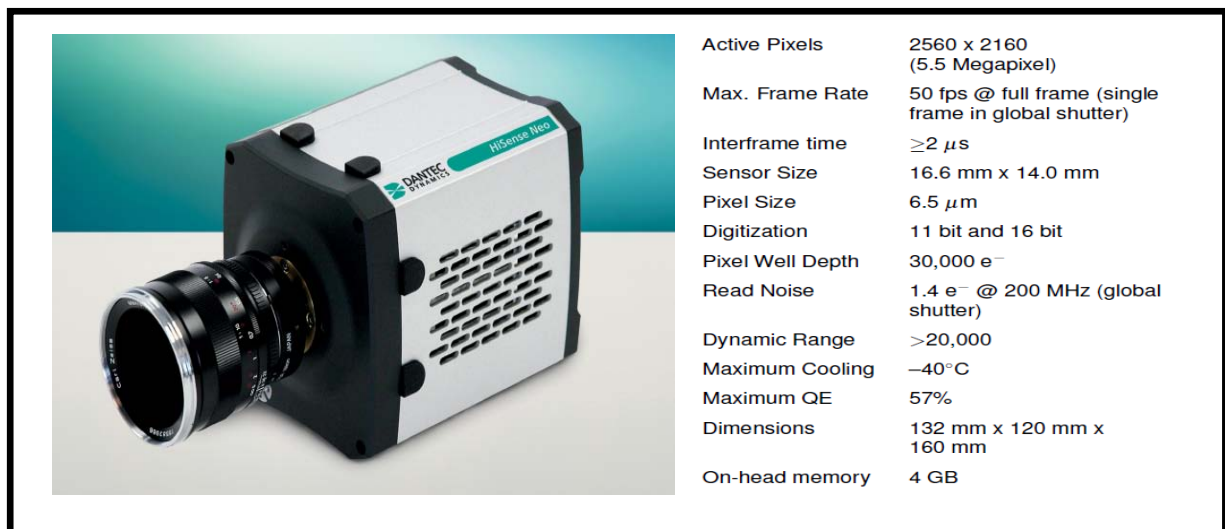


Figure II- 13. Camera of the PLIF system used

(iii) a control system in which all tasks concerning the management of the system, acquisition and image processing software used in this control system is "Dynamic Studio" version 2.30.

(iv) a synchronization box connected to the control system, the laser, camera and the switch.

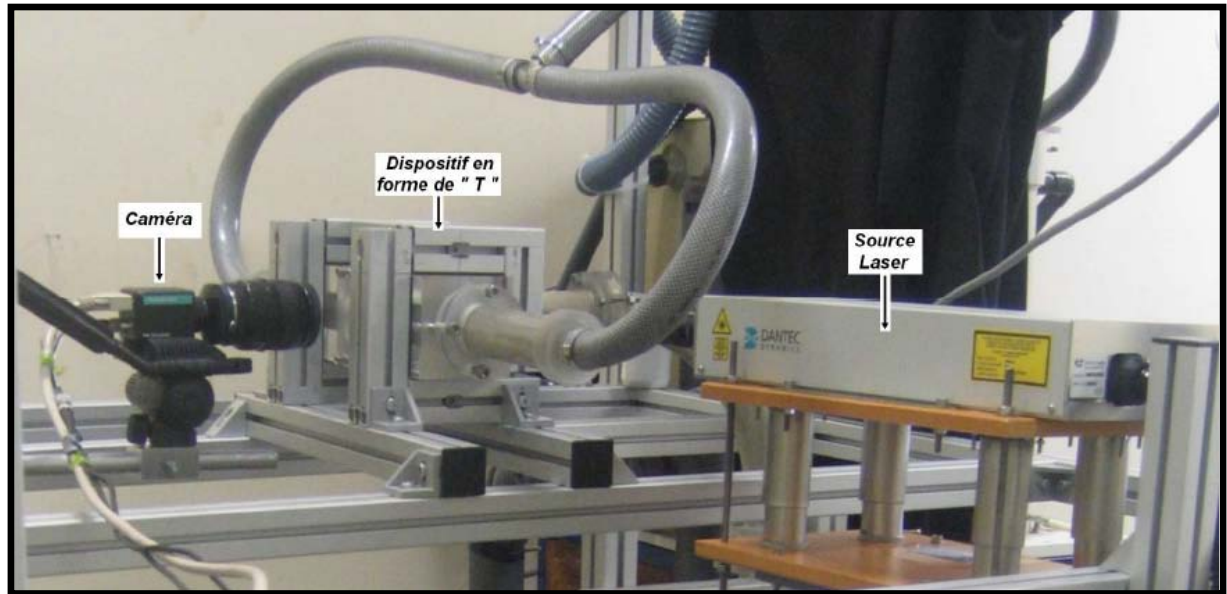


Figure II- 14.T shaped flow divider.

(v) a camera filter intended for diagnostics of liquid mixing using Laser Induced Fluorescence. This is done using a laser beam/sheet with the wavelength of 532 nm to excite the tracer species Rhodamine. The subsequent fluorescence is broad-band and is shifted towards red as compared to the excitation wavelength. The filter suppresses scattered laser light well and at the same time has a high transmission at the detection wavelengths above 570 nm.

II.2.2.2.Synchronization

Due to the temporal dependence of the flow, the PLIF measurements in precise moments in each of the oscillation period will only be possible by synchronization acquisition system with the movement of the piston. For this purpose, a pin is attached on the top of the crank, which works as a switch powered by 31.5V. The data acquisition system connected to this switch receives an intermittent signal from 0 to 4.5 Volts from the onset of the switch each contact with the tower top. Transmitting the signal from the switch to the center is acquired by means of the synchronization box. Once the acquisition system receives the signal, it waits hang a delay time, t_d , already stated by us in the acquisition software (Dantec Dynamics) and then acquisition is done.

The time delay, t_d , depends on two parameters:

(i) t_d depends on the frequency value of the parameter, α , or more simply the angular velocity, ω , of the crank.

(ii) t_d also depends on the precise instant in which the PLIF the measurement oscillation period must be achieved. This instant corresponds to a phase angle, ωt .

The position of the top pin on the circumference of the crank is such that the time of contact between the top pin and the switch, the phase of oscillation of the piston is equal to $\omega t = 180^\circ$. This means, if image acquisition is done at time ($t_d = 0$), then the velocity field obtained corresponds to the phase $\omega t = 180^\circ$. Taking into account the direction of movement of the piston (Fig. II-15) and the angular velocity of the crank, t_d can be calculated for other phases of oscillation. If the pulsation period is T :

$$t_d = \frac{i \cdot T}{4} = \frac{i \cdot (2\pi/\omega)}{4} = \frac{i \cdot \left(\frac{2\pi}{\frac{a^2 v}{r_0^2}} \right)}{4} \begin{cases} i = 0, & \text{if } \omega \cdot t = 180^\circ \\ i = 1, & \text{if } \omega \cdot t = 270^\circ \\ i = 2, & \text{if } \omega \cdot t = 0^\circ \\ i = 3, & \text{if } \omega \cdot t = 90^\circ \end{cases} \quad (\text{II- 17})$$

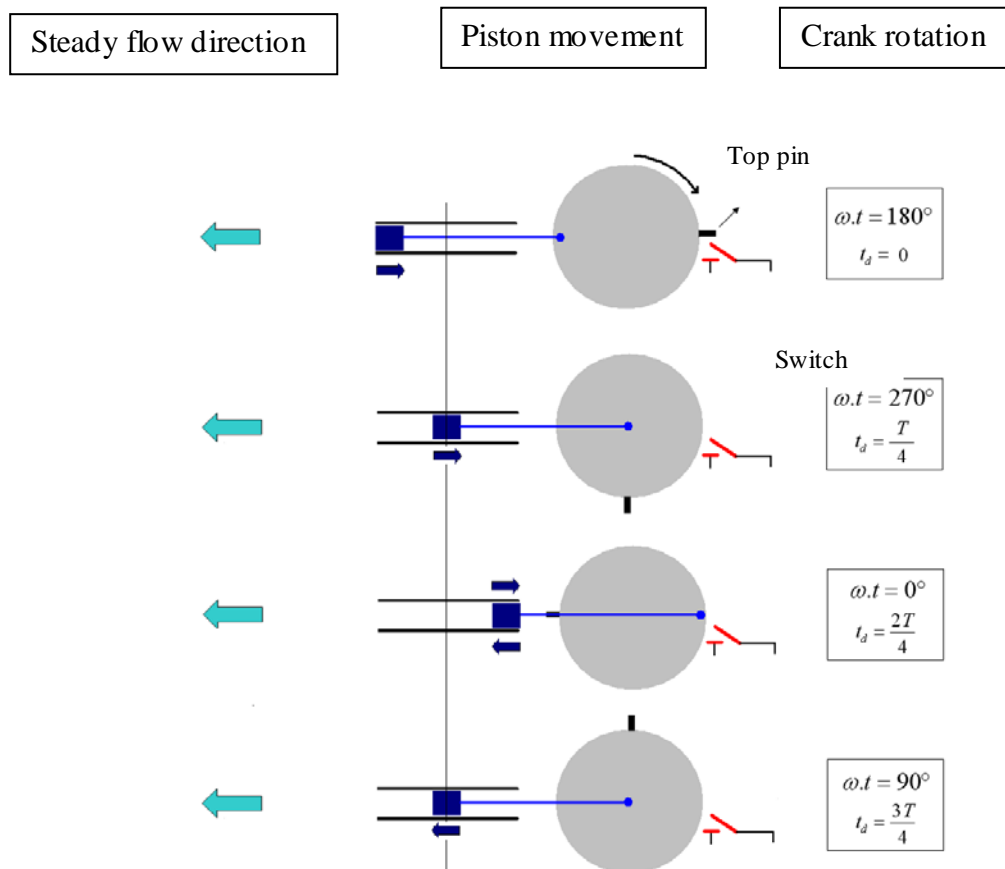


Figure II- 15. Piston positions at different phases of oscillation.

The calculated values for the time delay, t_d , are shown in Figure II-16. These values are entered in the "Dynamic Studio" software to control the photo taking time.

		Oscillation phase ($\omega.t$)			
		0°	90°	180°	270°
		Time delay t_d in μs			
Frequency parameter α	8.37	18072728	27109092	0	9036364
	10.26	11933174	17899761	0	5966587
	11.24	9940000	14910000	0	4970000
	12.14	8495726	12743590	0	4247863
	14.51	5952380	8928570	0	2976190
	15.4	5287234	7930851	0	2643617
	17.77	3976000	5964000	0	1988000
	20.53	2984984	4477476	0	1492492
24.5	2092632	3138948	0	1046316	

Figure II- 16. Time delay.

II.2.2.3. PLIF measurements and data treatment

Software Dynamic-Studio provided by Dantec Dynamics (version 2.30) is used for controlling the PLIF acquisitions and processing of images.

The camera is positioned in front of the viewing window (Fig. II-14) and the thickness of the laser plane is set to 2mm. After the camera focused on the illuminated section (outlet of the bend), the images of the flow in circular section of diameter 0.04 m are recorded. The dimensions of this framework for action in the first bend exit are 68.3 mm \times 68.3 mm and the resolution of the images obtained is 2048 pixels \times 2048 pixels.

To determine the scale factor, we selected the "Single Frame" acquisition and takes a single photo of the illuminated section. This picture is registered under the "Save for Calibration" in the database. In the option "Measure Scale Factor", two point are selected A and B at the ends of a diameter of the section specifying the value of their distance in millimeters in order to compute the scale factor that is required to convert the pixels in millimeters.

Once the scaling factor is determined, then the flow conditions are set by adjusting the length of the crank and the rotational speed of the flywheel in order to produce the different pulsation cases depending on Re_{st} , β and α (using Table II-1).

- **Stationary flow:** If the measurements relate to a steady flow (i.e. the pulse generator is not involved in the circuit of flow), the mode of trigger selected in the property class of the device is "internal", as laser and the camera will automatically trigger and measurements are taken several times to perform statistical processing.
- **Time-dependent flow:** For measurements in the case of a pulsated flow or sinusoidal, a cable connects the switch (see Figure II-17) to one input (Input 1) of the box synchronization. This time, the trigger mode selected is "external" because to reach measurement, the laser will not operate after a period t_d after the reception of the signal sent by the external switch (see Section II-2.2.2).

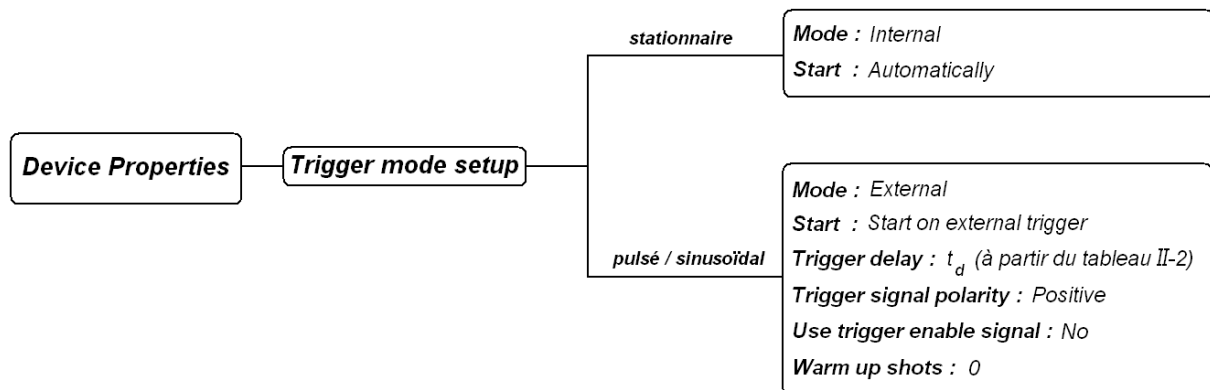
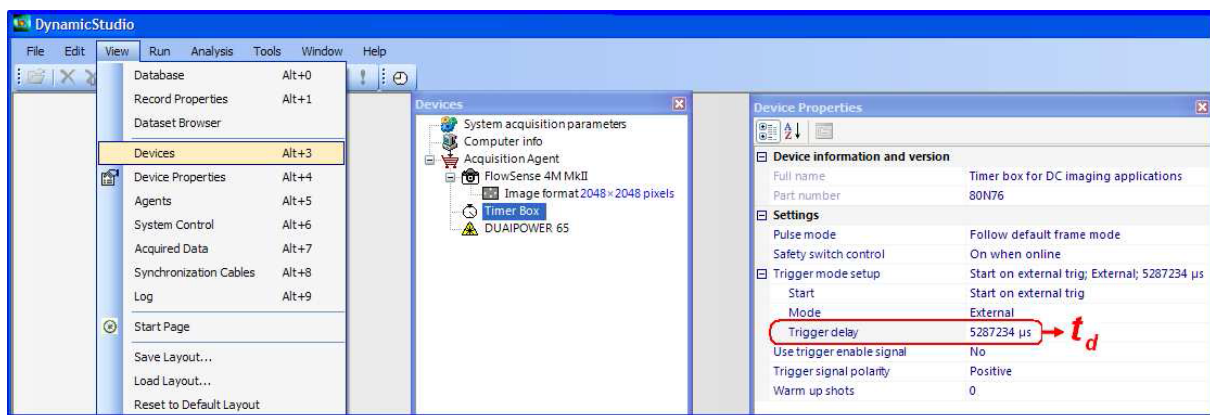


Figure II- 17. Trigger mode and Time delay PLIF System (Jarrahi, 2010)

After setting the configuration of the PLIF system, the time lag between laser exposure, Δt must be calculated for each case measurement. As explained in the section II.2.1.4, for a reliable, correct choice of this lag is essential. For a steady flow, Δt allows one to make measurements but a pulsatile flow, the appropriate value of Δt differs from swing

phase to another as the flow velocity varies during an oscillation period and Δt is strongly this speed dependent. This requires a search Δt for each phase oscillation where the measurement should be performed. Given that in this study, four time (phase) of the oscillation period corresponding to phases $\omega.t = 0^\circ, 90^\circ, 180^\circ$ and 270° are essentially covered, four Δt are to be calculated for each condition of flow pulsation.

II.3. The intermittent heat exchanger

II.3.1. Schematic arrangement

An experimental setup was designed and fabricated in the LTN Laboratory, especially dedicated to the study of different pulsatile conditions onto the heat transfer in a chaotic twisted pipe configuration. This setup is a closed circuit and is composed of a computerized controlled pulsation pumping system, a shell and tube heat exchanger, temperature measuring blocks and two thermostats. One of the thermostats is to control shell side temperature and the other one is to control the inlet temperature in the tube side. A 2 m straight tube between heat exchanger and pulsation pumping system is installed to ensure a developed flow at the inlet of heat exchanger. A chaotically twisted copper tube comprising of 12 bends is submerged in a rectangular tank to form a shell-and-tube heat exchanger. A schematic diagram of the experimental setup is shown in II-18.

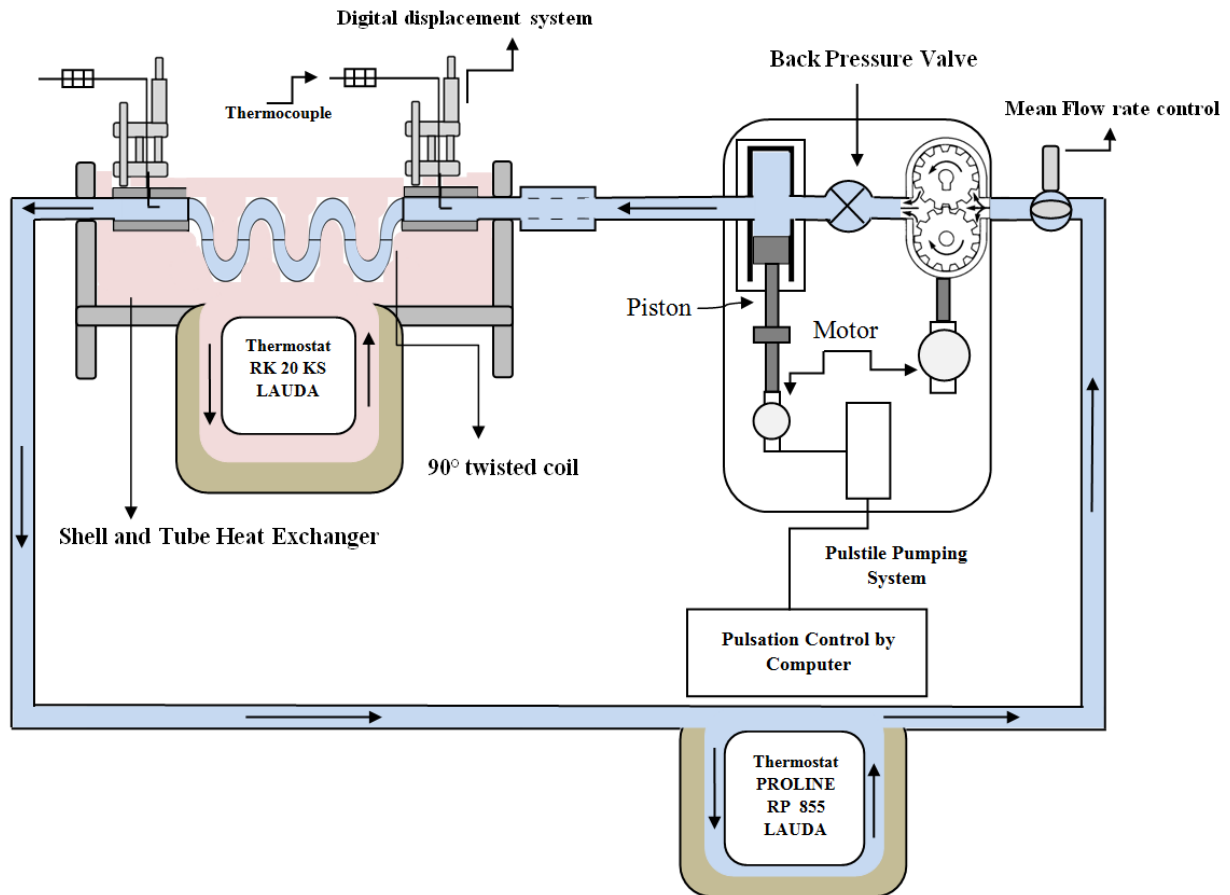


Figure II- 18. Experimental setup of the intermittent heat exchanger.

Digital displacement systems are used to move the K type thermocouples to measure the inlet and outlet temperatures. Thus entrance and exit temperatures of the tube side fluid are measured by two K-type thermocouples at inlet and at outlet and are fixed onto micrometric displacement systems. Therefore two probes at inlet and at outlet allow measurement of the intake and exit temperature profiles of the tube-side fluid along the tube diameter. The cold water with desired flow rate is pumped through a gear pump. The flow rate is controlled by a valve and measured through a flow meter. A platinum probe measures the fluid temperature in the shell. The working fluid in both shell side and tube side is water.

II.3.2. Pulsation pumping system

The pulsatile pumping system consists of a combination of a gear and a piston pump in series shown in Figure II- 19. The gear pump provides the steady mean component and is preloaded with a back-pressure valve at its discharge. A non-return back-pressure valve is installed after the gear pump discharge to avoid reverse flow as the reaction of the flow

pulsation. A piston pump composed of a stainless steel, honed cylinder housing of bore 20 mm and a stroke of 50 mm containing a piston. The capped end of the cylinder has the flow ports. The piston is driven by a servo motor attached to obtain the oscillating component piston actuated by a brushless linear motor. The movement is controlled in velocity mode by an analog signal between 0 to 10 V. This type of device has the advantage of allowing an easy transition to a sinusoidal, square and triangular signal wave forms.

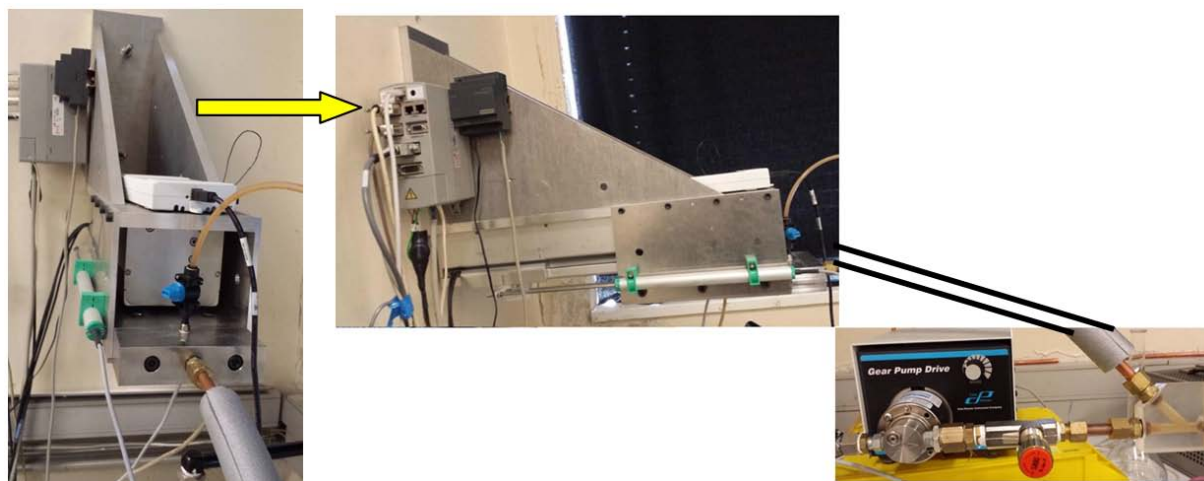


Figure II- 19. Pulsation system designed and assembled for the intermittent heat exchanger.

A function generator is produced under LABVIEW acquisition system with NI USB6211 case. The selected linear motor is capable of creating perturbation to the fluid of a maximum frequency of 8 Hz and a maximum instantaneous flow of 10 L/min. However the steering gear exhibited a gradual drift of the piston to its mechanical stops. To correct this problem, a linear position sensor is installed to check each time the position of the piston and make the necessary correction on the speed. This pulsation system is connected to the back-pressure valve and provides the oscillatory component of the flow wave form. In order to achieve reverse output flow, the piston pump draws fluid at a faster rate than the gear pump outputs. The gear drive used is of Cole-Parmer Instrument Company, works under maximum speed of 3000 rpm. The gear pump is driven with a constant flow rate to generate the mean flow, and the piston pump is driven with a variable voltage signal, however the system can easily be run from an analog signal generator or computer controlled digital signal generator with the appropriate hardware. Flow rates are measured by a Cole-Parmer Instrument Company flow meter.

II.3.3. Chaotic heat exchanger

The chaotic heat exchanger consists of a twisted tube of 1.15 m in length and an inner diameter of 8 mm. This twisted tube shown in Figure II- 20 is actually built by the assembly of series of 12 bends whose dimensions are: bend curvature radius 44 mm, curvature angle in bend plane 90°, curved length of a bend is 0.878 m and the straight length between every bend is 0.008m.

The heat exchanger is immersed in 300 mm×400 mm×250 mm rectangular shell of stainless steel filled with hot water. The hot fluid is kept constant in the shell side with a low-temperature thermostat RK 20 KS LAUDA. The cold fluid is circulated in the twisted tube, the inlet temperature is controlled by a cooling thermostat RP855 LAUDA.

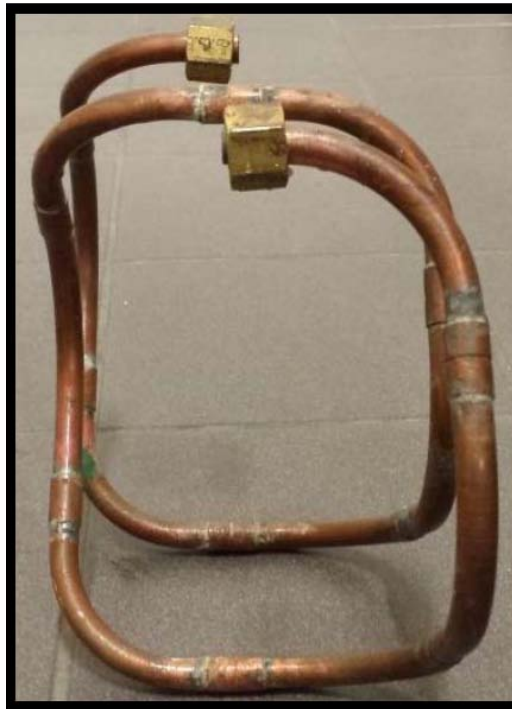


Figure II- 20. Chaotic twisted tube heat exchanger immersed in the tank.

The temperature measurements are recorded through an Agilent Bench Link Data Logger. To obtain the temperature profiles, thermocouples can be moved vertically from upper inner wall to the lower inner wall of the tube. Temperature is measured at 8 different

vertical points in the tube. The Figure II-21 shows digital displacement system and K type thermocouple.

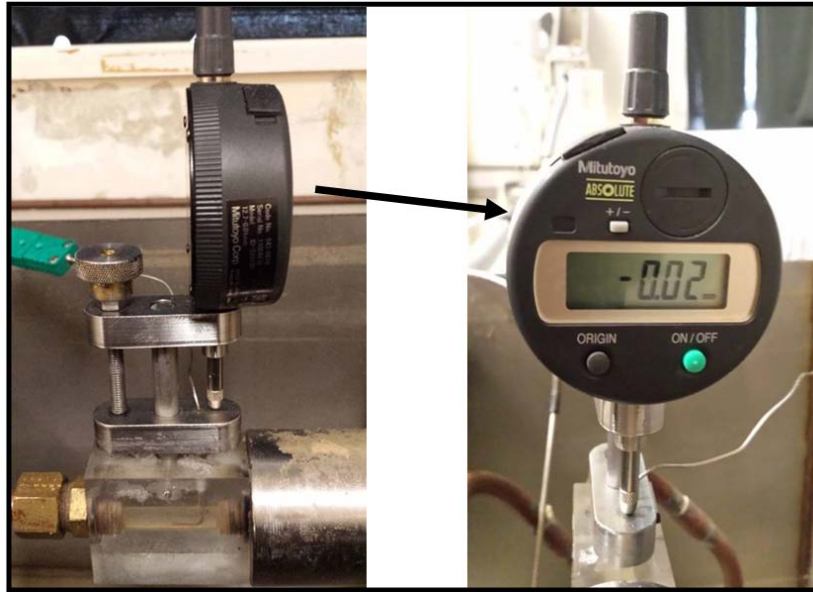


Figure II- 21. Digital displacement system and K type thermocouple.

II.3.4. Pulsation parameters and conditions

The velocity amplitude ratio β and the Womersley number α can be calculated in the following manner, in which V_{piston} is the velocity of the piston, Q_{sin} is the sinusoidal flow rate, S_{piston} is the cross-sectional area of the piston, and S_{tube} is the cross-sectional area of the tube used in the heat exchanger.

The velocity of the piston V_{piston} :

In the pulsation system the velocity is in Volts. Therefore to obtain velocity of the piston in m/s with our pulsation system used, we must multiply it with an scale factor of 0.1 to obtain velocity in m/s.

$$V_{piston} = 0.1 \times \text{Amplitude of the function generator} \quad (\text{II- 18})$$

The sinusoidal flow rate Q_{sin} is ;

$$Q_{sin} = V_{piston} \times S_{piston} \quad (\text{II- 19})$$

The sinusoidal maximum velocity $V_{sinusmax}$

$$V_{sinus\ max} = \frac{Q_{sin,max}}{S_{tube}} \quad (\text{II- 20})$$

The velocity amplitude ratio β

$$\beta = \frac{V_{sinus\ max}}{V_{steady}} \quad (\text{II- 21})$$

where V_{steady} is the steady velocity of the fluid flowing through the tube.

The Womersley number α is ;

$$\alpha = r_{tube} \times \left(\frac{\omega}{\vartheta}\right)^{\frac{1}{2}} \quad (\text{II- 22})$$

where $r_{tube} = 0.004$ m is the radius of the tube, ϑ is the kinematic viscosity of the water and ω is the angular frequency (i.e. $\omega = 2\pi f$ where f is the frequency).

The pulsation conditions imposed on the flow are recapitulated in Table II-4 and II-5. Table II-4 represents the different Womersley frequency parameter α calculated by adjusting frequency in the pulsation system used for thermal measurements.

f (Hz)	$\omega = 2\pi f$	α
0	0	0
0.4	2.512	6
0.6	3.768	8
0.8	5.024	9
1	6.28	10
1.25	7.85	11
1.5	9.42	12
1.75	10.99	13
2	12.56	14
2.5	15.7	16
3	18.84	17
3.5	21.98	19
4	25.12	20

Table II- 4 Amplitude frequency and Womersley parameters

Table II-5 represents the different velocity amplitude ratio β calculated by adjusting amplitude in the pulsation system to perform for thermal measurements for the intermittent heat exchanger.

Amplitude	V_{piston} m/s	Q_{sin} m ³ /s	$V_{sinus,max}$ m/s	β
0.16	0.016	0.000005024	0.1	1
0.32	0.032	0.000010048	0.2	2
0.48	0.048	0.000015072	0.3	3
0.64	0.064	0.000020096	0.4	4
0.96	0.096	0.000030144	0.6	6
1.28	0.128	0.000040192	0.8	8
1.6	0.16	0.00005024	1	10
2.08	0.208	0.000065312	1.3	13
2.56	0.256	0.000080384	1.6	16

Table II- 5 Amplitude and velocity amplitude ratios

Chapter 3

Mixing intensification by pulsatile flow

Objectives

The objective of this chapter is to study the transverse mixing due to various structures of secondary flow in the steady and pulsatile state, in a 90° pipe bent, which constitutes a basic element in vast categories of open loop mixers. Understanding the effects of pulsation for mixing enhancement in this geometry has a great importance for the development of applications in more complex geometries (helical or chaotic ones). The PLIF technique is used to measure the concentration field in the section, and the different structures can be observed and described. The mixing enhancement due to pulsation is evaluated by the degree of mixing, based on the concentration variance.

III.1. PLIF measurements

In this section, the mixing enhancement by a pulsatile flow in a 90° degree curved pipe is assessed by the tracer diffusion. Though Jarrahi (2010) has discussed in detail the structures of the secondary flow in this configuration, it still remains a lack of accurate information about mixing quantification.

At the exit of a 90° degree curved pipe with a curvature ratio $\theta = \frac{r_o}{r_c}$ equal to 0.09, PLIF measurements are carried out by injecting a tracer, Rhodamine 6G, at the center of the straight pipe through a needle of 1 mm diameter. The distance between the injection system and the inlet of 90° curved pipe is 500 mm.

III.1.1. Operating conditions

According to the definitions presented in Chapter I, the velocity of the pulsatile flow U_p is:

$$U_p = U_{st}(1 + \beta \sin(\omega t)) \quad (\text{III-1})$$

where U_{st} represents the steady component of the velocity, β is the velocity amplitude ratio and ω is the angular velocity of the sinusoidal component.

A T-shape structure is positioned at the exit of the curve to avoid problems of light refraction and a tracer injection system is installed at upstream (details are given in Chapter II). Hereafter, the obtained PLIF images are described and their alterations with flow rate oscillation are discussed, the tracer diffusion is discussed in a simple mixing process, then, visualizations and quantitative analysis are provided for the quantification of mixing with and without pulsation.

Table III-1 recapitulates the frequency values used for the runs, and the corresponding Womersley number α . By varying the motor speed from 167 rpm to 1004 rpm, the setup allows sinusoidal pulsations at a frequency in the range 0.03 Hz to 0.17 Hz, which correspond to Womersley parameter varying from 8 to 21 (calculation procedure is explained in Chapter II.1).

Electric motor speed, N_o (rpm)	Angular velocity, ω (rad/s)	Frequency, f (Hz)	Womersley parameter, α
167	0.18	0.03	8.4
251	0.26	0.04	10.3
301	0.32	0.05	11.3
351	0.37	0.06	12.2
501	0.53	0.08	14.5
565	0.59	0.09	15.4
752	0.79	0.13	17.8
952	1.00	0.16	20.0
1004	1.06	0.17	20.6

Table III-1 Frequency parameters imposed in the 90° curved pipe.

Table III-2 describes the different pulsation conditions used to perform the experiments in this study. The Reynolds number is taken at four values 420, 600, 800 and 1000, the amplitude velocity ratio is taken at values 1, 2 or 3 when technically possible and the Womersley frequency parameter α is taken at six different values between 8 and 21 when technically possible. As the pulsation conditions depend on the crank position and motor speed, it is not possible to obtain the pulsation conditions combinations with all values of α and β .

Reynolds number, Re_{st}	Fluid velocity, U_{st} (m/s)	Amplitude velocity ratio, β	Womersley frequency parameter α					
420	0.0105	1	8	10	-	15	18	-
		2	8	10	12	-	-	21
		3	-	-	-	15	-	-
600	0.015	1	8	10	12	-	-	-
		2	8	10	-	15	-	-
800	0.020	1	8	10	12	15	-	-
1000	0.025	1	8	10	11	15	-	-

Table III-2 Pulsation conditions imposed in the 90° curved pipe.

III.1.2. PLIF calibration

To calibrate a LIF setup, images must first be acquired at known experimental conditions *i.e.* concentration or intensity of laser as calibration images. For this calibration, the intensity of laser light for all concentrations is kept constant. A double cavity laser of the type Nd :YAG (65 mJ) which emits the beams with wavelength of 532 nm was used to carry out the measurements.

To get reference PLIF images, a series of images of a calibration test section corresponding to different concentrations is recorded. A series of 50 images for each concentration ranging between 0 to 100 $\mu\text{g/L}$ of a calibration test section corresponding to different concentrations is recorded. The gray value response of the camera is then monitored to ensure a linear response to the dye concentration. This procedure is used to find the appropriate maximum concentration solution. Calibration curve is obtained in such a way that the experimental setup, laser and the optical arrangements are on the same positions. An analog beam monitor is also used to monitor the laser energy.

Mean images of the 50 instantaneous images shown in Figure III-1 for each concentration tested: nine homogeneous solutions of known concentrations of Rhodamine 6G in the water between $C=0 \mu\text{g/L}$ to $C=100 \mu\text{g/L}$. We can clearly observe that the grey level of the images increases with the increase in the concentration.

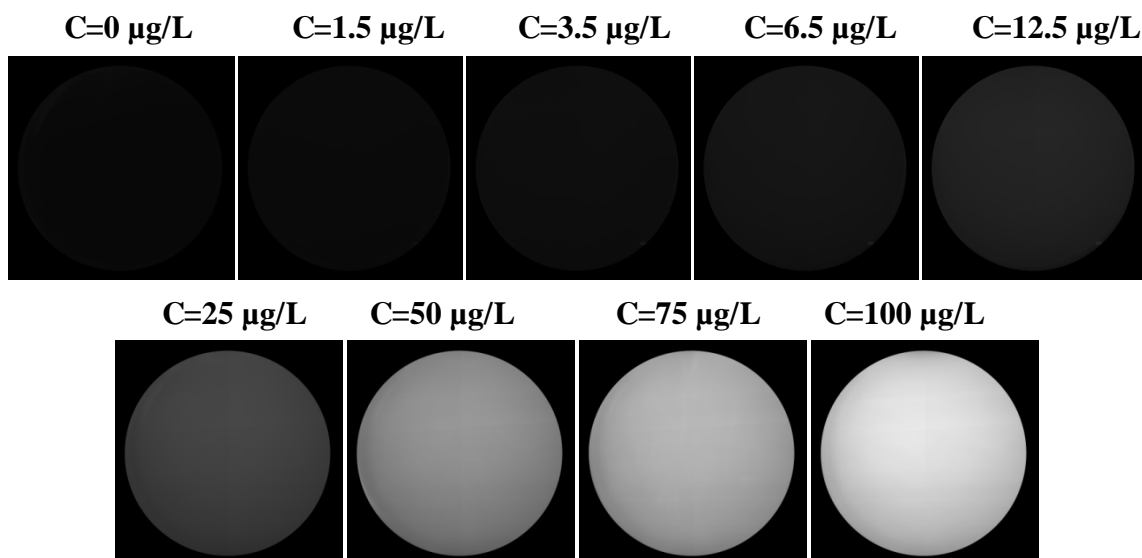


Figure III-1. Images for different concentration values of homogeneous solutions.

When all nominal concentration values have been entered along with laser pulse energies (if appropriate), the actual calibration can be performed. The linearity between the fluorescence signal (grey-level) and concentration defined locally is observed. It should be pointed out that the camera is sensible to detect even small concentration of 1.50 $\mu\text{g/L}$.

Figure III-2 shows PLIF calibration curve. The calibration curve includes for each and every pixel of the 2699540 pixels in the entire image, some of these will have stronger response to varying concentrations, and some will have weaker response.

The units of the luminous intensity are a.u. (arbitrary units). The measurements are carried out with an intensive surety of keeping the experimental conditions right from the calibration to the final experimental measurements constant. This means the laser intensity, camera aperture and position remain unchanged. The concentration C is then assigned to the detected fluorescence intensity I for each pixel $P(i,j)$ of the CCD camera ($i=1\dots 2048$, $j=1\dots 2048$). A linear correlation between I and C is verified. The calibration curve starts from a level different to zero, due to the luminosity in the laboratory.

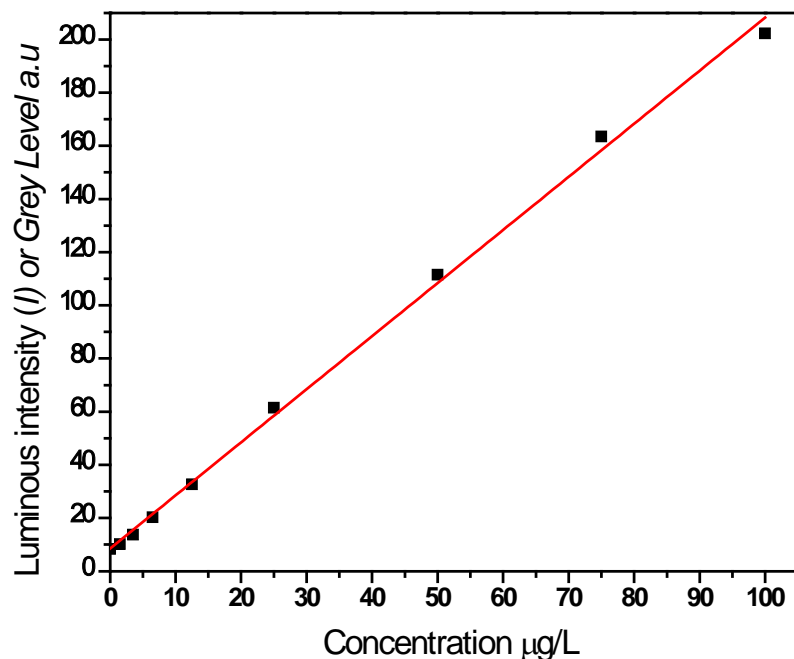


Figure III- 2. Calibration curve.

III.1.3. Mass balance of tracer dye for steady cases

Mass balance is carried out to verify the amount of tracer injected in the flow and the amount of tracer captured through the CCD camera. This is useful to know the threshold level of capturing the Rhodamine 6G of equipment used (i.e. CCD Camera, filter etc). This process allows to estimate the amount of tracer lost by the dilution and precision limit of the equipment used. Mass balance is verified by using the following relation:

$$C_0 = \frac{qC_q}{(Q + q)} \quad (\text{III-2})$$

where C_0 is the mean concentration injected in the section, C_q the concentration of solution injected, q the mean injection (colorant) flow rate and Q the main flow rate.

The Table III-3 recapitulates the measured injected concentration C_0 and the mean concentration \bar{C} measured on the section by the CCD camera used for experimentation. C_0 is measured by knowing the average mass flow rate and the concentration value of the tracer injected. For each Reynolds number Re_{st} it is then regulated in such a way that tracer does not disturb the streamlines of the main flow. It is assumed that amount of tracer is constant through the pipe section with a Reynolds number Re_{st} thus at the measuring point too. Then a mean concentration \bar{C} obtained through our PLIF setup, is compared with the C_0 injected. It is verified that the PLIF setup used is able to capture more than 90% of the injected concentration at $Re_{st}=420$. Then the amount of the concentration lost is in average around 14% for the different Reynolds numbers, it may be due to the threshold level of the camera, filter and other errors in experiment including human ones.

Reynolds number, Re_{st}	Q m^3/s	q m^3/s	$C_0 = \frac{qC_q}{(Q + q)}$ ($\mu g/L$)	\bar{C} ($\mu g/L$)	$\frac{(C_0 - \bar{C})}{C_0}$ measured
420	1.32×10^{-5}	4.7×10^{-8}	3.352	3.053	8.9%
600	1.88×10^{-5}	4.7×10^{-8}	3.711	3.023	18.5%
800	2.51×10^{-5}	4.7×10^{-8}	2.984	2.616	12.3%
1000	3.14×10^{-5}	4.7×10^{-8}	2.764	2.301	16.8%

Table III-3. Measured injected concentration C_0 and mean concentration \bar{C} observed by PLIF technique.

III.2. Qualitative study of mixing in pulsatile flow

III.2.1. Flow visualization in steady cases

Timité *et al.* [2005] presented an experimental and numerical studies of three-dimensional pulsatile flow in a twisted pipe in order to show the effects of chaotic advection on mixing in this flow configuration. PIV measurements for the same experimental setup were conducted by Jarrahi (2010). The secondary flow generated by centrifugal force, the pulsating velocity field and the change in curvature plane lead to irregular fluid particle trajectories. The studies revealed modifications in the trajectories evolution due to pulsation. The regular zones in the secondary flow decrease with an increase in the number of bends and with the pulsation conditions, i.e. Womersley pulsation frequency α and velocity-amplitude ratio β . These both phenomena contribute to the mixing and mass transfer enhancement.

Figure III-3 represents the tracer diffusion in steady state cases for four Reynolds numbers.

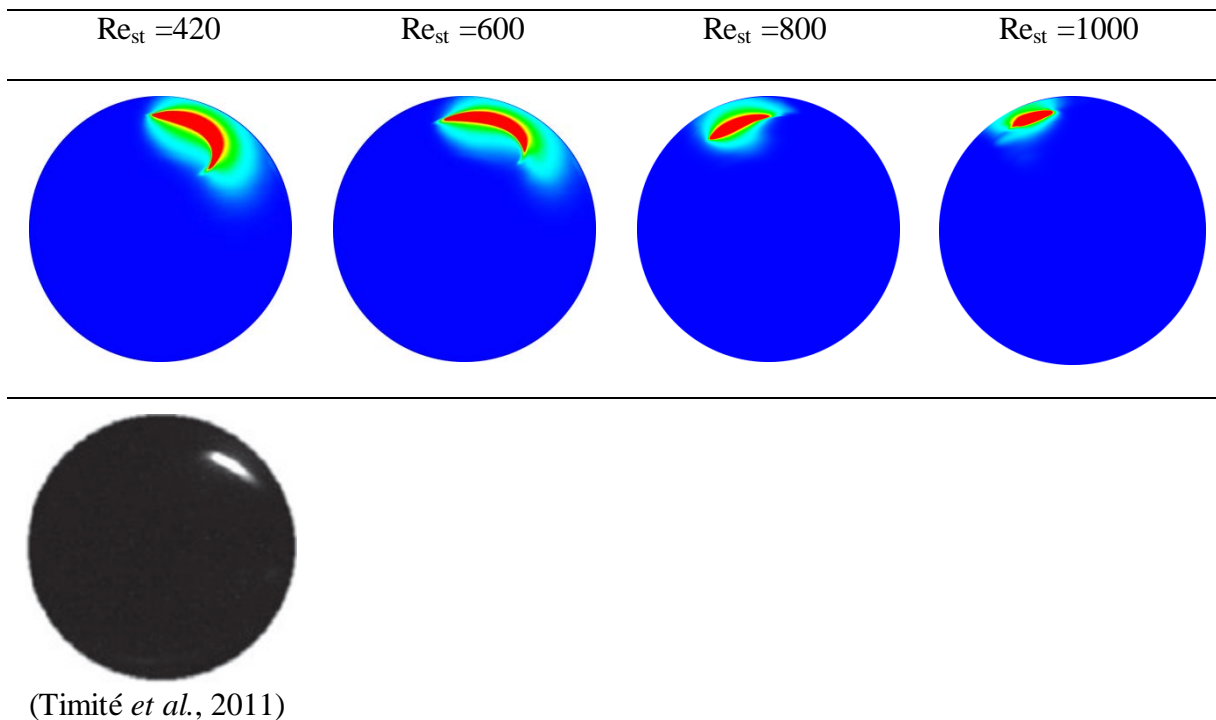


Figure III-3. Images obtained at the exit of a 90° curved pipe for different Reynolds numbers Re_{st} . The colors blue, green, and red show respectively the less, moderate and maximum concentration values.

The tracer remains near the upper wall. In the steady state flow fluid particles do not diverge and remain always in the upper part of the circular cross-section. Another phenomenon can be observed that the colorant spot in the pipe section decreases with the increase in Re_{st} . By comparing with results of Timité et al. (2011) we may observe that the colorant position in the circular section has remained in identical position. The PLIF technique clearly provides better quality images than Timité et al. (2011).

III.2.2. Flow visualization in pulsated cases

Due to pulsation imposition, the tracer dye deforms and occupies, under some pulsating conditions, more space in the pipe section compared to the steady cases. This is due to the pulsation effect that destructs or deforms Dean roll-cells structures in the flow. As mentioned in the introduction, different structures of secondary flow and mixing in a pulsatile flow through a curved pipe have already been investigated by some authors. The pulsation conditions when $\beta \geq 2$ and $\alpha \leq 15$ were found favorable conditions for mixing (Jarrahi *et al.*, 2009).

III.2.2.1. Influence of Reynolds number

Figure III-4 represents the tracer diffusion for different Reynolds numbers $420 \leq Re_{st} \leq 1000$ with pulsation condition $\alpha=10$ and $\beta=1$ and for the different phase angles of 0° , 90° , 180° and 270° . When the velocity amplitude ratio is unity ($\beta = 1$), the tracer is deformed in the boundary layer near the wall in the upper part of the section. Higher deformation of the tracer is observed and effective mixing zones are increased compared to the steady cases. Therefore, more surface is occupied by the tracer in the section. The tracer diffusion is different at different phase angles ωt and it seems difficult to see a mechanism which clearly depends on the Reynolds number.

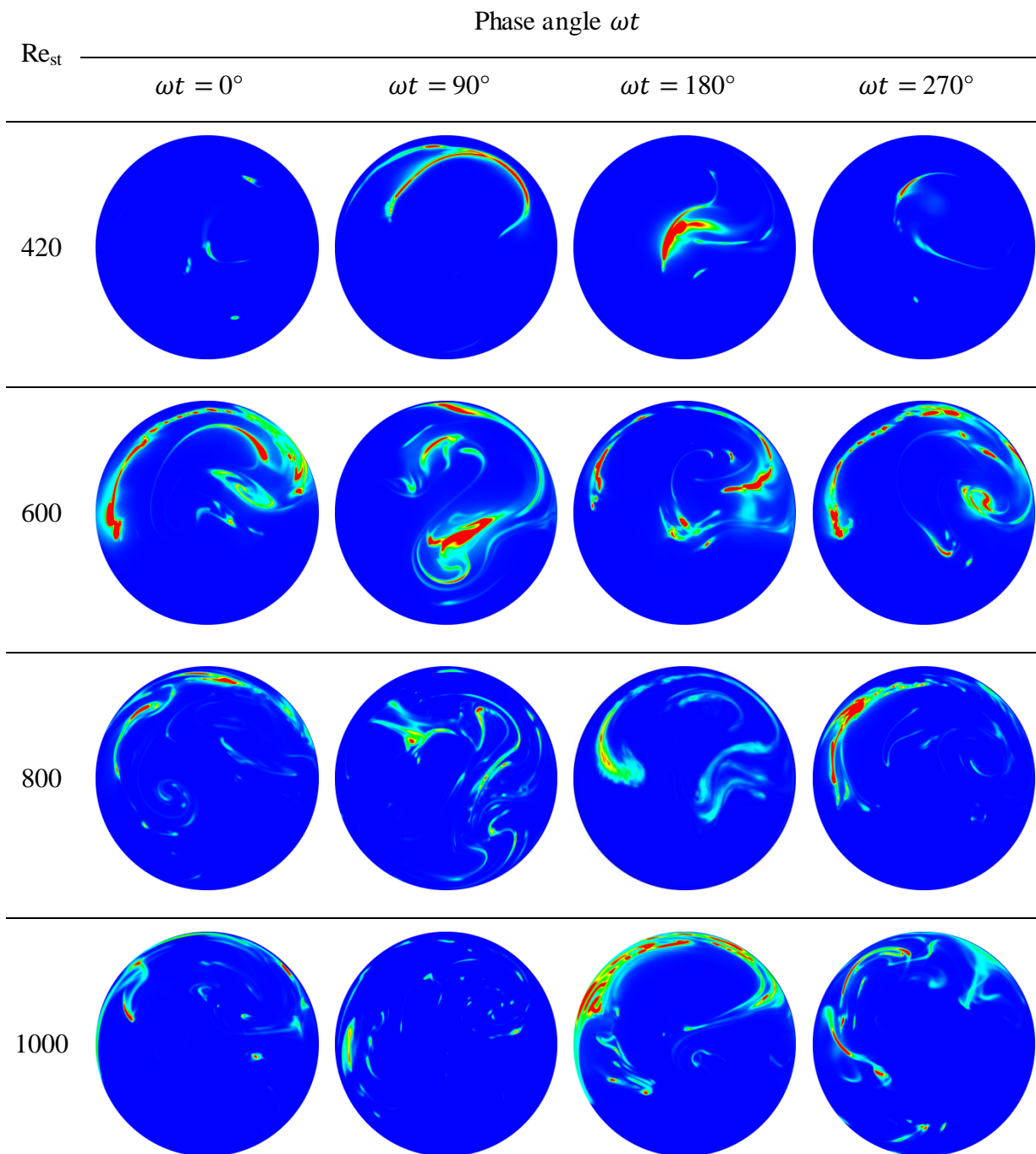


Figure III-4. Images obtained at the exit of a 90° curved pipe for different phase angles and Reynolds numbers, $\alpha=10$, $\beta=1$.

PLIF visualizations of the secondary flow for $Re_{st}=420$ and 600 , $\alpha=10$ and $\beta=2$ are shown in Figure III-5. The different pulsation conditions lead to different secondary flow patterns. When the velocity amplitude ratio is $\beta = 2$, the secondary flow is constantly modified with carrying one, two or three rotating roll cells with respect to the phase angle ωt or period of movement. The secondary flow structure becomes much more complex and the dye dispersion is enhanced as compare to the previous ones (i.e. $\beta=1$ and steady cases). The secondary flow at $\omega t=90^\circ$ and $\omega t=180^\circ$ is composed of two counter rotating Dean roll-cells. At the end of deceleration phase, i.e. $\omega t=270^\circ$, the both cells converge into single but bigger one on a very complex structure.

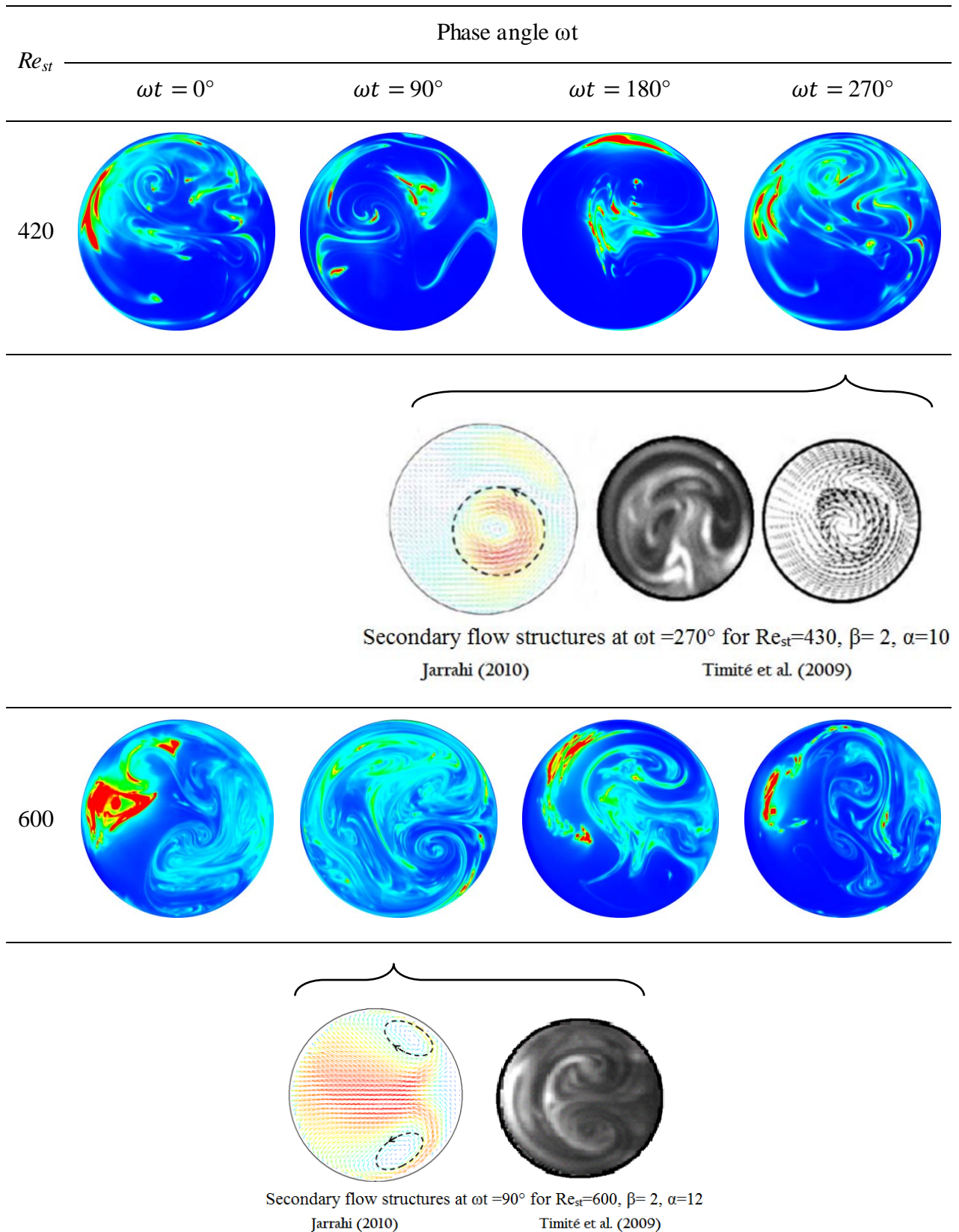


Figure III-5. Images obtained at the exit of a 90° curved pipe for different phase angles and Reynolds numbers for $\alpha=10$ and $\beta=2$.

III.2.2.2. Influence of velocity amplitude

Figure III-6 represents the tracer distribution for different velocity amplitude ratios $\beta=1, 2$ and 3 . We can observe the influence of β . The increase in velocity amplitude ratio results in more divergence of fluid particles. This increase in divergence creates more dye dispersion in the fluid, which leads to a better mixing.

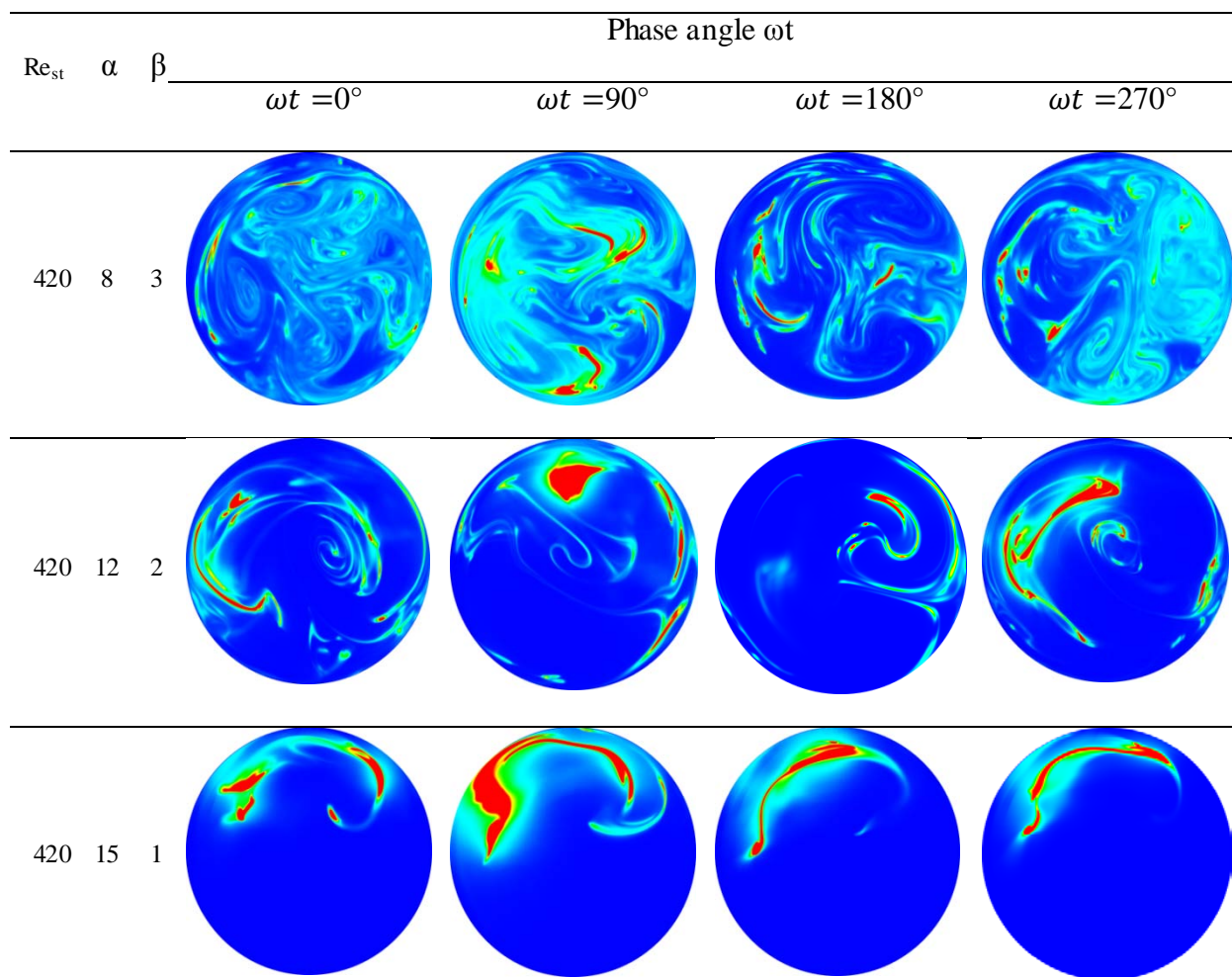
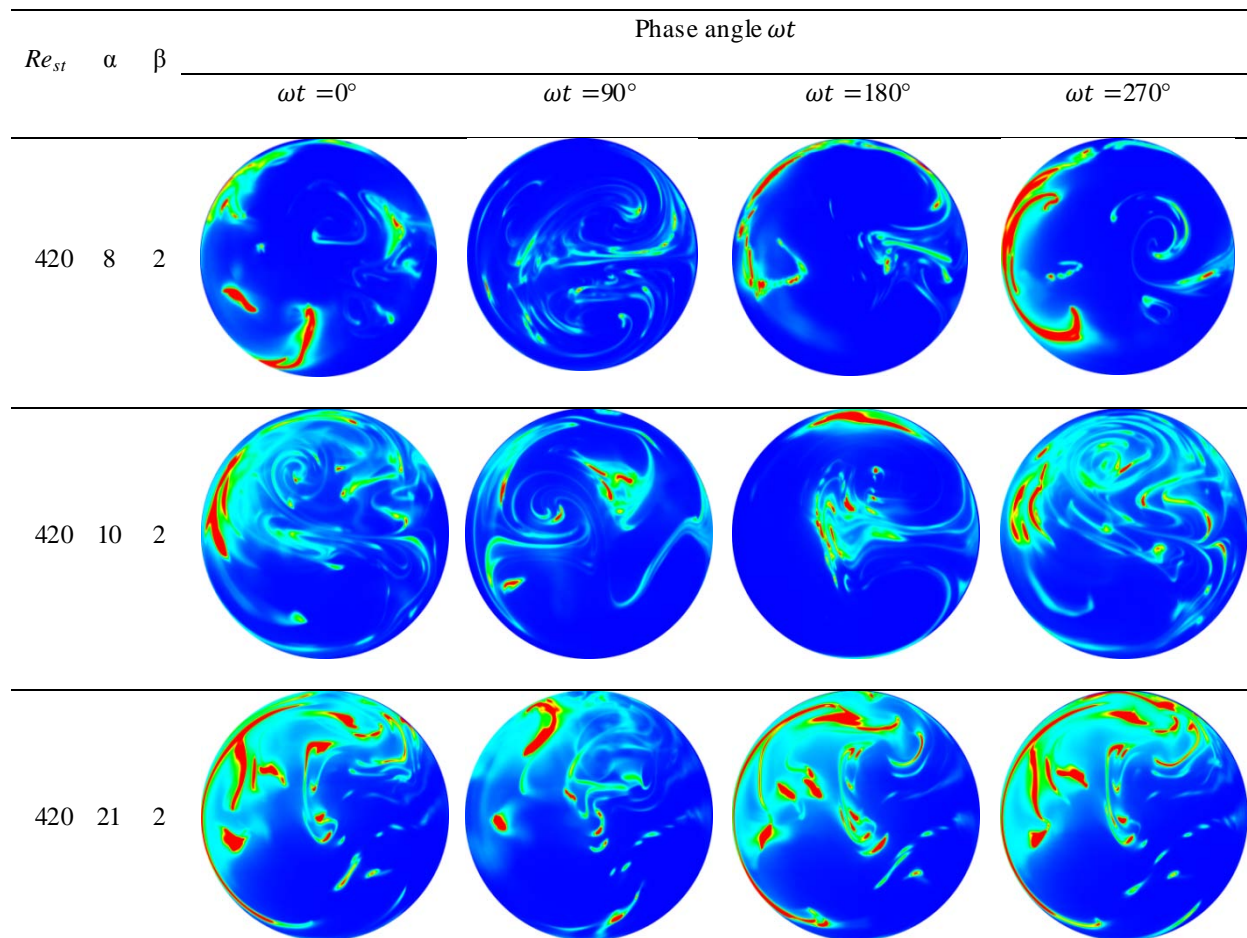
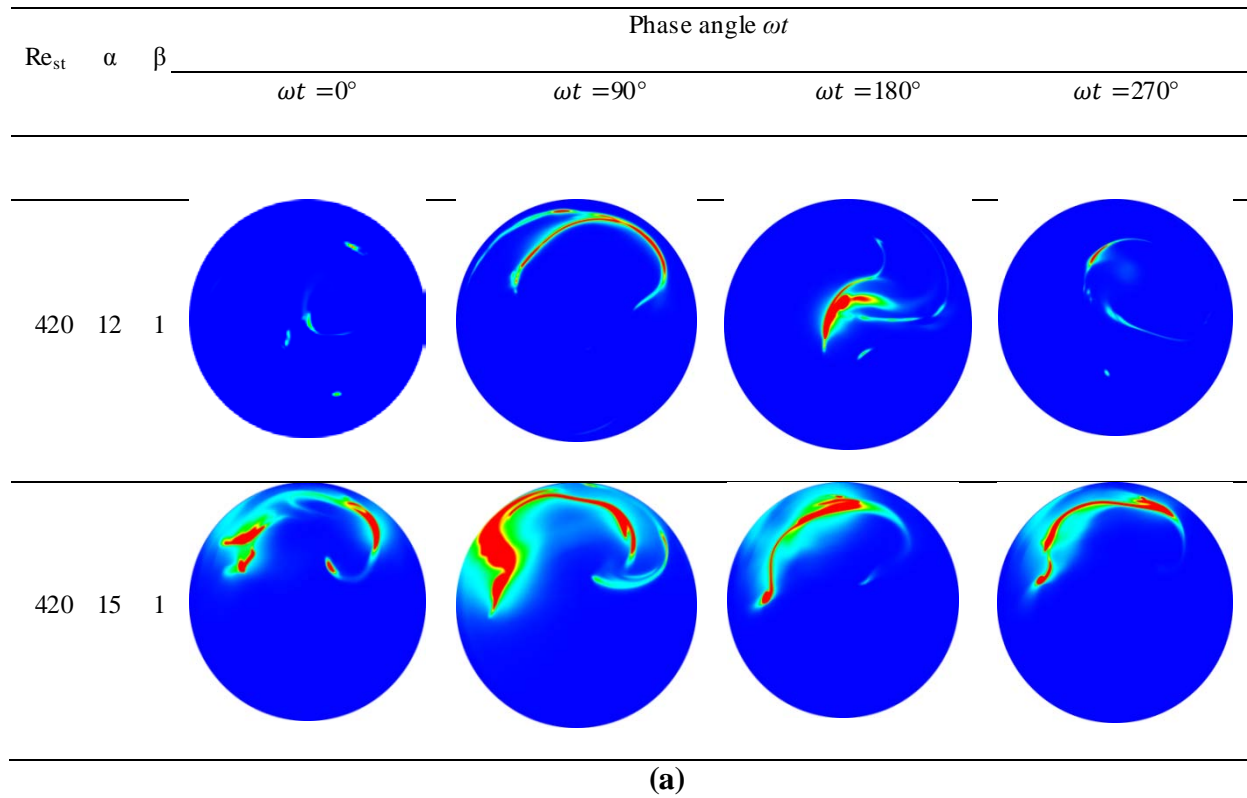


Figure III-6. Images obtained at the exit of a 90° curved pipe for Reynolds number $Re_{st}=420$ for $\alpha=8$ to 15 and $\beta=1$ to 3 .

III.2.2.3. Influence of the frequency

For a given Reynolds number and a constant velocity amplitude β , the variation of frequency parameter α makes the secondary flow remains more or less the same in structure, but it changes the quantitative mixing results.



(b) Figure III-7. Images obtained at the exit of a 90° curved pipe for Reynolds number $Re_{st}=420$ for (a) $\alpha=12$ to 15 and $\beta=1$, (b) $\alpha=8$ to 21 and $\beta=2$.

Therefore the quantitative results helps to select more favorable pulsation conditions a given Reynolds number Re_{st} . (b) Figure III-7 shows influence of Womersley parameter α on tracer distribution in the circular pipe section for two values of velocity amplitude β and a given Reynolds number $Re_{st}=420$.

We observe in Figure III-7 the mixing is increasing with increase in velocity amplitude ratio β . Also if we compare $\alpha=8$ and $\alpha=21$ for $\beta=2$ in Figure III-7, mixing is more evident in the case $\alpha=21$ as compared to $\alpha=8$ for $\beta=2$.

Figure III-8 shows influence of Womersley parameter α on tracer distribution in the circular pipe section for a constant velocity amplitude $\beta=1$ and Reynolds number $Re_{st}=600$. We may observe that as the α increases, the tracer deforms more than compared to the case of precedent value of the α . Tracer has occupied the maximum space in circular section with $\alpha=12$.

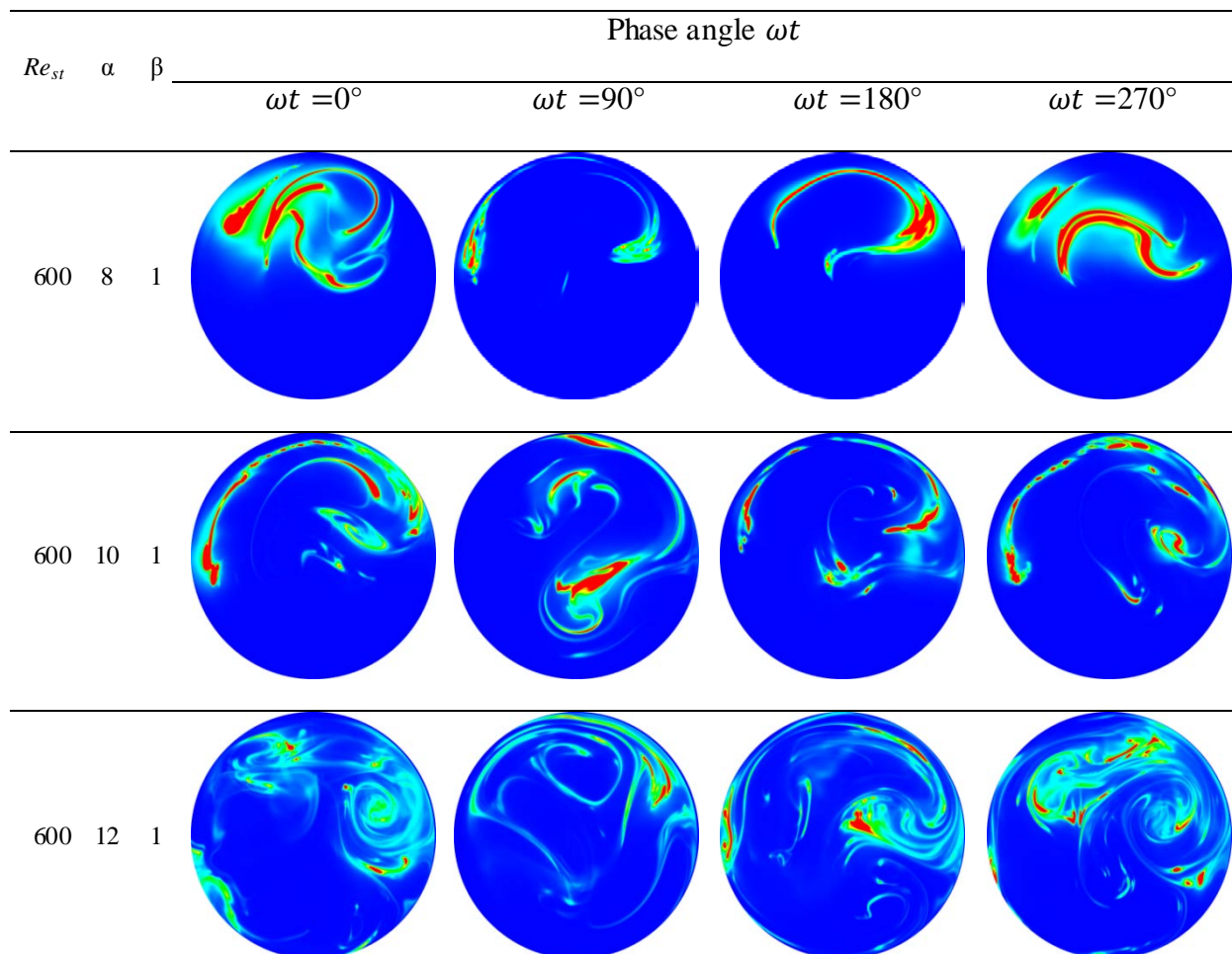


Figure III-8. Images obtained at the exit of a 90° curved pipe for Reynolds number $Re_{st}=600$ for $\alpha=8$ to 12 and $\beta=1$.

Figure III-9 shows influence of Womersley parameter α on tracer distribution in the circular pipe section for a constant velocity amplitude $\beta=1$ and Reynolds number $Re_{st}=800$. As the Womersley frequency parameter α increases to 12 and 15, the tracer lines deforms well on the circular section as compared to the smaller value of the $\alpha=8$. Tracer has occupied the maximum space in circular section with $\alpha=12$ and 15 with a phase angle $\omega t=90^\circ$.

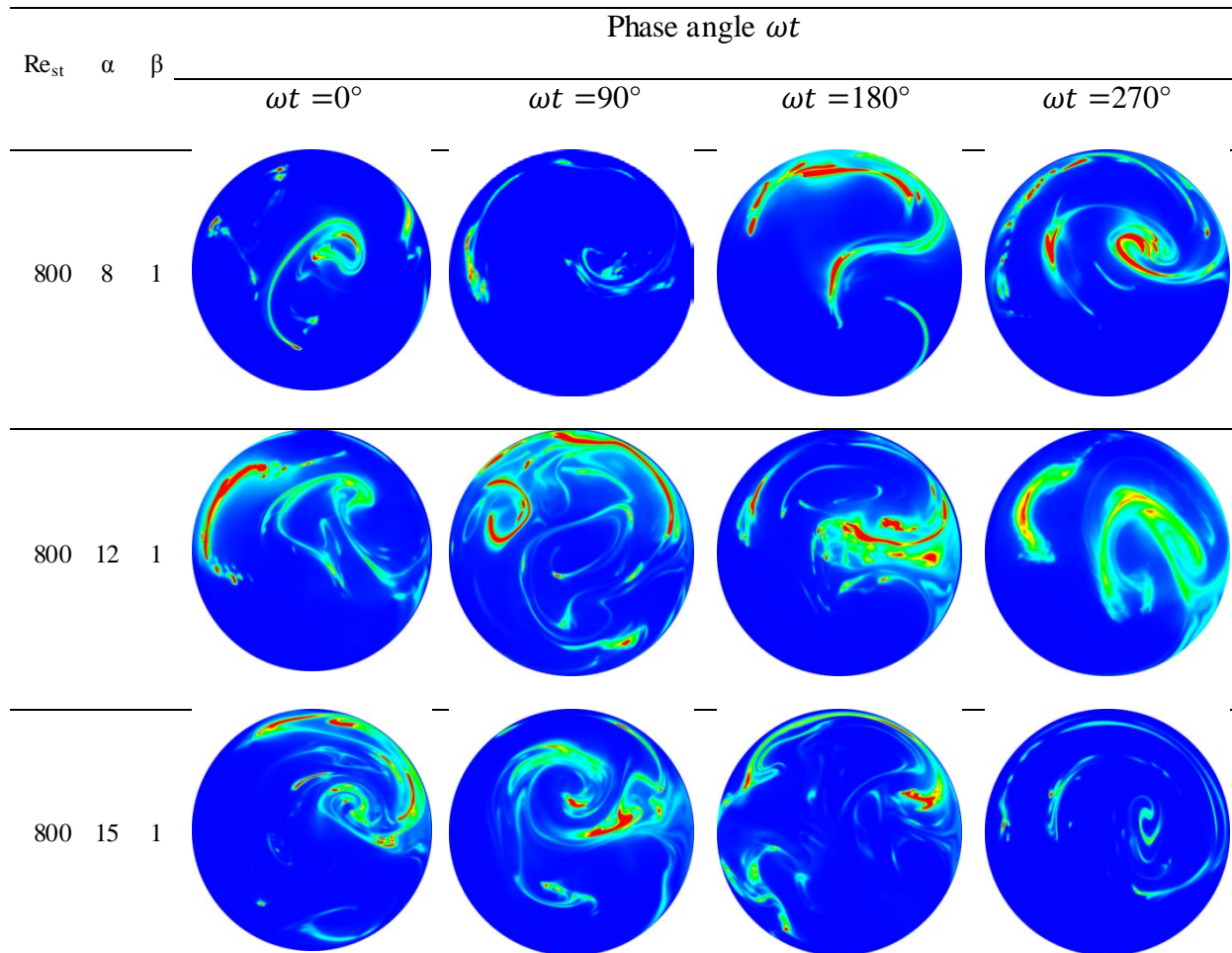


Figure III-9. Images obtained at the exit of a 90° curved pipe for Reynolds number $Re_{st}=800$ for $\alpha=8$ to 15 and $\beta=1$.

Figure III-10 shows influence of Womersley parameter α on tracer distribution in the circular pipe section for a constant velocity amplitude $\beta=1$ and Reynolds number $Re_{st}=1000$. As the Womersley frequency parameter α increases from 8 to 12 for a given $\beta=1$, the tracer amount is much more mixes with the main flow on the circular section as compared to the smaller value of the $\alpha=8$.

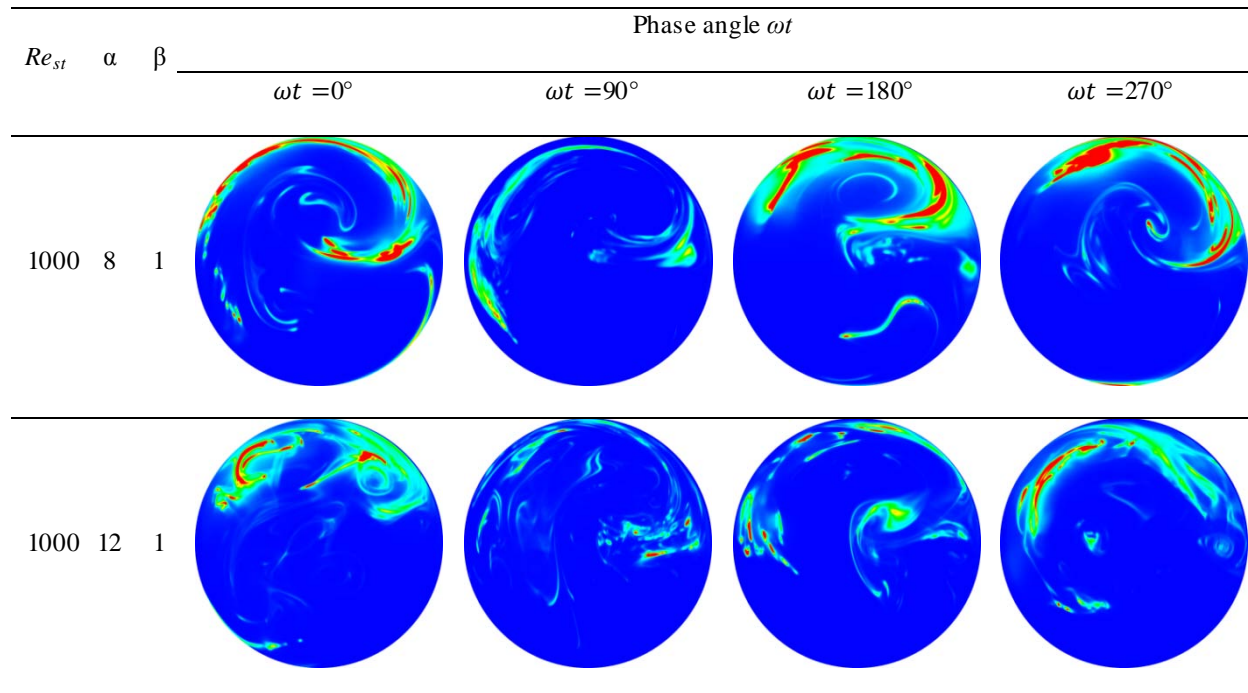


Figure III-10. Images obtained at the exit of a 90° curved pipe for Reynolds number $Re_{st}=1000$ for $\alpha=8$ to 12 and $\beta=1$.

III.3. Mixing intensification analysis in pulsatile flow

The mean concentration in the 90° curved pipe cross section have been used here as indications of mixing enhancement due to flow pulsation in the curved pipe. The standard deviation of the degree of mixing is also examined in order to provide a quantitative measurement for mixing homogeneity. The mean concentration is calculated in a numerical program using the concentration fields measured by the PLIF technique.

III.3.1. Determination of the degree of mixing

Mixing degree is calculated from the relation already discussed in Chapter I,

$$I_{mix} = 1 - \frac{\sigma^2}{\sigma_{max}^2} \quad \text{(III-34)}$$

where I_{mix} is the mixing intensity or degree of mixing, σ^2 is the variance and σ_{max}^2 is the maximum variance. The variance and maximum variance are computed by the equations III-2 and III-3 respectively.

$$\sigma^2 = \frac{1}{N} \sum_{i=1}^N (C_i - \bar{C})^2 \quad (\text{III-35})$$

$$\sigma_{max}^2 = \bar{C}(C_q - \bar{C}) \quad (\text{III-36})$$

Here C_q is the concentration injected in $\mu\text{g/L}$, \bar{C} is the mean concentration in $\mu\text{g/L}$, of N instantaneous C_i concentrations measured on the whole circular section by the CCD camera used for experimentation. It is already discussed, that the PLIF calibration curve defines the grey level with locally defined Rhodamine 6G homogeneous solutions of $0 \mu\text{g/L}$ to $100 \mu\text{g/L}$. Therefore, all experiments are conducted with the same PLIF calibration curve and the grey intensity is absolute in each run. Hence, the mixing degree obtained through different experimental conditions can be compared with that of other cases.

Figure III-11 shows an uncertainty measurement and an approximate error calculation curve according to the different phase angles. Six measurements for a given pulsation condition of $Re_{st}=600$, $\alpha=10$ and $\beta=1$ are carried out to calculate the error bar for degree of mixing. The coherent repeatability of the experiment is obtained and the respective values are in the limit of an error of $\pm 7\%$. The observed spread in the data points is consistent with the estimated uncertainty based on the propagation of errors.

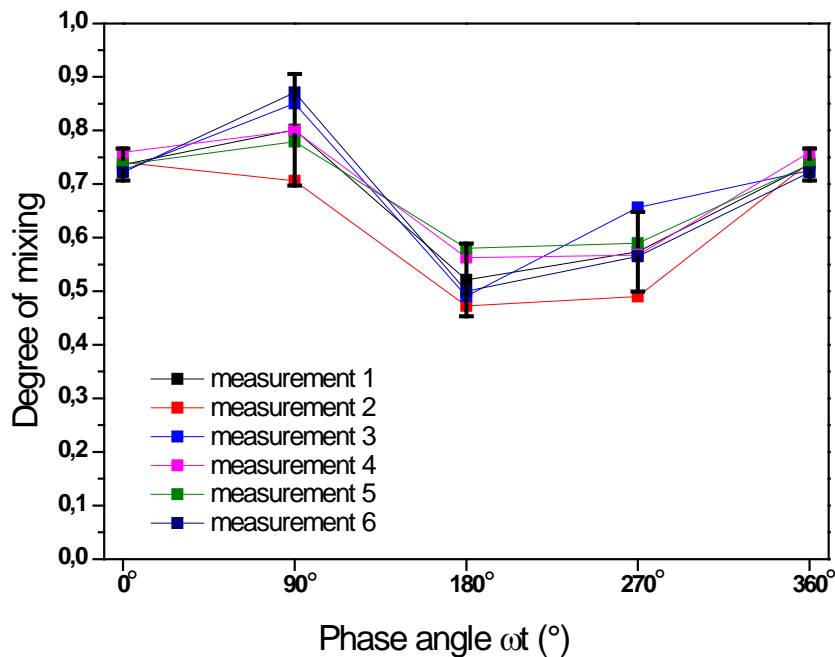


Figure III-11. Reproducibility study of degree of mixing for $Re_{st}=600$, $\alpha=10$, $\beta=1$.

Furthermore the standard deviation of the degree of mixing is examined in order to give a rough quantitative measure for mixing homogeneity. The standard deviation, which indicates the scattering of the degree of mixing values around their mean value, gives sufficient insight into the problem: the smaller the standard deviation, the more homogeneous the mixing. Figure III-12 plots the standard deviation of the degree of mixing for $Re_{st}=600$, $\alpha=10$ and $\beta=1$ versus the phase angle ωt . Standard deviation varies between the values of 0.015 in the case of phase angle 0° , to 0.065 in the case of phase angles 90° and 270° . An average value corresponding to the standard deviation is found to be 0.041.

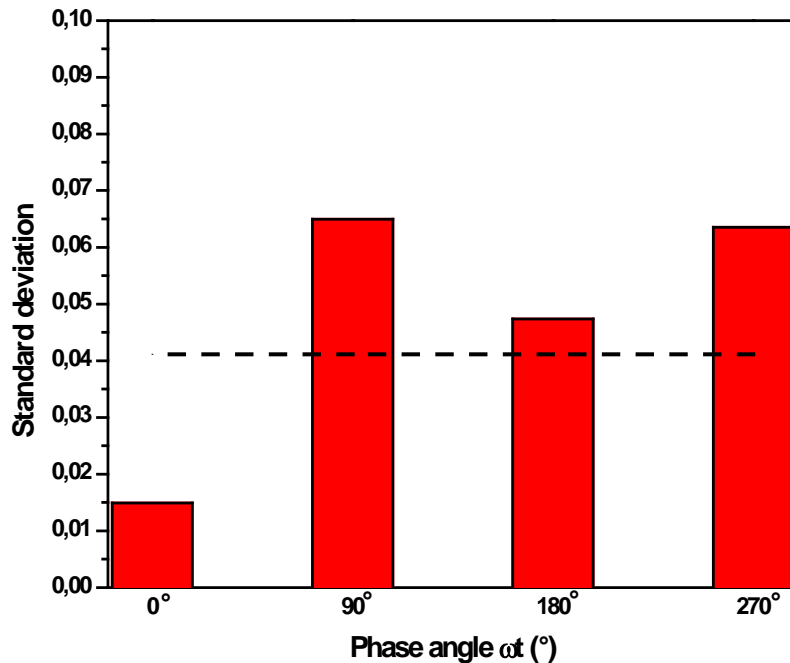


Figure III- 12 Standard deviation of mixing degree for $Re_{st}=600$, $\alpha=10$, $\beta=1$.

III.3.2. Influence of Reynolds number

Figure III-13 shows the enhancement of mixing as the function of Reynolds number Re_{st} for constant velocity amplitude ratio $\beta=1$. The degree of mixing represented in the Figure III-13 is calculated at phase angle $\omega t=0^\circ$, it means after a complete pulsation cycle. Degree of mixing in the case of steady flow is rather constant for the different Reynolds numbers, around 0.36. Degree of mixing increases as the Womersley frequency parameter α increases

from 0 to 15 and it increases more with increase in Re_{st} for pulsated cases. The maximum value of degree of mixing 0.85 is obtained for $Re_{st}=600$ and $\alpha=15$.

Figure III-14 shows the influence of Re_{st} on the enhancement of mixing for constant velocity amplitude ratio $\beta=1$ and the degree of mixing is calculated at phase angle $\omega t=90^\circ$. Here, we may observe that the maximum value of degree of mixing 0.84 is obtained for $Re_{st}=800$ and $\alpha=15$ after a rapid increase from a value of 0.50 at $Re_{st}=420$. The same trend is observed for the cases $\alpha=8$ and $\alpha=10$, but with lower values of degree of mixing, of about 14% to 20% less as compared to $\alpha=15$. For the case $Re_{st}=1000$ a slight decrease of degree of mixing is observed, but it is worth to notice that it seems to reach a plateau for $Re_{st}\geq 800$.

Figure III-15 shows the degree of mixing versus Reynolds number Re_{st} for constant velocity amplitude ratio $\beta=1$ and calculated at phase angle $\omega t=180^\circ$. We may observe that the maximum value of degree of mixing 0.77 is obtained for $Re_{st}=800$ with $\alpha=10$ and $\alpha=15$ while for $\alpha=8$ the maximum value of 0.68 is also obtained at $Re_{st}=800$. Globally, there is an increase of the degree of mixing between $Re_{st}=420-600$ and $Re_{st}=800-1000$, cases from which we can observe a plateau.

Figure III-16 represents the degree of mixing according to Reynolds number Re_{st} for constant velocity amplitude ratio $\beta=1$ and calculated at phase angle $\omega t=270^\circ$. We may observe that maximum value of degree of mixing 0.75 is obtained for $Re_{st}=1000$ with $\alpha=10$, the maximum value of 0.68 obtained for $\alpha=8$ (at $Re_{st}=800$) and the maximum value of 0.76 obtained for $\alpha=15$ (at $Re_{st}=600$). It is striking to note that at this phase angle the curve trend is slightly different from the three previous one: the maximum degree of mixing is obtained for $Re_{st}=800-1000$ and for $\alpha=8-15$ but the trend of the curves is not so clear as the previous one, on which we can observe two plateau at $Re_{st}=420-600$ and $Re_{st}=800-1000$. Also the enhancement between low Re_{st} and high Re_{st} is weaker in that case.

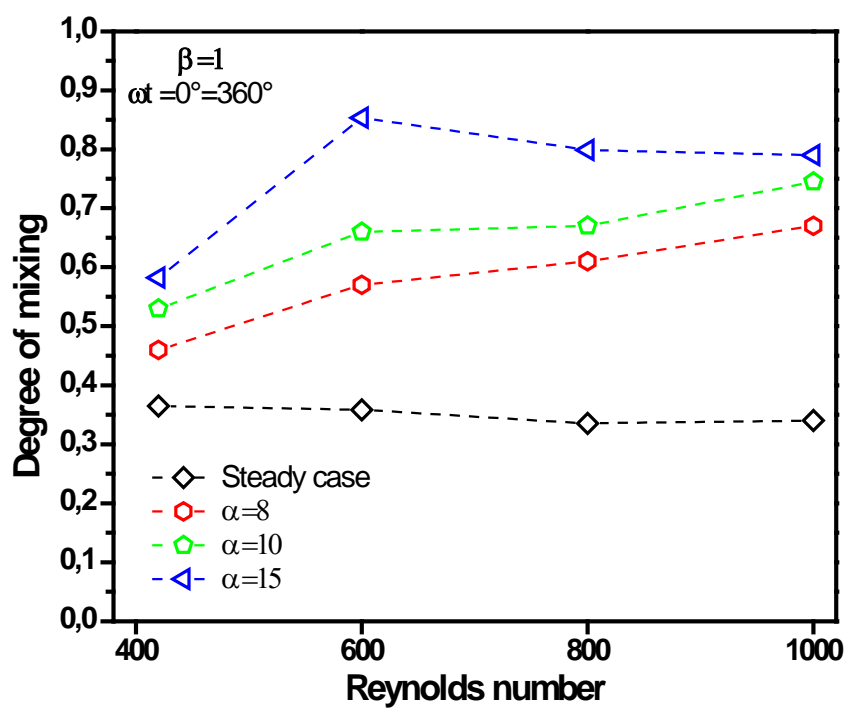


Figure III-13. Influence of Re_{st} on mixing intensity for $\beta=1$ at $\omega t=0^\circ$.

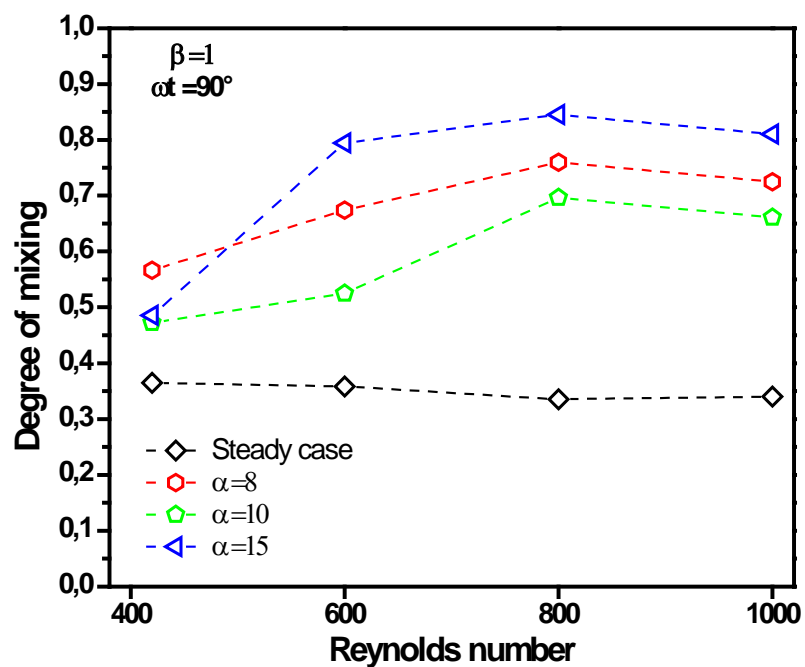


Figure III-14. Influence of Re_{st} on mixing intensity for $\beta=1$ at $\omega t=90^\circ$.

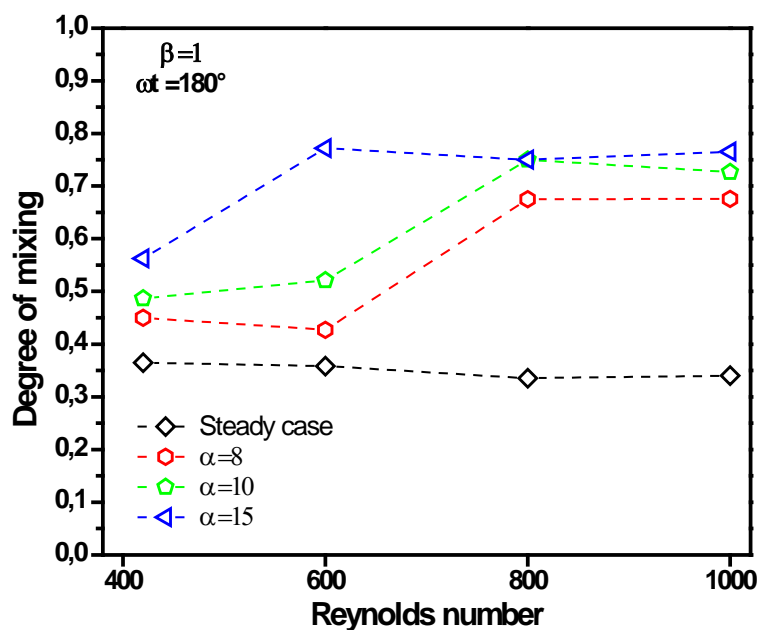


Figure III-15. Influence of Re_{st} on mixing intensity for $\beta=1$ at $\omega t=180^\circ$.

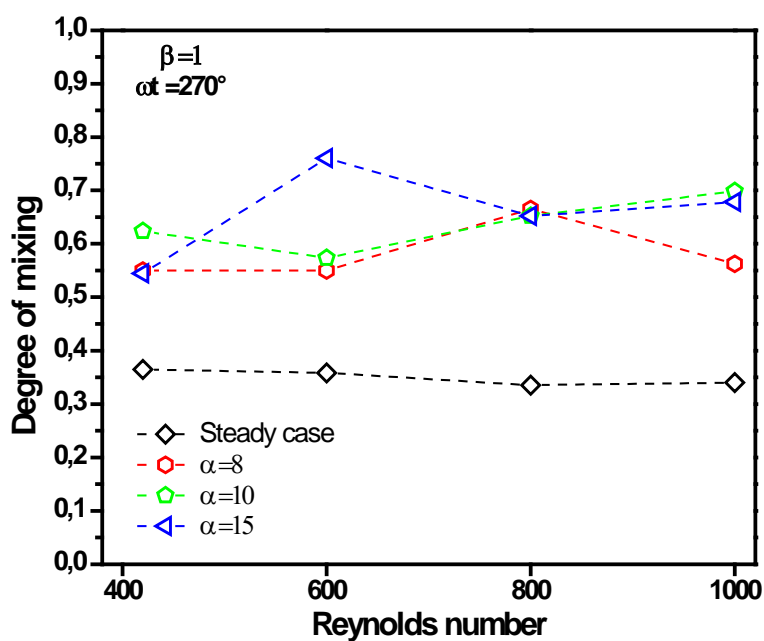


Figure III-16. Influence of Re_{st} on mixing intensity for $\beta=1$ at $\omega t=270^\circ$.

Figure III-17 represents the degree of mixing according to Reynolds number Re_{st} for constant velocity amplitude ratio $\beta=1$, here the mixing degree calculated is the average of the four phase angles ωt . We may observe that maximum value of degree of mixing 0.78 is obtained for $Re_{st}=600$ with $\alpha=15$, the maximum value of 0.7 obtained for $\alpha=10$ at $Re_{st}=1000$ and the maximum value of 0.68 obtained for $\alpha=8$ at $Re_{st}=800$. The global trend is an increase of the degree of mixing with the Reynolds number and a plateau seems to be attained for $Re_{st}=800$ at $\alpha=8-10$ and for $Re_{st}=600$ at $\alpha=15$.

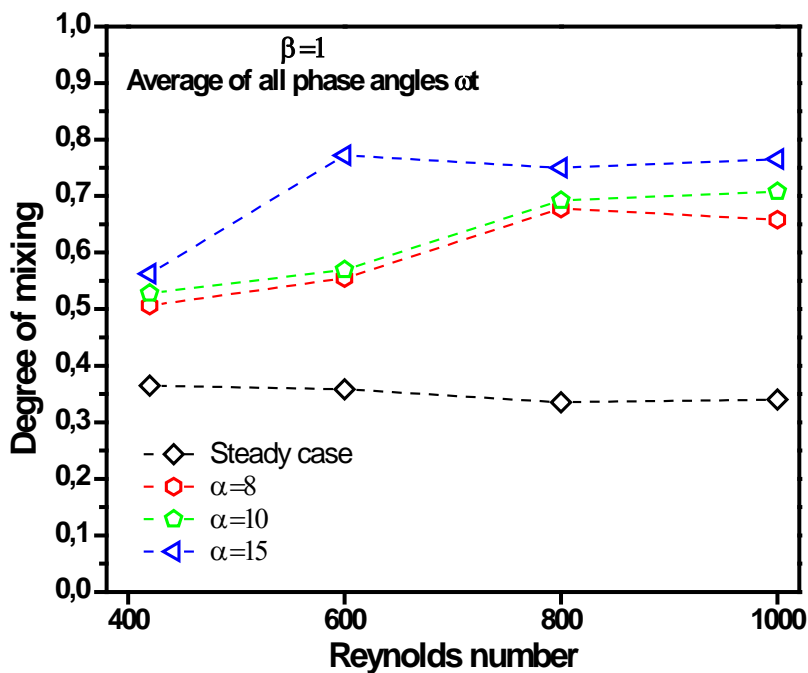


Figure III-17. Influence of Re_{st} on mixing intensity for $\beta=1$ for average of all phase angles ωt .

Figure III-18 shows influence of Re_{st} on relative mixing intensification ψ for $\beta=1$ for average of all phase angles ωt . The relative mixing intensity ψ is calculated by the following relation

$$\psi = \frac{I_{mix\ p} - I_{mix\ st}}{I_{mix\ st}} \quad (\text{III-37})$$

where $I_{mix\ p}$ is the degree of mixing obtained in pulsatile cases and $I_{mix\ st}$ is the degree of mixing obtained in steady cases.

We may observe that maximum value of relative mixing intensification $\psi=125\%$, 123% , 115% and 54% is obtained respectively for $Re_{st}=1000$, 800 , 600 and 420 at $\alpha=15$. Pulsations can increase more than 100% degree of mixing values in pulsated cases compared to steady cases.

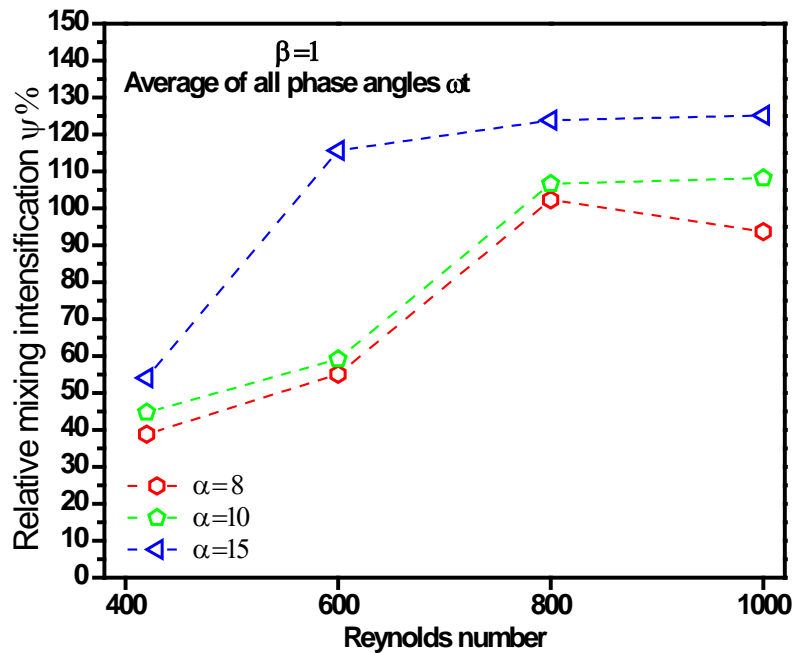


Figure III-18. Influence of Re_{st} on relative mixing intensification ψ in % for $\beta=1$ for average of all phase angles ωt .

III.3.3. Influence of the frequency

The degree of mixing is measured with increase in Womersley frequency parameter α and compared to steady cases. Figures III-19, III-20, III-21 and III-22 represent changes in mixing with phase angle ωt for different frequency parameters α over an oscillation period for $Re_{st}=420$, 600 , 800 and 1000 and $\beta=1$.

Figure III-19 shows the influence of three different values of $\alpha=8$, 10 and 15 on degree of mixing for different $Re_{st}=420$, 600 , 800 and 1000 at velocity amplitude ratio $\beta=1$ at $\omega t=0^\circ$. There is a gradual increase in degree of mixing values with increase in Womersley parameter α for all the Reynolds numbers. The maximum degree of mixing value 0.85 for $Re_{st}=600$ with $\alpha=15$ is observed.

Figure III-20 plots the influence of three different values of $\alpha=8, 10$ and 15 on degree of mixing for different $Re_{st}=420, 600, 800$ and 1000 at velocity amplitude ratio $\beta=1$ at $\omega t=90^\circ$. In this phase angle ωt , the degree of mixing values for $\alpha=10$ and 15 are almost plateau except in the case of $Re_{st}=1000$ and $Re_{st}=420$ for which there is a slight increase. The maximum degree of mixing value 0.84 for $Re_{st}=1000$ with $\alpha=15$ is observed.

Figure III-21 plots the influence of three different values of $\alpha=8, 10$ and 15 on degree of mixing for different $Re_{st}=420, 600, 800$ and 1000 at velocity amplitude ratio $\beta=1$ at $\omega t=180^\circ$. At this phase angle ωt , the degree of mixing values for $\alpha=15$ are almost the same for $Re_{st}=600, 800$ and 1000 with a maximum degree of mixing value 0.75 observed. Globally, the degree of mixing is increased with the Womersley frequency parameter.

Figure III-22 plots the influence of frequency parameter $\alpha=8, 10$ and 15 on degree of mixing for different $Re_{st}=420, 600, 800$ and 1000 with $\beta=1$ and phase angle $\omega t=270^\circ$. Maximum degree of mixing about 0.75 is observed for $Re_{st}=600$ with $\alpha=15$. Globally, it seems that for $\alpha>8$ a plateau is reached.

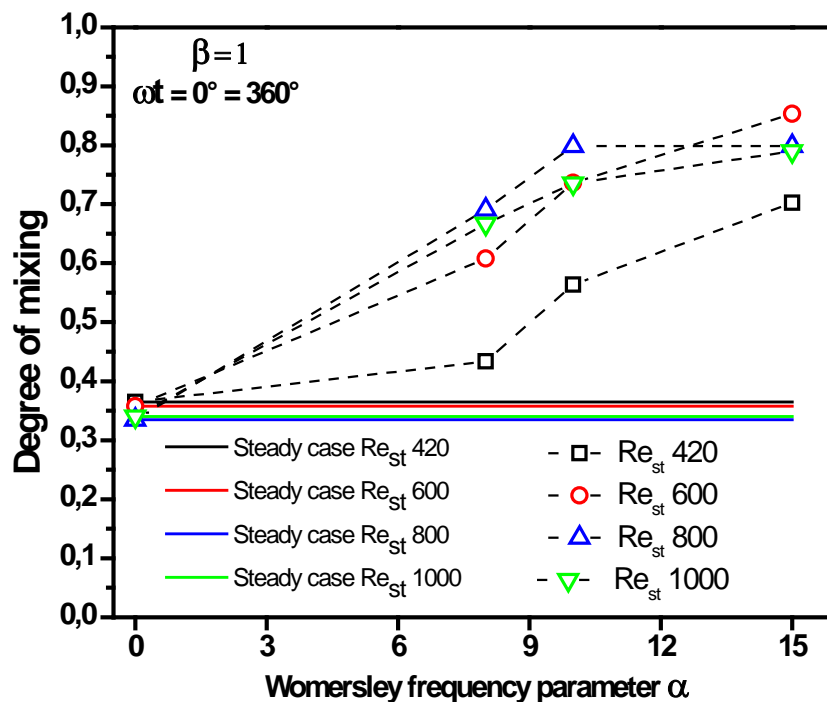


Figure III-19. Influence of α on mixing intensity for $\beta=1$ at phase angle $\omega t=0^\circ$.

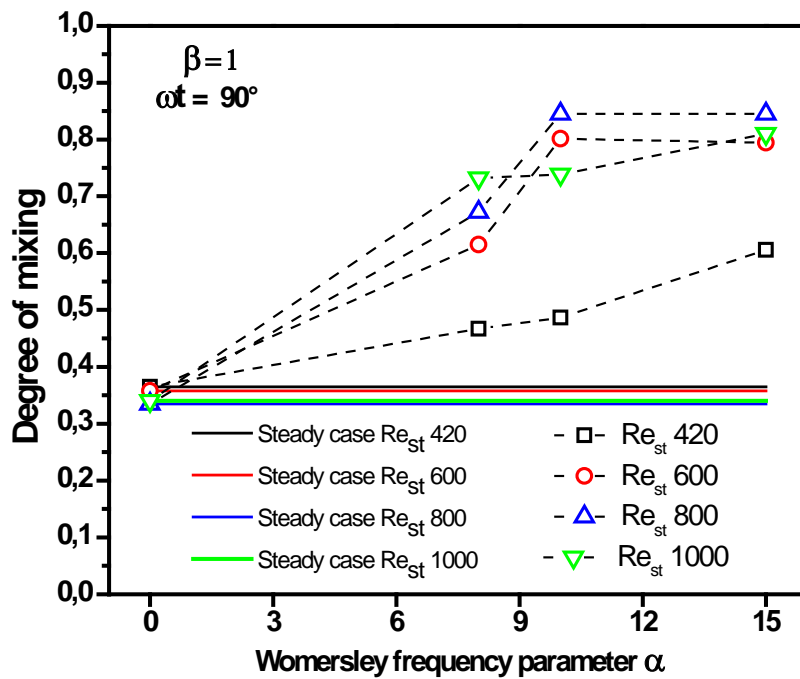


Figure III-20. Influence of α on mixing intensity for $\beta=1$ at phase angle $\omega t=90^\circ$.

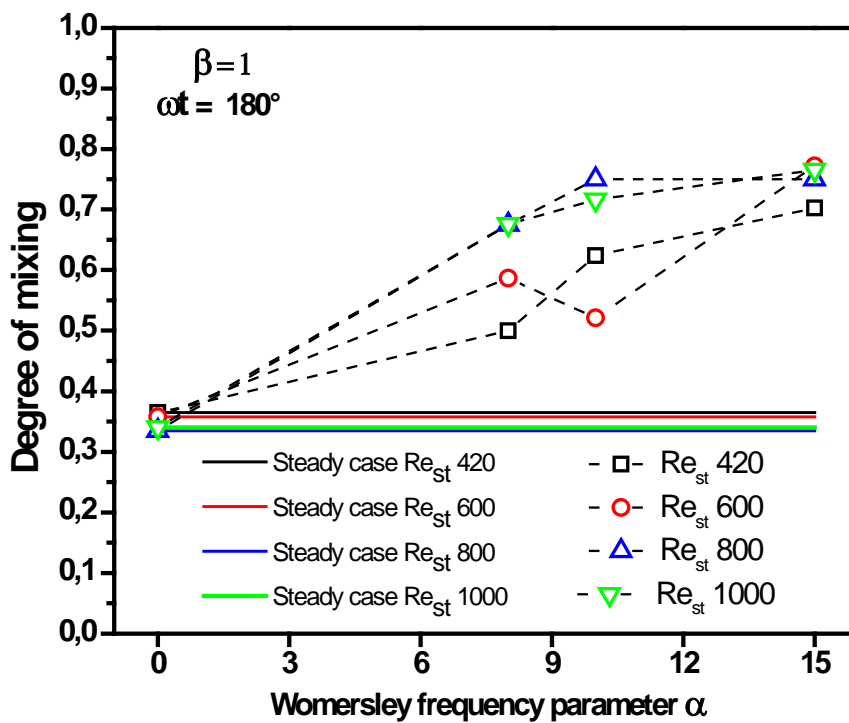


Figure III-21. Influence of α on mixing intensity for $\beta=1$ at phase angle $\omega t=180^\circ$.

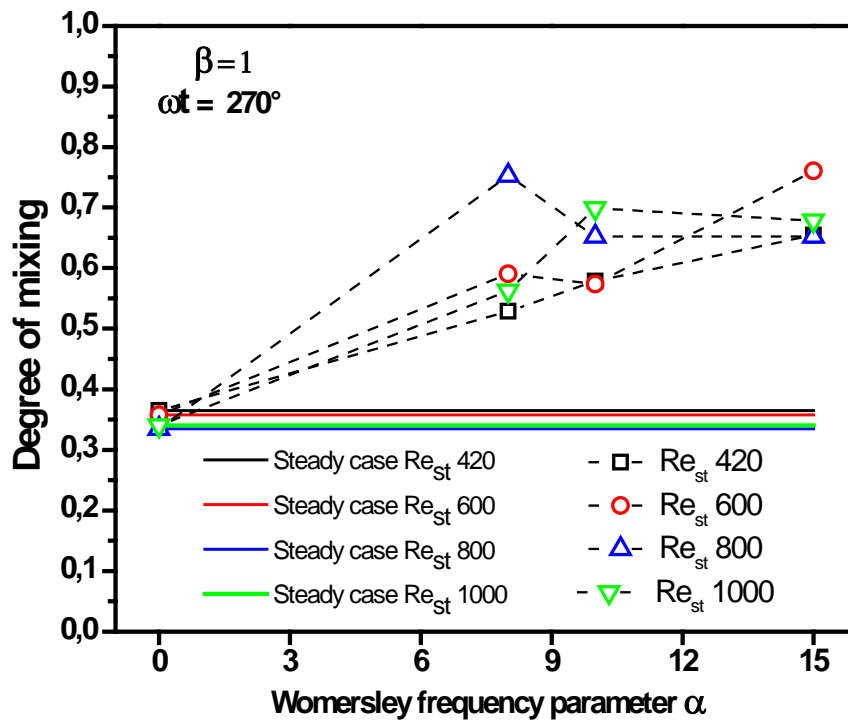


Figure III-22. Influence of α on mixing intensity for $\beta=1$ at phase angle $\omega t=270^\circ$.

Figure III-23 plots the influence of frequency parameter $\alpha=8, 10$ and 15 on the average of degree of mixing of all phase angles ωt , for different $Re_{st}=420, 600, 800$ and 1000 at $\beta=1$. Maximum degree of mixing about 0.80 is observed for $Re_{st}=600$ with $\alpha=15$. The global trend observed is an increase of the degree of mixing with the Womersley parameter.

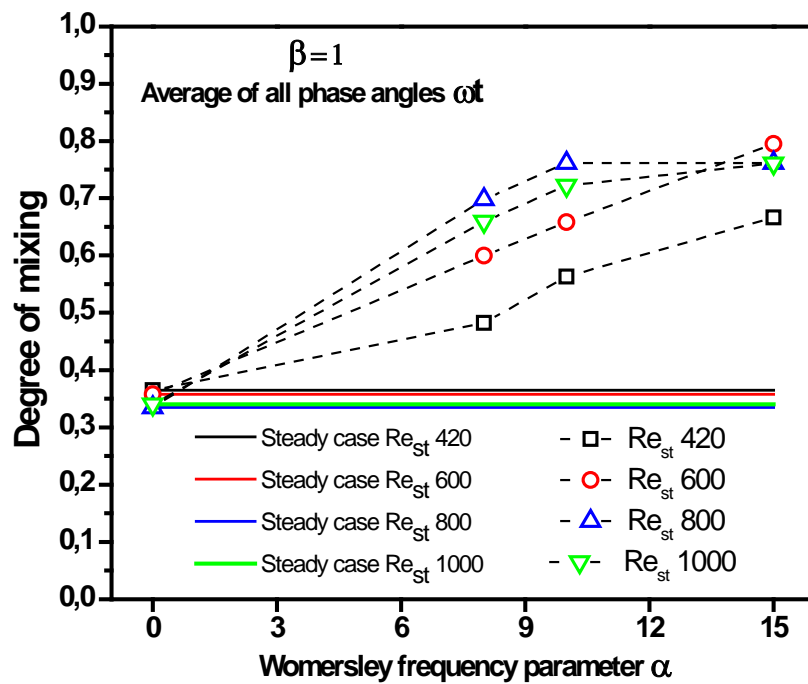


Figure III-23. Influence of α on mixing intensity for $\beta=1$ and average of all phase angles ωt .

Figure III-24 shows influence of α on relative mixing intensification ψ calculated for $\beta=1$ and the average of all phase angles ωt . We observe that maximum value of relative mixing intensification $\psi=85\%$, 123% , 127% , and 123% for respectively $Re_{st}=420$, 600 , 800 and 1000 with 15 . Globally, the trend is an increase of the enhancement of degree of mixing for the pulsated cases compared to the steady case, the enhancement is stronger for $Re_{st}=800-1000$ compared to $Re_{st}=600$ but for a Womersley value of 15 , the enhancement is the same for the three Reynolds numbers.

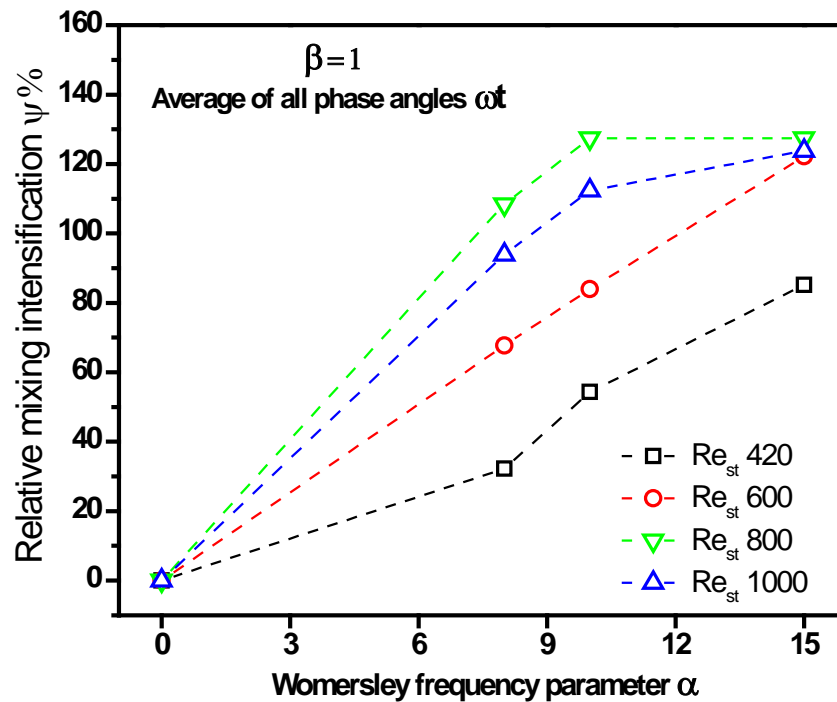
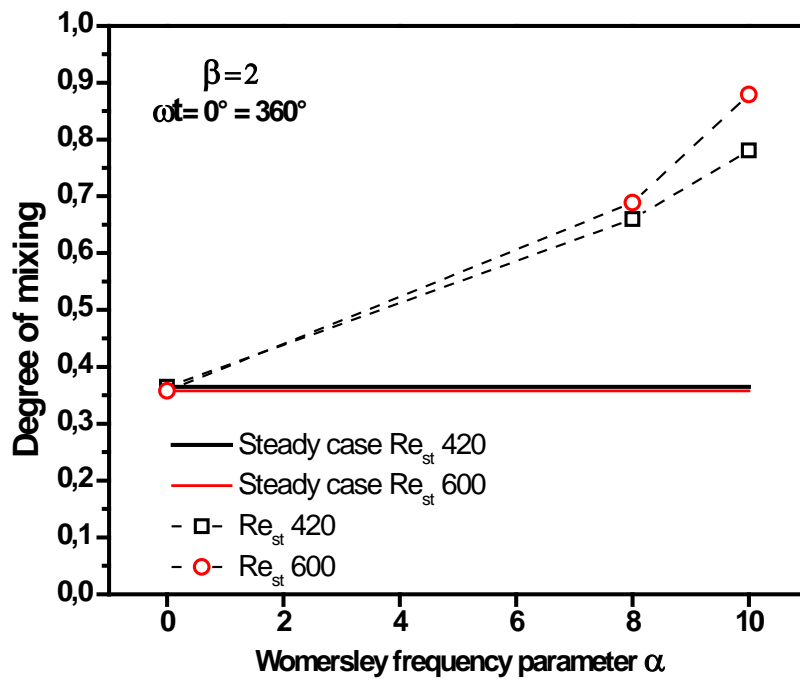
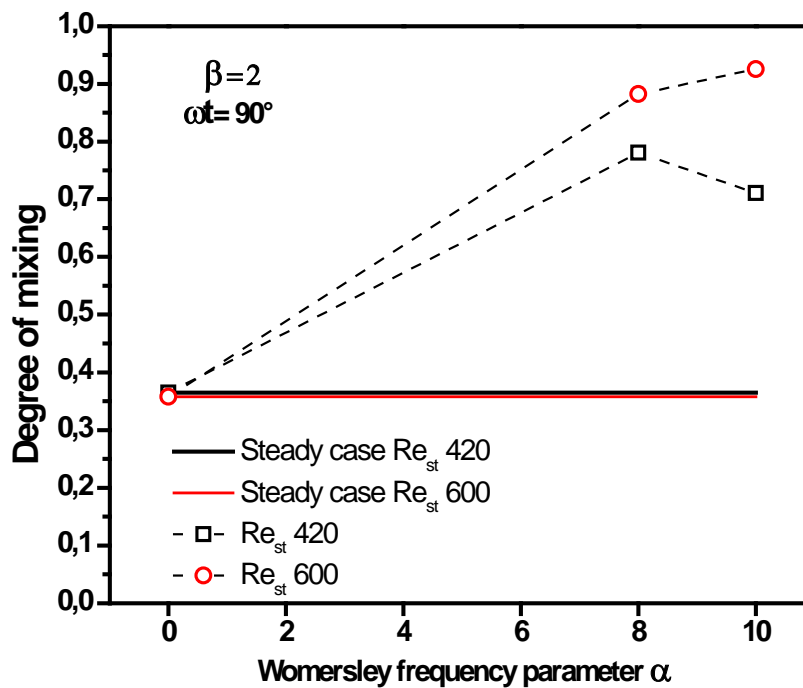


Figure III-24. Influence of α on relative mixing intensification ψ for $\beta=1$ and average of all phase angles ωt .

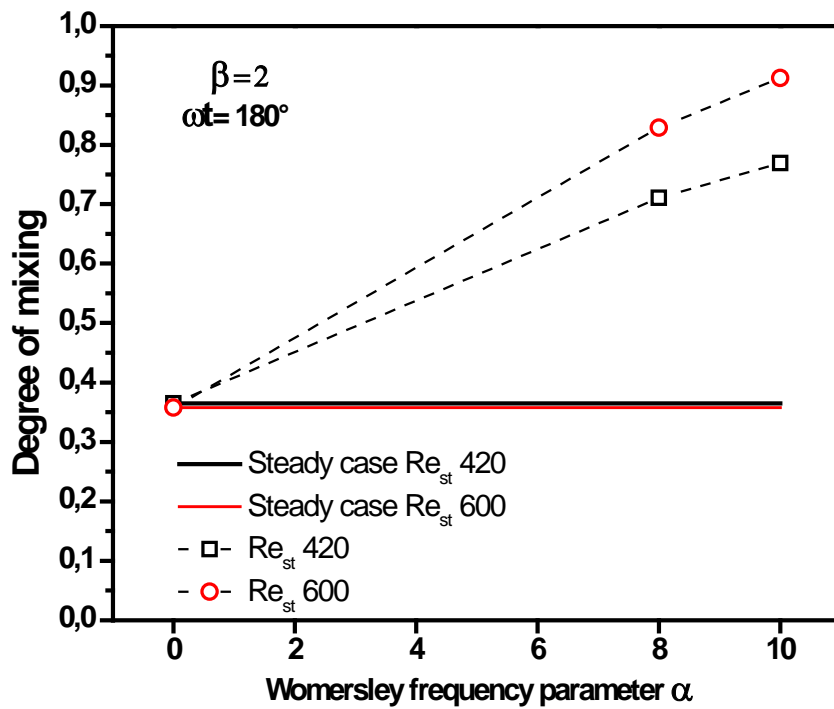
Figure III-25 plots the influence of frequency parameter $\alpha=8, 10$ on degree of mixing for different $Re_{st}=420$ and 600 at $\beta=2$ with different phase angles ωt . In Figure III-25 (a) at phase angle $\omega t=0^\circ$, the maximum degree of mixing about 0.87 is observed for $Re_{st}=600$ and 0.75 for $Re_{st}=420$ with $\alpha=10$. In Figure III-25 (b) at phase angle $\omega t=90^\circ$, the maximum degree of mixing about 0.93 is observed for $Re_{st}=600$ with $\alpha=10$ and the maximum degree of mixing about 0.78 is observed for $Re_{st}=420$ with $\alpha=8$. In Figure III-25 (c) at phase angle $\omega t=180^\circ$, the maximum degree of mixing about 0.92 and 0.76 is observed for $Re_{st}=600$ and 420 respectively with $\alpha=10$. In Figure III-25 (d) at phase angle $\omega t=270^\circ$, the maximum degree of mixing about 0.89 is observed for $Re_{st}=600$ $\alpha=10$. The maximum degree of mixing about 0.76 is observed for $Re_{st}=420$ and $\alpha=8$. Globally, in the cases of $\beta=2$, the enhancement of degree of mixing is stronger compared to the cases $\beta=1$.



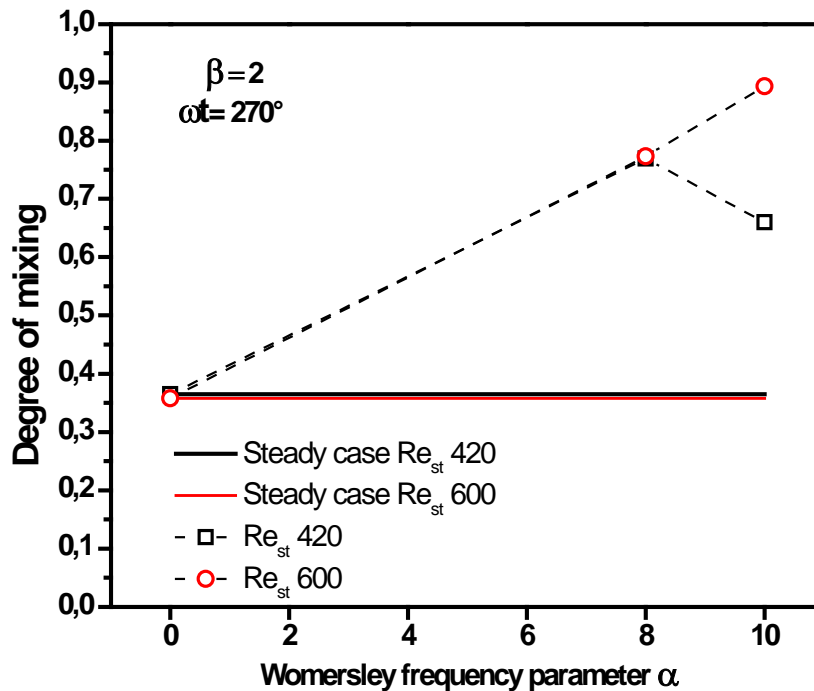
(a)



(b)



(c)



(d)

Figure III-25. Influence of α on mixing intensity for $\beta=2$ with different phase angles ωt . (a) $\omega t=0^\circ=360^\circ$, (b) $\omega t=90^\circ$, (c) $\omega t=180^\circ$, and (d) $\omega t=270^\circ$.

Figure III-26 shows influence of α on mixing intensity for $\beta=2$ with average of all phase angles ωt . We observe a maximum degree of mixing value of 0.90 for $Re_{st}=600$ with $\alpha=10$. While for the $Re_{st}=420$ there is same value of 0.73 for $\alpha=8$ and $\alpha=10$.

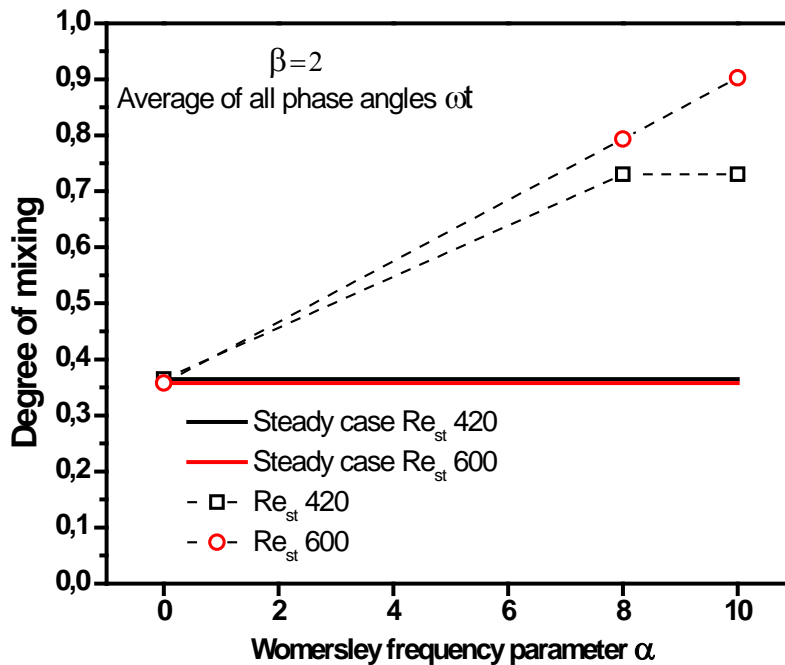


Figure III-26. Influence of α on mixing intensity for $\beta=2$ and average of all phase angles ωt .

Figure III-27 shows influence of Re_{st} on relative mixing intensification ψ for $\beta=2$ and average of all phase angles ωt . We observe a maximum value of relative mixing intensification $\psi=150\%$ for $Re_{st}=600$ at 10. Maximum value of relative mixing intensification $\psi 100\%$ is obtained for $Re_{st}=420$ at $\alpha=8$ and 10 because a plateau seems to be reached at this Womersley parameter value.

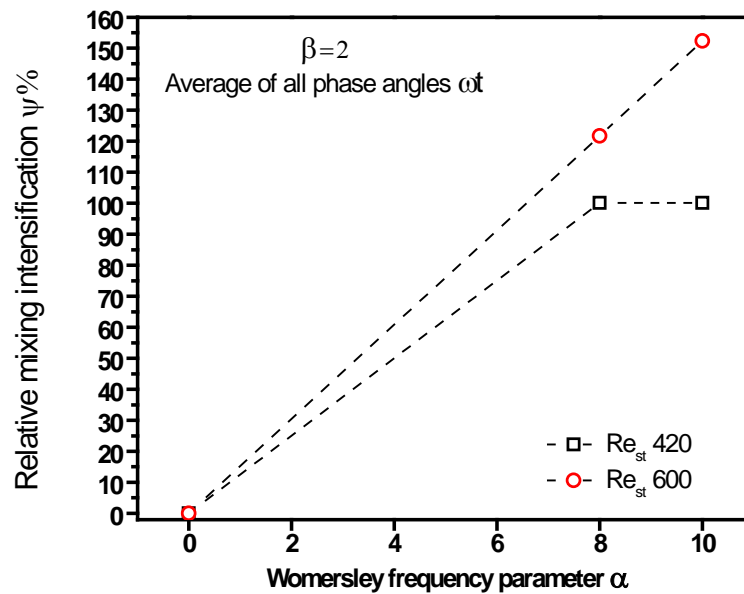


Figure III-27. Influence of α on relative mixing intensification ψ for $\beta=2$ for average of all phase angles ωt .

III.3.4. Influence of velocity amplitude

Figure III-28 shows influence of β on mixing intensity at phase angle $\omega t=0^\circ$. A strong point is that degree of mixing is increased in pulsated cases compared to steady cases, and it increases as the velocity amplitude ratio β increases. Maximum degree of mixing about 0.88 is observed for $Re_{st}=600$ and 0.78 for $Re_{st}=420$ at $\beta=2$ and $\alpha=10$.

Figure III-29 shows influence of β on mixing intensity at phase angle $\omega t=90^\circ$. Degree of mixing increases with the velocity amplitude ratio β . Maximum degree of mixing about 0.92 is observed for $Re_{st}=600$ and 0.78 for $Re_{st}=420$ at $\beta=2$ and $\alpha=8$.

Figure III-30 shows influence of β on mixing intensity at phase angle $\omega t=180^\circ$. Maximum degree of mixing about 0.92 is observed for $Re_{st}=600$ and 0.75 for $Re_{st}=420$ at $\beta=2$ and $\alpha=10$.

Figure III-31 shows influence of β on mixing intensity at phase angle $\omega t=270^\circ$. Maximum degree of mixing about 0.89 is observed for $Re_{st}=600$ and 0.75 for $Re_{st}=420$ at $\beta=2$ and $\alpha=10$.

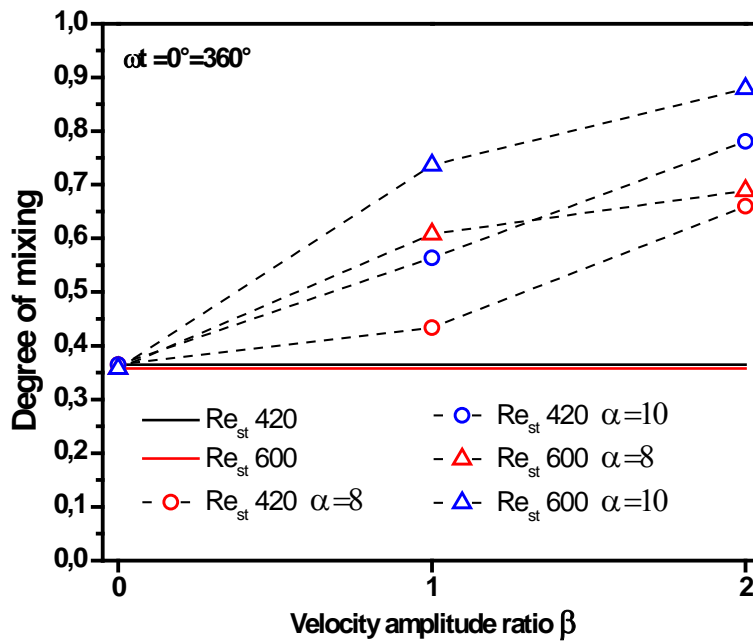


Figure III-28. Influence of β on mixing intensity at phase angle $\omega t = 0^\circ$.

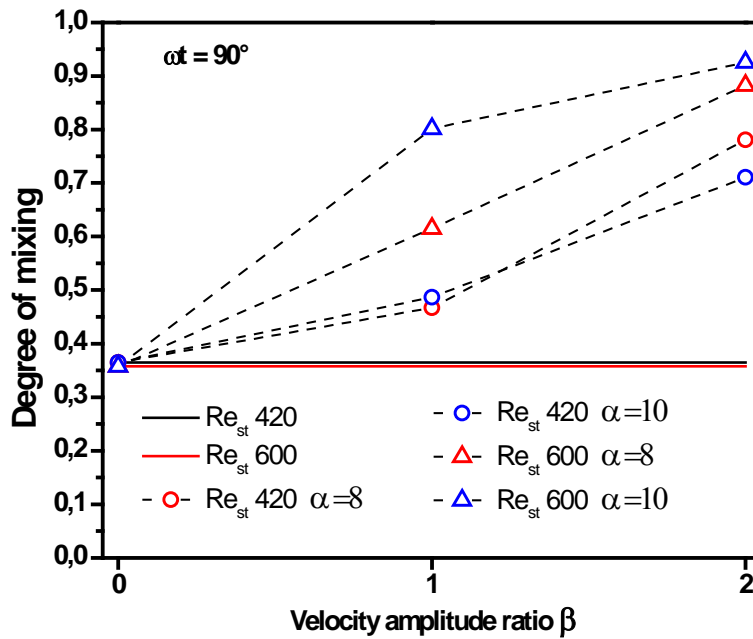


Figure III-29. Influence of β on mixing intensity at phase angle $\omega t = 90^\circ$.

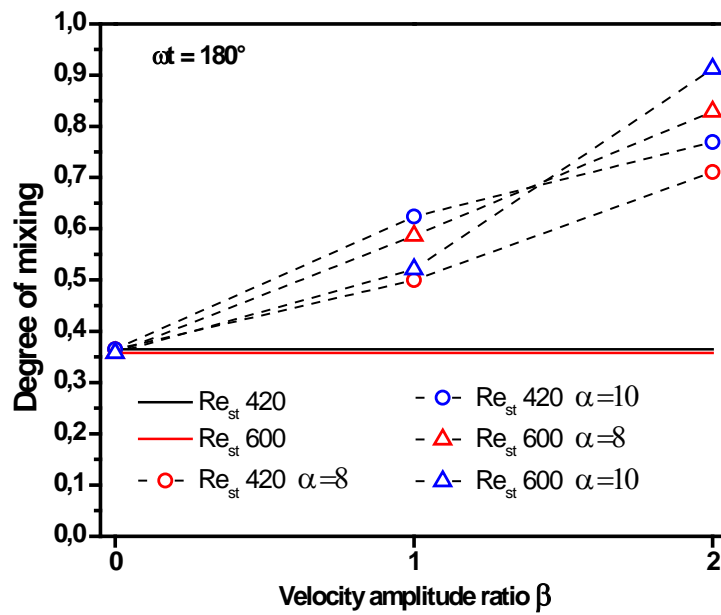


Figure III-30. Influence of β on mixing intensity at phase angle $\omega t = 180^\circ$.

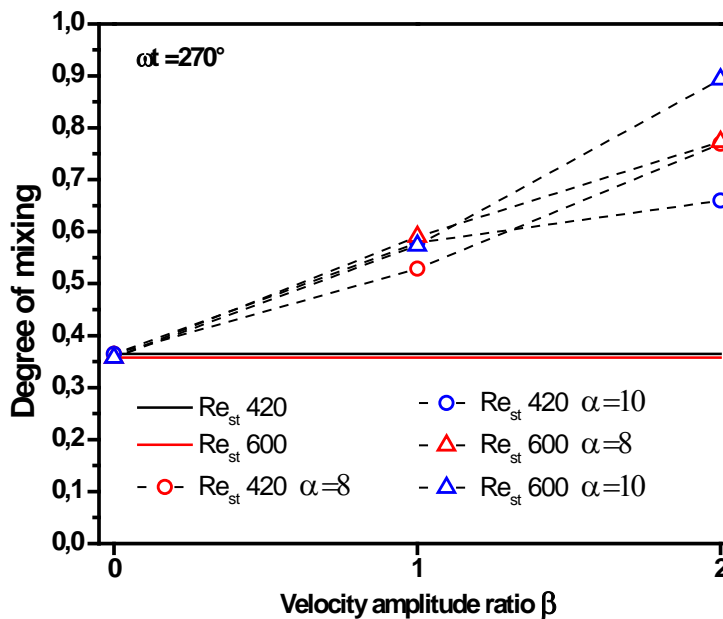


Figure III-31. Influence of β on mixing intensity at phase angle $\omega t = 270^\circ$.

Figure III-32 shows influence of β on mixing intensity with average of all phase angle ωt . We observe that degree of mixing value increases regularly with increase in velocity amplitude ratio β . Degree of mixing can be achieved up to 0.90 for $Re_{st} = 600$ with pulsation

conditions of $\beta=2$ and $\alpha=10$. For the $Re_{st}=420$, degree of mixing reaches up to 0.70 with $\beta=2$ and $\alpha=8-10$.

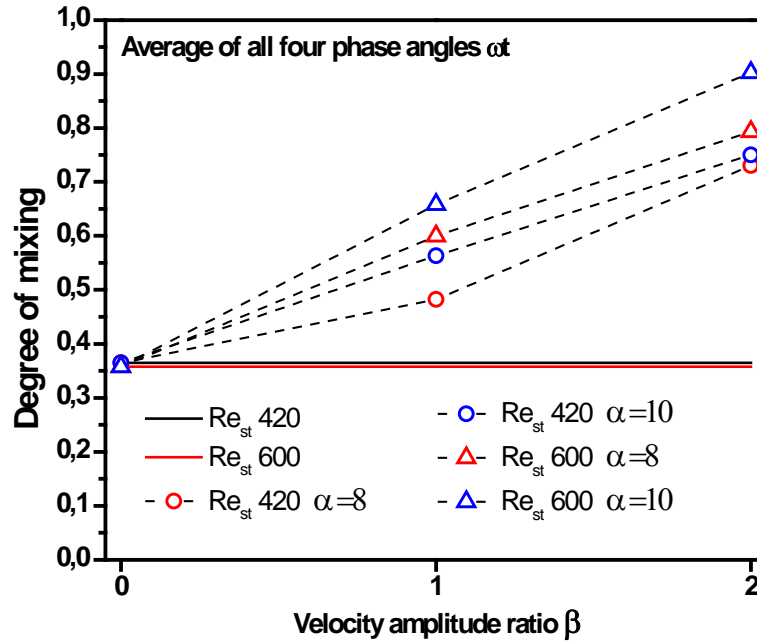


Figure III-32. Influence of β on mixing intensity with average of all phase angle ωt .

Figure III-33 shows influence of β on relative mixing intensification ψ for the average of all phase angles ωt . We observe that maximum value of relative mixing intensification $\psi=155\%$ for $Re_{st}=600$ with $\alpha=10$ and $\beta=2$. Maximum value of relative mixing intensification $\psi=107\%$ is obtained for $Re_{st}=420$ at $\alpha=10$ and $\beta=2$.

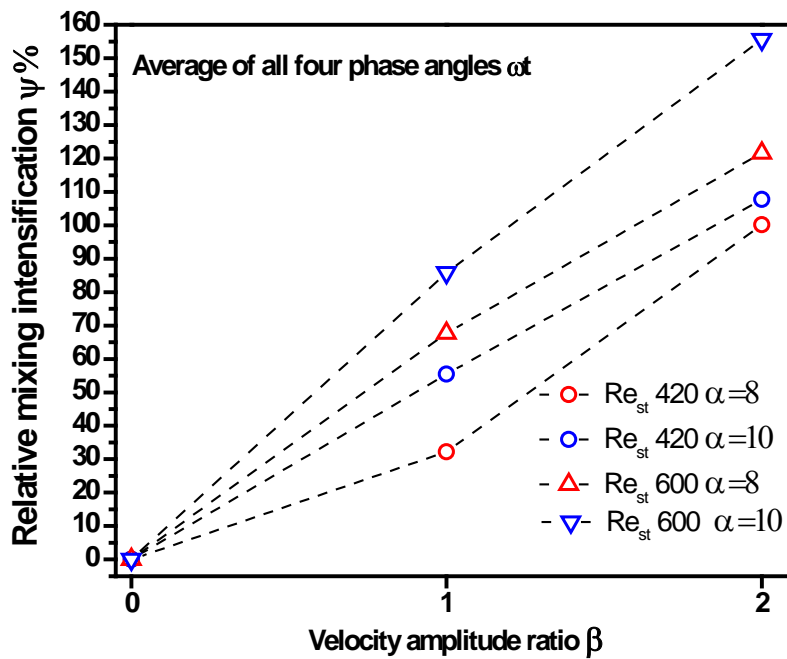


Figure III-33. Influence of velocity amplitude ratio β on relative mixing intensification ψ for average of all phase angles ωt .

III.3.5. Influence of phase angle ωt

At the lowest phase position, $\omega t = 0^\circ$, the pulsatile velocity $U_p(t)$ at the entrance of the curved pipe is equal to the mean steady flow velocity, U_{ms} . When the phase position is $\omega t = 90^\circ$, the pulsatile velocity at the entrance of the curved pipe reaches its highest value, i.e. $(1 + \beta)U_{ms}$ and the flow rate through the curved pipe is maximum. The deceleration zone of the oscillating velocity curve starts from this phase position. At the phase angle of 180° , similar to the phase position $\omega t = 0^\circ$, the pulsatile velocity becomes again equal to the mean steady flow velocity, U_{ms} . At $\omega t = 270^\circ$ the flow rate through the pipe is minimum. The variety of the observed structures at $\omega t = 270^\circ$ is much greater than what has been distinguished for previous phase positions (Jarrahi et al., 2011).

Figure III-34 shows changes in mixing degree with the phase angle ωt over an oscillation period for $Re_{st} = 420, 600, 800$ and 1000 and $\alpha = 8$ and $\beta = 1$. Here mixing degree increases between phase angles of 0° and 90° , at which it reaches its maximum value.

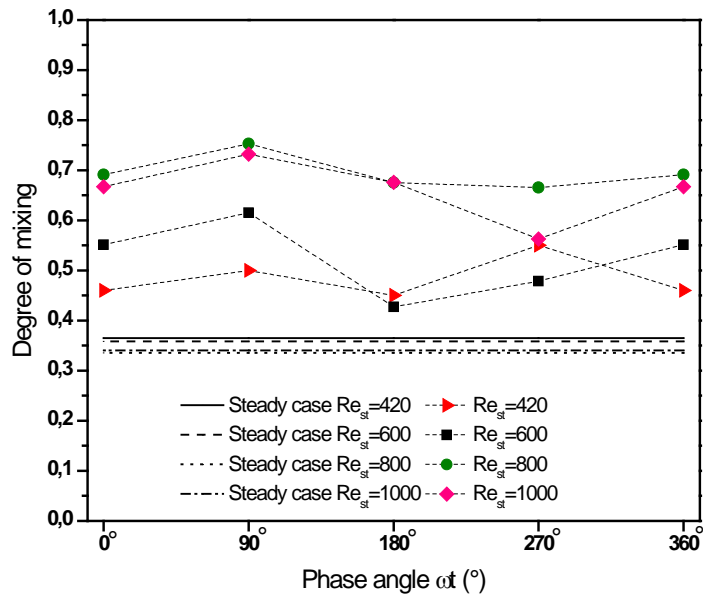


Figure III-34. Influence of phase angle ωt on mixing intensity for $\alpha=8$ and $\beta=1$.

Figure III-35 represents mixing degree versus the phase angle ωt over an oscillation period for $Re_{st}=420, 600, 800$ and 1000 and $\alpha=10$ and $\beta=1$. Here mixing degree increases between phase angles of 0° and 90° for all cases except in pulsation case of $Re_{st}=420$ where we observe the maximum degree of mixing about 0.65 at phase angle $\omega t=270^\circ$.

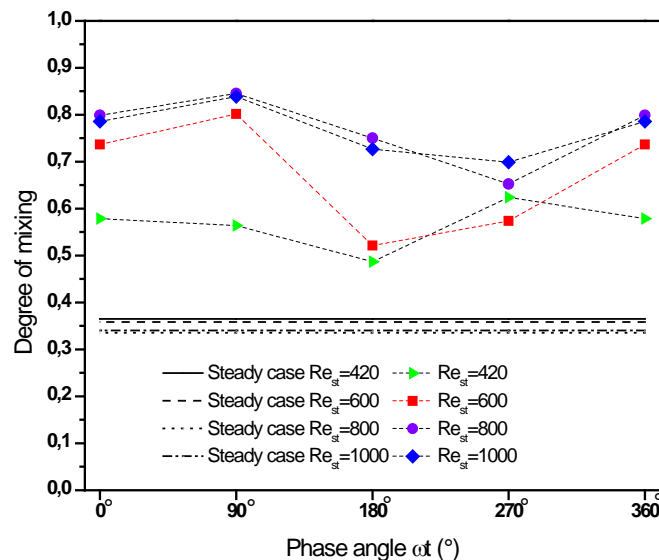


Figure III-35. Influence of phase angle ωt on mixing intensity for $\alpha=10$ and $\beta=1$.

Figure III-36 shows the influence of phase angle ωt on mixing intensity for $Re_{st}=420$ with $\beta=1$. Degree of mixing values vary with phase angles ωt . Maximum degree of mixing about 0.52 and 0.62 is observed for respectively $\alpha=8$ and 10 at the phase angles $\omega t=270^\circ$. Maximum degree of mixing about 0.58 is observed for $\alpha=12$ at the phase angles $\omega t=0^\circ$.

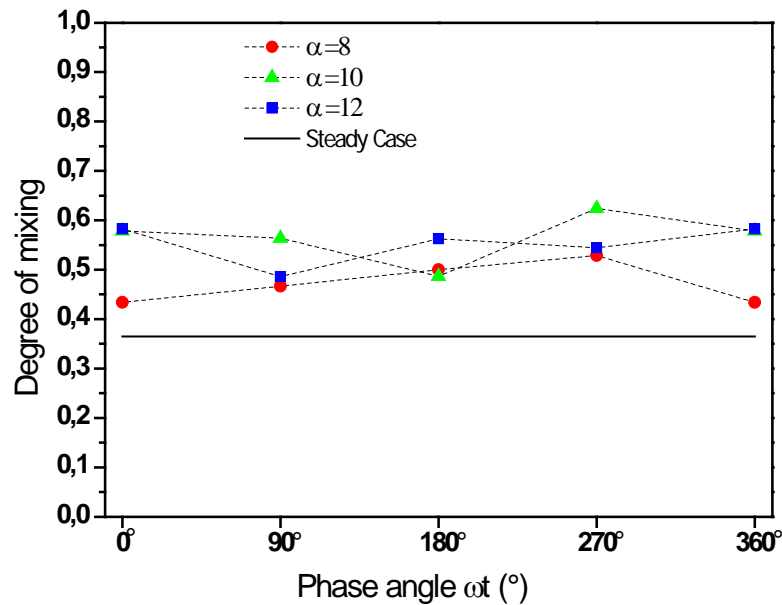


Figure III-36. Influence of phase angle ωt on mixing intensity for $Re_{st} 420$ at $\beta=1$.

Figure III-37 plots the influence of phase angle ωt on mixing intensity for $Re_{st}=600$ at $\beta=1$. Maximum degree of mixing about 0.85 is observed for $\alpha=15$ at the phase angles $\omega t=0^\circ$. For $\alpha=8$ and 10, a maximum degree of mixing about 0.63 and 0.84 is observed at the phase angle $\omega t=90^\circ$.

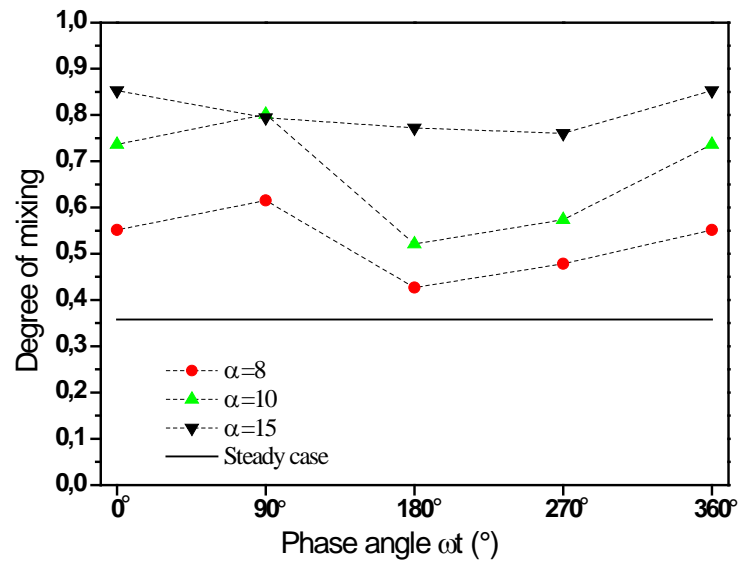


Figure III-37. Influence of phase angle ωt on mixing intensity for $Re_{st} = 600$ at $\beta = 1$.

Figure III-38 shows influence of phase angle ωt on mixing intensity for $Re_{st} = 800$ and $\beta = 1$. Maximum degree of mixing about 0.85 is observed for $\alpha = 15$ at the phase angle $\omega t = 90^{\circ}$. For $\alpha = 8$, maximum degree of mixing about 0.77 is observed at the phase angle $\omega t = 90^{\circ}$. Since, according to this paragraph, the maximum degree of mixing occurs at the phase angle $\omega t = 90^{\circ}$ for all studied values of α .

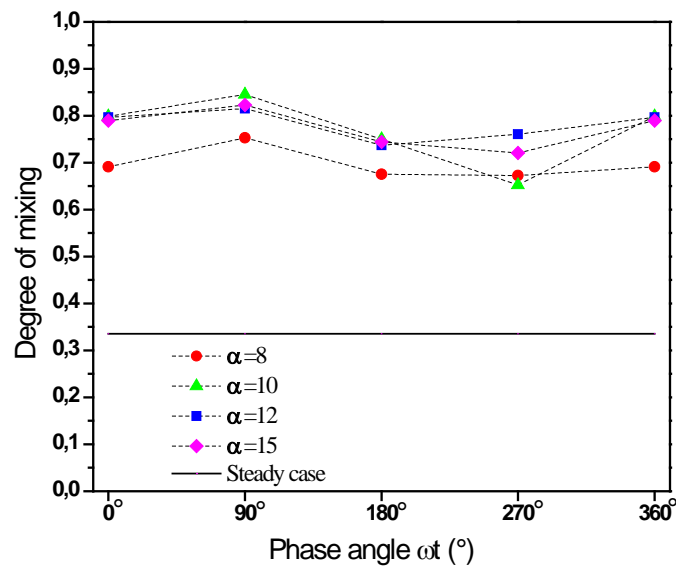


Figure III-38. Influence of phase angle ωt on mixing intensity for $Re_{st} = 800$ and $\beta = 1$

Figure III-39 shows influence of phase angle ωt on mixing intensity for $Re_{st}=1000$ and $\beta=1$. Maximum degree of mixing about 0.85 is observed for $\alpha=11$ during the phase angle $\omega t=90^\circ$. For $\alpha=8$ and 10, maximum degree of mixing about 0.73 is also observed at the phase angle $\omega t=90^\circ$. Since, according to this paragraph, the maximum degree of mixing occurs at $\omega t=90^\circ$ for all studied values of α .

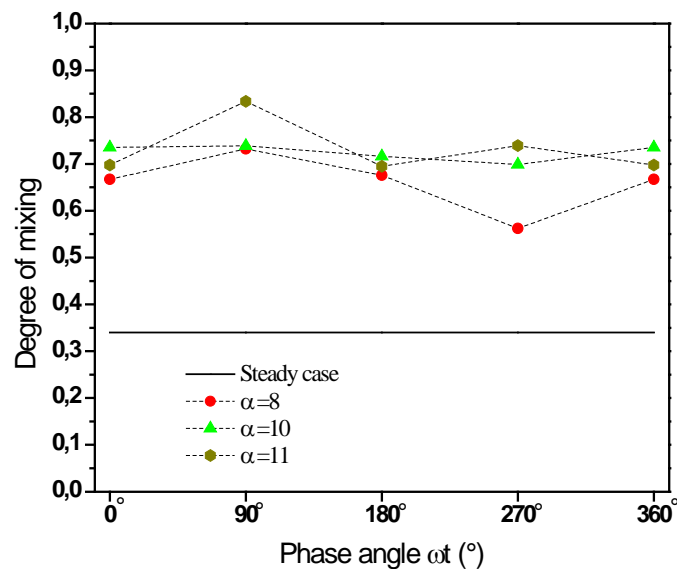


Figure III-39. Influence of phase angle ωt on mixing intensity for $Re_{st}=1000$ and $\beta=1$.

Figure III-40 shows influence of phase angle ωt on mixing intensity for $Re_{st}=420$ at $\alpha=8$. The degree of mixing fluctuates with respect to phase angle ωt . It increases with phase angle $\omega t=90^\circ$ and 270° while it has a weak value at phase angle $\omega t=0^\circ$ and 180° . A strong point is that degree of mixing is increased in pulsated cases compared to steady cases, and it increases as the velocity amplitude ratio β increases. Maximum degree of mixing about 0.77 is observed for $\beta=2$ during the phase angle $\omega t=270^\circ$. For $\beta=1$, maximum degree of mixing about 0.55, is observed at the phase angle $\omega t=270^\circ$.

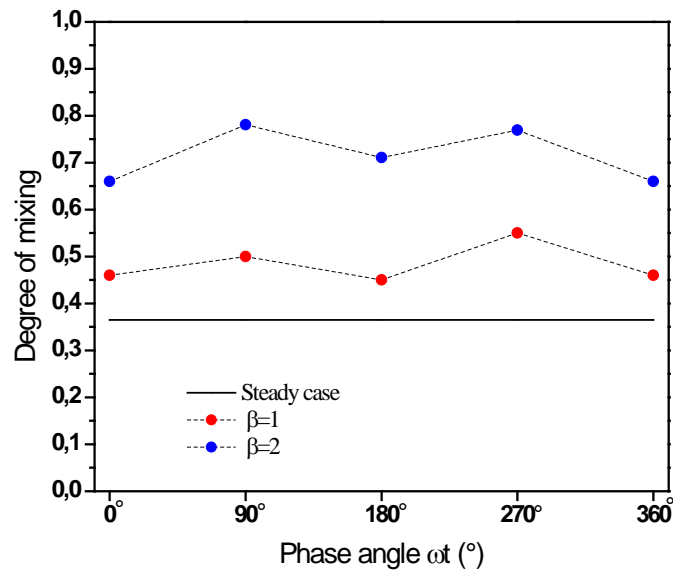


Figure III-40. Influence of phase angle ωt on mixing intensity for $Re_{st}=420$ at $\alpha=8$.

Figure III-41 shows influence of phase angle ωt on mixing intensity for $Re_{st}=600$ at $\alpha=10$. The maximum value of degree of mixing observed at phase angle $\omega t=90^\circ$ is about 0.94 for $\beta=2$. For $\beta=1$ during the phase angle $\omega t=90^\circ$ a maximum degree of mixing is found about 0.85.

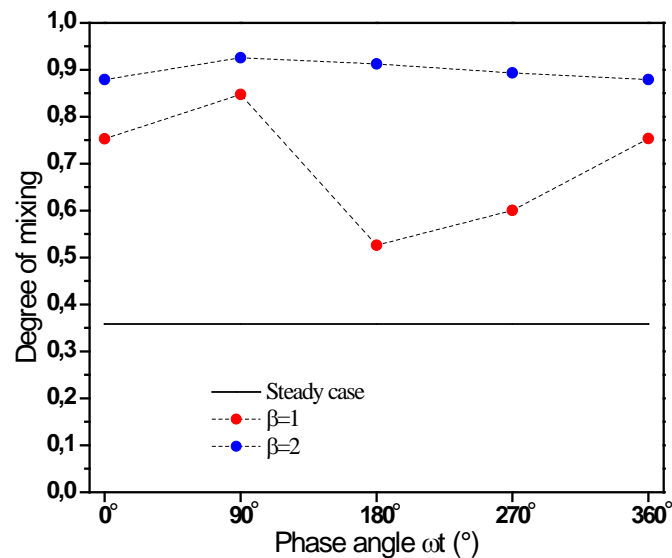


Figure III-41. Influence of phase angle ωt on mixing intensity for $Re_{st}=600$ at $\alpha=10$.

Concluding this section, the mixing degree increases between phase angles of 0° and 90° for $\alpha \leq 10$. Then it gradually decreases in the phase 180° of the oscillation period. Beyond this phase angle, it increases again until the phase 270° . However, for certain pulsation cases the frequencies $\alpha > 10$, the phase angle at which the mixing degree becomes maximum is greater than 90° ($\omega t > 90^\circ$). The increasing mixing degree in a phase between 0° and 90° in the oscillation period can be attributed to the acceleration of the flow in this part of the oscillation period (Jarrahi (2010), the vorticity and the strain rate play a significant role in transverse mixing increase between 0° and 90°).

III.4. Conclusions

Planer Laser Induced Florescence (PLIF) technique is used to measure the concentration field in a *developing* laminar pulsating flow through a circular 90° curved pipe. Planar laser induced fluorescence technique is for the first time implemented in the laboratory. Calibration of the experimental setup with PLIF technique is a delicate process and it takes a lot of time to perform the experiments for the different pulsation conditions.

The PLIF measurements are carried out for Reynolds numbers $Re_{st}=420, 600, 800$ and 1000 both for steady cases and pulsatile flows with Womersley numbers $8 \leq \alpha \leq 21$ and velocity component ratio $\beta=1, 2, 3$. The effects of these parameters on the mixing intensification are studied. The PLIF results of secondary flow for four different phase positions $\omega t=0^\circ, 90^\circ, 180^\circ$ and 270° are analyzed. The detailed PLIF measurements of the secondary flow showed that pulsatile flow in a curved pipe has a great influence on mixing intensity. The combination of the three control parameters: Reynolds number Re_{st} , frequency parameter α and velocity amplitude ratio β renders the resulting flow highly complex.

The influence of Re_{st} , α and β on mixing degree is analyzed. For pulsation cases, degree of mixing increases with the Reynolds number. The mixing degree in the configuration where the velocity-amplitude ratio β is equal to 2 reaches up to 0.94 for $Re_{st}=600$. At the exit of the curved pipe, we observe a difference in the degree of mixing value for different pulsation conditions. When the velocity amplitude ratio is unity ($\beta=1$), mixing is better in the boundary layer near the wall. On the other hand, when the velocity-amplitude ratio is $\beta=2$, the effective mixing zones are increased by occupying a larger surface.

We observe that maximum value of relative mixing intensification $\psi=155\%$ for $Re_{st}=600$ at $\alpha=10$ and $\beta=2$. Maximum value of relative mixing intensification $\psi=107\%$ is obtained for $Re_{st}=420$ at $\alpha=10$ and $\beta=2$.

In summary, the experimental results yielded certain information on tracer transport. The first type of information relates to the stretching and folding mechanisms. Two initially close trajectories diverge due to the effect of pulsation. Flow visualizations showed that the pulsation works to amplify the mixing by stretching the tracer lines in a larger space of the 90° curved circular pipe section.

Analysis of the dye deformation suggested that the pulsation imposition on a flow in 90° bend always generate better mixing in the tested operating conditions.

Chapter 4

Heat transfer intensification by pulsatile flow

Objective

This chapter is devoted to study the heat transfer enhancement by flow manipulation in a shell and tube heat exchanger. The configuration of the heat exchanger results of a succession of bent tubes chaotically twisted. By imposing pulsations to convert the steady flow into a pulsatile flow, some important improvements are measured and compared with the continuous flow. Effects of different pulsation parameters on the heat transfer enhancement are observed that makes this flow much more complex and favorable for efficient heat exchanger. Finally, optimum values for pulsation parameters are determined.

IV.1. Introduction

From the previous studies (summarized in Chapter 1), it can be observed that, due to variety of heat transfer control parameters, some conflicting results appear about effect of pulsation on heat transfer. Most investigators reported increase in heat transfer due to pulsated flow and some reported little increase, no increase, or even decrease in heat transfer for some configurations.

Therefore, this study is devoted to examine the effect of pulsation on heat transfer in a particular shell and tube heat exchanger. Three different wave forms *i.e.* sinusoidal, triangular and square signals are generated to obtain different pulsation conditions identified by Reynolds numbers in the range of $600 \leq Re_{st} \leq 5000$, Womersley numbers α varying between 0 to 20 *i.e.* frequency ranges between 0 and 4 Hz, and velocity amplitude ratio β between 1 to 16.

IV.2. Pulsatile flow and Dean configuration

Pulsatile flow is composed of a steady component and a superimposed periodical time varying component called oscillation. Oscillating flow itself is a special pulsatile flow which is governed by an oscillation alone, with a zero steady flow component. Important feature of

pulsatile flow is that it causes some alterations in the secondary flow in terms of stretching and folding of Dean roll-cells. Therefore, by adjusting pulsation parameters, one can make this flow more complex and favorable for efficiently heat transfer.

A temporal dependence imposed on a steady flow through a pipe, particularly in laminar flow regime, can modify the structures of main flow as well as the secondary flow. If this temporal dependence is imposed in the form of sinusoidal axial velocity, the structure of the flow can be more complex for certain conditions Jarrahi (2010). The velocity gradients are stronger in the secondary flow structures as compared to that in the main flow. These velocity gradients intensify the rate of stretching and folding, which are the main principles mechanisms in the mixing thus in uniform heating process in a heat exchanger.

The pulsatile flow used in this study is a compilation of a steady and an oscillation term, which may be of sinusoidal, triangular or square form. The equation for the pulsatile velocity U_p can be written in a general case as:

$$U_p(t) = U_{st} + U_{osc}(t) \quad (IV-1)$$

where U_{st} is the mean steady velocity and $U_{osc}(t)$ is the pure oscillating flow, which is the time-dependent component of the pulsatile velocity.

For the sinusoidal oscillation, if the amplitude of the sinusoidal oscillating flow is U_{sinmax} and the angular frequency of the oscillation is ω , with $\omega = 2\pi f$ where f is the frequency, then equation (IV-1) can be written as:

$$U_p(t) = U_{st} + U_{sinmax} \sin(\omega t) \quad (IV-2)$$

For the square oscillation, using Fourier expansion with cycle frequency f over time t , we can represent an ideal square wave with a peak to peak amplitude of two as an infinite series of the form:

$$U_p(t) = U_{st} + \frac{4}{\pi} \sum_{k=1}^{\infty} \frac{\sin(\omega t(2k-1))}{(2k-1)} \quad (IV-3)$$

For the triangular oscillation:

$$U_p(t) = U_{st} + \frac{8}{\pi^2} \sum_{k=0}^{\infty} (-1)^k \frac{\sin \omega((2k+1)t)}{(2k+1)^2} \quad (IV-4)$$

The angular frequency ω can also be described by a dimensionless parameter α also called the Womersley parameter, defined as:

$$\alpha = r_0 \left(\frac{\omega}{\vartheta} \right)^{\frac{1}{2}} \quad (\text{IV-5})$$

where r_0 is the radius of the pipe and ϑ is the kinematic viscosity of the fluid. The Womersley number is calculated with the same equation (IV-5) for all pulsation wave forms i.e. sinusoidal, triangular and square.

A velocity component ratio is defined as the ratio between the maximum oscillating amplitude of the oscillating velocity term and the average value of the steady velocity term. The velocity component ratio β is calculated by the following relations which depend of the pulsation wave form:

For sinusoidal signal:

$$\beta = \frac{U_{sinmax}}{U_{st}} \quad (\text{IV-6})$$

For triangular signal:

$$\beta = \frac{U_{triangularmax}}{U_{st}} \quad (\text{IV-7})$$

For square signal:

$$\beta = \frac{U_{squaremax}}{U_{st}} \quad (\text{IV-8})$$

IV.3. Pulsation conditions and measurements

A chaotically twisted tube comprised of 12 circular tube bends and every bend is 90° curved. This geometry is immersed in a rectangular shell, filled with water whose temperature is kept at a constant temperature of 52°C. Experiments are run for seven flow rates in the tube side corresponding to Reynolds numbers between 600 and 5000 with an inlet tube side temperature maintained at 11°C thanks to thermostat LAUDA PROLINE RP855. The experimental setup is discussed in detail in Chapter 2 and Table IV-1 recapitulates the details of the tested pulsation conditions.

Experiments are conducted for 7 Reynolds numbers in the range of $600 \leq Re_{st} \leq 5000$. The 13 Womersley frequency parameters are chosen in the range $0 \leq \alpha \leq 20$. The oscillation pulsations are in three different wave forms i.e. sinusoidal, triangular and square.

The velocity amplitude ratio β is generally chosen among 6 values in the range $0 \leq \beta \leq 6$. For the case $Re_{st}=800$ and sinusoidal pulsation, the velocity amplitude ratio is taken in the range $0 \leq \beta \leq 13$ among 9 values, in order to explore the influence of the amplitude ratio beyond its optimum value around $\beta \approx 6$. As we show that β values higher than 6 have a lower positive influence in terms of heat transfer enhancement, and even a negative influence for some operating conditions, it is the reason why the general study case of β is in the range 0–6.

For the triangular and square pulsations cases, the setup is not technically capable to produce a pulsated flow for values $\beta > 4$. Therefore we have studied the influence of β for the triangular and square pulsations wave forms in the range $0 \leq \beta \leq 4$.

Reynolds number Re_{st}	Womersley frequency parameter α	Velocity amplitude ratio β	Pulsation wave form
600		0, 1, 2, 3, 4, 6	Sinusoidal
800	0, 6, 8, 9, 10, 11, 12, 13, 14, 16, 17, 19, 20	0, 1, 2, 3, 4, 6, 8, 10, 13	Sinusoidal
		0, 1, 2, 3, 4	Square
			Triangular
1000			
1500			
2000		0, 1, 2, 3, 4, 6	Sinusoidal
2700			
5000			

Table IV-1. Pulsation conditions tested in this work.

IV.3.1. Verification of the pulsation flow

The pulse generator presented here produces pure sinusoidal, triangular and square oscillations. Figure IV-I shows the measurements of the axial velocity using a laser Doppler anemometer (DANTEC Dynamics). These measurements are carried out in the straight tube

of 2m long, located upstream of the heat exchanger, where the flow is assumed hydrodynamically established. This technique is pre-configured for instantaneous measurements and highly accurate with calibration coefficient uncertainty lower than 0.1%.



Figure IV- 1 Instantaneous velocity measurement through FlowExplorer laser Doppler anemometer

Table IV-2 shows specifications of the FlowExplorer laser Doppler anemometer.

Optical head		
Standard FlowExplorer	35 mW for the 1st and 2nd velocity components	
High Power FlowExplorer	90 mW for the 1st velocity component 70 mW for the 2nd velocity component	
FlowExplorer 300	300 mW for the 1st and 2nd velocity components	
Dimensions of optics head	98 x 98 x 396 mm	
Weight	5 kg	

Table IV-2. Specifications of the Flow Explorer laser Doppler anemometer.

Table IV-3 shows the measurement volume and velocity range of the FlowExplorer laser Doppler anemometer.

Measurement distance	285 mm		485 mm		735 mm	
Measurement volume diameter ⁽¹⁾	0.1 mm		0.17 mm		0.25 mm	
Measurement volume length ⁽¹⁾	1 mm		2.8 mm		6.3 mm	
Signal processor	BSA F30	BSA F60	BSA F30	BSA F60	BSA F30	BSA F60
Maximum velocity ⁽²⁾	27 m/s	212 m/s	45 m/s	352 m/s	68 m/s	528 m/s
Measurable velocity fluctuation	Better than 0.002% of the velocity range					

(1) Nominal values for one and two velocity component systems. (2) Standard and High Power FlowExplorer 1st velocity components.

Table IV-3. Measurement volume and velocity range of the FlowExplorer laser Doppler anemometer.

Figure IV-2, Figure IV-3 and Figure IV-4 represent measurements of instantaneous velocities compared to the correspondent theoretical case for the pulsation wave forms of respectively, sinusoidal, triangular and square signals. The red line on the three figures represents the theoretical case and permits to calculate the deviation of the measured velocity to the theoretical signal. The standard deviation is computed in the three cases given in Figure IV-2, Figure IV-3 and Figure IV-4. The values of the standard deviation are equal to: 0.0083 m/s (for the sinusoidal wave form), 0.036 m/s (for the triangular wave form) and 0.071 m/s (for the square wave form). The correspondence between the measured and the theoretical signals are rather great, especially for the sinusoidal and even for the triangular signals, the deviation is rather weak and the sinusoidal and triangular experimental cases are close to their theoretical cases. The measured square signal is quite deformed compared to the theoretical square case, in fact there are some fluctuations of the velocity around the plateau values and nevertheless the standard deviation is not so great because it is only twice that of the triangular case. Then, although the measured square velocity case is not so close to a perfect square signal, this case is named in the following square signal.

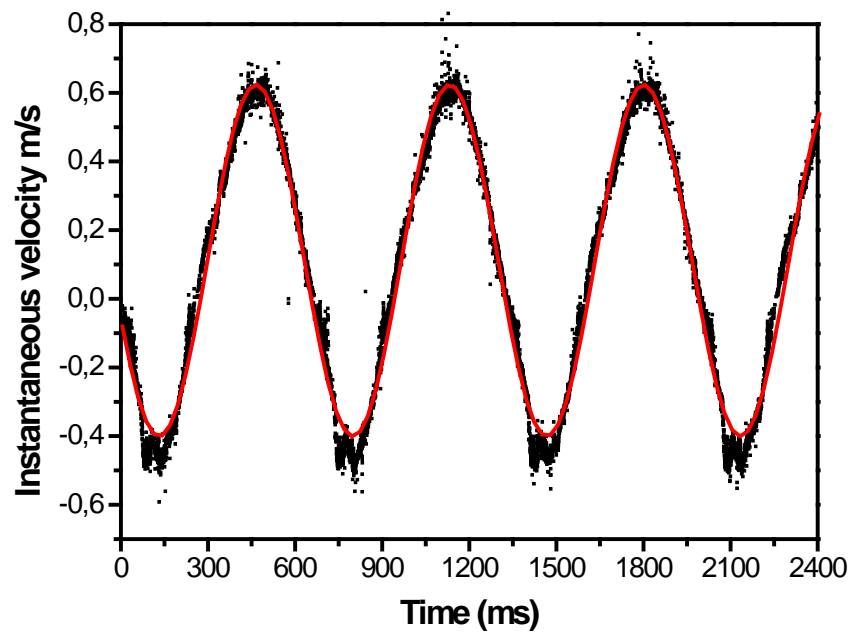


Figure IV- 2. Instantaneous velocity for $Re_{st}=800$, $\alpha=14$ and $\beta=4$ – Sinusoidal pulsation. The red line represents the theoretical case

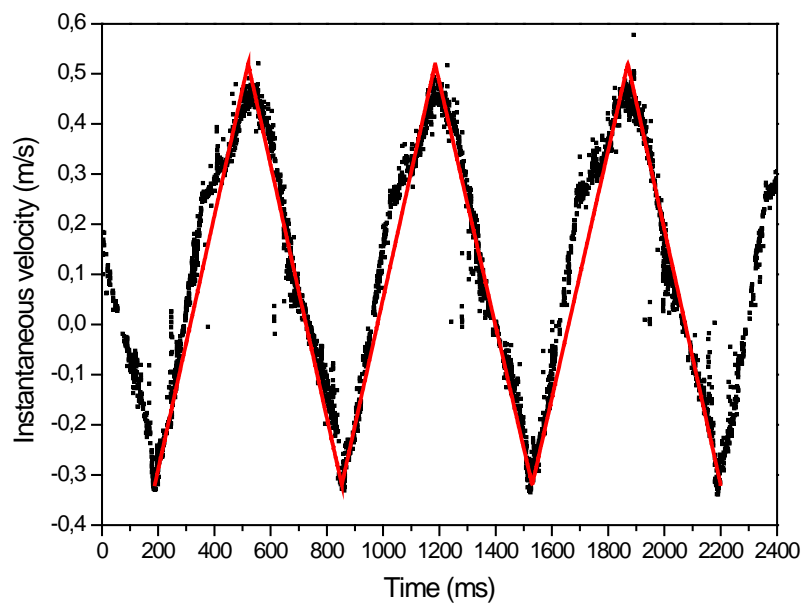


Figure IV- 3.. Instantaneous velocity for $Re_{st}=800$, $\alpha=14$ and $\beta=3$ – Triangular pulsation. The red line represents the theoretical case.

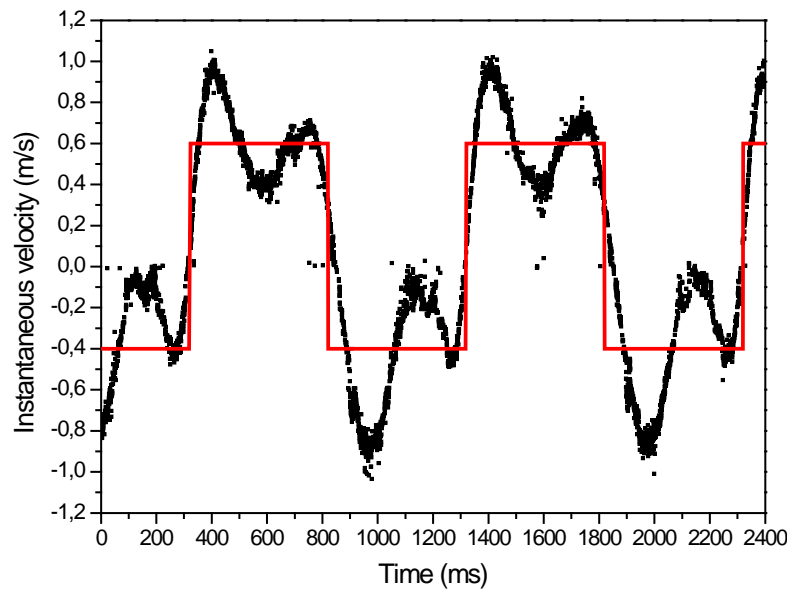


Figure IV- 4. Instantaneous velocity for $Re_{st}=800$, $\alpha=14$ and $\beta=4$ – Square pulsation. The red line represents the theoretical case.

IV.3.2. Quality of measurement

IV.3.2.1. Temperature measurement accuracy

Temperature profiles are measured on a 8 mm tube diameter at 8 different vertical locations with 1 mm vertical distance in each, at two locations in the chaotically twisted tube: at the entrance and at the exit of the heat exchanger. The inlet location of measurements of tube side temperature T_{inlet} is positioned at 20 mm before the first bent tube entrance and the outlet tube side temperature T_{outlet} is taken at 20 mm downstream the last bend exit. The experimental setup is conceived in a closed circuit and the hot fluid at the exit of the heat exchanger is re-used and cooled in order to be re-injected at the inlet of the heat exchanger, therefore it can be observed some variations in the tube side inlet temperature T_{inlet} , nevertheless this fact has no influence on the heat performances measurements as the interesting measured phenomenon is the overall heat transfer between the inlet and the exit, which must be independent of the inlet temperature. Hence the pertinent measured variable is the temperature difference ΔT for the tube side:

$$\Delta T = T_{outlet} - T_{it} \quad (IV-9)$$

Figure IV-5 shows temperature profiles $T_{outlet-i}$ at outlet of the chaotic tube for $Re_{st}=800$ and $\beta=3$ with sinusoidal pulsation, the i index standing for the different locations of

measurements in the profile. This graph is taken as an example to show that the temperature profiles obtained are flat and do not vary from the lower wall to the upper wall of the tube section at outlet. Flat profiles are firstly explained by the chaotic geometry, and secondly by the pulsations imposed on the tube side flow, each of these phenomena enhance the fluid mixing and then the thermal homogenization. Temperatures are measured after verifying the conditions are well established with pulsation i.e. inlet temperature and stable thermal measurements. At each point shown in the Figure IV-5 the temperature measurements are carried out for 3 minutes and every single point is the result of the arithmetic average of 300 instantaneous temperature values. As no variation is observed on each exit temperature profile, the outlet tube side temperature T_{outlet} is calculated as the average of the 8 $T_{\text{outlet}-i}$ temperatures, and is representative of the mean temperature at the exit of the heat exchanger.

$$T_{\text{ot}} = \text{mean}(T_{\text{outlet}-i}) \quad (\text{IV-10})$$

The inlet tube side temperature T_{inlet} is thus the mean of $T_{\text{inlet}-i}$.

$$T_{\text{it}} = \text{mean}(T_{\text{inlet}-i}) \quad (\text{IV-11})$$

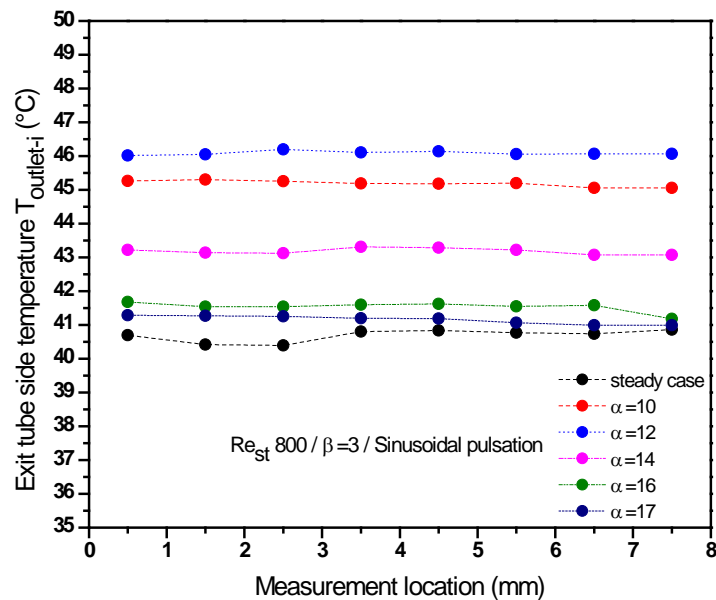


Figure IV- 5. Outlet temperature profiles $T_{\text{outlet}-i}$ for $Re_{\text{st}}=800$ and $\beta=3$ – Sinusoidal pulsation. Lower and upper walls are at 0 mm and 8 mm, respectively.

In the Figure IV-6, exit temperature variance values are plotted for $Re_{\text{st}}=800$, $0 \leq \alpha \leq 17$ and $\beta=3$ with sinusoidal pulsation. The variance in the steady case has the maximum value of

0.033 °C and the variances of the pulsated cases are comprised between 0.003°C and 0.022°C with the minimum variance for the case $\alpha=12$. Globally, the variances in temperature profiles are rather weak, indicating that the data points tend to be very close to the mean temperature value.

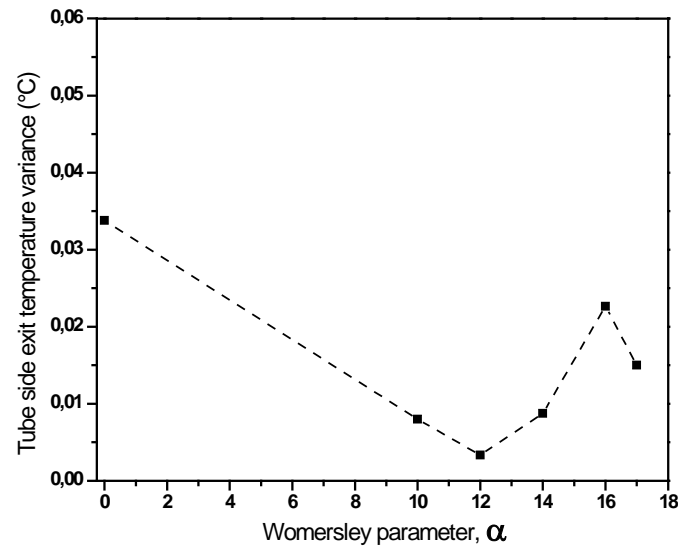


Figure IV- 6. Exit temperature variance for $Re_{st}=800$, $0 \leq \alpha \leq 17$ and $\beta=3$ – Sinusoidal pulsation.

Figure IV-7 shows tube side temperature difference ΔT calculated from the equations IV-9 and IV-10. Ten measurements for each operating condition are carried out to calculate the error bar for the experiments. The repeatability of the curves has been verified by retesting some experimental conditions several days apart. An overall error bar is calculated and worth $\pm 2.5\%$ of the data measurement, which means less than 1°C.

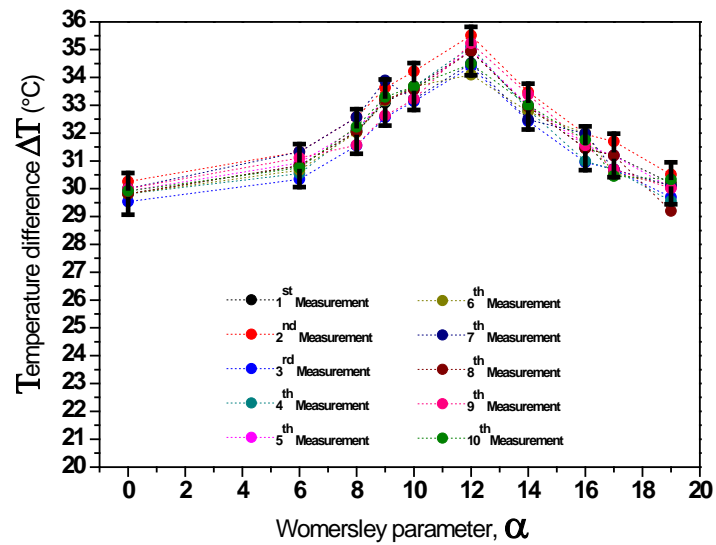


Figure IV- 7. Temperature difference ΔT obtained for $Re_{st}=800$ and $\beta=3$ – Sinusoidal pulsation.

IV.3.2.2. Standard deviation of measurement

Figure IV-8 shows standard deviation of the temperature difference ΔT in the steady and pulsated cases of the chaotic geometry for $Re_{st}=800$ and $\beta=3$.

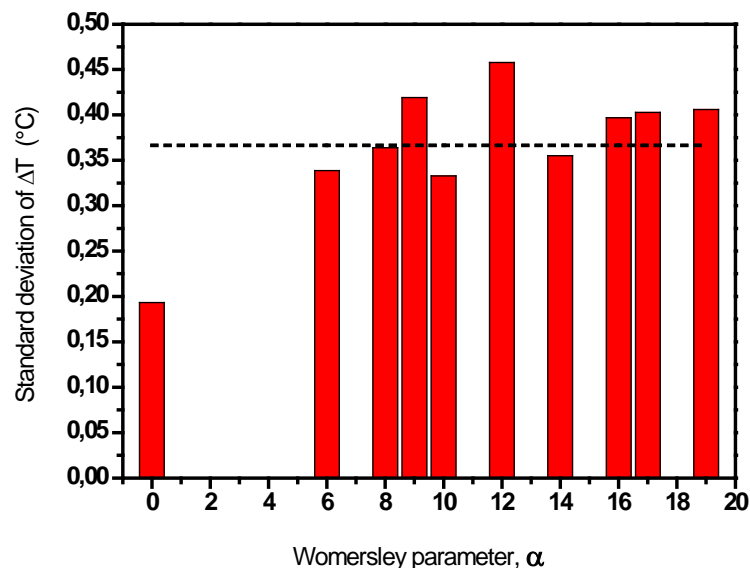


Figure IV- 8. Standard deviation of ΔT for $Re_{st}=800$ and $\beta=3$ – Sinusoidal pulsation.

Each bar represents the standard deviation of 10 experiments carried out with the same operating conditions. The observed standard deviation is smaller for steady cases compared to pulsated cases, approximately half. There is not a clear tendency of the frequency influence

for all the pulsated cases since the values are nearly constant for the pulsated cases. The dotted line in the Figure IV-8 represents the overall standard deviation, calculated for the whole 100 cases, and is equal to 0.366°C .

IV.3.2.3. Reproducibility of measurement

To evaluate the reproducibility of the measurements, three measurements of each case (steady or pulsated conditions) are carried out for Reynolds number $Re_{st}=800$, for the frequency parameter range $0 \leq \alpha \leq 19$ and the different velocity amplitude ratio β for the sinusoidal signal. Figures IV-9, IV-10 and IV-11 represent the temperature difference ΔT obtained for these operating conditions, respectively for $\beta=1, 2$ and 4 . The graphs show that the experiments conducted have an ability to be reproduced.

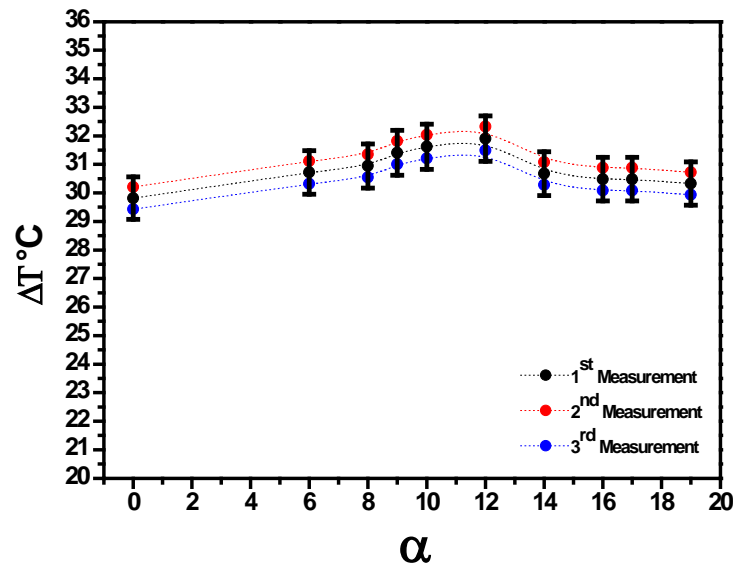


Figure IV- 9. Temperature difference ΔT obtained for $Re_{st}=800$ and $\beta=1$ – Sinusoidal pulsation.

The result values of Figures IV-9, IV-10 and IV-11 are to be commensurate to the same trend as in Figure IV-7 and they are obtained in distinct experimental trials according to the same reproducible experimental description and procedure. The graphs are found coherent and all the results are in the range of error bar of 2.5% of the data.

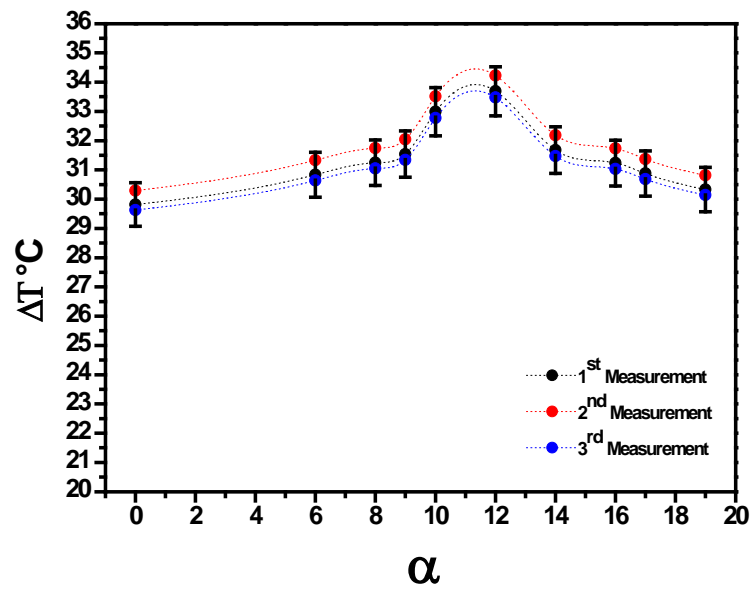


Figure IV- 10. Temperature difference ΔT obtained for $Re_{st}=800$ and $\beta=2$ – Sinusoidal pulsation.

It is worth to notice that the range of error bar of 2.5% of the data measurements is valid and nearly constant on the whole frequency parameter α and for the different cases of the amplitude velocity parameter β , independently of the temperature difference profile ΔT which is more or less deformed.

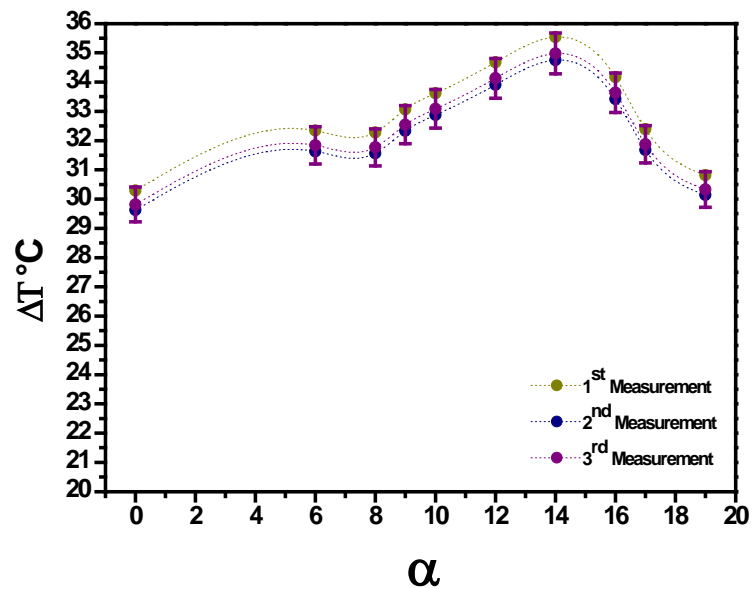


Figure IV- 11. Temperature difference ΔT obtained for $Re_{st}=800$ and $\beta=4$ – Sinusoidal pulsation.

IV.4. Study of heat transfer

Figure IV-12 shows fluid temperature difference profiles measured between the inlet tube side temperature and the outlet tube side temperature in steady cases. The temperature is measured at 8 different locations throughout the tube diameter.

It is observed that temperature difference profiles decrease with the increase of Reynolds number due to thermal balance. The tube side temperature difference profiles are nearly flat with a maximum difference observed for the smallest Reynolds numbers, equal to 2°C for Reynolds number of 1000. The temperature difference profiles are more flat for the highest Reynolds numbers, indicating that the temperatures inside the heat exchanger sections at high Reynolds numbers are more homogeneous.

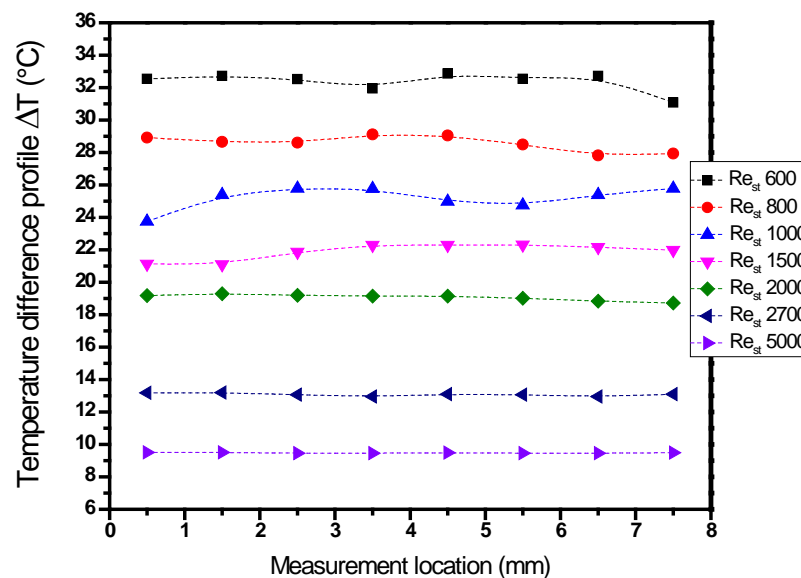
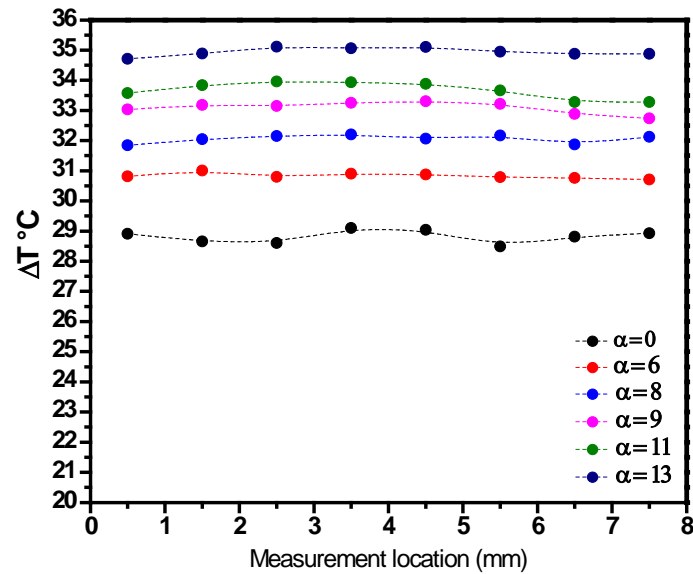


Figure IV- 12. Temperature difference profiles in steady cases for different Reynolds numbers Re_{st} .

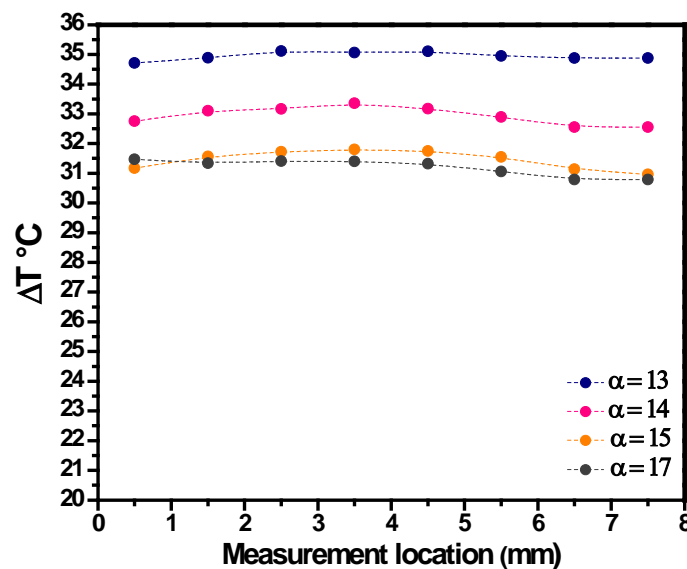
IV.4.1. Influence of frequency

Figure IV-13 shows the temperature difference ΔT profiles measured for Reynolds number $Re_{st}=800$, at the constant velocity amplitude ratio $\beta=3$ for different Womersley parameter α . It is observed that a very small and gradual change in the Womersley parameter α has a vital influence in term of the increase in temperature difference, and then in the increase of the heat transfer. The initial temperature difference in the steady case worth 29°C.

The Womersley parameter α change from 6 to 13 increases gradually the temperature difference ΔT from 31°C to 35°C while for $\alpha > 13$ the temperature difference declines: for $\alpha > 17$ the temperature difference is again equal to 31°C. Therefore $\alpha = 13$ appears as an optimum frequency parameter value for these operating conditions.



(a) $\alpha \leq 13$



(b) $\alpha \geq 13$

Figure IV- 13. Temperature difference profile for $Re_{st}=800$, $0 \leq \alpha \leq 17$ and $\beta=3$ – Sinusoidal pulsation.

IV.4.2. Influence of velocity amplitude

Figure IV-14 describes the influence of velocity amplitude ratio β on the temperature difference profiles in the heat exchanger, it is observed that the temperature difference regularly increases as the β ratio increases. The temperature difference is equal to 29 °C in average for the steady case, and is increased to 31.5°C for $\beta=1$ and until 35°C for $\beta=4$. However the increase is very weak between the cases $\beta=3$ and $\beta=4$ which seems to indicate that a saturation is nearly attained. Obtained temperature difference profiles are flat. For the certain case we also observed that temperature difference increases slightly even for $\beta>4$ till $\beta=10$.

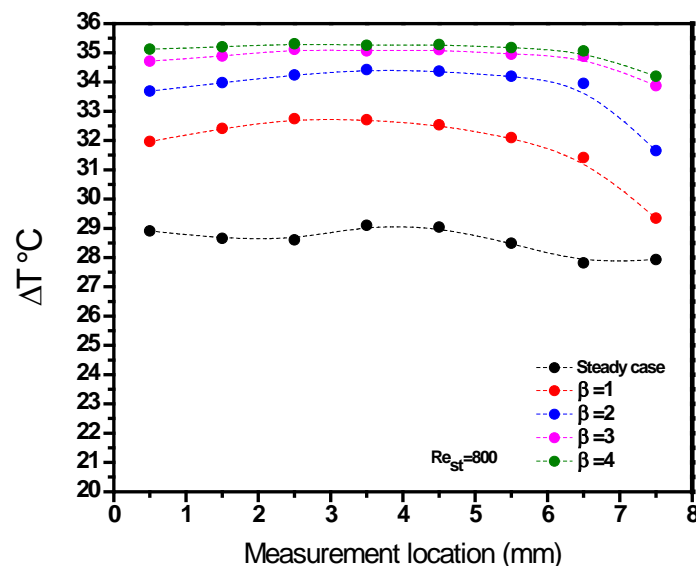


Figure IV- 14. Temperature difference profile for $Re_{st}=800$ for $\alpha=12$ – Sinusoidal pulsation.

IV.4.3. Influence of Reynolds number

Figure IV-15 represents the influence of Reynolds number Re_{st} on the temperature difference profiles for $\alpha=12$ and $\beta=3$. Here the tube side temperature difference profiles are nearly flat with a maximum difference observed for the smallest Reynolds numbers, equal to 1°C even for small Reynolds numbers. We may observe that pulsations have vital influence in increasing the temperature difference for $600 < Re_{st} \leq 2000$. There is also a slightly influence

of pulsation for $Re_{st} = 2700$ while comparing with its steady case as in Figure IV-12. For $Re_{st}=5000$ the pulsations have no influence to increase temperature difference.

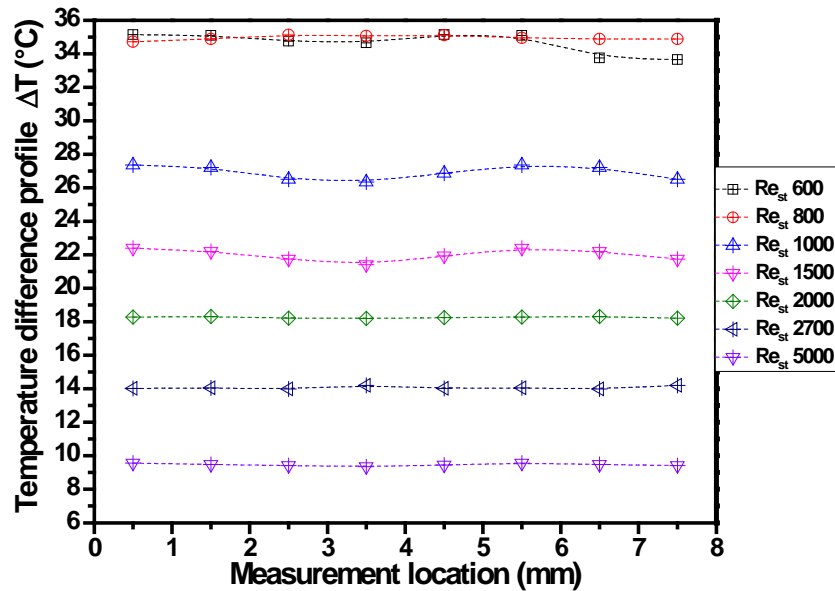


Figure IV- 15. Temperature difference profiles for $\alpha=12$ and $\beta=3$ – Sinusoidal pulsation.

IV.4.4. Influence of pulsation signal

Figure IV-16 shows the influence of pulsation signal on the temperature difference for $Re_{st}=800$, $\alpha=10$ and $\beta=4$. It can be observed that the square signal provides the better increase of temperature difference, thus of the heat transfer, compared to sinusoidal and triangular signals. The temperature difference for the steady case is in average 29°C though it attains 34.5°C for the square pulsation. The triangular pulsation signal exhibits almost the same values of temperature difference as the sinusoidal one but always shows a slight higher performance, of approximately 0.5°C . The square pulsation provides in average a temperature difference of 1.5°C more compared to sinusoidal one and 1°C compared to triangular one.

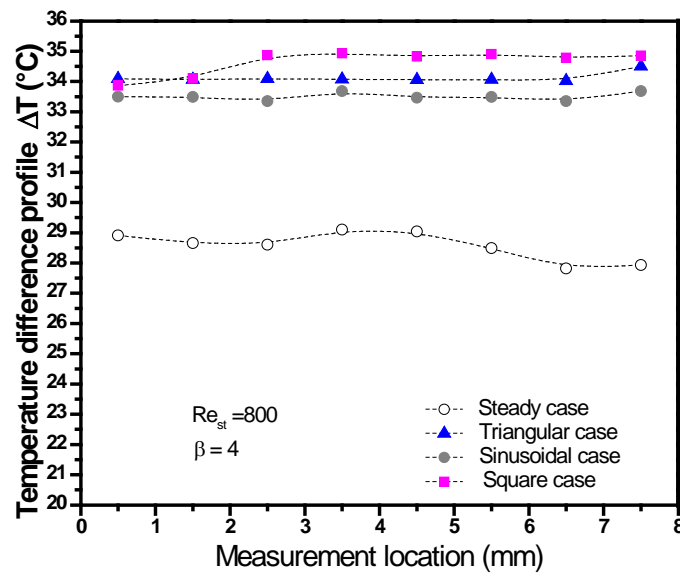


Figure IV- 16. Temperature difference profiles for different pulsation wave form for $Re_{st}=800$, $\alpha=10$ and $\beta=4$.

IV.5. Intensification of heat transfer

In all experiments, intake temperature of the fluid on the heat exchanger is regulated at 11°C . Shell-side temperature is maintained at 52°C , and the flow inside the shell is maintained at a fixed flow rate. Following equations are used to study the heat transfer intensification by pulsatile flow.

Heat exchanger efficiency is calculated as calculated by (Mokrani et al., 1997). Thermal energy received by the tube side flow is computed from

$$\varphi_t = \rho_t Q_t C_{pt} (T_{\text{outlet}} - T_{\text{inlet}}) \quad (\text{IV-12})$$

ρ_t , Q_t , C_{pt} are fluid density, flow rate and specific heat of the water.

The following expression is used to calculate the heat exchanger efficiency η .

$$\eta = \frac{\varphi_t}{(\rho Q C_p)(T_s - T_{\text{inlet}})} \quad (\text{IV-13})$$

The term (ρ_t, Q_t, C_{pt}) corresponds to the tube side fluid and T_s is the shell side temperature. Thus calculating heat exchanger efficiency can be reducing to calculate the ratio of two temperature differences:

$$\eta = \frac{(T_{\text{outlet}} - T_{\text{inlet}})}{(T_s - T_{\text{inlet}})} \quad (\text{IV-14})$$

Heat exchanger efficiency intensification χ representing the enhancement of the heat exchanger efficiency can be calculated from the relation;

$$\chi = \left(\frac{\eta_p - \eta_{st}}{\eta_{st}} \right) \quad (\text{IV-15})$$

where χ is the heat exchanger efficiency intensification, η_p and η_{st} are the heat exchanger efficiencies for pulsated cases and for steady cases respectively.

IV.5.1. Influence of frequency

Figure IV-17 shows the influence of the frequency parameter α on heat exchanger efficiency for a constant velocity amplitude ratio $\beta=3$. A gradual augmentation till a peak value is observed for heat exchanger efficiency. Heat exchanger efficiency η increases gradually from 0.69 (steady case) to 0.82, maximum value attained for $\alpha=14$. An increase of about 13% of efficiency is observed at $\alpha=14$ compared to steady state. For $\alpha>14$ a decline of the efficiency curve is observed and for the highest α almost the same value of the heat exchanger efficiency as that of steady case is observed. Therefore the value $\alpha=14$ can be observed as an optimum value of Womersley frequency parameter α in these operating conditions.

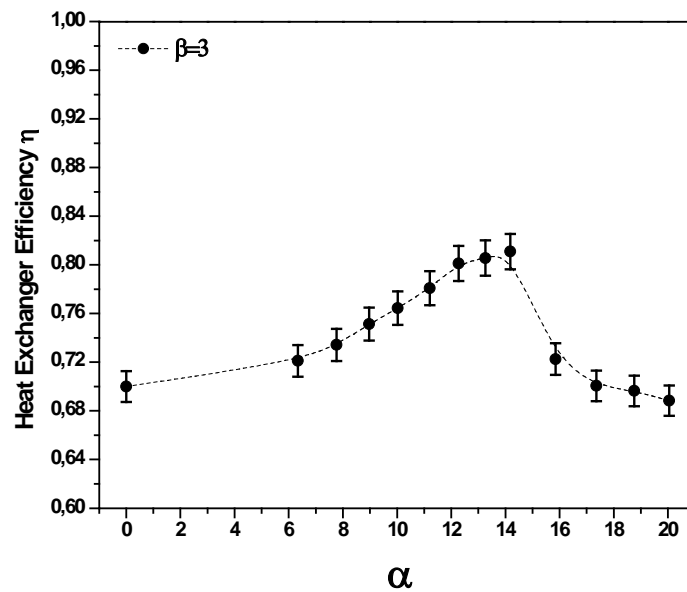


Figure IV- 17. Influence of α on heat exchanger efficiency for $Re_{st}=800$ and $\beta=3$ – Sinusoidal pulsation.

Figure IV-18 shows influence of α on heat exchanger efficiency for $Re_{st}=800$ with sinusoidal pulsation and for different velocity amplitude ratios β . The curve of heat exchanger efficiency is following the same tendency as previously observed: first a slight increase until attaining a peak value and then an abrupt decrease until attaining quite the same value as for the steady case for the highest α values. The peak value continuously increases with the increase of β value, but the increase becomes weaker for the β values higher than 6: it seems to attain a plateau in the enhancement phenomenon. The peak value for heat exchanger efficiency is observed at Womersley frequency parameter $\alpha=14$ for $\beta=[1, 2, 3, 4]$ and at $\alpha=12$ for $\beta=[6, 8, 10, 13]$.

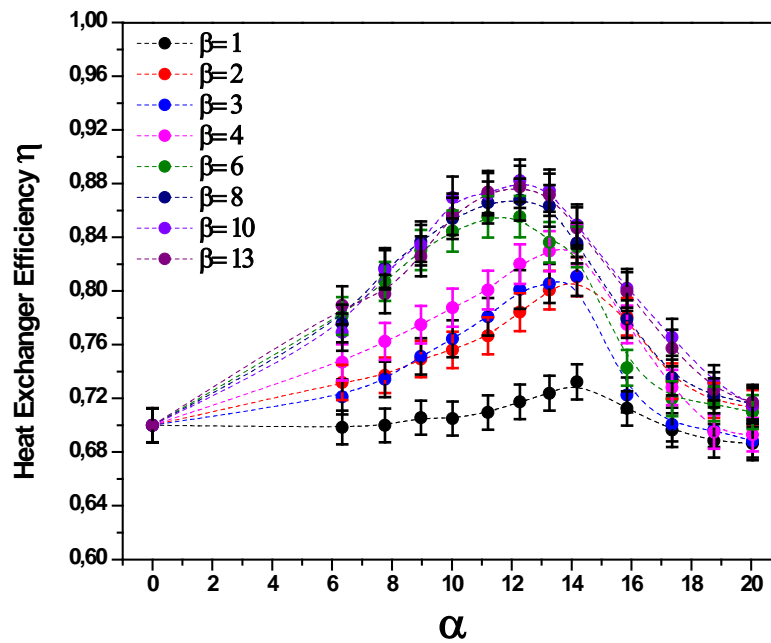


Figure IV- 18. Influence of α on heat exchanger efficiency for $Re_{st}=800$ – Sinusoidal pulsation.

Figure IV-19 shows the heat exchanger efficiency intensification χ i.e. the relative enhancement of the efficiency due to the pulsatile flow over that obtained in the steady state flow. Heat exchanger efficiency intensification χ exhibits bell-shaped curves with a slight increase of χ until attaining a peak value and then an abrupt decrease. The final value attained, for the highest α values, is nearly the same value as for the steady case, and even some values are lower than that in the steady case (for $\alpha > 17$ and $\beta < 4$) i.e. in these latter operating conditions, not only there is no enhancement but especially reduction of the heat transfer performances of the heat exchanger.

Heat exchanger efficiency intensification χ increases regularly with β increase, from $\beta=1$ to 13. For $\beta > 10$ there is rather no effect of increasing β as it seems to reach a saturation limit. A maximum heat exchanger efficiency intensification χ of 25% is achieved for $\alpha=12$ with $\beta=[10, 13]$. It is also observed that for a given Re_{st} and β value, an optimum Womersley frequency parameter α exists for the heat exchanger efficiency η of the chaotic heat exchanger. The optimum Womersley frequency parameter α relies between the values from 12 to 14, for the cases $\beta \geq 6$ and 14 for the cases $\beta < 6$.

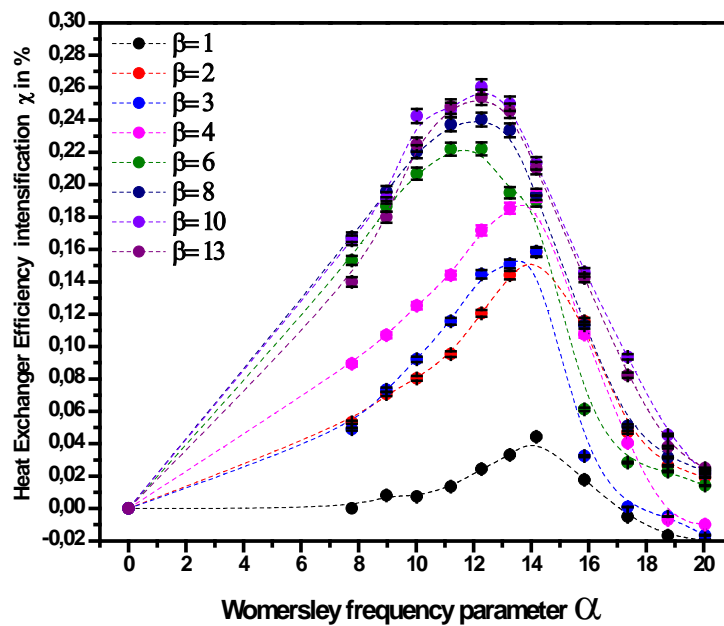


Figure IV- 19. Heat exchanger efficiency intensification χ for $Re_{st}=800$ – Sinusoidal pulsation.

IV.5.2. Influence of velocity amplitude

With the gradual increase in velocity amplitude ratios till it reaches the saturation point we may say that the fluid in the inner wall boundary layer occupying the heat near the shell side heated wall is transported in the direction of the interior flow with higher velocity, which increases the convective heat transfer effect, thus warmer fluid is passed far away to the colder fluid regions. As a result, the temperature profile near the wall is shattered and the heat enclosed in the boundary layer is transferred into the core flow.

Figure IV-20 shows an influence of velocity amplitude ratio β for a Reynolds number $Re_{st}=800$ and a frequency parameter $\alpha=12$. Heat exchanger efficiency increases gradually until $\beta=10$ from the value 0.69 for the steady case to the maximum value of 0.88, at which it seems to reach a saturation plateau for these operating conditions. Results show a higher heat transfer enhancement for higher velocity amplitude ratio β . A maximum increase of about 25% in efficiency, compared to steady case, is observed at $\beta=10$.

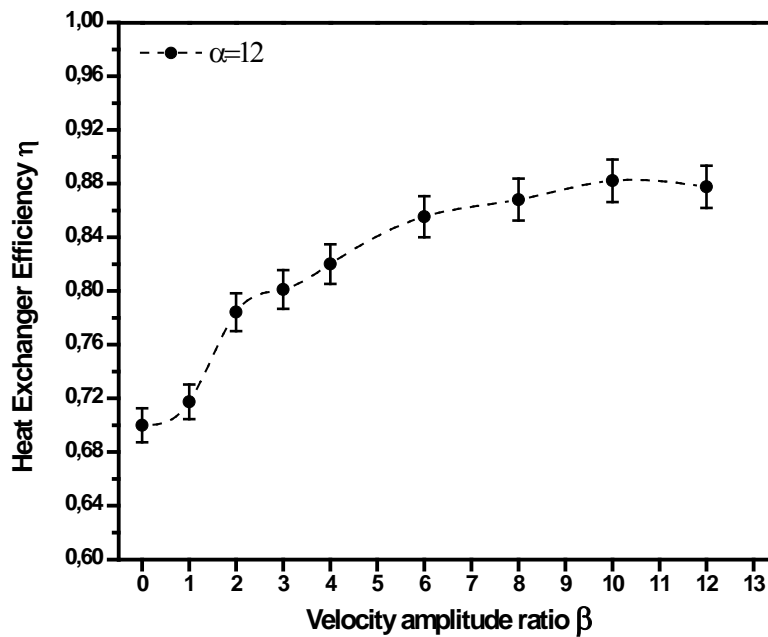


Figure IV- 20. Heat exchanger efficiency for $Re_{st}=800$ and $\alpha=12$ – Sinusoidal pulsation.

Figure IV-21 represents the influence of β on heat exchanger efficiency for $Re_{st}=800$ with sinusoidal pulsation. Figure IV-21 (a) shows that heat exchanger performance is improved with gradual increase of α from 0 to 12 for a fixed $Re_{st}=800$. From $\alpha>12$ a decrease in heat exchanger performance is observed in Figure IV-21 (b). For $\alpha=20$ almost the same values of efficiency are attained as that of steady case, i.e. no intensification is observed in these operating conditions. For small values of α , the saturation of the performances are attained for small values of β , i.e. for $\beta=6$ when $\alpha=6$, and this value increases as α increases, i.e. the saturation is at $\beta=10$ when $\alpha=12$. For higher values of α , the saturation seems to be obtained for the same value of β around 10, but the curves are slightly oscillating before reaching a stable saturation.

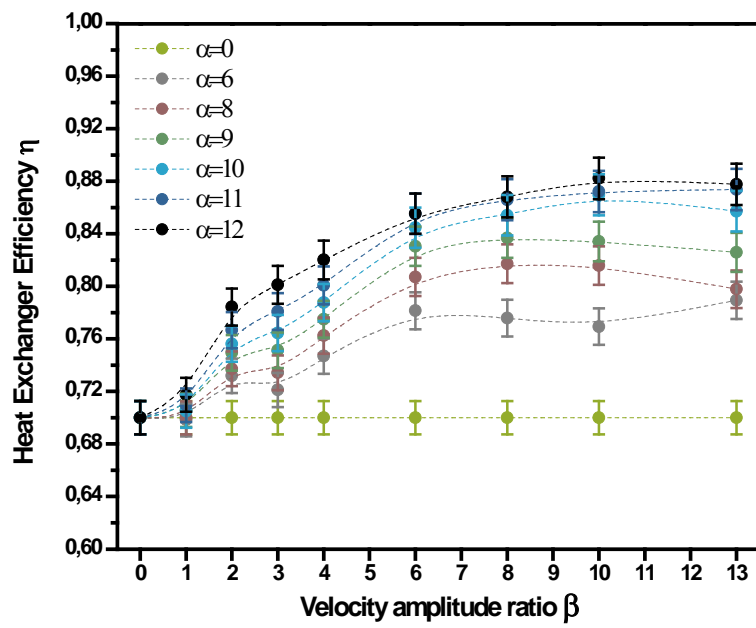
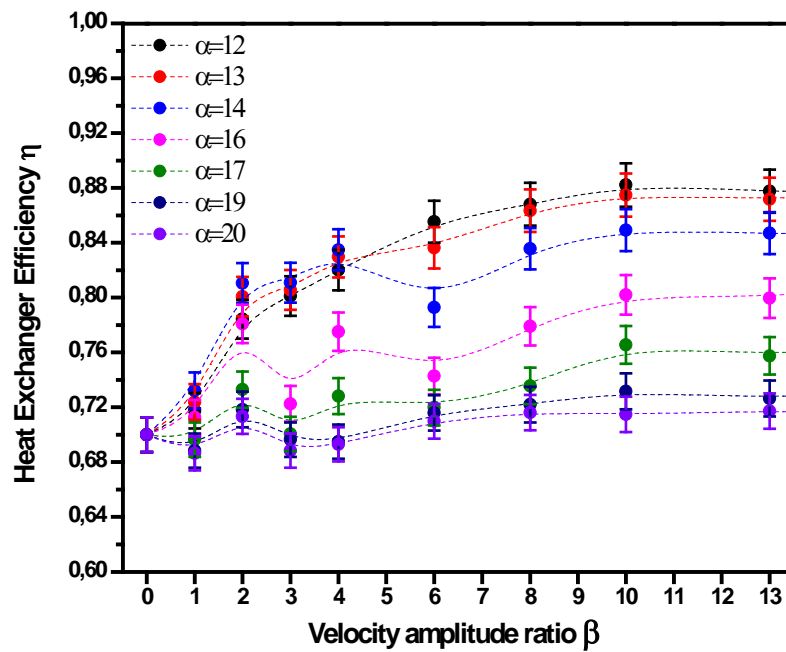
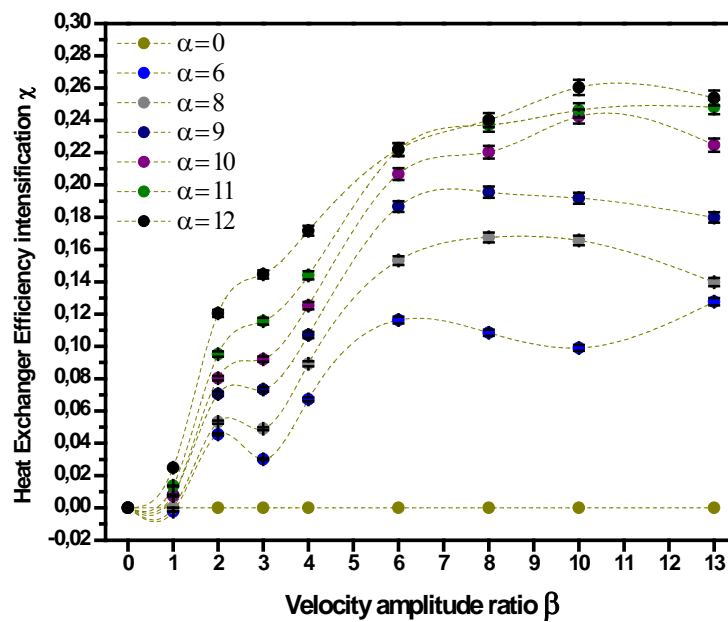
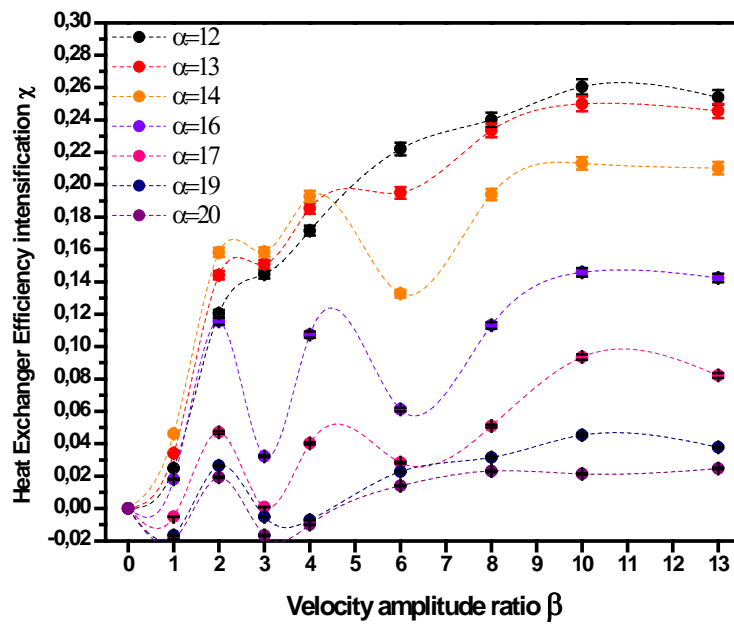
(a) $\alpha \leq 12$ (b) $\alpha \geq 12$ Figure IV- 21. Heat exchanger efficiency for $Re_{st}=800$ – Sinusoidal pulsation.

Figure IV-22 represents the heat exchanger efficiency intensification compared to the steady flow and shows that for a given Re_{st} and a given α , augmentation of β from 6 to 10 is favorable to the heat exchanger efficiency enhancement in this chaotic heat exchanger. The maximum enhancement is obtained for $\beta=6$ when $\alpha=6$, for $\beta=8$ when $\alpha=[8, 9]$ and for $\beta=10$ when $\alpha \geq 10$. For the highest α values ($\alpha \geq 16$), the oscillations of the curves are great, and even if the maximum enhancement is for $\beta=10$, this maximum is nearly attained for $\beta=2$. Beyond a β value higher than this saturation value, more energy is consumed to produce high pulsations but without enhancement of the heat exchanger efficiency η .

(a) $\alpha \leq 12$



(b) $\alpha \geq 12$

Figure IV- 22. Heat exchanger efficiency intensification χ for $Re_{st}=800$ – Sinusoidal pulsation.

IV.5.3. Influence of Reynolds number

Different pulsation conditions are imposed on Reynolds number Re_{st} ranging from 600 to 5000 to observe the effects of pulsation on heat transfer efficiency intensification. Figure IV-23 shows an influence of Reynolds numbers Re_{st} on heat exchanger efficiency for varying frequency with a constant velocity amplitude ratio $\beta=6$ and sinusoidal pulsation imposition. The curves are all bell-shaped with a maximum value attained for α is between 10 to 12.

This optimal value of α is between 10 to 12 for these operating conditions, and it appears that the heat exchanger efficiency decreases with the increase in Reynolds number, in other words the heat exchanger efficiency decreases with increase in flow rate in the tube side, especially the peak value seems to be greater for the smallest Reynolds numbers.

It can be observed that for higher frequencies $\alpha > 14$, the level of heat exchanger efficiency attained is rather the same as that for steady case, i.e. there is an optimal frequency not to exceed unless the performances decrease.

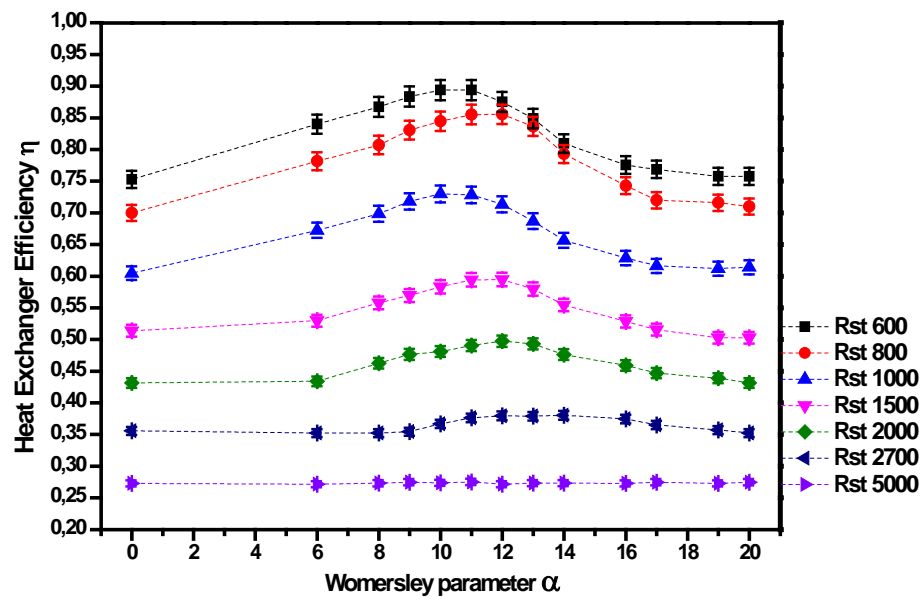


Figure IV- 23. Influence of Re_{st} on heat exchanger efficiency for $\beta=6$ – Sinusoidal pulsation.

Figure IV-24 shows the influence of Re_{st} on heat exchanger efficiency for $\alpha=12$ and $\beta=6$. We may observe that for a given α and β , the heat exchanger efficiency decreases with increase in Re_{st} , in this case the steady case provide an efficiency value of 0.75 at $Re_{st}=600$ and 0.25 at $Re_{st}=5000$, whereas in the pulsated case, the efficiency value is 0.88 at $Re_{st}=600$ and 0.25 at $Re_{st}=5000$. There is a significant increase in heat exchanger efficiency in the pulsated case compared to the steady case, for $Re_{st} \leq 2000$. In the transitional flow regime, pulsations have less but still positive influence on heat exchanger efficiency enhancement. However, for the turbulent flow, $Re_{st} > 2700$, pulsations have really no effect on the heat exchanger efficiency enhancement.

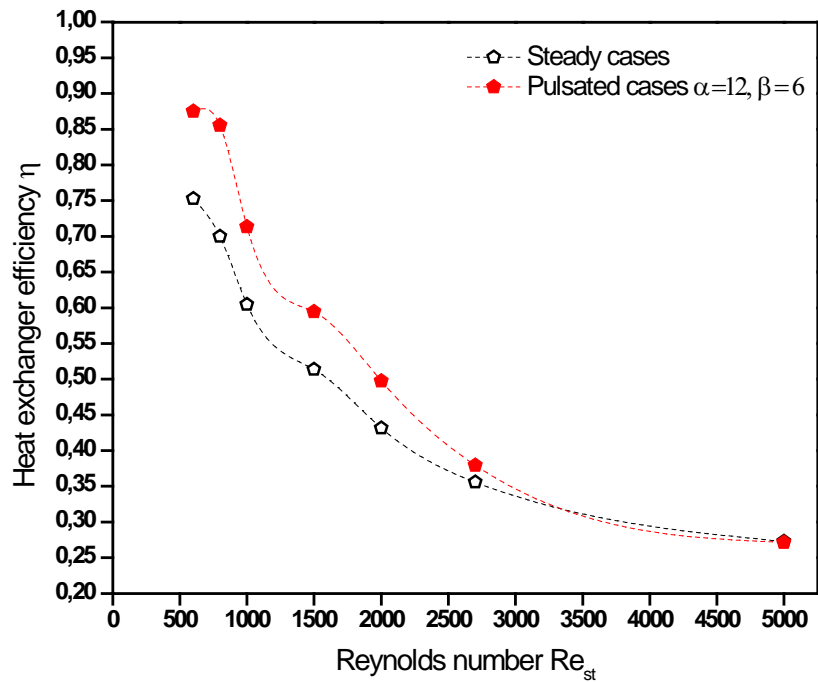


Figure IV- 24. Influence of Re_{st} on heat exchanger efficiency η for $\alpha=12$ and $\beta=6$ – Sinusoidal pulsation.

The Figure IV-25 shows heat exchanger efficiency intensification χ for $\beta=6$ with sinusoidal pulsation. The intensification of the heat exchanger efficiency exhibits a peak value for every Re_{st} and this peak value is higher for smaller Reynolds number, until Reynolds number 800 which seems to be an optimum Maximum heat transfer augmentation up to 16% is observed for $Re_{st}=800$. For higher Reynolds Re_{st} values, one can observe a decrease in the maximum augmentation, i.e. only 8% for $Re_{st}=1500$ and 2% for $Re_{st}=2700$.

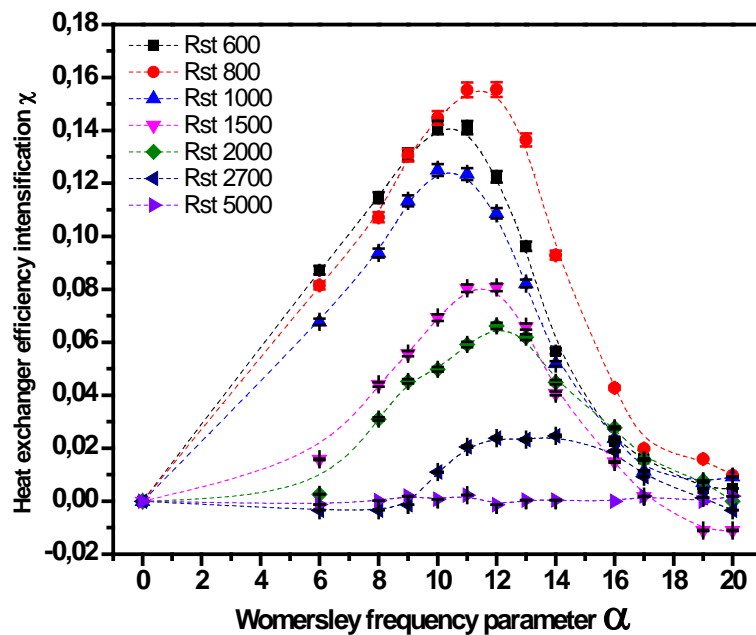


Figure IV- 25. Heat exchanger efficiency intensification χ for $\beta=6$ – Sinusoidal pulsation.

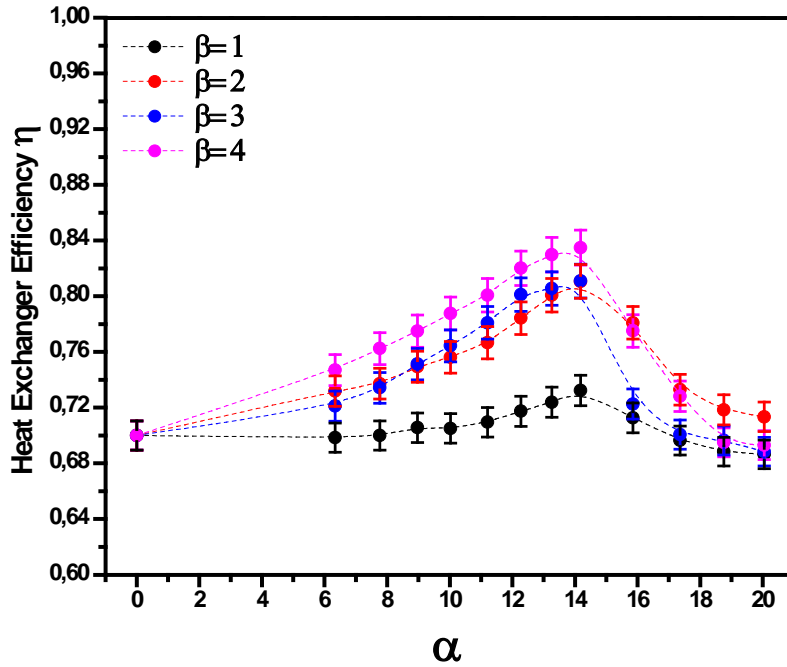
There is a more positive effect of pulsation on heat exchanger efficiency enhancement in laminar flow regime for a Reynolds number $Re_{st} \leq 800$ and there is no effect of pulsations in a complete turbulent regime for a Reynolds number $Re_{st} \geq 5000$.

IV.5.4. Influence of pulsation signal

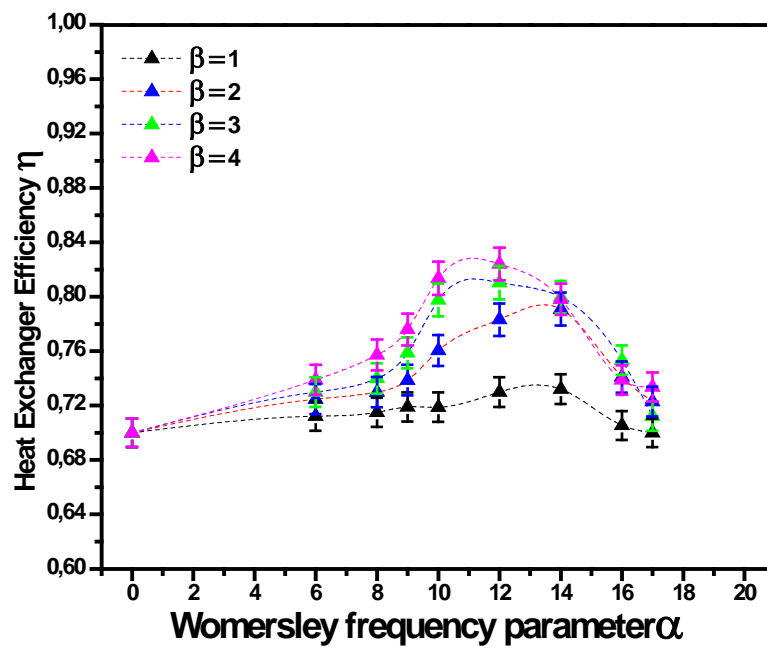
To observe the influence of pulsation wave forms on heat transfer intensification, three different types of pulsation signals, sinusoidal, square and triangular, are imposed on the steady flow.

Figure IV-26 represents the heat exchanger efficiency for $Re_{st}=800$ with (a) sinusoidal pulsation; (b) triangular pulsation and (c) square pulsation for $0 \leq \beta \leq 4$ and $0 \leq \alpha \leq 20$. Heat exchanger efficiency increases regularly with increase in velocity amplitude ratio β and it increases gradually with increase in α till an optimum value $\alpha=14$ with sinusoidal pulsation, $\alpha=12$ with triangular pulsation and $\alpha=10$ with square pulsation. Therefore it seems that for the different signal pulsations, a different optimum frequency is obtained: an early optimum

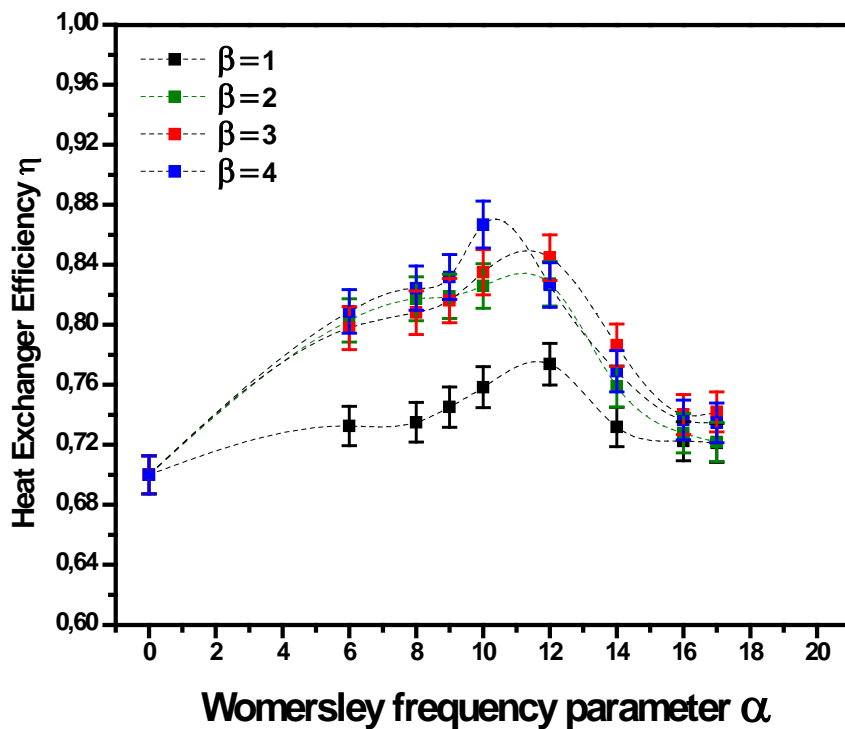
frequency value is obtained for the square pulsation, prior to triangular pulsation and sinusoidal pulsation.



(a) Sinusoidal pulsation



(b) Triangular pulsation



(c) Square pulsation

Figure IV- 26. Influence of the signal pulsation on heat exchanger efficiency for $Re_{st}=800$, for $\alpha \leq 20$ and $\beta \leq 4$.

Figure IV-27 represents the influence of different pulsation wave forms on heat exchanger efficiency for $Re_{st}=800$ with pulsation frequency parameter range $0 \leq \alpha \leq 17$ and for amplitude velocity ratio $\beta=1, 2, 3$ and 4.

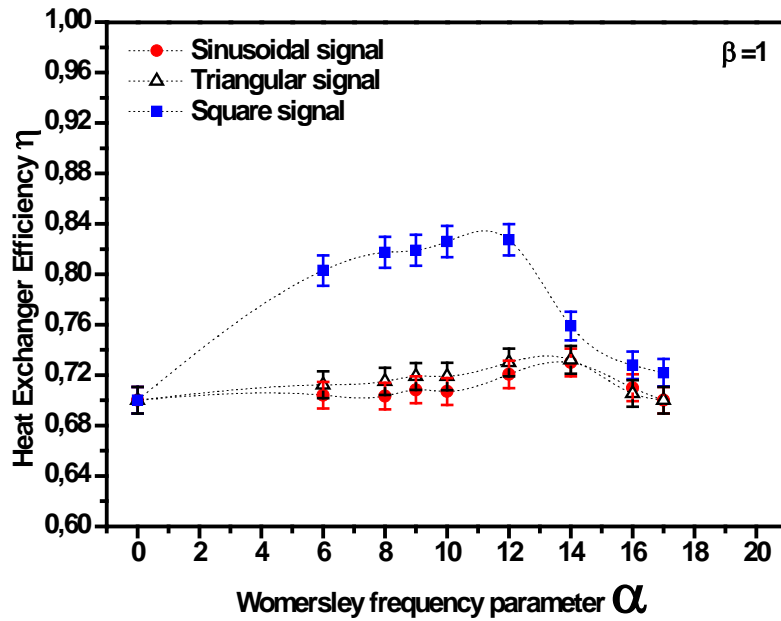
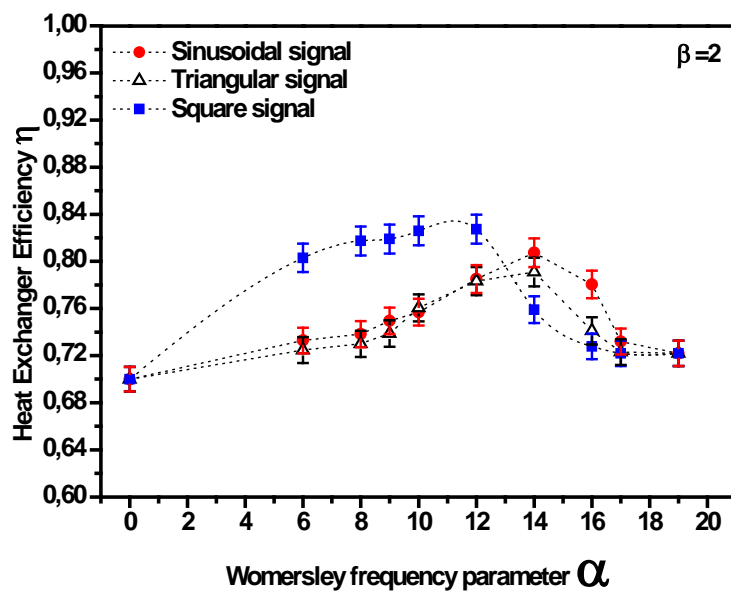
The pulsations generated through sinusoidal and triangular signals have similar effect on heat exchanger efficiency η enhancement: the difference between these two signals is only 1.5% over the whole range of operating conditions. Moreover, the results for $\alpha > 14$ are rather similar for all of the three signals.

However, the square pulsation wave form is found to be more favorable compared to sinusoidal and triangular ones, for cases $\alpha \leq 12$.

The great influence of the square signal is first to increase the maximum heat exchanger efficiency up to 83% instead of 74% for sinusoidal and triangular signals (for case $\beta=1$), and secondly to increase the heat exchanger efficiency for the cases $\alpha \leq 12$ (i.e. before

the peak): one can measure an enhancement of 10% of the heat exchanger efficiency with square signal compared to sinusoidal and triangular signals for $\beta=1$ for the cases $\alpha \leq 12$.

The comparative increase of the maximum heat exchanger efficiency is around 8% for $\beta=2$, 7% for $\beta=3$ and 5% for $\beta=4$ with $\alpha=10$: the increase of the maximum heat exchanger efficiency is decreasing with the augmentation of β .

(a) $\beta=1$ (b) $\beta=2$

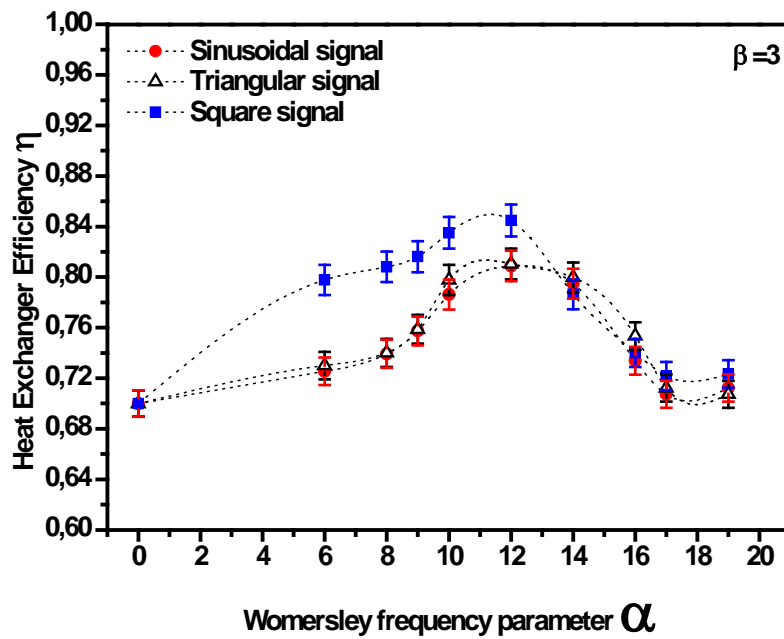
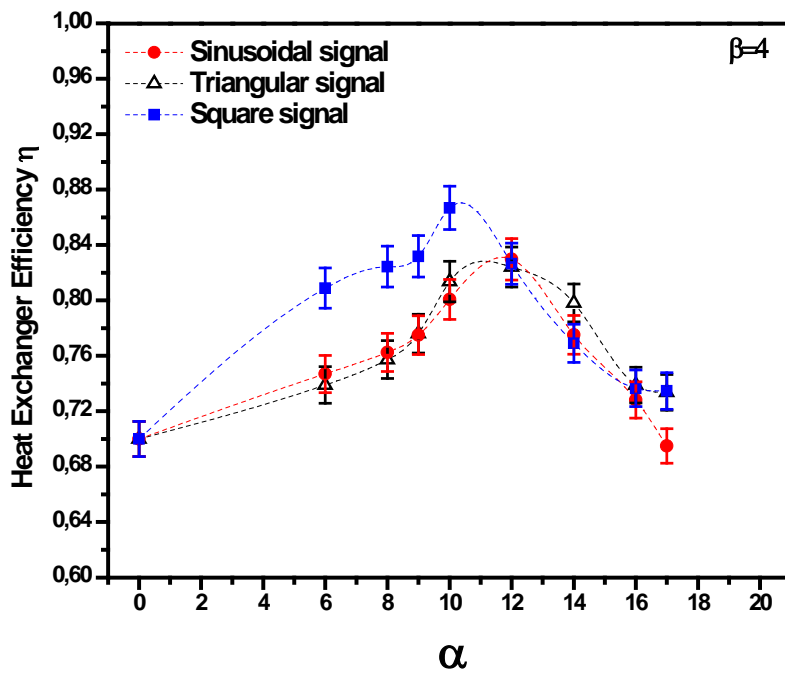
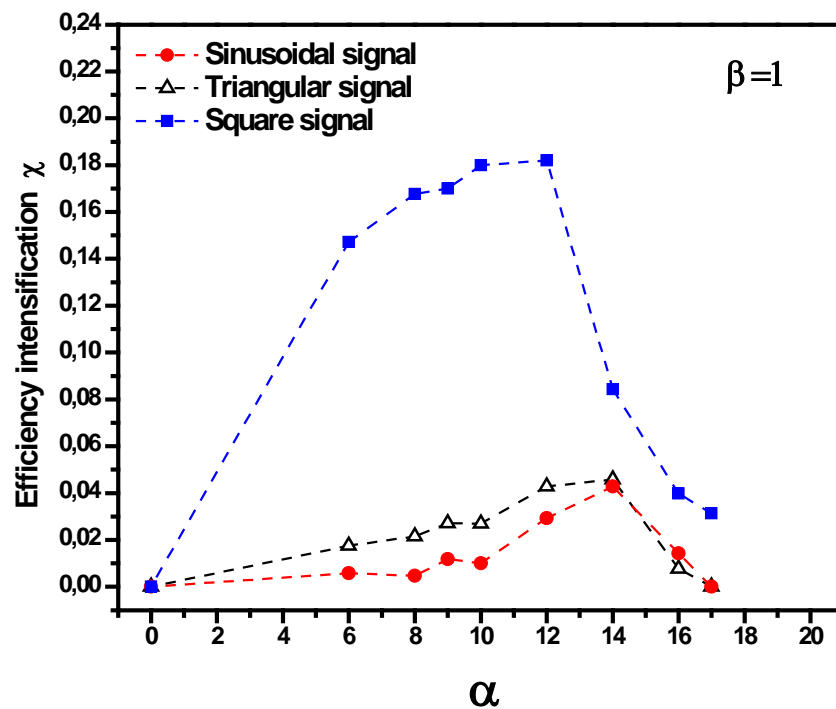
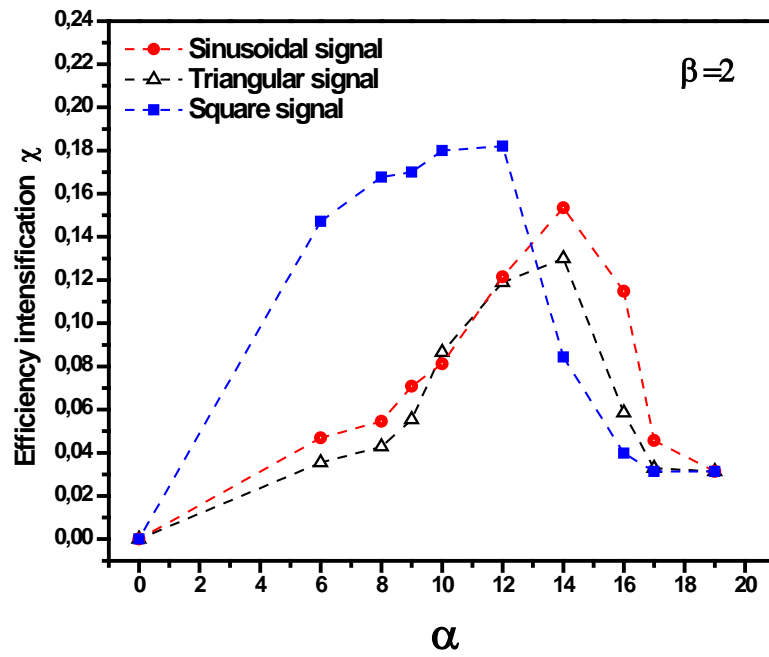
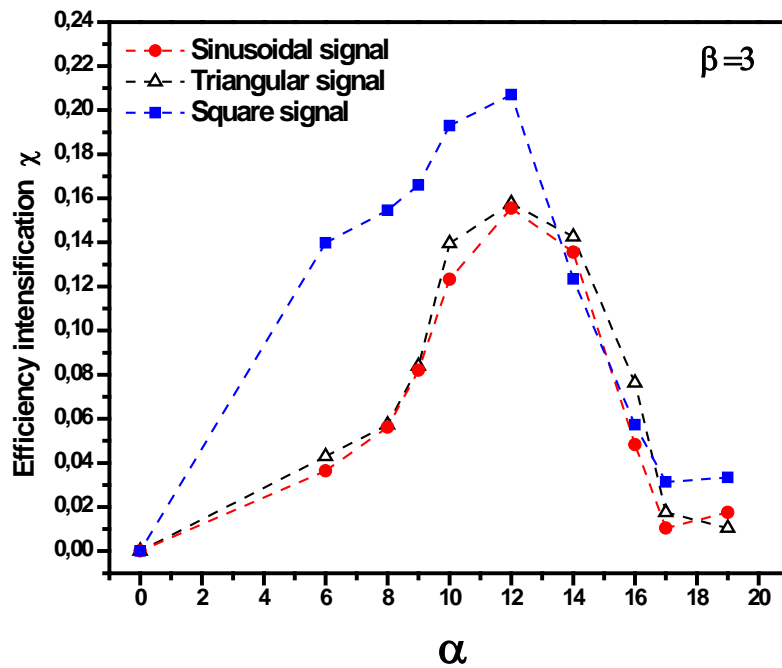
(c) $\beta=3$ (d) $\beta=4$ Figure IV- 27. Influence of the signal pulsation on heat exchanger efficiency for $Re_{st}=800$.

Figure IV-28 shows heat exchanger efficiency intensification χ due to different signal pulsation for $Re_{st} = 800$ and $\beta \leq 4$. The intensification of the heat exchanger efficiency exhibits a peak value for every α and β . This peak value is higher for square pulsation compare to sinusoidal and triangular pulsations. The peak value of heat exchanger efficiency intensification χ for square pulsation is $\alpha = 10$ to 12 for every β . Maximum heat transfer augmentation up to 24% is observed with square pulsation for $\beta = 4$. Heat transfer enhancement obtained through square signal pulsations is greater for $\beta = 1$ which is about 18% more from the enhancement obtained by triangular and sinusoidal pulsations. As the β increases from 2 to 4 we observe relatively less augmentation in heat transfer which is 9% for $\beta = 4$ with respect to the enhancement obtained by others two. This may be the trend to the saturation of influence of signal pulsation, which may be verified for the higher values of β for square wave pulsations.

(a) $\beta=1$

(b) $\beta=2$ (c) $\beta=3$

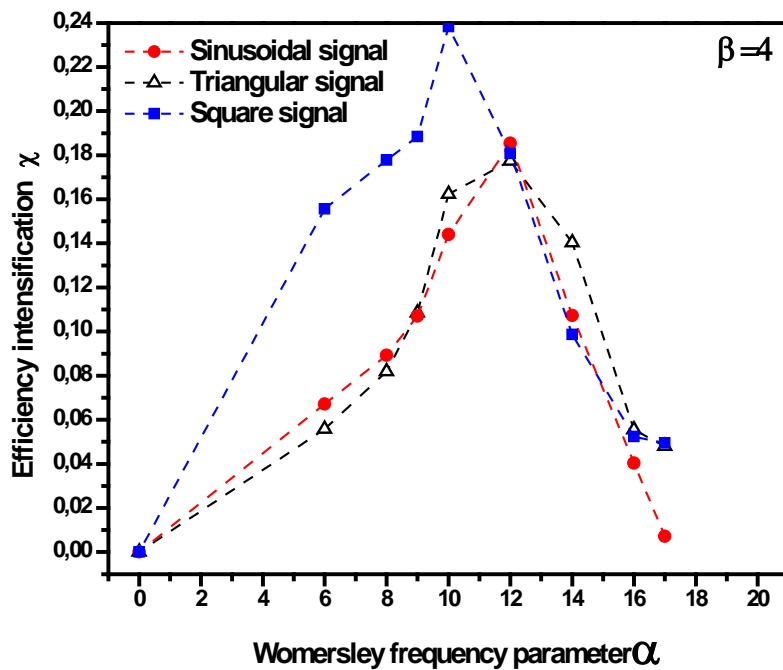
(c) $\beta=4$

Figure IV- 28. Influence of the signal pulsation on heat exchanger efficiency intensification χ for $Re_{st}=800$.

IV.6. Conclusions

An experimental setup is designed and fabricated to study the influence of pulsation on the heat transfer enhancement in a configuration of twisted bent pipes. Measurements are carried out for different operating conditions: Reynolds number Re_{st} in the range [600–5000], Womersley frequency parameter α in the range [0–20], velocity amplitude ratio β in the range [1–13] and three different types of pulsation signals i.e. sinusoidal, triangular and square signals. Thermal measurements are recorded at the entrance and at the exit of the chaotic twisted tube, while shell temperature is fixed.

The detailed measurements show that the combination of the four control parameters Reynolds number Re_{st} , Womersley frequency parameter α , velocity amplitude ratio β and different pulsation wave forms makes the heat transfer enhanced up to 24% for certain operating conditions, but the heat transfer can also not be increased, and even decreased for certain operating conditions.

It is observed that frequency has a vital influence on heat transfer intensification. An optimum Womersley frequency parameter α is observed between 12 and 14 for sinusoidal and triangular pulsation signals, and 10 for square signal.

Increase in Reynolds number Re_{st} decrease heat exchanger efficiency. Pulsated flow has a great influence on heat transfer efficiency η in laminar flow regime, enhancement up to 17% for sinusoidal pulsation signal. Pulsated flow has no effect on heat transfer enhancement when $Re_{st}=5000$ i.e. in complete turbulent regime.

Increase in velocity amplitude ratio β up to 6 is favorable for heat transfer enhancement, by producing enhancement up to 17 %. For $\beta>6$ the velocity amplitude ratio is found not to be efficient by producing the same enhancement as for cases with lower β values. In certain cases we observe a minor augmentation till $\beta=10$.

It is observed that different pulsation signals have different effect on heat transfer enhancement. Square signal compared to sinusoidal and triangular signals is found to provide better enhancement, especially for Womersley frequency parameter $\alpha<12$. Square signal increase the heat exchanger efficiency up to 10% more than the sinusoidal and triangular signals, and these two latter signals provide rather the same performances.

Chapter 5

Conclusion and prospects

V.1. Conclusions

This work is aimed to highlight the interest of pulsation imposition on steady flow for mixing enhancement and heat transfer intensification. Mixing study is carried out in a 90° curved pipe by analyzing the tracer deformation through a PLIF technique.

Two different experimental setup are used: the first one for mixing study, used by Timité (2005) and Jarrahi (2010) and modified to adapt it to the PLIF technique, and the second one, called intermittent heat exchanger, designed and fabricated at the LTN laboratory. The two experimental setups are used to study the influence of pulsated flows on mixing intensity and heat transfer enhancement respectively. Following is the general conclusions drawn by these two studies.

First, Planar Laser Induced Florescence (PLIF) technique is used in this work to measure the concentration field in a *developing* laminar pulsating flow through a circular 90° curved pipe. The PLIF techniques implemented for the first time in the LTN laboratory. The PLIF measurements are carried out for Reynolds numbers $Re_{st}=420, 600, 800$ and 1000 for steady cases and pulsatile flows with Womersley numbers α [8-21] and velocity component ratio $\beta=1, 2, 3$. The PLIF results of secondary flow for four different phase positions $\omega t=0^\circ, 90^\circ, 180^\circ$ and 270° are analyzed. The detailed PLIF measurements show that pulsatile flow in a curved pipe has a great influence on mixing intensity.

For pulsation cases, degree of mixing increases with the Reynolds number. The mixing degree in the configuration where the velocity amplitude ratio β is equal to 2 reaches up to 0.94 for $Re_{st}=600$. When the velocity amplitude ratio is unity ($\beta=1$), mixing is better in the boundary layer near the wall. On the other hand, when the velocity-amplitude ratio is doubled ($\beta=2$), the effective mixing zones are increased by occupying a larger surface.

In summary, the experimental results yielded certain information on tracer transport. The first type of information relates to the stretching and folding mechanisms. Two initially close trajectories diverge due to the effect of pulsation. Flow visualizations showed that the pulsation works to amplify the mixing by stretching the tracer lines in a larger space of the 90° curved circular pipe section. Analysis of the dye deformation suggested that the pulsation imposition on a flow in 90° bend can generate better mixing.

Second, heat transfer measurements are carried out for different pulsation conditions: steady Reynolds number Re_{st} in the range [600–5000], Womersley frequency parameter α in the range [0–20], velocity amplitude ratio β in the range [1–13] and three different types of pulsation signals, i.e. sinusoidal, triangular and square signals, are imposed on the steady flow rates. Temperature measurements are recorded at the entrance of the chaotic twisted tube and at the exit of it, while shell side temperature is fixed.

The results show that the four control parameters steady Reynolds number Re_{st} , Womersley frequency parameter α , velocity amplitude ratio β and different pulsation wave forms make the heat transfer enhanced up to 24% for certain operating conditions, but the heat transfer can also not be increased, and even decreased for certain operating conditions.

It is observed that frequency has a vital influence on heat transfer intensification. An optimum Womersley frequency parameter α is observed between 12 and 14 for sinusoidal and triangular pulsation signals, and 10 for square signal.

Increase in steady Reynolds number Re_{st} decreases the heat exchanger efficiency. It is found that pulsated flow has a great influence on heat transfer efficiency η in laminar flow regime, enhancement up to 17% for sinusoidal pulsation signal. Pulsated flow has no effect on heat transfer enhancement in turbulent regime.

Increase in velocity amplitude ratio β up to 6 is found favorable for heat transfer enhancement, by producing enhancement up to 17%. For $\beta > 6$ the velocity amplitude ratio is found not to be efficient by producing the same enhancement as for cases with lower β values.

It is also observed that different pulsation signals have different effect on heat transfer enhancement. Square signal compared to sinusoidal and triangular signals is found to provide better enhancement, especially for Womersley frequency parameter $\alpha < 12$. Square signal increases the heat exchanger efficiency up to 10% more than the sinusoidal and triangular signals, and these two latter signals provide rather the same performances.

V.2. Prospects

Prospects of this study are certainly various and rich, some examples are resumed hereafter.

For mixing study:

- PLIF measurements may be conducted to analyze mixing in the other 90° curved bends till the geometry becomes chaotic one. Five bent tubes are ready to be assembled in a chaotically configuration on the experimental setup in order to carry out PLIF measurements at the exit of two, three, four or five bent tubes chaotic mixer.
- Multiphase flow mixing can be studied by injecting different immiscible flow to observe the droplet formation and break up mechanisms.

For heat transfer study:

- Influence of square and triangular pulsation signals on heat transfer intensification for Reynolds numbers Re_{st} other than $Re_{st} = 800$ and for velocity amplitude ratio $\beta > 4$ can be implemented. This requires some modifications of the experimental setup in order to be able to carry out the same operating conditions for the square and triangular signals as for the sinusoidal signal.
- Other configuration of the helically or chaotic geometry can be tested on the experimental setup in order to quantify the influence of pulsated signals on the heat transfer on these geometries. Other geometries, such as tubes equipped with vortex generators, tri-dimensional milli-channels (which are available at the LTN laboratory), but also many other geometries can also be tested on this experimental setup.

Resumé français

Résumé français

L'intensification des transferts de masse et de chaleur dans un écoulement en conduite en régime laminaire revêt une grande importance pour certains secteurs de l'industrie (alimentaire, pharmacie, procédés et polymères), en particulier ceux pour lesquels la qualité des produits ne doit pas être modifiée en raison de contraintes de cisaillement élevées. Ces produits fluides sont souvent structurés à haute viscosité, avec des cellules ou de longues chaînes moléculaires susceptibles d'être cassées dans un régime turbulent. Améliorer la performance des échangeurs-mélangeurs qui opèrent en régime laminaire est encore l'objet de nombreuses études d'ingénierie.

Les échangeurs-mélangeurs constitués de tubes hélicoïdaux sont largement utilisés dans l'industrie de part leur plus grande efficacité par rapport à des géométries droites et pour leur facilité de mise en œuvre. Cela est dû à l'écoulement secondaire généré par la force centrifuge. Dans cet écoulement secondaire, les déplacements transversaux des particules de fluide augmentent et les dispersions axiales diminuent : les cellules de Dean formées [Dean (1927) et Dean (1928)] dans l'écoulement secondaire agissent comme des agitateurs internes qui permettent une meilleure homogénéisation de l'écoulement.

Pour améliorer le mélange et le transfert de chaleur en régime laminaire, une configuration géométrique plus complexe que la géométrie hélicoïdale, dite à advection chaotique à Dean alterné, a été proposée et étudiée précédemment au « Laboratoire de Thermocinétique de Nantes » (LTN) [Le Guer (1993), Castelain (1995), Mokrani (1997), Chagny-Regardin (2000), Lemenand (2002)]. Cette géométrie est composée d'une série de coudes agencés avec une alternance de $\pm 90^\circ$ entre les plans de courbure. Cette géométrie induit un chaos spatial des trajectoires fluides.

A chaque changement de plan de courbure, les cellules de Dean sont détruites et reformées dans une nouvelle orientation sous l'influence de la force centrifuge, ce qui crée un écoulement secondaire. Ce type de configuration a été évalué dans de nombreuses études antérieures comme (Aref, 1984), (Jones et al., 1989), (Acharya et al., 1992), (Peerhossaini et al., 1993), (Castelain et al., 1997), (Mokrani et al., 1997), (Chagny et al., 2000), (Castelain et al., 2001), (Lemenand et Peerhossaini, 2002), (Timité et al., 2010), (Habchi et al., 2009), (Funakoshi et Jang, 2012) et (Jarrahi et al., 2013).

Encouragés par les résultats obtenus dans la **géométrie chaotique**, constituée d'un agencement de tubes coudés avec rotation du plan de courbure entre chaque coude, sur des mesures thermiques de Mokrani (1997), Chagny et al. (2000), Lemenand (2002), et des mesures du mélange de Timité (2005) et Jarrahi (2010), ce travail de thèse a pour objectif d'analyser l'effet de la pulsation d'un écoulement pulsé sur l'intensification du mélange dans un coude à 90° et sur l'intensification du transfert de la chaleur dans une géométrie d'advection chaotique, comparativement à un écoulement stationnaire.

Dans le **premier chapitre** de cette thèse, des définitions du chaos sont rappelées et l'advection chaotique dans un écoulement de Dean alterné est expliquée. Des études antérieures sur le rôle de la dépendance temporelle de la modification de la structure des lignes d'écoulement dans les tubes coudés sont rappelées.

Timité (2005) a étudié les effets de la superposition de la dépendance de temps sur un écoulement de Dean alterné stable, l'idée étant d'imposer des pulsations sur un débit constant afin d'obtenir un écoulement plus complexe.

L'apparition d'une paire supplémentaire de cellules de rotation inverse, qui co-existe avec les cellules de Dean, dans un écoulement sinusoïdal dans un tube coudé a été démontrée pour la première fois par Lyne (1970). Cette structure complexe de l'écoulement secondaire obtenue en présence de la pulsation peut donc se traduire par un meilleur mélange par rapport aux cas stationnaires. Par des visualisations qualitatives menées par une technique LIF (Fluorescence Induite par Laser) dans une configuration chaotique constituée d'une série de six coudes alternés, Timité (2005) a analysé l'évolution des tourbillons de l'écoulement secondaire qui se développe au cours de la pulsation dans les tubes coudés. Il a démontré expérimentalement l'apparition de cet écoulement chaotique en surveillant la déformation des lignes de traceur. Une augmentation du chaos, qui fournit un meilleur mélange, par des pulsations a été confirmée par l'analyse de l'étirement de ces lignes de traceur.

Jarrahi (2010) a analysé plus profondément le rôle des structures de l'écoulement secondaire complexe formé par pulsation sur l'amélioration du mélange. A cet effet, pour l'écoulement secondaire à la sortie de chaque coude d'une configuration chaotique, les champs de vitesse ont été obtenus en utilisant une technique PIV (Particle Image Velocimetry). Jarrahi (2010) a utilisé ces champs de vitesses pour décrire la topologie des différentes structures qui se développent dans un écoulement laminaire pulsé dans un seul

coude, et dans la géométrie chaotique à Dean alterné. En outre, il a défini les conditions de pulsation favorables pour la mise en valeur du mélange par des critères pour la quantification du mélange basée sur des calculs de champs de tourbillon et des vitesses de déformation.

Le **deuxième chapitre** est consacré à une présentation détaillée des deux montages expérimentaux mis en œuvre : le premier banc est utilisé pour étudier l'intensification du mélange et le second banc pour analyser l'intensification des transferts thermiques. Les techniques de mesure, en particulier la technique de PLIF (Planar Laser Induced Fluorescence) mise en œuvre dans le premier montage, sont explicitées.

Deux montages expérimentaux différents sont utilisés dans ce but : le premier banc a été mis au point par Timité (2005) et utilisé par Jarrahi (2010), nous l'avons modifié pour l'adapter à la technique de PLIF qui permet d'analyser l'intensification du mélange dans un coude à 90° grâce à un écoulement pulsé sinusoïdal ; le second banc, appelé échangeur de chaleur intermittent, conçu et fabriqué au laboratoire LTN, permet des mesures thermiques pour mettre en évidence l'intensification des transferts thermiques grâce à un écoulement pulsé dans un échangeur chaotique à Dean alterné, constitué de tubes coudés avec rotation du plan de courbure entre chaque coude.

La pulsation est sinusoïdale dans le banc de mesure du mélange, et la forme de la pulsation peut être sinusoïdale, triangulaire ou carrée dans le banc de mesure thermique. Les deux montages expérimentaux sont utilisés pour étudier l'influence des écoulements pulsés sur l'intensification du mélange d'une part et l'amélioration du transfert de chaleur d'autre part, via l'étude de l'influence de différents paramètres : nombre de Reynolds $Re_{st} = \frac{U_{st} \cdot d}{\nu}$, paramètre de la fréquence de pulsation, dit de Womersley, $\alpha = r_o \left(\frac{\omega}{\nu} \right)^{\frac{1}{2}}$ et paramètre d'amplitude de la pulsation $\beta = \frac{U_p}{U_{st}}$.

L'objectif du **troisième chapitre** est de présenter les résultats obtenus par la technique de PLIF pour mesurer l'intensité de mélange obtenue en sortie d'un coude à 90° avec des écoulements stationnaires en régime laminaire comparativement à des écoulements pulsés sinusoïdaux. Les effets de différents paramètres de pulsation (nombre de Reynolds,

paramètres de fréquence et paramètre d'amplitude) sur le degré de mélange mesuré sont discutés.

Tout d'abord, la technique PLIF, mise en œuvre pour la première fois au laboratoire LTN, est utilisée dans ce travail pour mesurer le champ de concentration dans un écoulement laminaire à travers un tube circulaire coudé à 90°. Les mesures de PLIF sont effectuées pour les conditions opératoires suivantes : nombres de Reynolds $Re_{st}=420, 600, 800$ et 1000 , nombres de Womersley α compris dans l'intervalle $[8-21]$ et rapports d'amplitude de la vitesse $\beta=1, 2, 3$. Les mesures PLIF de l'écoulement secondaire sont effectuées pour quatre positions de phase différentes $\omega t=0^\circ, 90^\circ, 180^\circ$ et 270° . Les mesures de PLIF sont analysées et montrent que les pulsations dans un tube coudé ont une grande influence sur l'intensité de mélange.

Nous caractérisons le mélange par un paramètre de degré de mélange défini par $I_{mix} = 1 - \frac{\sigma^2}{\sigma_{max}^2}$ où σ^2 et σ_{max}^2 sont respectivement la variance et la variance maximum. Nous calculons une intensification du degré de mélange définie par $\psi = \frac{I_{mix\ p} - I_{mix\ st}}{I_{mix\ st}}$ où $I_{mix\ p}$ et $I_{mix\ st}$ sont les degrés de mélange respectivement pour les cas pulsés et stationnaires.

Nous avons effectué des mesures PLIF dans un coude avec des conditions opératoires : $420 \leq Re_{st} \leq 1000$ - $0 \leq \alpha \leq 21$ - $\beta=1$ à 2 . Le degré de mélange évolue selon la phase du signal sinusoïdal. Nous avons observé que

- Le degré de mélange dans la configuration pour laquelle le rapport d'amplitude de la vitesse $\beta=2$ atteint une valeur maximum de $0,94$ pour $Re_{st}=600$.
- Le degré de mélange augmente avec le nombre de Reynolds jusqu'à $Re_{st}=800$.
- Le degré de mélange augmente avec la fréquence avec un effet de saturation à partir de $\alpha=15$.
- Le degré de mélange augmente avec le rapport d'amplitude β .
- L'intensification du mélange atteint une valeur maximum de $\psi=155\%$ pour certains cas.

Le **quatrième chapitre** est consacré à l'étude de l'intensification du transfert de chaleur par des écoulements pulsés dans un échangeur chaotique à Dean alterné. Les effets de la pulsation, étudiée par quatre paramètres à savoir le nombre Reynolds, le paramètre de la

fréquence, le paramètre d'amplitude de la vitesse et différentes formes du signal, sont observés, mesurés et analysés. Les valeurs optimales favorables à un échangeur de chaleur plus efficace pour les conditions opératoires de la pulsation testées sont observées.

Les conditions de pulsations sont : nombre de Reynolds stationnaire Re_{st} dans la gamme [600-5000], le paramètre de fréquence Womersley α dans l'intervalle [0-20], le rapport d'amplitude de la vitesse β dans l'intervalle [1-13] et trois types de signaux de pulsations, sinusoïdaux, triangulaires et carrés, sont imposées à un écoulement à débit constant.

On caractérise l'intensification des transferts thermiques par l'utilisation d'un paramètre d'efficacité thermique en mesurant les températures à la sortie et à l'entrée dans l'échangeur chaotique et en calculant une efficacité thermique $\eta = \frac{(T_{outlet} - T_{inlet})}{(T_s - T_{inlet})}$. De plus nous évaluons de l'intensification de l'efficacité thermique par le calcul de $\chi = \left(\frac{\eta_p - \eta_{st}}{\eta_{st}} \right)$ où η_p et η_{st} sont les efficacités thermiques respectivement pour les cas pulsés et stationnaires.

Les mesures de température sont enregistrées à l'entrée de l'échangeur chaotique et à la sortie de celui-ci, tandis que la température du côté enveloppe est maintenue constante. Les résultats montrent que pour les conditions étudiées, le transfert de chaleur peut être amélioré jusqu'à 24%. Cependant pour certaines conditions opératoires, nous avons également observé que le transfert de chaleur peut ne pas être augmenté, et même être diminué dans certains cas. Il est observé que la fréquence a une influence vitale sur l'intensification du transfert de chaleur. Un paramètre de fréquence Womersley optimum est observé, pour des valeurs entre 12 et 14 pour les signaux de pulsations sinusoïdales et triangulaires, et une valeur de 10 pour le signal carré. L'augmentation du nombre de Reynolds diminue l'efficacité de l'échangeur de chaleur. On constate que le débit pulsé a une grande influence sur l'efficacité du transfert de chaleur η en régime d'écoulement laminaire, avec une amélioration jusqu'à 17% pour le signal de pulsation sinusoïdale, mais celui-ci ne procure pas d'amélioration du transfert de chaleur en régime turbulent.

L'augmentation du rapport d'amplitude de la vitesse β jusqu'à 6 est favorable à l'intensification du transfert de chaleur, en produisant une amélioration de l'efficacité thermique jusqu'à une valeur de 17%. Pour des rapports d'amplitude de la vitesse $\beta > 6$, ces conditions ne sont pas plus efficaces car nous observons une efficacité thermique identique à celle des cas avec des valeurs de β inférieures. Il est également observé que les signaux de pulsation ont des effets différents sur l'amélioration du transfert de chaleur. Le signal carré

assure une meilleure augmentation des transferts thermiques, par rapport aux signaux sinusoïdaux et triangulaires, en particulier pour des paramètres de fréquence Womersley $\alpha < 12$. Le signal carré augmente l'efficacité de l'échangeur thermique jusqu'à 10% de plus que les signaux sinusoïdaux et triangulaires, ces deux derniers signaux fournissant quasiment les mêmes performances.

Les **conclusions générales** de cette étude sont présentées dans le dernier chapitre ainsi que les **perspectives** pour les travaux futurs à mener dans la continuité de cette étude. Celles-ci sont diverses, quelques exemples sont repris ci-après.

Pour l'étude de mélange, des mesures PLIF peuvent être menées pour analyser le mélange dans une succession de coudes à 90°, agencés en configuration hélicoïdale ou en configuration chaotique. Cinq tubes coudés sont prêts à être assemblés sur le dispositif expérimental de manière à effectuer des mesures de PLIF à la sortie de deux, trois, quatre ou cinq tubes coudés. Le mélange d'un écoulement multiphasique peut également être étudié en injectant un fluide non miscible et en observant la formation des gouttelettes et les mécanismes de fractionnement.

Pour l'étude du transfert de chaleur, l'influence des signaux de pulsation carrés et triangulaires sur l'intensification du transfert de chaleur, pour des nombres de Reynolds Re_{st} autres que $Re_{st}=800$ et pour des rapports d'amplitude de la vitesse $\beta > 4$ pourront être mis en œuvre. Cela nécessite certaines modifications du dispositif expérimental afin d'être en mesure d'effectuer les mêmes conditions de fonctionnement pour les signaux carrés et triangulaires pour que le signal sinusoïdal. De plus, d'autres configurations d'échangeur de chaleur, des géométries en hélice, chaotiques ou autres peuvent être testées sur le dispositif expérimental de manière à quantifier l'influence de signaux pulsés sur le transfert de chaleur dans ces géométries. D'autres géométries telles que les tubes équipés de générateurs de vortex, des milli-canaux tridimensionnels (précédemment caractérisés pour leurs performances en mélange et disponibles au laboratoire LTN), mais aussi d'autres géométries pourront également être testées sur ce dispositif expérimental.

References

References

1. ACHARYA, N., SEN, M. & CHANG, H. C. 1992. Heat transfer enhancement in coiled tubes by chaotic advection. *International Journal of Heat and Mass Transfer*, 35, 2475-2489.
2. AKDAG, U. 2010. Numerical investigation of pulsating flow around a discrete heater in a channel. *International Communications in Heat and Mass Transfer*, 37, 881-889.
3. ANSARI, M. A. & KIM, K.-Y. 2009. Parametric study on mixing of two fluids in a three-dimensional serpentine micro-channel. *Chemical Engineering Journal*, 146, 439-448.
4. AREF, H. 1984. Stirring by chaotic advection. *Journal of Fluid Mechanics*, 143, 1-21.
5. B. O. OLAYIWOLA, P. W. 2009. Experimental Investigation of the Effects of Fluid Properties and Geometry on Forced Convection in Finned Ducts With Flow Pulsation. *J. Heat Transfer*, 131(5).
6. BAIRD, M. H. I., DUNCAN, G. J., SMITH, J. I. & TAYLOR, J. 1966. Heat transfer in pulsed turbulent flow. *Chemical Engineering Science*, 21, 197-199.
7. BEEBE, D. J., MENSING, G. A. & WALKER, G. M. 2002. Physics and applications of microfluidics IN BIOLOGY. *Annual Review of Biomedical Engineering*, 4, 261-286.
8. BERTELSEN, A. F. 1975. An experimental investigation of low Reynolds number secondary streaming effects associated with an oscillating viscous flow in a curved pipe. *Journal of Fluid Mechanics*, 70, 519-527.
9. CASTELAIN. 1995. *Etude expérimentale de la dynamique des fluides et des transferts thermiques dans un écoulement de Dean alterné en régime d'advection chaotique*. Thèse de Doctorat, , Université de Nantes et Ecole Centrale de Nantes.
10. CASTELAIN, C., MOKRANI, A., LE GUER, Y. & PEERHOSSAINI, H. 2001. Experimental study of chaotic advection regime in a twisted duct flow. *European Journal of Mechanics - B/Fluids*, 20, 205-232.
11. CHAGNY-REGARDIN-C. 2000. *Mélange et chauffage de fluides complexes à l'aide d'un échangeur de chaleur à effet d'advection chaotique*. Thèse de Doctorat, Ecole Polytechnique de l'Université de Nantes.
12. CHANG, T. J. M. 1985. Numerical simulation of fully developed sinusoidal and pulsatile (physiological) flow in curved tubes. *J. Fluid Mech*, 161, 175-198.

13. CHEN, Y. & ZHAO, J. 2006. Applications of the Strong Heat Transformation by Pulse Flow in the Shell and Tube Heat Exchanger. *Proceedings of the Sixth International Conference for Enhanced Building Operations, Shenzhen, China, November 6 - 9, 2006.*
14. CHOVÁN, T. & GUTTMAN, A. 2002. Microfabricated devices in biotechnology and biochemical processing. *Trends in Biotechnology*, 20, 116-122.
15. CRACIUNESCU OI, C. S. 2001. Pulsatile Blood Flow Effects on Temperature Distribution and Heat Transfer in Rigid Vessels. *J Biomech Eng*, 123(5):500-5.
16. CUNNINGHAM, D. D. 2001. Fluidics and sample handling in clinical chemical analysis. *Analytica Chimica Acta*, 429, 1-18.
17. DARLING, G. B. 1959. Heat Transfer to Liquid in Intermittent Flow Petroleum. *London*, 22:177.
18. DEAN, W. R. 1927. Note on the motion of fluid in a curved pipe. *Phil. Mag.*, 4208-223.
19. DEAN, W. R. 1928. The streamline motion of fluid in a curved pipe. *Phil. Mag.*, 5, 673-695.
20. DEPLANO V., S. M. 1999. Experimental and numerical study of pulsatile flows through stenosis: Wall shear stress analysis. *J. Biomechanics*, 32, 1081-1090.
21. ELSHAFEI, E. A. M., SAFWAT MOHAMED, M., MANSOUR, H. & SAKR, M. 2008. Experimental study of heat transfer in pulsating turbulent flow in a pipe. *International Journal of Heat and Fluid Flow*, 29, 1029-1038.
22. ELSHAFEI, E. A. M., SAFWAT.MOHAMED, M. & H MANSOUR, M. S. 2006. Experimental Study of Heat Transfer in Pulsating Turbulent Flow in a Pipe. *Proceedings of ICFDP 8: Eighth International Congress of Fluid Dynamics & Propulsion December 14-17, 2006, Sharm El-Shiekh, Sinai, Egypt ICFDP8-EG-165.*
23. EUSTICE, J. 1911. Experiments on streamline motion in curved pipes. *Proc. Roy. Soc.*, 119.
24. FUNAKOSHI, M. & JANG, B. 2012. Chaotic Mixing by a Flow in a Curved Pipe. *Procedia IUTAM*, 5, 169-172.
25. GLASGOW, I. & AUBRY, N. 2003. Enhancement of microfluidic mixing using time pulsing. *Lab on a Chip*, 3, 114-120.
26. HABCHI, C., LEMENAND, T., DELLA VALLE, D. & PEERHOSSAINI, H. 2009. Liquid/liquid dispersion in a chaotic advection flow. *International Journal of Multiphase Flow*, 35, 485-497.

-
27. HAMAKIOTES C.C., B. S. A. 1990. *Periodic flows through curved tubes: the effect of the frequency parameter. J. Fluid Mech*, 210, 353-370.
 28. HAVEMANN, H. A. & RAO, N. N. N. 1954. Heat Transfer in Pulsating Flow. *Nature*, 174, 41-41.
 29. HEMIDA, H. N., SABRY, M. N., ABDEL-RAHIM, A. & MANSOUR, H. 2002. Theoretical analysis of heat transfer in laminar pulsating flow. *International Journal of Heat and Mass Transfer*, 45, 1767-1780.
 30. JAFARI, M., FARHADI, M. & SEDIGHI, K. 2013. Pulsating flow effects on convection heat transfer in a corrugated channel: A LBM approach. *International Communications in Heat and Mass Transfer*, 45, 146-154.
 31. JARRAHI MOJTABA. 2010. *Intensification Du Melange Par Advection Chaotique Pulsée*. Thèse de Doctorat, École Polytechnique de l'Université de Nantes.
 32. KARAMI M., SHIRANI E., JARRAHI M., AND PEERHOSSAINI H., *Mixing by time-dependent orbits in spatiotemporal chaotic advection*, Journal of Fluids Engineering, Accepted 2014
 33. JARRAHI M., CASTELAIN C., AND PEERHOSSAINI H., *Mixing Enhancement by Pulsating Chaotic Advection*, Chemical Engineering and Processing : Process Intensification, **74**, 2013, pp. 1-13.
 34. JARRAHI M., CASTELAIN C., AND PEERHOSSAINI H., *Secondary Flow Patterns and Mixing in Laminar Pulsating Flow through a Curved Pipe*, Journal of Experiments in Fluids, **50 (6)**, 2011, pp. 1539-1558.
 35. JARRAHI M., CASTELAIN C., AND PEERHOSSAINI H., *Laminar Sinusoidal and Pulsatile Flows in a Curved Pipe*, Journal of Applied Fluid Mechanics, **4 (2)**, 2011, pp. 21-26.
 36. JONES, S. W., THOMAS, O. M. & AREF, H. 1989. Chaotic advection by laminar flow in a twisted pipe. *Journal of Fluid Mechanics*, 209, 335-357.
 37. KAKUTA, M., BESSOTH, F. G. & MANZ, A. 2001. Microfabricated devices for fluid mixing and their application for chemical synthesis. *Chem Rec*, 1, 395-405.
 38. KARAGOZ, I. 2001. Variation of momentum and thermal boundary layers for oscillatory flows in a channel. *International Communications in Heat and Mass Transfer*, 28, 379-388.
 39. KARAMERCAN, O. E. & GAINER, J. L. 1979. The Effect of Pulsations on Heat Transfer. *Industrial & Engineering Chemistry Fundamentals*, 18, 11-15.

-
40. KEIL, R. H. & BAIRD, M. H. I. 1971. Enhancement of Heat Transfer by Flow Pulsation. *Industrial & Engineering Chemistry Process Design and Development*, 10, 473-478.
 41. KHAKHAR, D. V., FRANJIONE, J. G. & OTTINO, J. M. 1987. A case study of chaotic mixing in deterministic flows: The partitioned-pipe mixer. *Chemical Engineering Science*, 42, 2909-2926.
 42. LASBET, Y. 2008. *Performances hydrodynamiques, thermiques et énergétiques de géométries chaotiques : Applications au refroidissement des PEMFC*. Thèse de Doctorat, Ecole Polytechnique de l'Université de Nantes.
 43. LASBET, Y., AUVITY, B., CASTELAIN, C. & PEERHOSSAINI, H. 2006. A chaotic heat-exchanger for PEMFC cooling applications. *Journal of Power Sources*, 156, 114-118.
 44. LE-GUER-Y. 1993. *Etude des phénomènes de transport en régime d'advection chaotique dans un écoulement ouvert*. Thèse de Doctorat, Université de Nantes et Ecole Centrale de Nantes.
 45. LEGUER, Y. 1993. *Etude des phénomènes de transport en régime d'advection chaotique dans un écoulement ouvert*. Ph.D. Dissertation, Université de Nantes et Ecole Centrale de Nantes.
 46. LEMENAND, T. & PEERHOSSAINI, H. 2002. A thermal model for prediction of the Nusselt number in a pipe with chaotic flow. *Applied Thermal Engineering*, 22, 1717-1730.
 47. LEMLICH, A., ARMOUR, J. C. 1965. Enhancement of Heat Transfer by Flow pulsations. *Chern. Eng. Prop. Symp. Ser.*, 61- 83.
 48. LEMLICH, R. 1961. Vibration and pulsation boost heat transfer. *Chemical Engineering* 171-176.
 49. LEMLICH, R. & HWU, C.-K. 1961. The effect of acoustic vibration on forced convective heat transfer. *AIChE Journal*, 7, 102-106.
 50. LIN J.Y., T. J. M. 1980. An experimental and numerical study of periodic flow in a curved tube. *J. Fluid Mech*, 100, 623-638.
 51. LUDLOW, J. C. 1975. MS. Thesis. *University of Virginia, Charlottesville, Va.*
 52. LYNE 1970. Unsteady viscous flow in a curved pipe. *J. Fluid Mech*, 45, 13-31.
 53. MARTINELLI, R. C., BOELTER, L. M. K. 1943. Heat transfer to a fluid flowing periodically at low frequencies in a vertical tube. *Transaction of ASME*, 789-798.

-
54. MCMICHAEL, W. J., HELLUMS, J. G. 1975. The Effect of Pulsations on Heat Transfer for Laminar Flow. *AIChE Journal*, 21: 743.
 55. MELDRUM, D. R. & HOLL, M. R. 2002. Microscale Bioanalytical Systems. *Science*, 297, 1197-1198.
 56. MOKRANI, A. 1997. Analyse expérimentale et numérique de deux procédés complémentaires de mélange et de transfert thermique en écoulement tridimensionnel ouvert : advection chaotique laminaire et écoulement turbulent eulérien. Thèse de Doctorat, Université de Nantes et Ecole Centrale de Nantes.
 57. MOSCHANDREOU, T. & ZAMIR, M. 1997. Heat transfer in a tube with pulsating flow and constant heat flux. *International Journal of Heat and Mass Transfer*, 40, 2461-2466.
 58. MULLER, W. K. 1957. Proceedings fifth Midwestern conference of fluid mechanics. *Ann Arbor, Mich*, p 146.
 59. MULLIN T., G. C. A. 1980. Oscillatory flow in curved pipes, part 1: The developing flow case. *J. Fluid Mech*, 98, 383-395.
 60. MUNSON, B. R. 1975. Experimental results for oscillating flow in a curved pipe. *Physics of Fluids*, 18, 1607-1609.
 61. NISHIMURA, T., OKA, N., YOSHINAKA, Y. & KUNITSUUGU, K. 2000. Influence of imposed oscillatory frequency on mass transfer enhancement of grooved channels for pulsatile flow. *International Journal of Heat and Mass Transfer*, 43, 2365-2374.
 62. OTTINO, J. M. 1989. The Kinematics of Mixing: Stretching, Chaos, and Transport.
 63. PAVLOVA, A., AND AMITAY, M. 2006. Electronic Cooling Using Synthetic Jet Impingement. *Trans. ASME, J. Heat Transfer*, 128, 897-907.
 64. PEDLEY, T. J. 1980. The fluid mechanics of large blood vessels. *Cambridge Monographs on Mechanics and Applied Mathematics*, 160-224.
 65. PEERHOSSAINI, H., GUER, Y. L. & CASTELAIN, C. 1993. Heat exchanger design based on chaotic advection. *Experimental and Thermal and Fluid Science*, 7, 333-334.
 66. PERSOONS, T., MCGUINN, A. & MURRAY, D. B. 2011. A general correlation for the stagnation point Nusselt number of an axisymmetric impinging synthetic jet. *International Journal of Heat and Mass Transfer*, 54, 3900-3908.
 67. PERSOONS, T., O'DONOVAN, T. S., AND MURRAY, D. B., 2009. Heat Transfer in Adjacent Interacting Impinging Synthetic Jets. *Proceedings of ASME Summer Heat Transfer Conference (HT2009)*, 1, 955-962.

-
68. S.W.JONES , T. O. M., AREF H 1989. Chaotic advection by laminar flow in twisted pipe. *J. Fluid Mech*, 209 335-357.
 69. SATO, K., HIBARA, A., TOKESHI, M., HISAMOTO, H. & KITAMORI, T. 2003. Microchip-based chemical and biochemical analysis systems. *Advanced Drug Delivery Reviews*, 55, 379-391.
 70. SCHULTE, T. H., BARDELL, R. L. & WEIGL, B. H. 2002. Microfluidic technologies in clinical diagnostics. *Clinica Chimica Acta*, 321, 1-10.
 71. SHUAI, X., CHENG, S. AND ANTONINI, G. 1994. Pulsation effects on convective heat transfer in the laminar flow of a viscous fluid. *The Canadian Journal of Chemical Engineering*, 72, 468 - 475.
 72. SIGGERS J.H., W. S. L. 2008. Unsteady flows in pipes with finite curvature. *J. Fluid Mech*, 600, 133-165.
 73. SIMON H.A., C. M. H., CHOW J.C.F 1977. Heat transfer in curved tubes with pulsatile fully developed laminar flows. *ASME J. Heat Transfer*, 99, 590-595.
 74. SIOUFFI M., D. V., PELISSIER R 1998. Experimental analysis of unsteady flows in stenosis. *J. Biomechanics*, 31, 11-19.
 75. STREMLER, M. A., HASELTON, F. R. & AREF, H. 2004. Designing for chaos: applications of chaotic advection at the microscale. *Philos Trans A Math Phys Eng Sci*, 362, 1019-36.
 76. SUMIDA 2007. Pulsatile entrance flow in curved pipes: effect of various parameters. *J. Exe. Fluids*, 43, 949-958.
 77. SUMIDA M., S. K., WADA H 1989. Pulsating flow in a curved pipe (secondary flow). *JSME Int. J*, 32, 523-531.
 78. SWANSON C.J., S. S. R., DONNELLY R 1993. Experimental investigation of periodic flow in curved pipes. *J. Fluid Mech*, 69-83, 256.
 79. TADA S., O. S., YAMANE R 1996. Classification of pulsating flow patterns in curved pipes. *J. Biomechanical Eng*, 118, 311-317.
 80. TAKAMI T., S. K., SUMIDA M 1984. Pulsating flow in curved pipes, 1st report, numerical and approximate analyse. *Bulletin of the JSME*, 27, 2706-2713.
 81. TALBOT L., G. K. O. 1983. Pulsatile entrance flow in a curved pipe. *J. Fluid Mech*, 127, 1-25.
 82. TIMITÉ. 2005. *Etude de l'écoulement de Dean alterné pulsé : Mise en évidence du comportement chaotique*. Thèse de Doctorat, Ecole Polytechnique de l'Université de Nantes.
-

-
83. TIMITÉ, B., CASTELAIN, C. & PEERHOSSAINI, H. 2011. Mass transfer and mixing by pulsatile three-dimensional chaotic flow in alternating curved pipes. *International Journal of Heat and Mass Transfer*, 54, 3933-3950.
84. TIMITÉ B., JARRAHI. M., CASTELAIN C., PEERHOSSAINI H 2009. Pulsating flow for mixing intensification in a twisted curved pipe. *J. Fluids Eng*, 131, 121104_1-121104_10.
85. VALIORGUE, P., PERSOONS, T., MCGUINN, A. & MURRAY, D. B. 2009. Heat transfer mechanisms in an impinging synthetic jet for a small jet-to-surface spacing. *Experimental Thermal and Fluid Science*, 33, 597-603.
86. VIJAYENDRAN, R. A., MOTSEGOOD, K. M., BEEBE, D. J. & LECKBAND, D. E. 2002. Evaluation of a Three-Dimensional Micromixer in a Surface-Based Biosensor†. *Langmuir*, 19, 1824-1828.
87. WEIGL, B. H., BARDELL, R. L. & CABRERA, C. R. 2003. Lab-on-a-chip for drug development. *Advanced Drug Delivery Reviews*, 55, 349-377.
88. WEST, F. B. A. T., A. T. 1952. The effect of pulsation on heat transfer in turbulent flow of water inside tubes. *Chemical Engineering Progress*, 48, 39-43.
89. WHITE, C. M. 1929. Streamline flow through curved pipes. *Proc. Roy. Soc.*, 123, 645.
90. YIN, D. & MA, H. B. 2014. Analytical solution of heat transfer of oscillating flow at a triangular pressure waveform. *International Journal of Heat and Mass Transfer*, 70, 46-53.
91. ZABIELSKI L., M. A. J. 1998. Unsteady blood flow in a helically symmetric pipe. *J. Fluid Mech.*, 370, 321-345.
92. ZALOSH R.G., N. W. G. 1973. Pulsating flow in a curved tube. *J. Fluid Mech*, 59, 693-705.
93. ZUMBRUNNEN, D. A., AND AZIZ, M. 1993. Convective Heat Transfer Enhancement Due to Intermittency in an Impinging Jet, *Trans. ASME, J. Heat Transfer*, 115, 91-97.

Abstract

The aim of this study is to investigate mixing and heat transfer enhancement through superposition of a temporal dependence on steady flow in bent tubes.

First, a mixing study is carried out in a 90° curved pipe by analyzing the tracer deformation through a PLIF technique. Measurements are performed for the steady Reynolds numbers range [420–1000], frequency parameters [8–21] and velocity component ratios [1–3]. Effects of each parameter (Re_{st} , α and β) on mixing intensity are discussed. In particular, the intensification of the mixing degree can reach up to 59% compared to the steady case.

Second, a heat exchanger is used to perform thermal measurements, carried out for the same parameters: Re_{st} in the range [600–5000], α in the range [0–20], β in the range [1–13] and adding the effect of the pulsation signals: sinusoidal, triangular and square. The heat exchanger, designed and fabricated at the LTN laboratory, is composed of a succession of bent tubes configured in a chaotic twisted tube geometry. Temperature profiles measurements are recorded at the entrance and exit. Pulsated flow show an increase of the heat transfer efficiency for laminar flow regime, but no effect for turbulent flow. At the optimal value of the pulsation condition, the heat transfer is enhanced up to 24% compared to steady case.

In both cases, and in the appropriate range of the operating parameters, the interest of pulsatile flow is demonstrated by a significant intensification of the transfers.

Keywords: Transfer intensification, mixing, heat transfer, pulsatile flows, PLIF, bent tubes.

Résumé

Ce travail étudie l'intensification du mélange et du transfert thermique par la superposition d'une dépendance temporelle sur des écoulements stationnaires dans des tubes coudés.

Dans un premier cas de figure, une étude du mélange est mise en œuvre dans un tube coudé à 90°, par l'analyse de la distribution d'un traceur par la technique PLIF. Les mesures sont effectuées pour des nombres de Reynolds stationnaires Re_{st} [420–1000], des paramètres de fréquence α [8–21] et des rapports d'amplitude de la vitesse β [1–3]. Les effets de chaque paramètre (Re_{st} , α et β) sur le degré de mélange sont discutés. En particulier, l'intensification du degré de mélange peut atteindre 59% par rapport au cas stationnaire.

Un deuxième montage expérimental permet des mesures thermiques dans un échangeur de chaleur. Les mêmes paramètres que précédemment sont étudiés dans des gammes un peu différentes (Re_{st} entre [600-5000], α entre [0-20], β entre [1-13]), en ajoutant l'effet du signal de pulsation : sinusoïdal, triangulaire ou carré. L'échangeur de chaleur, conçu et fabriqué au LTN, est composé d'une succession de tubes coudés, configurée selon une géométrie chaotique à Dean alterné. Les profils de température sont enregistrés à l'entrée et à la sortie de l'échangeur. L'écoulement pulsé montre une amélioration de l'efficacité du transfert de chaleur en régime laminaire, mais pas d'effet en écoulement turbulent. Des conditions de pulsation optimales améliorent le transfert de chaleur jusqu'à 24% par rapport au cas stationnaire.

Dans les deux cas et pour des conditions opératoires appropriées, l'intérêt d'un écoulement pulsé est démontré par une intensification significative des transferts.

Mots clés : Intensification des transferts, mélange, transfert thermique, écoulements pulsés, PLIF, tubes coudés.